

Stratum corneum model membranes:
molecular organization in relation to
skin barrier function

The investigations described in this thesis were performed at the division of Drug Delivery Technology of the Leiden/Amsterdam Center for Drug Research (LACDR), Leiden University, Leiden, The Netherlands. The studies described in this thesis were financially supported by a grant from the Technology Foundation (STW, project LGP 7503). The printing of this thesis was financially supported by STW, LACDR and the Leiden University library.

Cover image: Gothic bell tower of the church of St-André in Grenoble, France (1298).

Printed by Wöhrmann Print Service, Zutphen, The Netherlands

Stratum corneum model membranes: molecular organization in relation to skin barrier function

Proefschrift

ter verkrijging van
de graad van Doctor aan de Universiteit Leiden,
op gezag van Rector Magnificus prof. mr. P.F. van der Heijden,
volgens besluit van het College voor Promoties
te verdedigen op dinsdag 25 oktober 2011
klokke 15:00

door

Daniël Groen
geboren te Den Haag
in 1979

Promotiecommissie

Promotor: Prof. Dr. J.A. Bouwstra

Overige leden:
Prof. Dr. M. Danhof
Prof. Dr. W. Jiskoot
Prof. Dr. W.J. Briels
Prof. Dr. M.J. Lawrence
Prof. Dr. J.P. Abrahams

Stellingen

Behorende bij het proefschrift

Stratum corneum model membranes:
molecular organization in relation to skin barrier function

1. The barrier function of the skin is fundamental to life on dry land. (*D. Attenborough, Life on Earth, Little, Brown and Company, Boston, 1980*)
2. Understanding the permeability barrier function of the skin is important for rational design of transdermal drug delivery systems as well as for our understanding the etiology, and possible treatment, of a range of skin diseases in which barrier function is compromised. (*J.R. Hill and P.W. Wertz, BBA 1616, 2003, p121-126*)
3. The stratum corneum substitute, prepared with synthetic lipids only, closely mimics the stratum corneum lipid organization and can replace human stratum corneum in permeability studies. (*This thesis*)
4. Because of its adjustable lipid composition, the stratum corneum substitute is a suitable model to mimic the lipid organization in stratum corneum of diseased skin. (*This thesis*)
5. Whether an orthorhombic or hexagonal lipid packing is present in stratum corneum, is of less importance for a proper barrier function than the presence of a proper lamellar organization. (*This thesis*)
6. The presence of water is not required to form a proper lipid organization in a lipid model, mimicking that in human stratum corneum.
7. Many papers in the scientific literature on percutaneous absorption represent a complex blend of physicochemical theory and physiological practicalities. (*Brian W. Barry, Dermatological Formulations: Percutaneous Absorption, Marcel Dekker inc, New York, 1983*)
8. If you wish to make an apple pie from scratch, you must first invent the universe. (*Carl Sagan, Cosmos, 1980, p. 218.*)
9. The propositions in a thesis are a rudimentary organ that lost its function many years ago.

Table of contents

Chapter 1	Introduction, aim and outline of this thesis	1
Part I		
Chapter 2	Two new methods for preparing a unique stratum corneum substitute	29
Chapter 3	Is an orthorhombic lateral packing and a proper lamellar organization important for the skin barrier function?	61
Chapter 4	Investigating the barrier function of skin lipid models with varying compositions	91
Part II		
Chapter 5	Model membranes prepared with ceramide EOS, cholesterol and free fatty acids form a very unique lamellar phase	121
Chapter 6	New insights into the stratum corneum lipid organization by x-ray diffraction analysis	151
Chapter 7	Disposition of ceramide in model lipid membranes determined by neutron diffraction	175
Chapter 8	Summary and perspectives	205

Introduction

1. The skin barrier function

The natural function of the skin is to act as a barrier against unwanted influences from the environment. The skin consists of three layers, from the superficial to the innermost layer: the epidermis, the dermis and the hypodermis (subcutaneous fat tissue) (1), see figure 1. The epidermis also consists of various layers, of which the stratum corneum (SC) is the uppermost nonviable layer. This very thin layer is only 15 to 20 μm thick and acts as the main barrier against permeation of substances (2, 3).

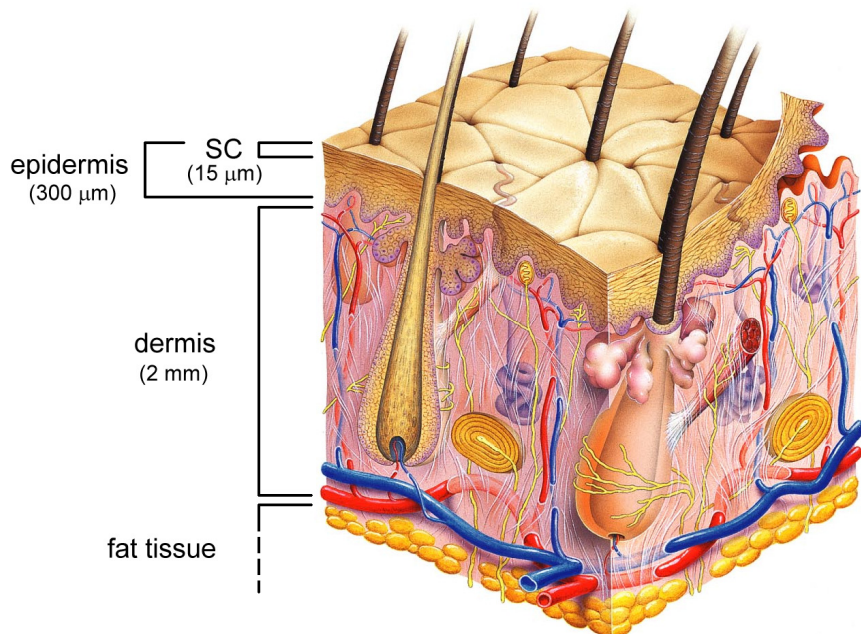


Figure 1: Schematic overview of the different tissue layers in the skin. This figure is adapted from Benjamin Cummings, Pearson Education Inc. copyright 2009.

Chapter 1

The excellent barrier properties of the SC can be ascribed to its unique structure and composition. The SC is generated by the underlying viable epidermis. As the structure of the SC is very different from that of the viable epidermis, many events occur during SC formation within a very short time period. The viable epidermis is densely populated with keratinocytes that are generated in its basal layer. During the formation of the SC, keratinocytes move into the direction of the skin surface. When passing the viable epidermis-SC interface, the cells transform into dead flattened cells (corneocytes). Simultaneously, the cornified envelope, a densely cross linked protein layer surrounding the corneocytes, is formed by sequential deposition of various proteins. Subsequently, a monolayer of non-polar lipids is esterified to the cornified envelope. Besides the formation of the corneocytes, an intercellular lipid matrix is formed, composed of non-polar lipids.

1.1 The structure of the SC

As described above, the SC consists of corneocytes (dead flattened cells) surrounded by the highly impermeable cornified envelope. The corneocytes are embedded in a lipid matrix as “bricks in mortar”, see figure 2. The lipids in the intercellular regions form crystalline lipid lamellae. The corneocytes and the lipid lamellae are oriented approximately parallel to the skin surface. As the lipid lamellae form a continuous pathway for diffusion of substances across the SC, the lipid domains are considered to play a dominant role in the skin barrier function (12). Furthermore, the orientation of the lamellae as well as the lipid organization is suggested to contribute largely to the excellent barrier function of the SC.

1.1.1 Permeation pathway through the SC

Although hair follicles, sweat glands and sebaceous glands are potential routes of compound penetration, the total surface covered by these appendages is only around 0.1%. For this reason compounds applied onto

the skin are considered to penetrate primarily via the transepidermal route into the deeper regions of the skin. During this penetration process, compounds may follow the intercellular or transcellular pathway, depicted in figure 2.

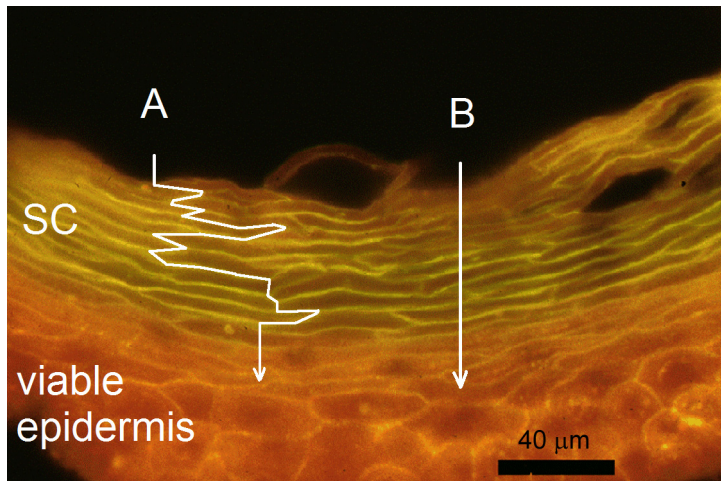


Figure 2: Fluorescence image of Nile red-stained human SC, presented in (9). Depicted are two possible transepidermal penetration pathways: The intercellular route (A) only involves transport along the lipid lamellae, whereas the transcellular route (B) directly crosses the corneocytes and intervening lipids. This figure is reprinted by permission from the American Association of Pharmaceutical Scientists, copyright 2001.

Because of the highly impermeable character of the cornified envelope, the tortuous intercellular pathway has been suggested to be the preferred route for most drug molecules (13). Although this is still a subject of debate, several studies have indeed reported transport mainly along the intercellular space in the SC (14-16). Moreover, it has been demonstrated that drug permeation across the SC increases many folds after lipid extraction (17), again demonstrating an important function of the lipids for a proper skin barrier. Hence, knowledge of the structure and biophysical properties of the intercellular lipid matrix is crucial for understanding the skin barrier function.

1.1.2 Intercellular lipid composition and organization in the SC

The lipid matrix in the intercellular region is mainly composed of ceramides (CER), cholesterol (CHOL) and free fatty acids (FFA), in an approximately equimolar ratio (18-22). However, there is a high inter-individual variability in this lipid composition (23). The CER consist of two long saturated hydrocarbon chains and a small polar headgroup. Each of the twelve CER subclasses identified in human SC contains a sphingoid base and a fatty acid, which are linked by an amide bond between the carboxyl group of the fatty acid and the amino group of the base (18, 21, 22, 24). The sphingoid moiety can be sphingosine (S), phytosphingosine (P), 6-hydroxysphingosine (H) or dihydrosphingosine (dS), whereas the fatty acid moiety is non-hydroxylated (N) or α -hydroxylated (A) with chain lengths of predominantly 24 to 26 carbon atoms. The most remarkable CER are the acylceramides. These CER consist of an unusual long ω -hydroxy fatty acid of 30 to 34 carbon atoms to which an unsaturated linoleic acid is ester-linked (EO). In figure 3 the molecular structure of the main CER subclasses in human SC are presented. The FFA fraction in SC mainly consists of saturated hydrocarbon chains with the prevalent chain lengths being C22 and C24 (25).

In 1987 the use of ruthenium tetroxide as a post-fixation agent made it possible to visualize the unique lamellar arrangement of the intercellular lipids in an electron microscope (7, 26). Multiple lamellae, consisting of a broad-narrow-broad sequence of electron lucent bands were observed demonstrating an unusual arrangement, see figure 4. A few years later small-angle X-ray diffraction (SAXD) measurements on human, pig and mouse SC revealed the presence of a long periodicity phase (LPP) with an approximately 13 nm repeat distance (27-32). Besides the LPP, another lamellar phase was observed using X-ray diffraction. The periodicity of this phase is approximately 6 nm and it is therefore referred to as the short periodicity phase (SPP). In addition to the lamellar phases (LPP and SPP),

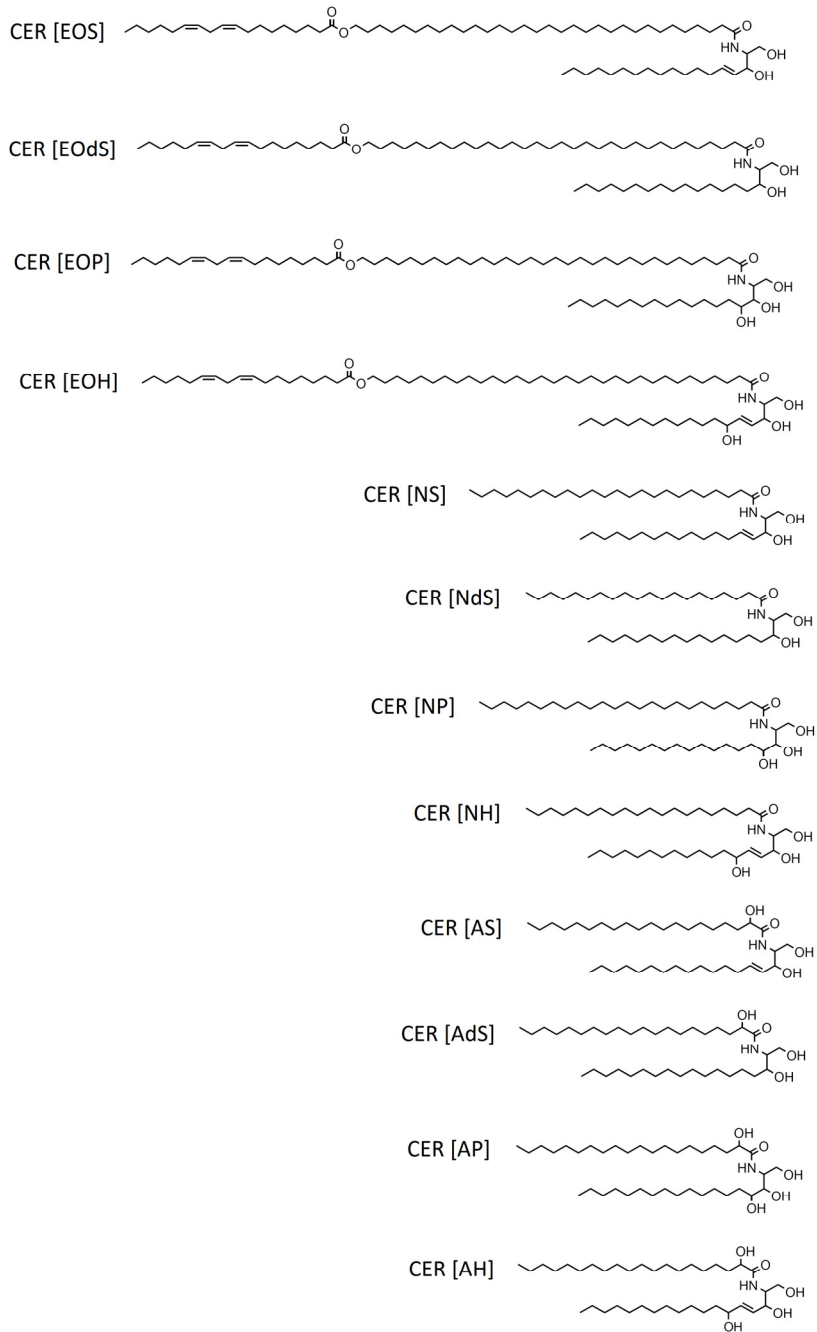


Figure 3: Molecular structure of the CER present in human SC.

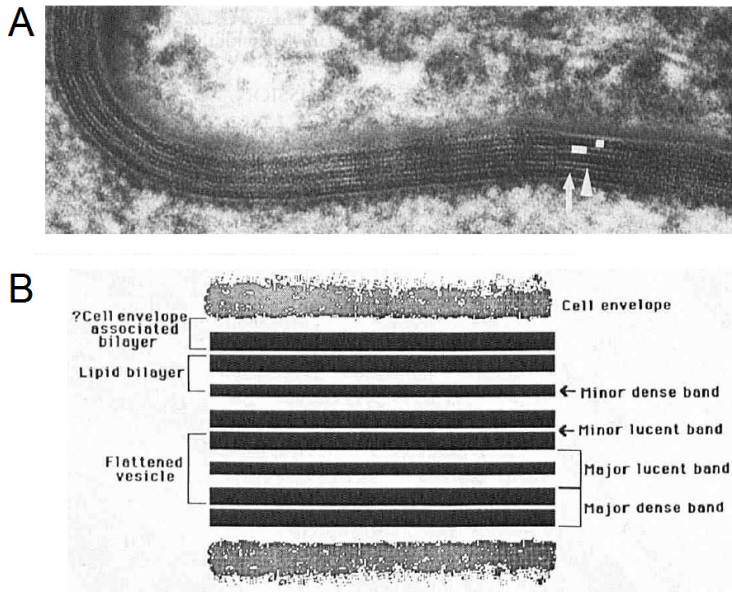


Figure 4: A) Electron micrograph of lamellar lipid structures in the intercellular space of the outer SC of neonatal mouse skin B) Schematic diagram of the intercellular space in figure A. Both figures are from (7), reprinted by permission from MacMillan Publishers Ltd: JID, copyright 1987.

the presence of phase separated crystalline CHOL is also observed in SC (33, 34). In subsequent studies using model lipid mixtures it was found that the presence of CER EOS (see figure 3), is a prerequisite for the formation of the LPP (35-37). Although over the years, a lot of information has been gathered on the SC lipid organization and the role the various lipid classes play in this organization (26, 33, 35, 37), until now the detailed molecular structure of the LPP is not known. In previous studies, several attempts have been made to determine an electron density profile of the LPP, using SAXD. White et al. performed the first calculations using a block shaped electron density profile (27). Our group performed electron density calculations in which the electron density profiles were simulated by Gaussian curves (28, 29). However, both studies suffered from the fact that no swelling of the

lamellae could be induced and therefore no unique electron density profile could be determined. More recently, McIntosh used a mixture of isolated pig CER, CHOL, and palmitic acid and performed X-ray diffraction studies (38). The results indicated a repeating unit consisting of two layers. However, due to the low resolution of the electron density profile the lipid organization in the unit cell could not be unraveled.

Concerning the molecular structure of the SPP, in several other studies progress has been made on the fundamental interactions between the lipid classes using simplified ternary or quaternary lipid mixtures. The mixtures included mainly CER AP with a short acyl chain length of 18 carbon atoms, CHOL and cholesterol sulfate. In these studies the neutron scattering length density profile was determined of CER rich phases with a short periodicity (39-41). However, the phases formed in these mixtures all contain repeat distances much smaller than observed for the SPP in SC. Because the model mixtures described above do not closely resemble the composition in SC, the molecular structure of these CER rich phases might be different from the structure of the SPP (42, 43).

Besides the lamellar organization, the packing of the lipids within these lamellae is also of importance for the barrier function of human skin. The packing density decreases in the order orthorhombic>hexagonal>liquid, see figure 5. Wide-angle X-ray diffraction studies revealed that, at a skin temperature of around 32°C, the lipids in human SC are predominantly forming an orthorhombic packing, although a subpopulation of lipids form a coexisting hexagonal packing (44, 45). It is almost impossible using X-ray diffraction to determine whether a liquid phase coexists with the crystalline phases, as its broad reflection in the diffraction pattern is obscured by the reflections attributed to keratin present in the interior of corneocytes.

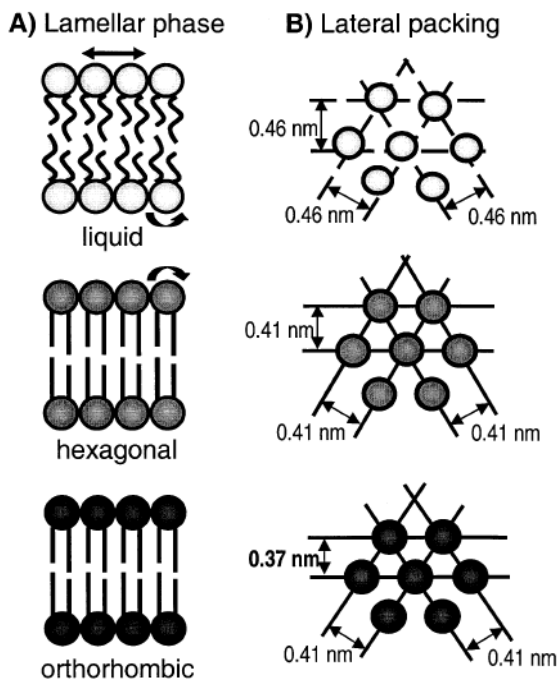


Figure 5: Schematic overview of the types of lateral lipid packing A) Side view showing the lamellae B) Top view showing the lateral packing of the hydrocarbon chains. This figure is from (11), reprinted by permission from MacMillan Publishers Ltd: JID, copyright 2001.

2. Lipid organization in SC of diseased skin

Diseased skin generally displays defects in the SC structure which may lead to a reduced skin barrier function. For example, in lamellar ichthyosis (LI) patients the activity of one of the enzymes involved in the formation of the densely packed cell envelope is reduced, most probably rendering a more permeable cornified envelope (46, 47). Not only enzymes involved in the synthesis of protein structures in SC are impaired in diseased skin. In several skin diseases the activity of enzymes involved in the synthesis of the lipids may be altered as well. For example, in type 2 Gaucher's disease

patients, the level of glucocerebrosidase is strongly reduced, resulting in a strong increase in the ratio of glucosylceramides/CER, leading to an altered lipid organization and a subsequent reduction in the skin barrier function (48-50). This demonstrates that the CER are very important for a proper barrier function. In LI skin, in addition to small changes in CER composition, the level of FFA is strongly reduced compared to that observed in healthy SC (51). Furthermore, SAXD studies with SC of LI skin revealed an altered lamellar organization, as the diffraction peaks in the scattering profile were located at higher scattering angle revealing smaller spacings than in SC of healthy skin (51). Freeze fracture electron microscopy and electron diffraction techniques have also been used to study the lipid organization in LI patients (11). The results showed that the lamellae in LI skin exhibit strong undulations compared to normal skin, confirming an altered lamellar organization. Another example is atopic eczema (AE), which is frequently observed in children especially in the industrialized countries. There is increasing evidence that the impaired skin barrier function is causative for AE. A defect barrier facilitates the transport of allergens and irritants into the skin resulting in skin inflammation. As this disease is a major problem for the western society, many research groups devoted on the skin barrier are now focusing their research on AE. However, there is only limited information about the lipid composition and organization in SC of AE skin. It has been reported that in the SC of AE patients the enzymes sphingomyelin deacylase ceramidase and glucosylceramide deacylase are increased in activity, resulting in a decreased CER level (52-60). Although the CER composition and the ratio between the FFA, CHOL and CER are reported, almost no information is available on the changes in the SC lipid organization in AE patients. In 2001 the lipid organization in three AE patients was investigated with freeze fracture electron microscopy and electron diffraction (ED) in a limited number of patients (11). In these patients the frequency of the hexagonal lateral packing was significantly increased compared to that in normal skin. In the 1980s, the lipid organization in essential fatty acid

Chapter 1

deficient (EFAD) SC has also been elucidated (26, 61). It appeared that elimination of linoleic acid from the diet of pigs resulted in a progressive increase in the oleate content in CER EOS at the expense of the linoleate content. This increase in CER EOS-oleate content was accompanied by a strong reduction in the skin barrier. This change in lipid composition is of interest to study, as in normal skin the CER EOS-oleate/CER EOS-linoleate ratio increases dramatically during the winter season and is also observed to be one of the characteristics of cosmetically dry skin (62, 63).

Furthermore, in psoriasis skin the keratinization process is deranged and the barrier function decreased (64). Analysis of CER from the psoriatic scale, compared to those from normal human SC, revealed a reduction in the CER EOS levels and in the CER containing the phytosphingosine base (65, 66). Recessive X-linked ichthyosis skin is also characterized by an impaired skin barrier function (67). As far as the lipid composition is concerned, a strongly increased level of cholesterol sulphate has been reported which also accounts for the pathological scaling (67-69). In previous studies it was shown that an increase in cholesterol sulphate level resulted in a change in the lipid organization. However, whether this change in lipid organization is responsible for the skin barrier impairment is not yet known.

As shown above, diseased skin often parallels with an altered SC lipid composition, which may lead to a change in the lipid organization. This in turn may be an important factor for the impaired skin barrier function. In order to understand the effects of an aberrant lipid organization in dry or diseased skin, information on the relation between lipid composition, lipid organization and barrier function is crucial. However, this is difficult to obtain with diseased human skin, as this is almost not available and in addition SC has a very complex structure. This makes it difficult to delineate the link between lipid organization and lipid composition in diseased human skin. Furthermore, as it is impossible to modulate systematically the lipid composition in SC, the use of lipid membranes in which the lipid composition can be varied on demand, offers an attractive alternative.

3. SC lipid models

3.1 Ternary and quaternary lipid mixtures

These mixtures generally incorporate one or two individual CER, a fatty acid and CHOL. As the focus is usually on only one CER class, the advantage of these simple systems is that the interpretations of the lipid organization are more detailed than in multi-component systems. Therefore, these mixtures are well suited to investigate fundamental interactions between different lipid classes (70-73). For example, It has been shown that, regardless of the type of lateral packing, hydrogen bonds between headgroups play an important role in the order-disorder transition temperature (70).

However, the limited chain length variation in the ternary and quaternary systems renders them more crystalline and due to a mismatch between the CER and FFA chain lengths the systems often exhibit phase separation (41, 74, 75). In human SC up to 12 CER classes and multiple FFA are present exhibiting a broad variation in chain lengths. This variation in chain length and headgroup architecture increases the ability to form solid mixtures and reduces the formation of separate phases (76). Another difference between single component CER mixtures and the more complex mixtures is the inability to form the LPP in the former. Because of the high crystalline character, the absence of the LPP and the tendency towards phase separation, the ternary and quaternary mixtures are less suited as models to mimic the lipid phase behaviour in SC.

3.2 Multi component lipid mixtures

Before the synthetic CER classes became available, models mimicking the SC lipid composition were prepared using CER isolated from native SC. In 2001 we observed for the first time that mixtures prepared from CHOL and isolated human CER form two lamellar phases with periodicities of 5.4 and 12.8 nm, closely mimicking the lipid phase behavior in human SC (36). In

Chapter 1

these mixtures, however, the lipids form a hexagonal lateral packing independent of the CER:CHOL ratio. With these mixtures, studies were also performed focusing on the role of CER EOS. Phase behavior studies with equimolar CHOL:CER mixtures lacking CER EOS revealed that the LPP was only weakly present, indicating that CER EOS plays a prominent role in the formation of the LPP (35, 77).

Furthermore, studies with lipid mixtures containing CHOL, CER and FFA have also been performed. To mimic the FFA composition in SC, a FFA mixture containing predominantly long chain FFA (C22 and C24) has been used. In the presence of FFA the formation of the SPP was promoted and two lamellar phases were formed with periodicities of 13.0 and 5.5 nm, mimicking even more closely the lipid organization in intact SC. Furthermore, the addition of long chain FFA induced a phase transition from a hexagonal to an orthorhombic lattice and therefore increased the lipid density in the structure (78).

In contrast to the above studies in which solely mixtures prepared with CER isolated from native tissue were used, in more recent studies the lipid organization in mixtures prepared with various synthetic CER with a defined acyl chain length was also investigated (79). The lipid organization in equimolar mixtures of CHOL, synthetic CER and FFA closely resembled that in SC, as both LPP (12.2 nm) and SPP (5.4 nm) were present and the lateral packing of the lipids was orthorhombic. Furthermore, CHOL was also observed in phase separated crystalline domains, similarly as in SC. No additional phases could be detected. Interestingly, only in the presence of FFA a dominant formation of the LPP was observed. This observation is different from that made with mixtures prepared with natural CER. This difference in phase behavior might be related to the limited acyl chain length variation in the synthetic CER mixtures.

The above studies demonstrate that mixtures with CHOL, FFA and synthetic CER can offer an attractive tool to unravel the importance of individual CER for a proper SC lipid organization. Up to now, only the relation between lipid

composition and organization was discussed. However, it is also of importance to correlate the lipid composition and organization to the barrier function. Therefore, to examine whether mixtures applied on an appropriate substrate could be used to replace native SC in permeation studies, a SC substitute (SCS) was developed (43). The barrier properties of the SCS were evaluated in a series of in vitro passive diffusion studies, using three structurally related compounds; p-amino benzoic acid (PABA), ethyl-PABA and butyl-PABA (80). Of these 3 model drugs PABA is the most hydrophilic compound and the lipophilicity increases with increasing ester chain length. The diffusion profiles of all 3 model compounds across 12 μm thick lipid membranes closely resembled those of human SC. Furthermore, exclusion of CER EOS from the lipid mixture revealed a reduced barrier function of the SCS, demonstrating that CER EOS is not only very important for the proper skin lipid phase behavior, but also for the skin barrier function.

Although a lot of information has been gathered on the SC lipid organization and the role the various lipid classes play in this organization, a detailed molecular structure of the LPP and SPP has not yet been presented. More knowledge on these molecular structures can be gained by performing additional X-ray and neutron diffraction studies using mixtures with CER, CHOL and FFA.

3.3 Molecular models for the SC lipid organization

In literature, several molecular models for the lipid organization in SC have been proposed: The stacked monolayer model (8), the domain mosaic model (4), the single gel phase model (6) and the sandwich model (10, 37). The stacked monolayer model presented in 1989 describes the molecular arrangement in the LPP for the first time. Based on the broad-narrow-broad pattern obtained after ruthenium tetroxide fixation of pig skin, a trilayer model was proposed. In this model the CER are arranged in a planar arrangement and the linoleic moiety of CER EOS is randomly distributed in the two broad layers adjacent to the narrow central layer in the repeating unit, see figure 6.

Furthermore, in the stacked monolayer model the CHOL interfacial area is assumed to be similar to that of CER in a planar alignment. However, this is not in agreement with the interfacial areas as reported for CHOL (0.37 nm^2) and CER in a planar (0.25 nm^2) alignment by Dahlén and Pascher (81).

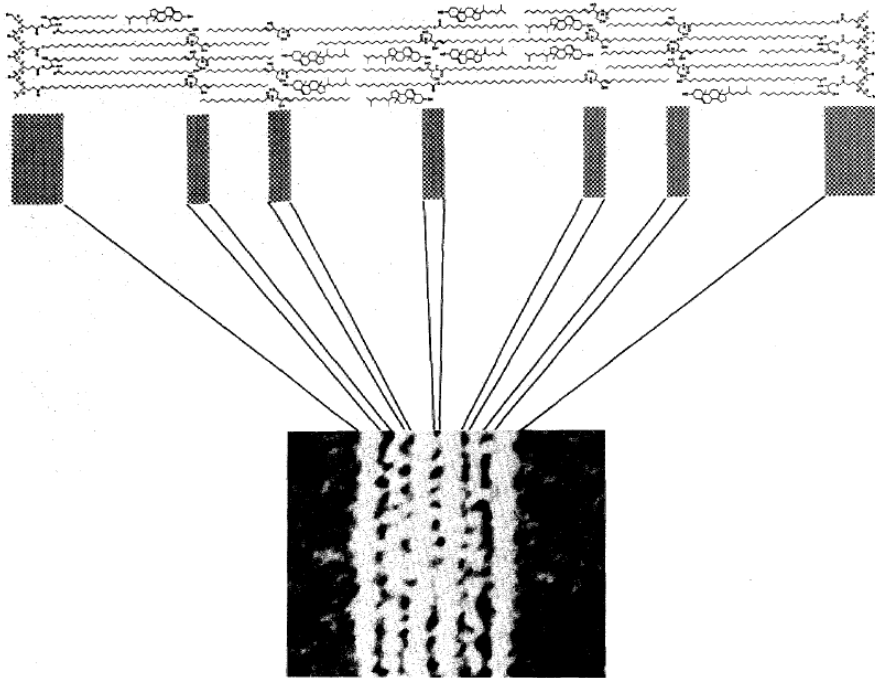


Figure 6: The stacked monolayer model as proposed in (8). A proposed molecular arrangement of one Landmann unit and two corneocyte lipid envelopes with associated monolayers, explaining the pattern of intercellular lamellae where the lucent bands are broad-narrow-broad-broad-narrow-broad. This figure is reprinted by permission from MacMillan Publishers Ltd: JID, copyright 1989.

More recently, Hill and Wertz presented a follow up of the stacked monolayer model again based on the same ruthenium tetroxide data (5), but now including more detailed knowledge on the chemical reaction of ruthenium tetroxide fixation. In this model the linoleate of CER EOS is

located in the central layer, but the CHOL interfacial area is again assumed to be similar to that of CER in a planar arrangement, see figure 7.

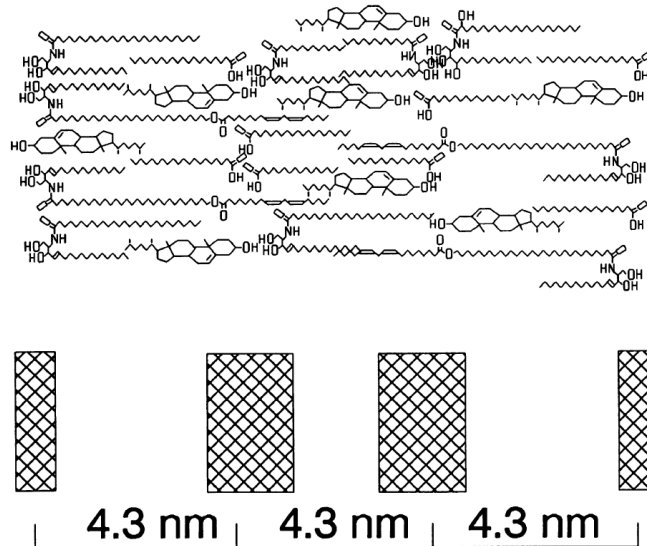


Figure 7: Proposed molecular model as presented in (5), also based on the broad-narrow-broad pattern in ruthenium tetroxide fixed pig SC. Shaded boxes represent the pattern of reduced ruthenium on a corresponding portion of a transmission electron micrograph. This figure is reprinted by permission from Elsevier, copyright 2003.

In 1993 Forslind proposed for the first time a model that incorporates the presence of a liquid phase in the SC. This model postulated the presence of a continuous liquid phase from the superficial layers of the SC down to the viable epidermis, the so-called domain mosaic model, see figure 8. Although this was the first model including the presence of a liquid phase in SC lipid structures, until now no experimental data are available to verify this model.

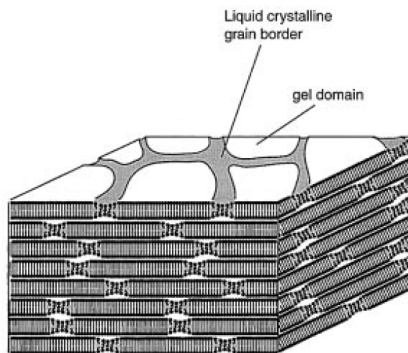


Figure 8: The domain mosaic model as presented in (4). Reprinted by permission from *Acta Dermato-Venereologica*, copyright 1994.

In a more recent paper, another model has been proposed for the SC lipid organization, called the single gel phase model, see figure 9. According to this model the intercellular lipids within the SC exist as a single and coherent lamellar gel phase without domain boundaries. In this gel phase the hydrocarbon chains are packed simultaneously in a hexagonal (close to hydrocarbon chain ends) and an orthorhombic ordering (close to polar headgroups). If this is the case, the orthorhombic and hexagonal phases should always coexist. This has not been observed in electron diffraction studies, in which diffraction patterns were measured attributed either to only a hexagonal or to only an orthorhombic phase (45, 82). Furthermore, in proposing the single gel phase model no attention has been paid to the role the individual lipids play in the lipid organization. For example, the crucial role CER EOS plays in the formation of the 13 nm lamellar phase and the presence (or absence) of long-chain FFA that facilitate the formation of the orthorhombic packing in vitro as well as in vivo, was not taken into consideration.

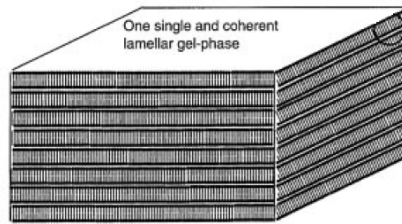


Figure 9: The single gel phase model as presented in (6). Reprinted by permission from Macmillan Publishers Ltd, JID, copyright 2001.

Finally, the sandwich model proposed by our group suggests that the lipids within the LPP are organized in a tri-layer structure: two broad layers with a crystalline (orthorhombic) structure are separated by a narrow central lipid layer with fluid domains, see figure 10.

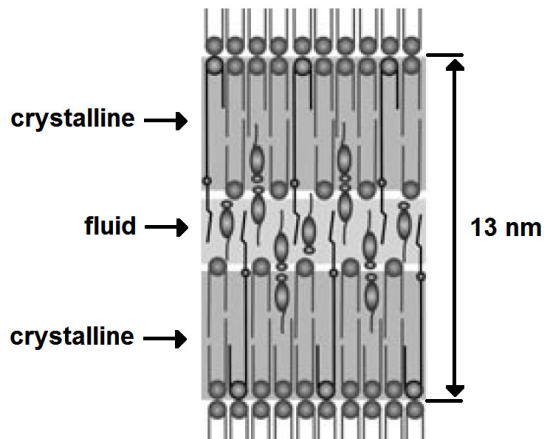


Figure 10: The sandwich model as presented in (10). Reprinted by permission from Acta Dermato-Venereologica, copyright 2000.

This broad-narrow-broad pattern of hydrocarbon chains corresponds to the images obtained with electron microscopy of the SC intercellular lamellae (figure 4). CHOL and the linoleic acid moieties of the acylceramides CER

EOS, CER EOH and CER EOP are proposed to be located in the central narrow layer, whereas crystalline packed CER are present on both sides of this central layer (83). Due to their unusual long structure, the acylceramides are able to span a layer and extend into another layer. The acylceramides are therefore thought to contribute to the stability of the 13 nm phase. The central, non-continuous fluid phase may be of importance for proper elasticity of the lamellae and for the enzyme activity in the SC, as enzymes are unlikely to be active in crystalline phases. In the sandwich model the CHOL is suggested to be located near the linoleate chains in the central layer. More recent data, however, revealed that the CHOL molecule prefers to arrange with saturated hydrocarbon chains rather than with unsaturated chains (84-86). Therefore it is more likely that CHOL is located in the crystalline layers adjacent to the narrow central layer than in the central layer with unsaturated linoleate chains. Furthermore, as Kessner et al recently suggested, the CER molecules in the sandwich model are arranged in the hairpin conformation while it can not be excluded that the CER molecules are arranged in a fully extended conformation (72).

Several models for the molecular structure of the intercellular lipids were discussed above. In conclusion, there is no consensus on the best model for the intercellular lipid arrangement in SC and therefore continuing research is necessary to gain more insight into the molecular organization of the SC lipids.

4. This thesis

4.1 Aim of this thesis

As described above, the SC forms the main barrier function of the skin and the lipid domains in the SC are considered to play a dominant role in this barrier function.

In previous studies a synthetic SC substitute (SCS) was developed to replace native SC in permeability studies. The SCS consists of synthetic SC

lipids (CER, CHOL and FFA) casted on a porous substrate. One of the advantages of the SCS is that its lipid composition can be modified to mimic that in SC of dry or diseased skin. This modified SCS can subsequently be assessed on its barrier function in permeation studies. Furthermore, the unique SC lipid organization can be investigated using SC lipid models in FTIR, SAXD and neutron diffraction studies.

The objectives of this thesis are:

- 1) To improve the preparation method of the SCS to obtain a lower lipid loss during preparation, a more uniform lipid layer thickness and a better reproducibility in terms of thickness and lipid organization.
- 2) To investigate the lateral and lamellar lipid organization in SC in more detail, using the SCS in permeation studies and SC lipid models in FTIR and X-ray and neutron diffraction studies. Concerning the lamellar organization, more knowledge can be gained especially on the molecular structure of the LPP in SC and on the role of CER EOS in the formation of this phase.
- 3) To evaluate the barrier properties of SCS mimicking the SC lipid composition in dry or diseased skin, to assess whether or not the altered SC lipid organization in diseased skin results in a decreased barrier function.

4.2 Outline of this thesis

In the studies described in **Part I** of this thesis the SCS is used as a tool to study the relation between lipid composition, organization and barrier function in one model. In chapter 2 we describe two new methods to prepare the SCS, in order to improve reproducibility and to increase the efficiency of the preparation method. Subsequently the properties of the SCS prepared by the different methods are investigated and the most optimal preparation method is selected for future studies. In the studies described in chapter 3 we use the SCS to determine whether a change in the lateral lipid organization affects the permeability of the SCS. We examine the effect of the orthorhombic to hexagonal phase transition on the barrier function of SCS and compared it with human SC. In the studies described in chapter 4

Chapter 1

we examine SCS that mimic selected changes in lipid composition reported for dry or diseased skin.

In the studies described in **Part II** the molecular organization in the repeating units of the SC lamellar phases is investigated. As CER EOS plays an important role in the formation of the LPP, in the studies described in chapter 5 we investigate whether CER EOS in the absence of the other CER subclasses, mixed with CHOL and FFA, forms similar phases as observed in SC. In the studies described in chapter 6 the molecular structure in the unit cell of the LPP present in SC is investigated into detail. This characteristic LPP is suggested to be very important for the barrier function of the skin. To gain more insight into the molecular organization of this lamellar phase, we perform SAXD studies using various lipid mixtures mimicking the lipid composition in SC, with a slight variation in repeat distance of the LPP. Finally, in the studies described in chapter 7 the molecular structure of the SPP, also present in SC, is investigated into detail. To gain more insight into the molecular organization of the SPP we perform neutron diffraction studies on a mixture that incorporates a deuterated CER subclass.

References

1. Schaefer, H., and T. E. Redelmeier. 1996. Principles of percutaneous absorption. Karger, Basel.
2. Blank, I. H., and R. J. Scheuplein. 1969. Transport into and within Skin. *British Journal of Dermatology* 81:4-8.
3. Scheuplein, R. J., and I. H. Blank. 1971. Permeability of the skin. *Physiol Rev* 51:702-747.
4. Forslind, B. 1994. A domain mosaic model of the skin barrier. *Acta Derm Venereol* 74:1-6.
5. Hill, J. R., and P. W. Wertz. 2003. Molecular models of the intercellular lipid lamellae from epidermal stratum corneum. *Biochim Biophys Acta* 1616:121-126.
6. Norlen, L. 2001. Skin barrier structure and function: the single gel phase model. *J Invest Dermatol* 117:830-836.
7. Madison, K. C., D. C. Swartzendruber, P. W. Wertz, and D. T. Downing. 1987. Presence of intact intercellular lipid lamellae in the upper layers of the stratum corneum. *J Invest Dermatol* 88:714-718.
8. Swartzendruber, D. C., P. W. Wertz, D. J. Kitko, K. C. Madison, and D. T. Downing. 1989. Molecular models of the intercellular lipid lamellae in mammalian stratum corneum. *J Invest Dermatol* 92:251-257.
9. Talreja, P. S., N. K. Kleene, W. L. Pickens, T. F. Wang, and G. B. Kasting. 2001. Visualization of the lipid barrier and measurement of lipid pathlength in human stratum corneum. *AAPS PharmSci* 3:art. no.-13.
10. Bouwstra, J. A., F. E. Dubbelaar, G. S. Gooris, and M. Ponc. 2000. The lipid organisation in the skin barrier. *Acta Derm Venereol Suppl (Stockh)* 208:23-30.
11. Pilgram, G. S., D. C. Vissers, H. van der Meulen, S. Pavel, S. P. Lavrijsen, J. A. Bouwstra, and H. K. Koerten. 2001. Aberrant lipid organization in stratum corneum of patients with atopic dermatitis and lamellar ichthyosis. *J Invest Dermatol* 117:710-717.
12. Simonetti, O., A. J. Hoogstraate, W. Bialik, J. A. Kempenaar, A. H. Schrijvers, H. E. Bodde, and M. Ponc. 1995. Visualization of diffusion pathways across the stratum corneum of native and in-vitro-reconstructed epidermis by confocal laser scanning microscopy. *Arch Dermatol Res* 287:465-473.
13. Williams, M. L., and P. M. Elias. 1987. The extracellular matrix of stratum corneum: role of lipids in normal and pathological function. *Crit Rev Ther Drug Carrier Syst* 3:95-122.
14. Bodde, H. E., I. Vandenbrink, H. K. Koerten, and F. H. N. Dehaan. 1991. Visualization of In vitro Percutaneous Penetration of Mercuric-Chloride - Transport through Intercellular Space Versus Cellular

- Uptake through Desmosomes. *Journal of Controlled Release* 15:227-236.
15. Johnson, M. E., D. Blankschtein, and R. Langer. 1997. Evaluation of solute permeation through the stratum corneum: lateral bilayer diffusion as the primary transport mechanism. *J Pharm Sci* 86:1162-1172.
 16. Meuwissen, M. E., J. Janssen, C. Cullander, H. E. Junginger, and J. A. Bouwstra. 1998. A cross-section device to improve visualization of fluorescent probe penetration into the skin by confocal laser scanning microscopy. *Pharm Res* 15:352-356.
 17. Rastogi, S. K., and J. Singh. 2001. Lipid extraction and transport of hydrophilic solutes through porcine epidermis. *Int J Pharm* 225:75-82.
 18. Wertz, P. W., M. C. Miethke, S. A. Long, J. S. Strauss, and D. T. Downing. 1985. The composition of the ceramides from human stratum corneum and from comedones. *J. Invest. Dermatol.* 84:410-412.
 19. Robson, K. J., M. E. Stewart, S. Michelsen, N. D. Lazo, and D. T. Downing. 1994. 6-Hydroxy-4-sphingenine in human epidermal ceramides. *J. Lipid. Res.* 35:2060-2068.
 20. Stewart, M. E., and D. T. Downing. 1999. A new 6-hydroxy-4-sphingenine-containing ceramide in human skin. *J. Lipid. Res.* 40:1434-1439.
 21. Ponec, M., A. Weerheim, P. Lankhorst, and P. Wertz. 2003. New acylceramide in native and reconstructed epidermis. *J. Invest. Dermatol.* 120:581-588.
 22. Masukawa, Y., H. Narita, E. Shimizu, N. Kondo, Y. Sugai, T. Oba, R. Homma, J. Ishikawa, Y. Takagi, T. Kitahara, Y. Takema, and K. Kita. 2008. Characterization of overall ceramide species in human stratum corneum. *J Lipid Res* 49:1466-1476.
 23. Weerheim, A., and M. Ponec. 2001. Determination of stratum corneum lipid profile by tape stripping in combination with high-performance thin-layer chromatography. *Arch Dermatol Res* 293:191-199.
 24. van Smeden, J., L. Hoppel, R. van der Heijden, T. Hankemeier, R. J. Vreeken, and J. A. Bouwstra. LC-MS analysis of stratum corneum lipids: Ceramide profiling and discovery. *J Lipid Res.*
 25. Wertz, P. 1991. Epidermal lipids. In *Physiology, Biochemistry and Molecular Biology of the Skin*. L. A. Goldsmith, editor. Oxford University Press, Oxford. 205-235.
 26. Hou, S. Y., A. K. Mitra, S. H. White, G. K. Menon, R. Ghadially, and P. M. Elias. 1991. Membrane structures in normal and essential fatty acid-deficient stratum corneum: characterization by ruthenium tetroxide staining and x-ray diffraction. *J Invest Dermatol* 96:215-223.

27. White, S. H., D. Mirejovsky, and G. I. King. 1988. Structure of lamellar lipid domains and corneocyte envelopes of murine stratum corneum. An X-ray diffraction study. *Biochemistry* 27:3725-3732.
28. Bouwstra, J. A., G. S. Gooris, J. A. van der Spek, and W. Bras. 1991. Structural investigations of human stratum corneum by small-angle X-ray scattering. *J Invest Dermatol* 97:1005-1012.
29. Bouwstra, J. A., G. S. Gooris, J. A. van der Spek, S. Lavrijsen, and W. Bras. 1994. The lipid and protein structure of mouse stratum corneum: a wide and small angle diffraction study. *Biochim Biophys Acta* 1212:183-192.
30. Bouwstra, J. A., G. S. Gooris, W. Bras, and D. T. Downing. 1995. Lipid organization in pig stratum corneum. *J. Lipid Res.* 36:685-695.
31. Norlen, L. 2003. Skin barrier structure, function and formation - learning from cryo-electron microscopy of vitreous, fully hydrated native human epidermis. *Int J Cosmet Sci* 25:209-226.
32. Norlen, L. 2007. Nanostructure of the stratum corneum extracellular lipid matrix as observed by cryo-electron microscopy of vitreous skin sections. *Int J Cosmet Sci* 29:335-352.
33. Garson, J. C., J. Doucet, J. L. Leveque, and G. Tsoucaris. 1991. Oriented structure in human stratum corneum revealed by X-ray diffraction. *J Invest Dermatol* 96:43-49.
34. Bouwstra, J. A., G. S. Gooris, J. A. van der Spek, and W. Bras. 1991. Structural investigations of human stratum corneum by small-angle X-ray scattering. *J. Invest. Dermatol.* 97:1005-1012.
35. McIntosh, T. J., M. E. Stewart, and D. T. Downing. 1996. X-ray diffraction analysis of isolated skin lipids: reconstitution of intercellular lipid domains. *Biochemistry* 35:3649-3653.
36. Bouwstra, J. A., G. S. Gooris, F. E. Dubbelaar, and M. Ponc. 2001. Phase behavior of lipid mixtures based on human ceramides: coexistence of crystalline and liquid phases. *J Lipid Res* 42:1759-1770.
37. Bouwstra, J. A., G. S. Gooris, F. E. Dubbelaar, and M. Ponc. 2002. Phase behavior of stratum corneum lipid mixtures based on human ceramides: the role of natural and synthetic ceramide 1. *J Invest Dermatol* 118:606-617.
38. McIntosh, T. J. 2003. Organization of skin stratum corneum extracellular lamellae: diffraction evidence for asymmetric distribution of cholesterol. *Biophys J* 85:1675-1681.
39. Kiselev, M. A., N. Y. Ryabova, A. M. Balagurov, S. Dante, T. Hauss, J. Zbytovska, S. Wartewig, and R. H. Neubert. 2005. New insights into the structure and hydration of a stratum corneum lipid model membrane by neutron diffraction. *Eur Biophys J* 34:1030-1040.
40. Ruettinger, A., M. A. Kiselev, T. Hauss, S. Dante, A. M. Balagurov, and R. H. Neubert. 2008. Fatty acid interdigitation in stratum corneum model membranes: a neutron diffraction study. *Eur Biophys J* 37:759-771.

41. Schroter, A., D. Kessner, M. A. Kiselev, T. Hauss, S. Dante, and R. H. Neubert. 2009. Basic nanostructure of stratum corneum lipid matrices based on ceramides [EOS] and [AP]: a neutron diffraction study. *Biophys J* 97:1104-1114.
42. de Jager, M. W., G. S. Gooris, I. P. Dolbnya, W. Bras, M. Ponec, and J. A. Bouwstra. 2004. Novel lipid mixtures based on synthetic ceramides reproduce the unique stratum corneum lipid organization. *J Lipid Res* 45:923-932.
43. de Jager, M., W. Groenink, J. van der Spek, C. Janmaat, G. Gooris, M. Ponec, and J. Bouwstra. 2006. Preparation and characterization of a stratum corneum substitute for in vitro percutaneous penetration studies. *Biochim. Biophys. Acta* 1758:636-644.
44. Bouwstra, J. A., G. S. Gooris, M. A. Salomonsdevries, J. A. Vanderspek, and W. Bras. 1992. Structure of Human Stratum-Corneum as a Function of Temperature and Hydration - a Wide-Angle X-Ray-Diffraction Study. *International Journal of Pharmaceutics* 84:205-216.
45. Pilgram, G. S., A. M. Engelsma-van Pelt, J. A. Bouwstra, and H. K. Koerten. 1999. Electron diffraction provides new information on human stratum corneum lipid organization studied in relation to depth and temperature. *J Invest Dermatol* 113:403-409.
46. Yang, J. M., K. S. Ahn, M. O. Cho, K. Yoneda, C. H. Lee, J. H. Lee, E. S. Lee, E. Candi, G. Melino, B. Ahvazi, and P. M. Steinert. 2001. Novel mutations of the transglutaminase 1 gene in lamellar ichthyosis. *J Invest Dermatol* 117:214-218.
47. Egberts, F., M. Heinrich, J. M. Jensen, S. Winoto-Morbach, S. Pfeiffer, M. Wickel, M. Schunck, J. Steude, P. Saftig, E. Proksch, and S. Schutze. 2004. Cathepsin D is involved in the regulation of transglutaminase 1 and epidermal differentiation. *J Cell Sci* 117:2295-2307.
48. Holleran, W. M., E. I. Ginns, G. K. Menon, J. U. Grundmann, M. Fartasch, C. E. McKinney, P. M. Elias, and E. Sidransky. 1994. Consequences of beta-glucocerebrosidase deficiency in epidermis. Ultrastructure and permeability barrier alterations in Gaucher disease. *J Clin Invest* 93:1756-1764.
49. Sidransky, E., M. Fartasch, R. E. Lee, L. A. Metlay, S. Abella, A. Zimran, W. Gao, P. M. Elias, E. I. Ginns, and W. M. Holleran. 1996. Epidermal abnormalities may distinguish type 2 from type 1 and type 3 of Gaucher disease. *Pediatr Res* 39:134-141.
50. Doering, T., R. L. Proia, and K. Sandhoff. 1999. Accumulation of protein-bound epidermal glucosylceramides in beta-glucocerebrosidase deficient type 2 Gaucher mice. *FEBS Lett* 447:167-170.
51. Lavrijsen, A. P., J. A. Bouwstra, G. S. Gooris, A. Weerheim, H. E. Bodde, and M. Ponec. 1995. Reduced skin barrier function parallels

- abnormal stratum corneum lipid organization in patients with lamellar ichthyosis. *J Invest Dermatol* 105:619-624.
52. Murata, Y., J. Ogata, Y. Higaki, M. Kawashima, Y. Yada, K. Higuchi, T. Tsuchiya, S. Kawainami, and G. Imokawa. 1996. Abnormal expression of sphingomyelin acylase in atopic dermatitis: an etiologic factor for ceramide deficiency? *J Invest Dermatol* 106:1242-1249.
 53. Hara, J., K. Higuchi, R. Okamoto, M. Kawashima, and G. Imokawa. 2000. High-expression of sphingomyelin deacylase is an important determinant of ceramide deficiency leading to barrier disruption in atopic dermatitis. *J Invest Dermatol* 115:406-413.
 54. Macheleidt, O., H. W. Kaiser, and K. Sandhoff. 2002. Deficiency of epidermal protein-bound omega-hydroxyceramides in atopic dermatitis. *J Invest Dermatol* 119:166-173.
 55. Okamoto, R., J. Arikawa, M. Ishibashi, M. Kawashima, Y. Takagi, and G. Imokawa. 2003. Sphingosylphosphorylcholine is upregulated in the stratum corneum of patients with atopic dermatitis. *J Lipid Res* 44:93-102.
 56. Ishibashi, M., J. Arikawa, R. Okamoto, M. Kawashima, Y. Takagi, K. Ohguchi, and G. Imokawa. 2003. Abnormal expression of the novel epidermal enzyme, glucosylceramide deacylase, and the accumulation of its enzymatic reaction product, glucosylsphingosine, in the skin of patients with atopic dermatitis. *Lab Invest* 83:397-408.
 57. Proksch, E., J. M. Jensen, and P. M. Elias. 2003. Skin lipids and epidermal differentiation in atopic dermatitis. *Clin Dermatol* 21:134-144.
 58. Jensen, J. M., R. Folster-Holst, A. Baranowsky, M. Schunck, S. Winoto-Morbach, C. Neumann, S. Schutze, and E. Proksch. 2004. Impaired sphingomyelinase activity and epidermal differentiation in atopic dermatitis. *J Invest Dermatol* 122:1423-1431.
 59. Choi, M. J., and H. I. Maibach. 2005. Role of ceramides in barrier function of healthy and diseased skin. *Am J Clin Dermatol* 6:215-223.
 60. Ishikawa, J., H. Narita, N. Kondo, M. Hotta, Y. Takagi, Y. Masukawa, T. Kitahara, Y. Takema, S. Koyano, S. Yamazaki, and A. Hatamochi. Changes in the ceramide profile of atopic dermatitis patients. *J Invest Dermatol* 130:2511-2514.
 61. Melton, J. L., P. W. Wertz, D. C. Swartzendruber, and D. T. Downing. 1987. Effects of essential fatty acid deficiency on epidermal O-acylsphingolipids and transepidermal water loss in young pigs. *Biochim Biophys Acta* 921:191-197.
 62. Rogers, J., C. Harding, A. Mayo, J. Banks, and A. Rawlings. 1996. Stratum corneum lipids: the effect of ageing and the seasons. *Arch Dermatol Res* 288:765-770.
 63. Conti, A., J. Rogers, P. Verdejo, C. R. Harding, and A. V. Rawlings. 1996. Seasonal influences on stratum corneum ceramide 1 fatty

- acids and the influence of topical essential fatty acids. *Int J Cosmet Sci* 18:1-12.
64. Marks, J., S. Rogers, B. Chadkirk, and S. Shuster. 1981. Clearance of Chronic Plaque Psoriasis by Anthralin - Subjective and Objective Assessment and Comparison with Photochemotherapy. *British Journal of Dermatology* 105:96-99.
 65. Motta, S., M. Monti, S. Sesana, R. Caputo, S. Carelli, and R. Ghidoni. 1993. Ceramide composition of the psoriatic scale. *Biochim. Biophys. Acta* 1182:147-151.
 66. Motta, S., S. Sesana, R. Ghidoni, and M. Monti. 1995. Content of the different lipid classes in psoriatic scale. *Arch Dermatol Res* 287:691-694.
 67. Zettersten, E., M. Q. Man, J. Sato, M. Denda, A. Farrell, R. Ghadially, M. L. Williams, K. R. Feingold, and P. M. Elias. 1998. Recessive x-linked ichthyosis: role of cholesterol-sulfate accumulation in the barrier abnormality. *J Invest Dermatol* 111:784-790.
 68. Elias, P. M., M. L. Williams, M. E. Maloney, J. A. Bonifas, B. E. Brown, S. Grayson, and E. H. Epstein, Jr. 1984. Stratum corneum lipids in disorders of cornification. Steroid sulfatase and cholesterol sulfate in normal desquamation and the pathogenesis of recessive X-linked ichthyosis. *J Clin Invest* 74:1414-1421.
 69. Williams, M. L., and P. M. Elias. 1981. Stratum corneum lipids in disorders of cornification: increased cholesterol sulfate content of stratum corneum in recessive x-linked ichthyosis. *J Clin Invest* 68:1404-1410.
 70. Rerek, M. E., D. van Wyck, R. Mendelsohn, and D. J. Moore. 2005. FTIR spectroscopic studies of lipid dynamics in phytosphingosine ceramide models of the stratum corneum lipid matrix. *Chemistry and Physics of Lipids* 134:51-58.
 71. Chen, X., S. Kwak, M. Lafleur, M. Bloom, N. Kitson, and J. Thewalt. 2007. Fatty acids influence "solid" phase formation in models of stratum corneum intercellular membranes. *Langmuir* 23:5548-5556.
 72. Kessner, D., A. Ruettinger, M. A. Kiselev, S. Wartewig, and R. H. Neubert. 2008. Properties of ceramides and their impact on the stratum corneum structure. Part 2: stratum corneum lipid model systems. *Skin Pharmacol Physiol* 21:58-74.
 73. Brief, E., S. Kwak, J. T. Cheng, N. Kitson, J. Thewalt, and M. Lafleur. 2009. Phase behavior of an equimolar mixture of N-palmitoyl-D-erythro-sphingosine, cholesterol, and palmitic acid, a mixture with optimized hydrophobic matching. *Langmuir* 25:7523-7532.
 74. Percot, A., and M. Lafleur. 2001. Direct observation of domains in model stratum corneum lipid mixtures by Raman microspectroscopy. *Biophys J* 81:2144-2153.

75. Velkova, V., and M. Lafleur. 2002. Influence of the lipid composition on the organization of skin lipid model mixtures: an infrared spectroscopy investigation. *Chem Phys Lipids* 117:63-74.
76. Gooris, G. S., and J. A. Bouwstra. 2007. Infrared spectroscopic study of stratum corneum model membranes prepared from human ceramides, cholesterol, and fatty acids. *Biophys J* 92:2785-2795.
77. Bouwstra, J. A., G. S. Gooris, F. E. Dubbelaar, A. M. Weerheim, A. P. Ijzerman, and M. Ponec. 1998. Role of ceramide 1 in the molecular organization of the stratum corneum lipids. *J Lipid Res* 39:186-196.
78. Bouwstra, J. A., G. S. Gooris, F. E. Dubbelaar, A. M. Weerheim, and M. Ponec. 1998. pH, cholesterol sulfate, and fatty acids affect the stratum corneum lipid organization. *J Investig Dermatol Symp Proc* 3:69-74.
79. de Jager, M. W., G. S. Gooris, M. Ponec, and J. A. Bouwstra. 2005. Lipid mixtures prepared with well-defined synthetic ceramides closely mimic the unique stratum corneum lipid phase behavior. *J Lipid Res* 46:2649-2656.
80. de Jager, M., W. Groenink, R. Bielsa i Guivernau, E. Andersson, N. Angelova, M. Ponec, and J. Bouwstra. 2006. A novel in vitro percutaneous penetration model: evaluation of barrier properties with p-aminobenzoic acid and two of its derivatives. *Pharm. Res.* 23:951-960.
81. Dahlen, B., and I. Pascher. 1979. Molecular Arrangements in Sphingolipids - Thermotropic Phase-Behavior of Tetracosanoylphytosphingosine. *Chemistry and Physics of Lipids* 24:119-133.
82. Pilgram, G. S., A. M. Van Pelt, F. Spies, J. A. Bouwstra, and H. K. Koerten. 1998. Cryo-electron diffraction as a tool to study local variations in the lipid organization of human stratum corneum. *J Microsc* 189:71-78.
83. Bouwstra, J., G. Pilgram, G. Gooris, H. Koerten, and M. Ponec. 2001. New aspects of the skin barrier organization. *Skin Pharmacol Appl Skin Physiol* 14 Suppl 1:52-62.
84. Brzustowicz, M. R., V. Cherezov, M. Caffrey, W. Stillwell, and S. R. Wassall. 2002. Molecular organization of cholesterol in polyunsaturated membranes: microdomain formation. *Biophys J* 82:285-298.
85. Harroun, T. A., J. Katsaras, and S. R. Wassall. 2006. Cholesterol hydroxyl group is found to reside in the center of a polyunsaturated lipid membrane. *Biochemistry* 45:1227-1233.
86. Kucerka, N., D. Marquardt, T. A. Harroun, M. P. Nieh, S. R. Wassall, D. H. de Jong, L. V. Schafer, S. J. Marrink, and J. Katsaras. 2010. Cholesterol in bilayers with PUFA chains: doping with DMPC or POPC results in sterol reorientation and membrane-domain formation. *Biochemistry* 49:7485-7493.

Chapter 2

Two new methods for preparing a unique stratum corneum substitute

Daniël Groen, Gert S. Gooris, Maria Ponec, Joke A. Bouwstra

Biochim Biophys Acta, vol. 1778, no. 10, pp. 2421-2429.

Abstract

Stratum corneum lipids play an important role in the barrier function of skin. An *in vitro* permeation model consisting of synthetic lipids has previously been developed to replace human stratum corneum (SC) in permeation studies. This model is referred to as the stratum corneum substitute (SCS). In order to improve its reproducibility and to increase the efficiency in preparing the SCS, two new preparation methods are developed. Subsequently the properties of the SCS prepared by the various methods, i.e. the manual airbrush method, the rotor airbrush method and the linomat method, are investigated. The results show that the SCS prepared with the various methods share the properties of a uniform lipid composition and lipid distribution. Furthermore, irrespective of the preparation method, the lipids form crystalline lamellar phases, mimicking the lipid organization and orientation in human SC. As a result, permeation profiles of benzoic acid through SCS are very similar to human SC. The rotor method increases the efficiency and reproducibility of the manual airbrush method, while the linomat method reduces the lipid loss during preparation and results in SCS with a more uniform membrane thickness. In conclusion, the linomat method was chosen as the preferred method for preparing the substitute.

1. Introduction

The uppermost layer of the human skin, the stratum corneum (SC) consists of flattened dead skin cells (corneocytes) surrounded by lipid lamellae. The lipid domains in the SC form the only continuous pathway through the SC and are suggested to act as the main barrier for diffusion of substances through the skin (1). The main lipid classes in SC are ceramides (CER), cholesterol (CHOL) and free fatty acids (FFA) (2-5). The lipids are arranged in two coexisting lamellar phases; a long periodicity phase (LPP) with a repeat distance of ~13 nm and a short periodicity phase (SPP) with a repeat distance of ~6 nm (6, 7). Furthermore, within the lamellae the lipids form mainly a crystalline lateral packing. The lipid organization and its orientation approximately parallel to the skin surface play an important role in the skin barrier function (8). A more detailed analysis of the lipid composition revealed that the FFA has lipid chain lengths of mainly 22 and 24 C atoms (9). In addition, there are nine subclasses of CER in human SC (5). The CER consist of either a sphingosine (S), phytosphingosine (P) or a 6-hydroxysphingosine (H) base, whereas the acyl chain is a nonhydroxy (N), α -hydroxy (A) or ω -hydroxy chain (10). The corresponding nonhydroxy and α -hydroxy CER are therefore denoted as CER NP, CER NS, CER NH, CER AP, CER AS and CER AH. The ω -hydroxy CER possess a longer chain length (mainly between C₃₀ and C₃₄) and have a linoleic acid chemically bound to their ω -hydroxy group (indicated with EO). They are denoted as CER EOP, CER EOS and CER EOH.

As there is a great interest in the administration of drugs via the skin, there is a need for predictive in-vitro permeation models. Isolated human epidermis or SC can serve as an excellent in-vitro model but human skin is scarcely available and the inter-individual variability of human skin is substantial. Furthermore, with respect to diseased skin, for which many topical drugs are developed, it is virtually impossible to obtain skin for in-vitro diffusion studies. Animal skin as an alternative is not an optimal choice as it

has different permeation properties than human skin. In addition, after 2009 there will be an EU ban on the use of animal skin for the testing of cosmetic products.

Because of the crucial role of the lipids in the skin barrier function, in previous studies an in-vitro model based on SC lipids was developed, referred to as the stratum corneum substitute (SCS) (11, 12). The SCS consists of a porous substrate covered with a layer of synthetic SC lipids. These lipids mimic very closely the molecular organization and orientation of the SC lipid lamellae. An advantage of the SCS is that its composition can be easily modified which allows us to study the relationship between lipid composition, molecular organization and barrier function in just one model. With the SCS we also have the unique possibility to mimic the lipid composition and organization of dry or diseased skin.

In previous studies, the SCS was prepared by spraying a lipid solution onto a substrate with a modified airbrush method. This preparation method results in a SCS with excellent barrier properties similar to SC. However, the spraying process is labor intensive and a substantial part of the lipid solution is lost to the air. Therefore the preparation method of the SCS requires further optimization. In the present study a method is developed to scale up the production of SCS making it less labor intensive. In addition, an alternative preparation method is presented to minimize the loss of lipids to the air. In order to validate the various preparation methods, the qualities of SCS prepared with the various methods are compared. The SCS are characterized concerning their 1) lipid composition and distribution, 2) thickness and profile of the lipid layer, 3) lipid loss during spraying, 4) lipid packing, 5) lamellar organization and orientation and 6) variation in equilibration temperature and permeation properties.

2. Materials and Methods

2.1 Materials

Synthetic CER(EOS)C30-linoleate, CER(NS)C24, CER(NP)C24, CER(NP)C16, CER(AS)C24 and CER(AP)C24 were generously provided by Cosmoferm B.V. (Delft, The Netherlands). Palmitic acid (C16:0), stearic acid (C18:0), arachidic acid (C20:0), behenic acid (C22:0), tricosanoic acid (C23:0), lignoceric acid (C24:0), cerotic acid (C26:0) and cholesterol were purchased from Sigma-Aldrich Chemie GmbH (Schnelldorf, Germany). Perdeuterated palmitic and behenic acid were purchased from Larodan (Malmö, Sweden), perdeuterated stearic and arachidic acid from Cambridge Isotope Laboratories (Andover, Massachusetts) and perdeuterated lignoceric acid was purchased from Arc Laboratories B.V. (Apeldoorn, The Netherlands). Benzoic acid, trypsin (type III, from bovine pancreas), and trypsin inhibitor (type II-S from soybean) were obtained from Sigma-Aldrich (Zwijndrecht, The Netherlands). Dialysis membrane disks (cutoff value of 5000 Da) were obtained from Diachema (Munich, Germany). Nuclepore polycarbonate filter disks (pore size 50 nm) were purchased from Whatman (Kent, UK). All organic solvents are of analytical grade and manufactured by Labscan Ltd. (Dublin, Ireland). All other chemicals are of analytical grade and the water is of Millipore quality.

2.2 Isolation of SC from human skin

SC was isolated from abdominal or mammary skin, which was obtained within 24 h after cosmetic surgery. After removal of the subcutaneous fat tissue, the skin was dermatomed to a thickness of approximately 250 μm using a Padgett Electro Dermatome Model B (Kansas City, KS, USA). The SC was separated from the epidermis by trypsin digestion [0.1% in phosphate-buffered saline (PBS), pH 7.4], after overnight incubation at 4°C and subsequently at 37°C for 1 h. The SC was then placed in a 0.1% solution of trypsin inhibitor and rinsed twice with Millipore water.

Until use, the SC was stored in a silica-containing box under gaseous nitrogen or argon in the dark to prevent oxidation of the intercellular SC lipids.

2.3 Preparation of the SCS

2.3.1 Preparing the lipid mixture

For the preparation of the SCS, CHOL, synthetic CER and FFA were used. The following synthCER composition was selected: CER(EOS)C30, CER(NS)C24, CER(NP)C24, CER(AS)C24, CER(NP)C16 and CER(AP)C24 in a 15:51:16:4:9:5 molar ratio which closely resembles the CER composition in pig SC (13). This synthCER composition is similar to that used in our previous studies (12, 14). The acyl chain length is either 30 C atoms (C30), 24 C atoms (C24) or 16 C atoms (C16). For the free fatty acids mixture (FFA), the following composition was selected: C16:0, C18:0, C20:0, C22:0, C23:0, C24:0 and C26:0 at molar ratios of 1.8, 4.0, 7.7, 42.6, 5.2, 34.7 and 4.1 respectively. This chain length distribution is based on a FFA composition in SC (9). To achieve lipid mixtures at an equimolar CHOL:synthCER:FFA composition appropriate amounts of individual lipids were dissolved in chloroform : methanol (2:1). After evaporation of the organic solvent under a stream of nitrogen, the lipid mixtures were re-dissolved in hexane : ethanol (2:1) at a lipid concentration of 4.5 mg/ml. In some studies the protonated FFA were replaced by the deuterated FFA using a slightly different FFA composition, namely DFFA(5) with C16, C18, C20, C22 and C24 at molar ratios of 1.8, 4.0, 7.6, 47.8 and 38.8 respectively.

2.3.2 Spraying of SCS with an airbrush

An evolution solo airbrush (Airbrush Service Almere, The Netherlands) connected to gaseous nitrogen was used to spray the lipid mixtures onto a polycarbonate filter disk with a pore size of 50 nm. For the manual spraying of SCS the same procedure is followed as published

Two new methods for preparing a unique stratum corneum substitute

previously (11, 12). For spraying multiple SCS simultaneously, the airbrush was equipped with an automated rotor developed by the fine mechanical and electronics department of our university, see figure 1 for a schematic presentation.

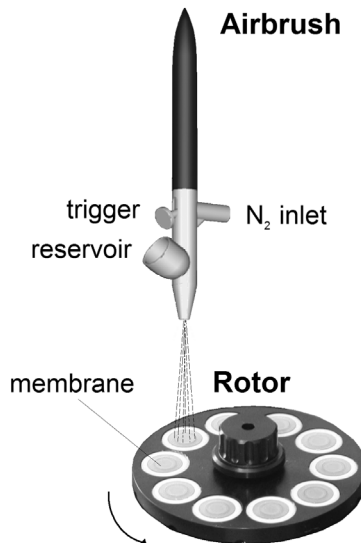


Figure 1: Schematic representation of the airbrush equipped with a rotor that contains ten filters. The rotor cap, mechanics and electronics are not shown. The airbrush is filled with lipid solution and under a stepping rotation the filters are sprayed up to a 1000 times in total.

The rotor can contain up to ten SCS filters and rotates the filters under the airbrush nozzle in a continuous stepping movement. The spraying is automatically discontinued during each movement of the rotor. The rotor is covered by a cap with a circular opening positioned exactly below the nozzle at a distance of 7.7 cm. The nozzle and the cap are not rotating but held in the same position. In this way only 1 filter positioned below the opening is sprayed, while the other filters are protected from dust by the cover. Due to the rotating movement all filters are sprayed sequentially. A nitrogen stream

Chapter 2

is flowing underneath the cap to dry the SCS after each spray. The filters are sprayed on average around 70 to 100 times per SCS, depending mainly on the volume of lipid solution inserted which varies between 500 to 800 μl per SCS. The drying period (between sprays) is 16 s per SCS and the spray-time is 1.5 s per SCS. The (N_2) spray pressure is ~ 1.09 bar.

2.3.3 Spraying of SCS with a modified Linomat

A Linomat IV (Camag, Muttenz, Switzerland) was extended with a y-axis arm developed by the fine mechanical and electronics department of our university. The linomat device makes use of a Hamilton syringe (100 μl) and mechanics to spray a confined (programmable) volume of sample solution from a distance of ~ 1 mm to the porous filter substrate. With the y-axis in use, the linomat is capable of spraying lipids in a rectangular shape, by a continuous zigzag movement. The linomat sprays the lipid solution with a flow of 5.0 $\mu\text{l}/\text{min}$ at a movement speed of 1.01 cm/s in a square of 8 x 8 mm. The amount of lipid solution used is ~ 200 μl per SCS. Therefore in 40 minutes it covers the circular diffusion area (of 6 mm diameter).

2.3.4 Equilibration of SCS

After spraying with the manual/rotor airbrush or linomat, the lipid-loaded filters were equilibrated at 70°C or 80°C for a period of at least 10 minutes and subsequently cooled down to room temperature in approximately 30 min.

2.4 SCS lipid composition and distribution

The lipid composition and distribution was determined by two methods. One-dimensional high performance thin layer chromatography (HPTLC) was used to establish the distribution of the various lipid classes over the filter surface. Briefly, the lipid-loaded filters were cut into two circular parts: the centre (diameter 4 mm; area 12.6 mm^2) and the periphery (diameter 9 mm; area 51.0 mm^2) as shown in figure 2. The lipids were

Two new methods for preparing a unique stratum corneum substitute

extracted in 0.5 ml chloroform : methanol (2:1) by extensive vortexing and were subsequently dried under a nitrogen flow and re-dissolved in chloroform : methanol to obtain an equal lipid concentration for the two fractions. Aliquots were applied on a silica plate (Merck, Darmstadt, Germany) under a flow of nitrogen using a linomat. After eluting with different organic solvent mixtures (15), the silica plate was sprayed with copper sulphate.

A Bio-Rad FTS4000 Fourier transform infrared spectrometer (FTIR) (Cambridge MA, USA) equipped with a broad-band mercury cadmium telluride detector, cooled with liquid nitrogen, was used to measure the infrared absorption of SCS with perdeuterated FFA. The spectra were collected in transmission mode as a co addition of 64 scans at 4.0 cm^{-1} resolution. All samples were measured at room temperature under continuous dry air purge.

In order to be able to obtain a local absorption spectrum from a well defined small region in the membrane a pinhole of 1.4 mm in diameter (developed by the fine mechanical department) was designed and used to measure a spectrum at five positions on the SCS (see figure 3A). From the peak integration of the CH_2 and CD_2 stretching vibrations at 2849 and 2088 cm^{-1} respectively, the absorption spectra intensity ratio between CER and perdeuterated FFA could be obtained for each position. A change in intensity ratio indicates a change in CER/FFA composition. The contribution of CHOL to the vsCH_2 vibration is neglected because of its much shorter lipid tail. All samples were measured at room temperature.

2.5 Thickness and lateral organization of the SCS lipid layer

In order to determine the thickness of the SCS by the absorption in the FTIR spectrum, first the relation between the infrared absorption and layer thickness was determined. For this purpose the spraying speed of the linomat was lowered, so that a complete SCS is sprayed in 17 homogeneous layers. The FTIR spectrum in the center of the SCS was measured through

the pinhole after each additional sprayed layer with the linomat. After each measurement the FTIR absorption was calculated from peak integration of the CH₂ rocking vibration ($\rho_r\text{CH}_2$ at 720 cm⁻¹). After the relationship between the FTIR absorption and the layer thickness was established, the infrared absorption of the CH₂ rocking vibration was used as a parameter to determine the uniformity of the SCS thickness. The pinhole was set at the center and at 1 and 2 mm radial distance from the center (see figure 3A). Subsequently the FTIR spectrum was measured and absorption was determined using the $\rho_r\text{CH}_2$ at 720 cm⁻¹.

From the same FTIR spectrum also the packing of the lipids can be determined. This information is provided by the CH₂ scissoring vibrations (δCH_2) around 1467 cm⁻¹. In addition the SCS was prepared with perdeuterated FFA. This allows determining whether FFA and CER participate in one lattice. This information can be obtained from the CD₂ scissoring mode (δCD_2). The contour of this band is located at approximately 1088 cm⁻¹. All FTIR measurements were performed at room temperature.

2.6 Lipid Loss during spraying

For the airbrush and linomat preparation methods the lipid yield on the filter surface was determined. After spraying, the membrane was weighed and the empty membrane weight was subtracted. The resulting lipid layer weight (after spraying) was divided by the amount of lipids used during spraying multiplied by 100%, to obtain the percentage lipid yield on the filter. Also, the yield inside the diffusion area was determined. After spraying and equilibration, the circular membrane diffusion area of 6 mm diameter was punched and weighed, the empty membrane weight was subtracted. The remaining lipid weight was again divided by the amount of lipids used during spraying and multiplied by 100% to obtain the percentage lipid yield inside the diffusion area on the filter.

2.7 Lamellar organization and orientation determined by SAXD

Small-angle X-ray diffraction was used to acquire information about the lamellar organization (i.e., the repeat distance of a lamellar phase) and the orientation of the lamellae. The scattering intensity I (in arbitrary units) was measured as a function of the scattering vector q (in reciprocal nm). The latter is defined as $q=(4\pi\sin\theta)/\lambda$, in which θ is the scattering angle and λ is the wavelength. From the positions of a series of equidistant peaks (q_n), the periodicity, or d-spacing, of a lamellar phase was calculated using the equation $q_n=2n\pi/d$, n being the order number of the diffraction peak. One dimensional intensity profiles were obtained by transformation of the 2D SAXD pattern from Cartesian (x,y) to polar (ρ,θ) coordinates and subsequently integrating over θ from 60 to 120 degrees. All measurements were performed at the European Synchrotron Radiation Facility (ESRF, Grenoble) using station BM26B (16). The X-ray wavelength and the sample-to-detector distance were 0.124 nm and 1.6 m, respectively. Diffraction data were collected on a two-dimensional multiwire gas-filled area detector with 512×512 pixels of 0.25 mm spatial resolution. The spatial calibration of this detector was performed using silver behenate ($d=5.838$ nm). A filter with lipid layers was mounted parallel to the primary beam in a temperature controlled sample holder with mica windows. Static diffraction patterns were collected at room temperature. The temperature-induced phase changes were measured by collecting successive diffraction patterns, while the temperature of the sample was raised from 20 to 80°C at a rate of 1°C/min, subsequently kept at this temperature for 10 min and then reduced in temperature to 20°C at a rate of 5°C/min. During the dynamic measurements each diffraction curve was collected for a period of 2 min.

2.8 Diffusion studies on human SC and SCS

In vitro permeation studies were performed using PermeGear in-line diffusion cells (Bethlehem PA, USA) with a diffusion area of 0.28 cm². SC on a supporting dialysis membrane (5000 Da, apical side facing the donor

Chapter 2

chamber) or the SCS was mounted in the diffusion cell and was hydrated for 1 h in phosphate buffered saline (PBS: NaCl, Na₂HPO₄, KH₂PO₄ and KCL in MQ water with a concentration of 8.13, 1.14, 0.20 and 0.19 g/l respectively) at pH 7.4 prior to the experiment. The donor compartment was filled with 1400 µl of benzoic acid solution in PBS (pH 7.4) at a 2.0 mg/ml concentration. Benzoic acid has a log P_{oct/water} value of 1.9. The acceptor phase consisted of PBS (pH 7.4), which was flushed at a flow rate of about 2 ml/h. The acceptor phase was stirred with a magnetic stirrer. The exact volume per collected fraction was determined by weighing. Each experiment was performed under occlusive conditions, by closing the opening of the donor compartment with adhesive tape. The temperature of the SC or SCS was maintained at ~32°C during the total length of the experiment, using a thermo-stated water bath. Fractions were collected for 18 h at a 1 h interval. Diffusion studies were performed on SCS from the manual airbrush, rotor airbrush and linomat method, as well as SCS equilibrated at 70 and 80°C. Steady state fluxes and lag-times were determined from a plot of the cumulative permeated amount. The steady state flux is the slope of the linear part of this graph. The lag-time is determined by regression of this linear part to the time at y=0.

3. Results

The SCS was constructed with the three methods; the manual airbrush method used in previous studies, the automated rotor airbrush method and the linomat method. In order to characterize the SCS, the lipid composition and distribution, membrane thickness, lipid yield, lipid organization, and the barrier function of the SCS prepared by the different methods have been examined.

Two new methods for preparing a unique stratum corneum substitute

3.1 Lipid composition and distribution

In order to determine the uniformity of the lipid composition along the surface of SCS, HPTLC and FTIR are employed. Using HPTLC, the mean lipid composition of the inner and outer ring of the SCS is examined. The results are provided in figure 2. From this figure it is obvious that no differences in lipid profile are observed between inner and outer ring of SCS prepared by the manual airbrush, rotor airbrush and linomat. This indicates that the mean lipid composition and distribution in the central and peripheral part of the SCS manufactured by the three methods is similar.

More detailed information about the fluctuations in FFA/CER ratio at various positions along the SCS surface is obtained by using FTIR.

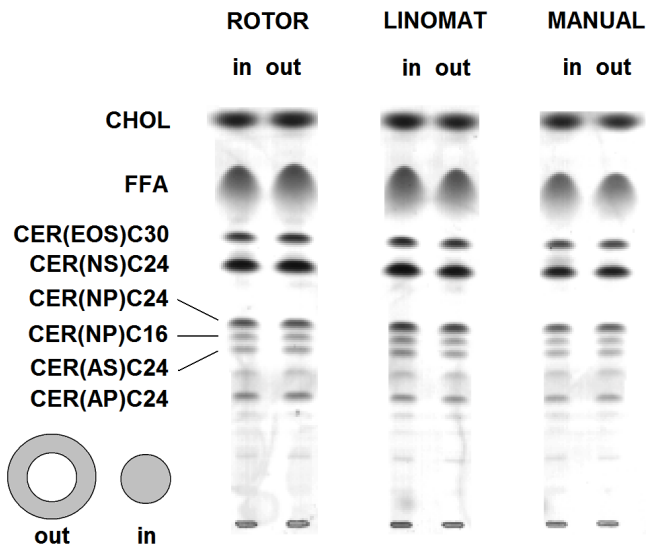


Figure 2: HPTLC pattern of the center part (in) and outer ring (out) of SCS prepared with the three methods. No differences in lipid composition are visible between inner and outer membrane.

When using deuterated FFA, in the FTIR spectrum the fluctuations in ratio of peak intensities of νCH_2 (located at 2849 cm^{-1}) and νCD_2 (located

at 2088 cm^{-1}) is directly related to the fluctuations in molar ratios of the protonated CER and deuterated FFA chains, respectively. A change in the integrated peak ratio of vsCH_2 : vsCD_2 is indicative for a change in the molar ratio of the protonated and deuterated chains. The integrated vsCH_2 : vsCD_2 peak ratios of the five selected locations (see figure 3A) are shown in table 1, for SCS prepared with the manual-, rotor airbrush and linomat method. For each preparation method, the variation in vsCH_2 : vsCD_2 peak ratio (between the different locations at the SCS) is very low, demonstrating a uniform CER : FFA ratio within the five selected positions. However, for the manual airbrush and linomat method, between SCS (at each position), a larger standard deviation for the vsCH_2 : vsCD_2 peak ratio was observed than for the rotor method. This can be explained by the fact that the SCS from the rotor airbrush are all prepared simultaneously in one run, resulting in a very reproducible thickness of the SCS.

Table 1:
 $\text{vsCH}_2/\text{vsCD}_2$ ratio measured at 5 positions (see also figure 3A) on SCS prepared with the three methods.

position	1	2	3	4	5
Rotor SCS (n=3)	3.20 \pm 0.02	3.18 \pm 0.02	3.16 \pm 0.04	3.23 \pm 0.05	3.26 \pm 0.07
Linomat SCS (n=3)	2.5 \pm 0.2	2.5 \pm 0.2	2.4 \pm 0.2	2.5 \pm 0.2	2.6 \pm 0.2
Manual SCS (n=3)	2.5 \pm 0.2	2.3 \pm 0.3	2.3 \pm 0.2	2.3 \pm 0.3	2.5 \pm 0.2

3.2 Thickness and cross section of the lipid layer

A uniform thickness of the lipid layer of the SCS is important when performing permeation experiments. In order to determine the SCS thickness at a predetermined position in the SCS, first a linear relation between the peak intensity of the $\nu_r\text{CH}_2$ rocking vibration at 720 cm^{-1} in the FTIR spectrum and the number of sprayed layers was determined. After each layer sprayed with the linomat, the IR absorption was determined by FTIR. The results are displayed in figure 3B. The graph clearly shows that

Two new methods for preparing a unique stratum corneum substitute

there is a linear relationship between the layer thickness of the SCS, expressed by the number of layers sprayed with the linomat, and its infrared absorbance around 720 cm^{-1} (the contours of the $\rho_r\text{CH}_2$ rocking vibration). Thus, by measuring the intensity of the $\rho_r\text{CH}_2$ mode, the relative thickness of a prepared membrane can be determined.

Using the linear relationship between the intensity of the absorption peak of the $\rho_r\text{CH}_2$ rocking vibration and the membrane thickness, the homogeneity in thickness of the lipid layer of SCS can be determined by measuring this $\rho_r\text{CH}_2$ rocking vibration intensity at various selected locations on the stratum corneum substitute. These locations are chosen in a cross section at the center and 1 and 2 mm out of the center. Figure 3C shows the relative infrared absorbance of the $\rho_r\text{CH}_2$ contour at the various positions on SCS, in which the intensity of the $\rho_r\text{CH}_2$ contour in the center of the membrane is set to 100%. From this figure it is obvious that for all three methods the layer thickness is highest in the center of the SCS and reduces towards the edge of the diffusion area. Furthermore, the linomat method delivers SCS with a more homogeneous layer thickness than SCS prepared with the rotor- or manual airbrush method.

3.3 Lipid loss during spraying

The distance between the nozzle and the supporting membrane using the airbrush method is 7.7 cm for the rotor and 5 to 10 cm for the manual holder, while the distance between the needle tip and the supporting membrane using the linomat method is only 1 mm. This may result in differences in lipid loss. Therefore the lipid yield in the diffusion area of the membrane is determined by weighing. For the manual airbrush, rotor airbrush and the linomat method, the recovery of lipids sprayed on the filter is respectively $68\pm 19\%$ ($n=3$), $52\pm 4\%$ ($n=5$) and $93\pm 4\%$ ($n=3$) of the total amount of lipids used for spraying. However, the recovery of lipids inside the diffusion area is $8\pm 1\%$ ($n=4$) for the manual airbrush, $10\pm 1\%$ ($n=4$) for the rotor airbrush and $31\pm 2\%$ (with $n=13$) for the linomat method. The recovery

Chapter 2

in the diffusion area is less than the total recovery because a relatively small area of the membrane is used for diffusion. From these results it is clear that the airbrush method has a much lower lipid yield than the linomat preparation method.

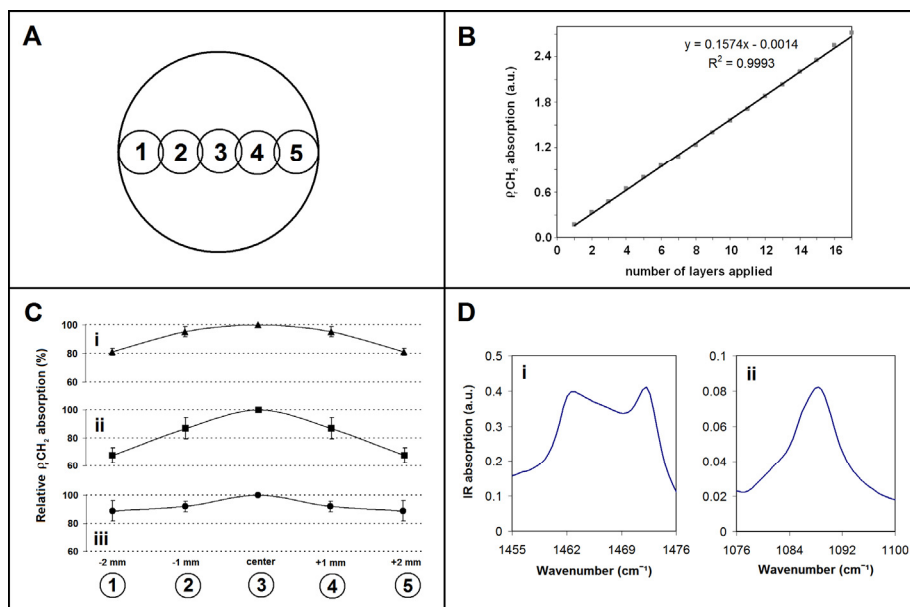


Figure 3: Overview of FTIR results. A) The five positions on SCS that were selected for the FTIR absorption measurements for determining variations in membrane thickness and DFFA/CER absorption ratio. B) The peak intensity of the FTIR rocking mode ($p\text{rCH}_2$) is plotted as function of the number of lipid layers sprayed with the linomat application method. A linear relationship is observed. C) Lipid layer cross section of SCS prepared with the rotor airbrush (i), manual airbrush (ii) and linomat (iii) ($n=3$ per method). The profile is calculated using the correlation between peak intensity and membrane thickness shown in B). The positions of the measurements are provided in (a). D) (i) Typical CH_2 scissoring mode in the FTIR spectrum obtained for SCS prepared with the three spraying methods. A doublet is observed with absorption maxima at 1463 and 1472 cm^{-1} indicative for the presence of an orthorhombic lateral packing. (ii) typical CD_2 scissoring mode for SCS with perdeuterated FFA. A singlet is observed with maximum at 1088 cm^{-1} indicative for participation of FFA and CER in one lattice.

3.4 Lipid packing

Information on the lipid packing can be obtained from the δCH_2 contours in the FTIR spectrum. If the δCH_2 band is a singlet at around 1467 cm^{-1} , the lipids form either a liquid or a hexagonal packing. However, when lipids form an orthorhombic packing, chains in scissoring mode interact via a short-range coupling resulting in splitting of the δCH_2 vibration known as factor group splitting. As a consequence the contour is a doublet located between 1463 cm^{-1} and 1473 cm^{-1} . The spectrum of the δCH_2 mode representative for SCS is provided in figure 3D-i. This spectrum reveals a doublet at 1463 and 1472 cm^{-1} respectively with a weak singlet around 1467 cm^{-1} . No difference in the scissoring contours was observed between SCS prepared using the different methods. Therefore, in SCS membranes the lipid packing is mainly orthorhombic with a small population of lipids forming a hexagonal packing.

When the FFA is replaced with deuterated FFA, information on the mixing of FFA and CER in one lattice can be obtained. If CER and deuterated FFA participate in one lattice, decoupling takes place and the doublet in the δCD_2 mode (present in a mixture with only deuterated FFA) changes into a singlet at 1088 cm^{-1} in the CER:CHOL:FFA(deuterated) mixtures (17). The δCD_2 band typical for SCS prepared with any of the three methods is shown in figure 3D-ii. A singlet was observed at all five positions (see figure 3A) on the SCS indicating that deuterated FFA and CER participate in the same crystal lattice.

3.5 Lamellar organization and orientation

Besides the lateral organization (lipid packing), the formation of the lamellar phases and their orientation are both assumed to be crucial for the skin barrier function. The lamellar organization is examined by small angle X-ray diffraction using a two-dimensional detection. Figure 4A shows a typical two-dimensional X-ray diffraction pattern of the lipids in the SCS

prepared with the linomat method. Equal patterns have been acquired for SCS prepared with the other two methods. The high intensity at the meridian (see arrow in figure 4A) demonstrates that the lipid lamellae have a preferred orientation parallel to the surface of the SCS.

In figure 4B the intensity profile of the integrated SAXD pattern is plotted. From the position of the diffraction peaks two lamellar phases can be identified with repeat distances of 11.6 and 5.4 nm. The diffraction orders 1 to 4 of the long periodicity phase (LPP, with $d = 11.6$ nm) are located at $q = 0.54, 1.10, 1.62$ and 2.15 nm^{-1} respectively. The 1st and 2nd order of the short periodicity phase (SPP, with $d \sim 5.7$ nm) are located at $q = 1.10$ and 2.15 nm^{-1} . Besides the two lamellar phases, phase separated CHOL could be identified by the peaks located at $q = 1.86$ and 3.73 nm^{-1} .

Finally two peaks are observed at $q = 1.43$ and 2.86 nm^{-1} , which should be assigned to another lipid structure. As these peaks were never identified in the diffraction pattern of stratum corneum (7, 18, 19), additional studies were performed to observe whether the formation of this phase could be avoided. One of the critical parameters is the elevated equilibration temperature after spraying. Therefore, for an unequilibrated SCS (prepared by the linomat method), the phase behavior was examined as a function of temperature during heating and cooling. The result is provided in figure 4C. The measurement starts at room temperature, and upon heating, between 70 and 80°C all diffraction peaks disappear. After the SCS is kept at 80°C for 10 minutes (equilibration), the SCS is cooled down to 20°C at a rate of 5°C/min. During this cooling process, first a diffraction peak attributed to the SPP (at $q = 1.2 \text{ nm}^{-1}$) as well as the CHOL peak appear around 60°C, and at slightly lower temperature also the diffraction peaks of the LPP appear. Interestingly, this thermal treatment did not result in the reappearance of the peaks attributed to the 4.4 nm phase. In a similar dynamic experiment an unequilibrated SCS was equilibrated at 75 instead of 80°C, it was striking that the diffraction peak at 4.4 nm and the CHOL peak did not disappear at 75°C and were still present after equilibration (data not shown).

Two new methods for preparing a unique stratum corneum substitute

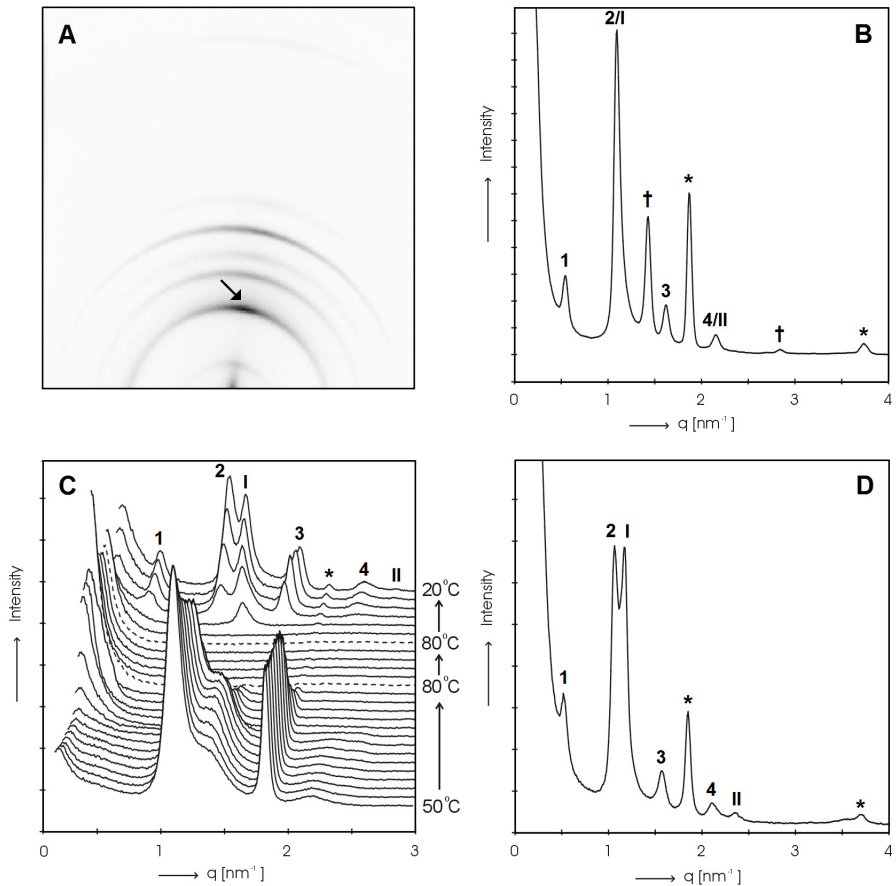


Figure 4: Overview of SAXD results. A) Typical 2D SAXD pattern of SCS equilibrated at 70°C. The arrow denotes the position of the intensity maximum. B) Intensity profile of integrated SAXD pattern of SCS equilibrated at 70°C. The orders attributed to the LPP are located at q -values of 0.54 (1st order), 1.10 (2nd order), 1.62 (3rd order) and 2.15 nm⁻¹ (4th order). The 1st and 2nd order peak of the SPP (indicated by I and II) are located at q -values of 1.10 and 2.15 nm⁻¹. The asterisk (*) indicates the reflections of crystalline cholesterol (q values at 1.86 and 3.74 nm⁻¹) and † denotes the two reflections attributed to the additional phase with a periodicity of 4.4 nm (q values at 1.43 and 2.83 nm⁻¹). C) Intensity profiles as a function of temperature. The X-ray diffraction profile has been measured from 50 to 80°C, equilibrated during 10 minutes and subsequently cooled with a cooling rate of 5°C/min. In heating, between 75 and 80°C all ordering disappears. In the cooling process, between 70 and 50°C the LPP and SPP are formed. D) X-ray diffraction profile of SCS equilibrated at 80°C. The orders 1 to 4 of the LPP are located at $q = 0.52, 1.06, 1.57$ and 2.11 nm⁻¹, the orders I and II of the SPP are located at $q = 1.17$ and 2.35 nm⁻¹). After equilibration at 80°C the additional phase is not formed and the spacing of the LPP is longer as compared to the LPP in (A). This is clearly visible by the split peaks at the first order of the SPP and second order LPP in (D).

For this reason, in preparing SCS, it was decided to adapt the equilibration temperature from 70 to 80°C. Figure 4D shows the SAXD pattern of SCS (prepared by the linomat method) after equilibration at 80°C; it is obvious that the 4.4 nm phase disappeared and the intensity of the first order cholesterol peak reduced, in comparison with SCS equilibrated at 70°C (figure 4A). Furthermore, the repeat distance of the long periodicity phase increased to 12.2 nm more closely mimicking the lipid organization in stratum corneum.

As a clear difference in phase behavior was observed when equilibrating the SCS at 70 or 80°C, polarization microscopy was conducted to study the presence of crystals at the two equilibration temperatures. In figure 5 two typical polarization microscopic images are shown for SCS equilibrated at 70°C and 80°C. It can be seen that the degree of mosaicity is greatly reduced at 80°C, while at 70°C needle-shaped crystals are present. Because the cholesterol fraction is reduced with a temperature rise from 70°C to 80°C (as concluded from SAXD results), the needle-shaped crystalline domains observed at 70°C may originate from phase separated cholesterol. This hypothesis was further investigated with SCS prepared with a reduced cholesterol content (molar ratio of CER/CHOL/FFA = 2/1/2). This SCS equilibrated at 70°C indeed showed a lower number of crystals than SCS prepared using equimolar CER:CHOL:FFA mixtures (images not shown).

3.6 Variation in equilibration temperature and permeation properties

As a difference in lipid organization was observed when equilibrating the SCS at 70°C or 80°C, it was decided to perform permeation studies using SCS equilibrated either at 70 or 80°C. In figure 6A the permeation profiles of benzoic acid are depicted of SCS prepared at 70 or 80°C using either the linomat or rotor method.

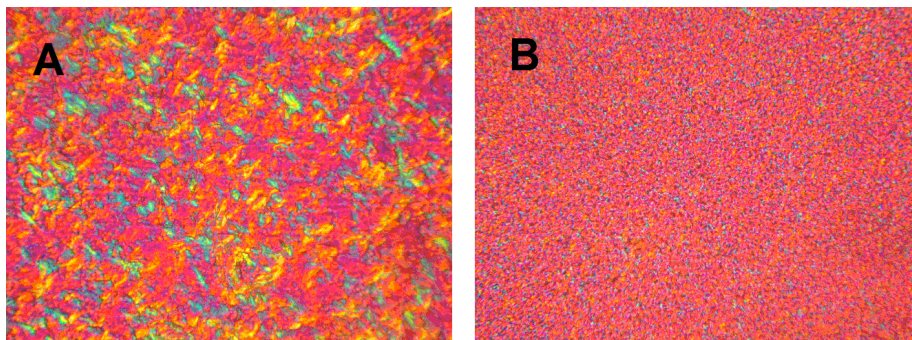


Figure 5: Transmission polarization images (40x magnification) of SCS equilibrated at 70°C (A) and SCS equilibrated at 80°C (B). The mosaicity due to cholesterol crystals is drastically reduced at 80°C.

When the SCS is equilibrated at 80°C, the lag-time (τ) is 1.2 ± 0.2 h, while equilibration at 70°C results in a τ of 3.4 ± 0.8 h. Furthermore, the steady state flux across SCS equilibrated at 70°C is 18 ± 1 $\mu\text{g}/\text{cm}^2/\text{h}$ which is significantly lower than the steady state flux across SCS equilibrated at 80°C were $J_{ss} = 25 \pm 2$ $\mu\text{g}/\text{cm}^2/\text{h}$. In an additional series of studies the benzoic acid flux across the SCS prepared with the different methods has been determined and compared to that across SC. The SCS were all equilibrated at 80°C, the fluxes are shown in figure 6B. It can be seen that the permeation profiles of SCS prepared with the three methods are very similar to each other. Furthermore, the steady state flux of the SCS closely resembles the steady state flux of human SC; the J_{ss} are on average 24 ± 2 $\mu\text{g}/\text{cm}^2/\text{h}$ for SCS and 22 ± 3 $\mu\text{g}/\text{cm}^2/\text{h}$ for SC. The lag-time is shorter for SC than for the SCS; τ is -0.1 ± 0.3 h for SC and 1.1 ± 0.5 h for SCS.

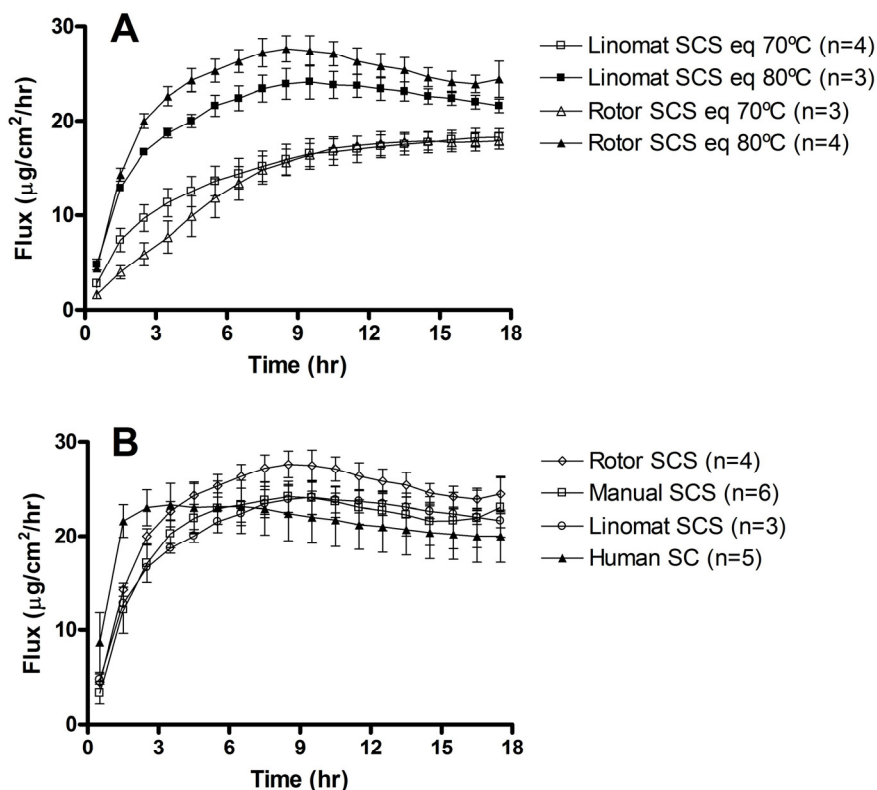


Figure 6: Permeation studies at 32°C on SCS with benzoic acid used as model drug. (a) SCS previously equilibrated at 70°C and 80°C (two preparation methods) and (b) SCS (pre-eq. at 80°C) prepared with the three methods, compared to human SC. SCS equilibrated at 80°C displays a shorter lag-time and higher steady state flux than SCS equilibrated at 70°C. The three different methods for preparing SCS result in very similar diffusion profiles, with a steady state flux comparable to human SC, however with a larger lag-time than SC.

4. Discussion

The main purpose of our studies is to construct a SCS that can be used as an in vitro permeation model. This is of interest for at least two

Two new methods for preparing a unique stratum corneum substitute

reasons. First, the SCS can serve as a model for human stratum corneum to screen compounds on their skin permeability or study the effect of formulations on the permeation profile. Second, the SCS offers the unique opportunity to study the relationship between lipid composition, lipid organization and permeability in one model. This is of particular importance for understanding the reduced skin barrier function in diseased skin. For screening purposes several reconstructed skin models are already commercially available. However, although these models are very useful for skin irritation tests (20, 21), they show an impaired barrier compared to human skin. This makes these models less attractive as an alternative for human skin in permeation studies (22), (23).

When used for permeation purposes, the SCS should i) be prepared in a very reproducible manner, ii) be homogeneous in composition and in membrane thickness and iii) mimic lipid organization and orientation of human SC. These properties of SCS, and its permeation properties, will be discussed below.

4.1 Optimal preparation with the linomat method

In our present study, besides the manual airbrush and rotor method, the linomat method was used to prepare the SCS. Kuempel et al also used the linomat for spraying lipids on a Millipore filter disk (24) and they showed for the first time that it is possible to form the broad-narrow-broad pattern characteristic for SC lipid organization using RuO₄ staining. However, their studies were different from ours in at least three aspects. i) Kuempel et al used total lipid extracts of pig SC without isolation of the CER, while we use mixtures based on synthetic CER. As we noticed in previous studies, the preparation method of mixtures prepared with synthetic CER is different from that prepared with isolated CER, especially with respect to the choice of the optimal equilibration temperature (14). ii) Kuempel et al did not modify the linomat by adding an extra arm, which allows spraying of lipids in a predefined area of the supporting membrane. This may indicate that their

supporting membrane is not homogeneously covered with lipids. This limits the use of these membranes in permeation studies. iii) Kuempel et al concluded that in the absence of hydration no broad-narrow-broad structure (visualized by RuO_4 staining) could be obtained. The latter is likely correlated with the formation of the LPP. Using our application method it is possible to form the LPP in the absence of water. Furthermore, in our previous study we showed that hydration at elevated temperature results in phase separation between lipid and water domains in the membrane (12) creating a leaky SCS, which cannot be used in permeation studies.

The linomat application method showed some advantages above the rotor and manual air-brush spraying methods. First, the loss of lipids for the linomat method was much lower than for the airbrush spraying methods, which is most probably due to the shorter nozzle to membrane distance. Second, the membrane thickness is more uniform using the linomat application method instead of the airbrush spraying methods.

HPTLC and the ratio of the absorption of the CH_2/CD_2 symmetric stretching frequencies in the FTIR spectrum both revealed that in all SCS the lipid composition parallel to the SCS surface is quite homogeneous. However, in contrast to the rocking frequencies used to determine the SCS thickness, the CH_2 and CD_2 stretching absorptions used to determine the uniformity of the SCS composition, are not linearly correlated with the SCS thickness. The signal of the MCT detector used to measure the infrared spectra is nonlinear with sample absorption in the region around 2800 cm^{-1} , which is the region of the CH_2 stretching mode used to determine CH_2/CD_2 ratio and thus the lateral homogeneity in the lipid membrane. Therefore, a variation in membrane thickness (different absorption) in this region, will affect to some extent the CH_2/CD_2 intensity ratio of the stretching mode. The membranes prepared by the rotor airbrush method were thinner than those prepared by the linomat and manual rotor method, which resulted in higher CH_2/CD_2 stretching peak ratios of the SCS prepared by the rotor airbrush method, see table 1.

Two new methods for preparing a unique stratum corneum substitute

4.2 FTIR as a non-destructive tool to measure thickness and lipid distribution

The average membrane thickness and cross section of the lipid layer are assessed by FTIR without destruction of the SCS. This makes it an elegant method for quality control of prepared SCS as the measurements can be performed prior to a permeation study. Another control is the assessment of lipid distribution by FTIR using perdeuterated fatty acids. If the distribution of lipid components over the membrane surface is not uniform, the LPP that is crucial for the barrier function (11), may not be formed.

Pidgeon et al demonstrated already in 1989 that FTIR can be used to quantify the lipid content in organic lipid solutions and extracted membrane preparations (25). Although our method presented in this paper is based on the method of Pidgeon, there are some differences. We quantify the lipid thickness of the SCS by integration of the peak intensity of the rocking vibration, whereas Pidgeon used an internal standard combined with the stretching vibrations. We did not choose for an internal standard as this might affect the lipid organization and therefore the permeability of the SCS. Also, we chose for the rocking vibrations because we observed that only in this region of the spectrum the absorption was linear with the lipid quantity.

Furthermore, it is well known that the steady state flux of a substance through a membrane according to Fick's Law is linear dependent on the reciprocal membrane thickness. Therefore a homogeneous reproducible thickness is a prerequisite for the SCS when used in screening studies. Variation in thickness of the SCS prepared with the two airbrush methods is larger than that of the SCS prepared by the linomat method, although even when using the linomat method there is still a small variation in thickness. This may be due to the equilibration step at elevated temperatures. At these temperatures the lipids are in the hexagonal to liquid phase transition, which will result in a small additional spreading over a larger surface area.

4.3 The SCS closely mimics the stratum corneum lipid organization

In human SC the lipids are organized mainly in an orthorhombic lateral packing, which is considered to play an important role in the skin barrier function (26-28). Therefore, it is a prerequisite that the SCS form an orthorhombic (very tight) lateral lipid packing. As demonstrated in figure 3D-i, the lipids form the orthorhombic lateral packing. Furthermore, as the inter peak distance of the doublet is approximately 9.2 cm^{-1} approaching the maximum splitting of 11 cm^{-1} , this indicates that the crystalline domain sizes exceed that of 100 lipids (29). In previous studies, FTIR was used to study the mixing properties of perdeuterated palmitic acid and protonated CER in one lattice (29, 30). In the study of Moore et al, palmitic acid and bovine brain CER type III form their own separate orthorhombic phases. This contrasts our finding that FFA and CER participate in one lattice. Their model however was less complex than ours, with only 3 lipid components: a single CER, CHOL and palmitic acid. The smaller number of components in that mixture may facilitate phase separation.

Not only the orthorhombic packing, but also the LPP has been suggested to be important for the barrier function (11). The diffraction pattern of the SCS shows the coexistence of the LPP and SPP, similarly as in human SC. However, after equilibration of the SCS at 70°C an additional unknown phase was formed not present in SC. This phase disappeared after using an equilibration temperature of 80°C . This is in contrast to the phase behavior of lipids casted on mica in previous studies, in which an equilibration temperature of 70°C was sufficient (14). Very recently, we observed that the solvent choice for spraying lipids accounts for the difference in required equilibration temperature. When sprayed on mica, the lipids dissolved in chloroform:methanol (2:1 v/v) form the LPP and SPP, while the lipids dissolved in hexane:ethanol (2:1 v/v) result in formation of the additional unknown phase (data not shown). Most probably, when using hexane:ethanol (2:1 v/v) some lipid components are dissolved less readily,

Two new methods for preparing a unique stratum corneum substitute

which results in a crystallization of these components forming separate lipid domains during the spraying process.

In the two-dimensional detection plane, the arc-shaped form of the reflections in the diffraction pattern in figure 4A indicates that the majority of the lamellae are oriented parallel to the surface of the membrane. This arc-shaped pattern is very similar to that observed for SC (not shown) indicating that the SCS has a very similar lamellar orientation.

4.4 SCS as a permeability model can replace human SC

For our permeation studies we chose a model compound similar to the compounds used previously (11), namely benzoic acid (BA). As we observed differences in the phase behavior after equilibration at 70 and 80°C we have first investigated the effect of equilibration temperature on the permeability of SCS. It appeared that for the lower equilibration temperature of 70°C (where a separate phase exists) the SCS permeability for BA is slightly lower and the lag-time longer. Equilibration at 80°C resulted in a shorter lag-time, which mimics more closely the diffusion profile across human SC. This demonstrates that it is important to mimic the lipid phase behaviour in SC as closely as possible.

Subsequently, the SCS were prepared with all three methods and after equilibration at 80°C their permeability was compared to SC. No significant differences in BA permeability were observed regardless of the preparation method used. Although the diffusion profiles through the SCS revealed a slightly longer lag-time than the diffusion profiles through SC, the steady state fluxes through SCS were very similar to those through SC. Therefore, the SCS can serve as an excellent permeability model and replace stratum corneum in diffusion studies.

In conclusion, in this study it has been shown that the preparation of SCS is feasible with any of the tested preparation methods; manual airbrush, rotor airbrush or linomat. The SCS prepared with the three methods

displayed the desired properties of a uniform lipid composition, the presence of an orthorhombic lateral organization, the distinct phases with a lamellar orientation approximately parallel to the membrane surface and permeation properties similar to human SC. The linomat method was selected as the most appropriate method for preparing the SCS, as the spraying was most efficient and the membrane thickness was more uniform compared to the two airbrush methods.

Acknowledgements

We would like to thank the company Cosmoferm B.V. for the provision of the synthetic ceramides, our fine mechanical department and our electronics department of Leiden University for the development of the airbrush setup and modifications to the linomat and diffusion setup. The Netherlands Organization for Scientific Research (NWO) is acknowledged for the provision of the beam time and we thank the personnel at the DUBBLE beam line 26 at the ESRF for their support with the x-ray measurements, as well as the group of crystallography at the University of Amsterdam for additional x-ray measurements.

References

1. Simonetti, O., A. J. Hoogstraate, W. Bialik, J. A. Kempenaar, A. H. Schrijvers, H. E. Bodde, and M. Ponec. 1995. Visualization of diffusion pathways across the stratum corneum of native and in-vitro-reconstructed epidermis by confocal laser scanning microscopy. *Arch. Dermatol. Res.* 287:465-473.
2. Wertz, P. W., M. C. Miethke, S. A. Long, J. S. Strauss, and D. T. Downing. 1985. The composition of the ceramides from human stratum corneum and from comedones. *J. Invest. Dermatol.* 84:410-412.
3. Robson, K. J., M. E. Stewart, S. Michelsen, N. D. Lazo, and D. T. Downing. 1994. 6-Hydroxy-4-sphinganine in human epidermal ceramides. *J. Lipid. Res.* 35:2060-2068.
4. Stewart, M. E., and D. T. Downing. 1999. A new 6-hydroxy-4-sphinganine-containing ceramide in human skin. *J. Lipid. Res.* 40:1434-1439.
5. Ponec, M., A. Weerheim, P. Lankhorst, and P. Wertz. 2003. New acylceramide in native and reconstructed epidermis. *J. Invest. Dermatol.* 120:581-588.
6. Bouwstra, J. A., G. S. Gooris, J. A. van der Spek, and W. Bras. 1991. Structural investigations of human stratum corneum by small-angle X-ray scattering. *J. Invest. Dermatol.* 97:1005-1012.
7. Bouwstra, J. A., G. S. Gooris, W. Bras, and D. T. Downing. 1995. Lipid organization in pig stratum corneum. *J. Lipid Res.* 36:685-695.
8. Bouwstra, J., G. Gooris, and M. Ponec. 2002. The lipid organisation of the skin barrier: liquid and crystalline domains coexist in lamellar phases
journal of Biological Physics 28:211-223.
9. Wertz, P. 1991. Epidermal lipids. In *Physiology, Biochemistry and Molecular Biology of the Skin*. L. A. Goldsmith, editor. Oxford University Press, Oxford. 205-235.
10. Motta, S., M. Monti, S. Sesana, R. Caputo, S. Carelli, and R. Ghidoni. 1993. Ceramide composition of the psoriatic scale. *Biochim. Biophys. Acta* 1182:147-151.
11. de Jager, M., W. Groenink, R. Bielsa i Guivernau, E. Andersson, N. Angelova, M. Ponec, and J. Bouwstra. 2006. A novel in vitro percutaneous penetration model: evaluation of barrier properties with p-aminobenzoic acid and two of its derivatives. *Pharm. Res.* 23:951-960.
12. de Jager, M., W. Groenink, J. van der Spek, C. Janmaat, G. Gooris, M. Ponec, and J. Bouwstra. 2006. Preparation and characterization of a stratum corneum substitute for in vitro percutaneous penetration studies. *Biochim. Biophys. Acta* 1758:636-644.

13. Bouwstra, J. A., G. S. Gooris, K. Cheng, A. Weerheim, W. Bras, and M. Ponc. 1996. Phase behavior of isolated skin lipids. *J. Lipid Res.* 37:999-1011.
14. de Jager, M. W., G. S. Gooris, M. Ponc, and J. A. Bouwstra. 2005. Lipid mixtures prepared with well-defined synthetic ceramides closely mimic the unique stratum corneum lipid phase behavior. *J. Lipid. Res.* 46:2649-2656.
15. Weerheim, A., and M. Ponc. 2001. Determination of stratum corneum lipid profile by tape stripping in combination with high-performance thin-layer chromatography. *Arch. Dermatol. Res.* 293:191-199.
16. Bras, W. 1998. An SAXS/WAXS beamline at the ESRF and future experiments. *Journal of Macromolecular Science-Physics* B37:557-565.
17. Gooris, G. S., and J. A. Bouwstra. 2007. Infrared spectroscopic study of stratum corneum membranes prepared from human ceramides, cholesterol, and fatty acids. *Biophys. J.* 92:2785-2795.
18. White, S. H., D. Mirejovski, and G. I. King. 1988. Structure of lamellar lipid domains and corneocytes envelopes of murine stratum corneum. *Biochemistry*:3725-3732.
19. Bouwstra, J. A., G. S. Gooris, J. A. van der Spek, and W. Bras. 1991. Structural investigations of human stratum corneum by small-angle X-ray scattering. *J Invest Dermatol* 97:1005-1012.
20. Kandarova, H., M. Liebsch, E. Schmidt, E. Genschow, D. Traue, H. Spielmann, K. Meyer, C. Steinhoff, C. Tornier, B. De Wever, and M. Rosdy. 2006. Assessment of the skin irritation potential of chemicals by using the SkinEthic reconstructed human epidermal model and the common skin irritation protocol evaluated in the ECVAM skin irritation validation study. *Altern. Lab. Anim.* 34:393-406.
21. Tornier, C., M. Rosdy, and H. I. Maibach. 2006. In vitro skin irritation testing on reconstituted human epidermis: reproducibility for 50 chemicals tested with two protocols. *Toxicol. In Vitro* 20:401-416.
22. Schmook, F. P., J. G. Meingassner, and A. Billich. 2001. Comparison of human skin or epidermis models with human and animal skin in in-vitro percutaneous absorption. *Int. J. Pharm.* 215:51-56.
23. Netzlaff, F., C. M. Lehr, P. W. Wertz, and U. F. Schaefer. 2005. The human epidermis models EpiSkin, SkinEthic and EpiDerm: an evaluation of morphology and their suitability for testing phototoxicity, irritancy, corrosivity, and substance transport. *Eur J Pharm Biopharm* 60:167-178.
24. Kuempel, D., D. C. Swartzendruber, C. A. Squier, and P. W. Wertz. 1998. In vitro reconstitution of stratum corneum lipid lamellae. *Biochim. Biophys. Acta* 1372:135-140.
25. Pidgeon, C., G. Apostol, and R. Markovich. 1989. Fourier transform infrared assay of liposomal lipids. *Anal. Biochem.* 181:28-32.

Two new methods for preparing a unique stratum corneum substitute

26. Pilgram, G. S., D. C. Vissers, H. van der Meulen, S. Pavel, S. P. Lavrijsen, J. A. Bouwstra, and H. K. Koerten. 2001. Aberrant lipid organization in stratum corneum of patients with atopic dermatitis and lamellar ichthyosis. *J. Invest. Dermatol.* 117:710-717.
27. Bouwstra, J. A., G. S. Gooris, W. Bras, and D. T. Downing. 1995. Lipid organization in pig stratum corneum. *J Lipid Res* 36:685-695.
28. Pilgram, G. S., J. van der Meulen, G. S. Gooris, H. K. Koerten, and J. A. Bouwstra. 2001. The influence of two azones and sebaceous lipids on the lateral organization of lipids isolated from human stratum corneum. *Biochim. Biophys. Acta* 1511:244-254.
29. Moore, D. J., M. E. Rerek, and R. Mendelsohn. 1997. Lipid domains and orthorhombic phases in model stratum corneum: evidence from Fourier transform infrared spectroscopy studies. *Biochem. Biophys. Res. Commun.* 231:797-801.
30. Mimeault, M., and D. Bonenfant. 2002. FTIR spectroscopic analyses of the temperature and pH influences on stratum corneum lipid phase behaviors and interactions. *Talanta*:395-405.

Chapter 3

Is an orthorhombic lateral packing and a proper lamellar organization important for the skin barrier function?

Daniël Groen, Dana S. Poole, Gert S. Gooris, Joke A. Bouwstra

Biochim Biophys Acta, vol. 1808, issue 6, pp. 1529-1537.

Abstract

The lipid organization in the stratum corneum (SC), plays an important role in the barrier function of the skin. SC lipids form two lamellar phases with a predominantly orthorhombic packing. In previous publications a lipid model was presented, referred to as the stratum corneum substitute (SCS), that closely mimics the SC lipid organization and barrier function. Therefore, the SCS serves as a unique tool to relate lipid organization with barrier function. In the present study we examined the effect of the orthorhombic to hexagonal phase transition on the barrier function of human SC and SCS. In addition, the SCS was modified by changing the free fatty acid composition, resulting in a hexagonal packing and perturbed lamellar organization. By measuring the permeability to benzoic acid as function of temperature, Arrhenius plots were constructed from which activation energies were calculated. The results suggest that the change from orthorhombic to hexagonal packing in human SC and SCS, does not have an effect on the permeability. However, the modified SCS revealed an increased permeability to benzoic acid, which we related to its perturbed lamellar organization. Thus, a proper lamellar organization is more crucial for a competent barrier function than the presence of an orthorhombic lateral packing.

Is an orthorhombic lateral packing important for the skin barrier function?

1. Introduction

The uppermost layer of the human skin, the stratum corneum (SC), consists of flattened protein-rich dead cells (corneocytes) surrounded by intercellular lipids. The intercellular lipid domains in the SC form the only continuous pathway through the SC and are suggested to act as the main barrier for diffusion of substances through the SC (3). The main lipid classes in the SC are ceramides (CER), cholesterol (CHOL) and free fatty acids (FFA) (4-8). The lipids are arranged in two coexisting lamellar phases; a long periodicity phase (LPP) with a repeat distance of around 13 nm and a short periodicity phase (SPP) with a repeat distance of around 6 nm (9, 10). Furthermore, at the skin temperature of around 30-32°C in human SC the orthorhombic lateral packing is dominantly present, although a subpopulation of lipids also forms a hexagonal lateral packing. When increasing the temperature of SC, a transition is noticed from an orthorhombic to a hexagonal lateral packing between 30 and 40°C. Both the lateral and lamellar lipid organization are considered to play an important role in the barrier function of the skin (11-13). A detailed analysis of the lipid composition revealed that the FFA have a wide chain length distribution, in which the chain lengths of 22 and 24 carbon atoms are most abundantly present (14). In addition, there are eleven subclasses of CER identified in human SC (4, 7, 8).

As the lipids play a crucial role in the barrier function, a large number of studies have been performed to understand the complex lipid phase behaviour underlying the skin barrier function. These studies, performed using isolated as well as synthetic CER mixtures, have markedly contributed to our present knowledge on the SC lipid organization and the role the lipid subclasses play in the lipid phase behaviour (12, 15-22). However, in these studies no information was obtained about the relation between lipid organization and skin barrier function. In order to study this, we developed a SC lipid model consisting of a porous substrate covered by a lipid film prepared from synthetic CER, CHOL and FFA. This lipid membrane mimics

the lipid organization and lipid orientation in SC closely and is referred to as the stratum corneum substitute (SCS) (23-25). As the lipid composition can easily be modified, this lipid membrane allows us to study the relationship between lipid composition, molecular organization and barrier function in just one model. In a previous study using the SCS, it was observed that the LPP plays an important role in the skin barrier function (23). However, only little information is available on the role the orthorhombic lateral packing plays in forming a proper skin barrier function. One of the key parameters to monitor the skin barrier function is the trans epidermal water loss (TEWL). In a very recent study the TEWL has been related to the degree of orthorhombic lateral packing present in SC in vivo in humans (26).

In the present study we examine whether the formation of the very dense orthorhombic packing and the formation of the characteristic lamellar phases observed in SC are crucial for the lipid barrier function in SC. As model compound we use benzoic acid (BA), a medium lipophilic low MW molecule. To examine the lipid organization in the SCS models, Fourier transform infrared spectrometry (FTIR) and small-angle x-ray diffraction (SAXD) are used. To determine the importance of the orthorhombic lateral packing for the SC lipid barrier, diffusion studies are performed during a step-wise increase in temperature from 15 to 45°C, sampling the temperature of the orthorhombic-hexagonal phase transition. To determine whether a simultaneous change in lateral packing and in the lamellar phases has a profound effect on the SC lipid barrier, a SCS with short free fatty acids is prepared, referred to as the short FFA SCS. This composition was selected as short chain FFAs are encountered in SC of human skin equivalents (27).

Is an orthorhombic lateral packing important for the skin barrier function?

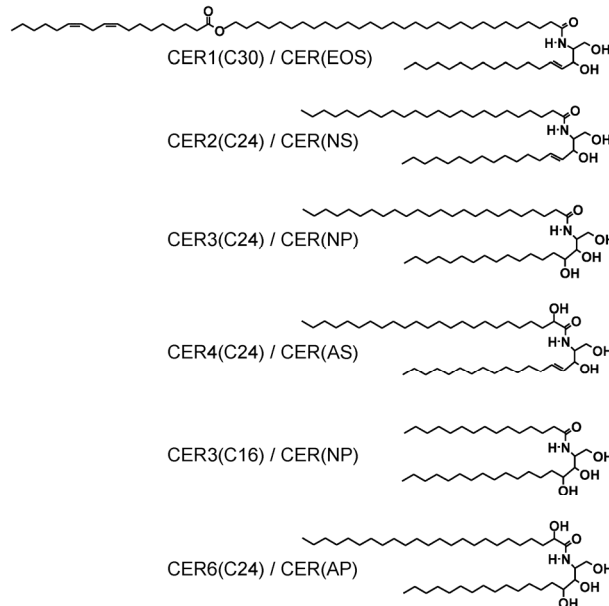


Figure 1: Molecular structure of the synthetic CER used in the SCS. The nomenclature is according to Motta et al (1).

2. Materials and Methods

2.1 Materials

In these studies we used 5 CER subclasses, see figure 1. The CER subclasses consist of either a sphingosine (S) or phytosphingosine (P) base, whereas the acyl chain is a nonhydroxy (N), α -hydroxy (A) or ω -hydroxy chain (1). The acyl chain length is either 16 carbons (C16), 24 carbons (C24) or 30 carbons (C30). The corresponding nonhydroxy and α -hydroxy CER are denoted as CER NS (C24), CER NS (C16), CER NP (C24) and CER AP (C24). In an additional CER subclass a linoleic acid is ester linked to the ω -hydroxy group (indicated by EO) with a sphingosine base. This CER is denoted as CER EOS (C30). These ceramides were generously provided by Cosmoferm B.V. (Delft, The Netherlands). Myristic acid (C14:0), palmitic acid (C16:0), stearic acid (C18:0), arachidic acid (C20:0), behenic acid (C22:0),

tricosanoic acid (C23:0), lignoceric acid (C24:0), cerotic acid (C26:0) and cholesterol were purchased from Sigma-Aldrich Chemie GmbH (Schnelldorf, Germany). The deuterated FFA with chain length of C16:0 and C22:0 were obtained from Larodan (Malmö, Sweden) and C14:0, C18:0 and C20:0 were purchased from Cambridge Isotope laboratories (Andover MA, USA). Benzoic acid, trypsin (type III, from bovine pancreas), and trypsin inhibitor (type II-S from soybean) were obtained from Sigma-Aldrich (Zwijndrecht, The Netherlands). Dialysis membrane disks (cutoff value of 5000 Da) were obtained from Diachema (Munich, Germany). Nuclepore polycarbonate filter disks (pore size 50 nm) were purchased from Whatman (Kent, UK). All organic solvents are of analytical grade and manufactured by Labscan Ltd. (Dublin, Ireland). All other chemicals are of analytical grade and the water is of Millipore quality.

2.2 Isolation of SC from human skin

SC was isolated from abdominal or mammary skin, which was obtained from the hospital within 24 h after cosmetic surgery. After removal of the subcutaneous fat tissue, the skin was dermatomed to a thickness of approximately 250 μm using a Padgett Electro Dermatome Model B (Kansas City KS, USA). The SC was separated from the epidermis by trypsin digestion [0.1% in phosphate-buffered saline (PBS), pH 7.4], after overnight incubation at 4°C and subsequently at 37°C for 1 h. The SC was then placed in a 0.1% solution of trypsin inhibitor and washed twice with Millipore water. Until use, the SC was stored in a silica-containing box under gaseous argon in the dark to prevent oxidation of the intercellular SC lipids. Before FTIR measurements, the SC was rehydrated for 24h at 100% relative humidity.

2.3 Preparation of the lipid mixtures

For the preparation of the SCS, synthetic CER, CHOL and FFA were used in equimolar ratio. For the SCS, the following synthCER composition was selected (see also figure 1): CER EOS (C30), CER NS (C24), CER NP

Is an orthorhombic lateral packing important for the skin barrier function?

(C24), CER AS (C24), CER NP (C16) and CER AP (C24) in a 15:51:16:4:9:5 molar ratio, similar as observed in pig SC (16). For the free fatty acid mixture (FFA), the following composition was selected: C16:0, C18:0, C20:0, C22:0, C23:0, C24:0 and C26:0 at a molar ratio of 1.8:4.0:7.7:42.6:5.2:34.7:4.1 respectively. This chain length distribution is based on the reported FFA composition in SC (14). For the model with shorter FFA chain length, a FFA mixture with the following composition was used; C14:0, C16:0, C18:0, C20:0 and C22:0 in molar ratios of 8.9:43.5:38.6:4.3:4.7. The same composition and molar ratios were used for the deuterated short chain FFA mixture used in FTIR studies. For each SCS model the appropriate amount of individual lipids was dissolved in hexane:ethanol (2:1 v/v) at a lipid concentration of 4.5 mg/ml.

Preparation of the lipid mixture for FTIR was the same as above, but instead 1.5 mg of lipids was dissolved in chloroform:methanol (2:1, v/v).

2.4 Spraying of the lipid mixtures onto a porous substrate for use in permeation studies, small angle X-ray diffraction measurements and electron microscopic studies

A Camag Linomat IV (MuttENZ, Switzerland) was extended with a y-axis arm. The linomat device makes use of a Hamilton syringe (100 μ l) and mechanics to spray a confined (programmable) volume of sample solution (lipids in hexane:ethanol at 4.5 mg/ml concentration) from a distance of 1 mm onto the porous filter substrate. With the y-axis arm, the linomat is capable of spraying lipids in a rectangular shape by a continuous zigzag movement. The spraying flow rate is 5.0 μ l/min under a stream of nitrogen gas at a movement speed of 1 cm/s. The area of spraying is 8 \times 8 mm. The amount of lipid solution used is 200 μ l per SCS. After spraying, the lipid films were equilibrated for 10 minutes at elevated temperature. The SCS and short FFA SCS were equilibrated at 80°C and 60°C respectively. After equilibration, the membranes were cooled down to room temperature in approximately 30 minutes.

2.5 Spraying of the lipid mixtures onto a AgBr window for use in fourier transform infrared studies

Sample preparation for FTIR was the same as above, but instead 1.5 mg of lipids was sprayed by the Linomat from chloroform:methanol (2:1, v/v) in an area of 1 cm² on an AgBr window. The sample was equilibrated for 10 min and slowly cooled down to room temperature. The SCS and short FFA SCS were equilibrated at 80°C and 60°C respectively. Subsequently, the lipid layer was covered with 25 µl of deuterated acetate buffer pH 5 (50 mM). After buffer application, the sample was kept at 37°C for 24h to obtain a full hydration. Finally, to homogenize the sample, five freeze-thawing cycles of 3h each were carried out between -20°C and RT (28).

2.6 Permeability studies

In vitro permeation studies were performed using PermeGear inline diffusion cells (Bethlehem PA, USA) with a diffusion area of 0.28 cm². The SC was supported by a dialysis membrane (5000 Da, apical side facing the donor chamber). The SC and SCS were mounted in the diffusion cells and were hydrated for 1 h in phosphate-buffered saline (PBS: NaCl, Na₂HPO₄, KH₂PO₄ and KCL in MQ water with a concentration of 8.13, 1.14, 0.20 and 0.19 g/l respectively) at pH 7.4 prior to the experiment. The donor compartment was filled with 1.4 ml of BA (MW 122 g/mol) solution in PBS (pH 7.4) at a 2.0 mg/ml concentration. BA has a logK_{o/w} value of 1.7. The acceptor phase consisted of PBS (pH 7.4), which was perfused at a flow rate of about 2 ml/h and was stirred with a magnetic stirrer. The volume per collected fraction was determined by weighing. Each experiment was performed under occlusive conditions, by closing the opening of the donor compartment with adhesive tape. The temperature of the SC or SCS during permeation was controlled by a thermo-stated water bath. To determine the activation energy for permeation, at predetermined time intervals the temperature of the SCS or SC was increased in steps of 3°C within a time interval of 10 min. Fractions were collected at a 1 h interval. Steady state

Is an orthorhombic lateral packing important for the skin barrier function?

fluxes (J_{SS}) were calculated from the horizontal part of the flux profile. For the data analysis, the following Arrhenius-type equations were used (29):

$$D = \frac{D_0}{\exp(E_D/RT)} \quad \text{or} \quad \ln(D) = \ln(D_0) - \frac{E_D}{RT} \quad (1)$$

Where R is the gas constant, D is the diffusivity of the permeating compound and D_0 denotes the hypothetical diffusivity at infinite temperature. During steady state conditions, the flux equals to:

$$J_{SS} = \frac{C \cdot K \cdot D}{L} \quad (2)$$

In which C, and K are respectively the donor concentration (under sink conditions) and partition coefficient of the permeating compound, while L is the penetration pathlength through SC or SCS. Since D is strongly related to temperature (see equation 1) and K and L are only moderately affected by the temperature, we can rewrite equation 1 by using equation 2 to obtain:

$$R \ln(J_{SS}) = R \ln(J_{SS_0}) - E_p (1/T) \quad (3)$$

Following equation 3, the natural logarithm of the obtained steady state fluxes (multiplied by the gas constant) was plotted as function of the inverse absolute temperature. Subsequently, the activation energy for permeation (E_p) was calculated directly from the slope of a linear fit through the data.

2.7 Fourier Transform Infrared spectral measurements

All spectra were acquired on a BIORAD FTS4000 FTIR spectrometer (Cambridge MA, USA) equipped with a broad-band mercury cadmium telluride detector, cooled by liquid nitrogen. The sample cell was closed by two AgBr windows. The sample was under continuous dry air purge starting 1 hour before the data acquisition. The spectra were collected in transmission mode, as a co-addition of 256 scans at 1 cm^{-1} resolution during 4 minutes. In order to detect phase transitions, the sample

temperature was increased at a heating rate of 0.25°C/min resulting in a 1°C temperature rise per recorded spectrum. The spectra were collected between 0°C and 90°C and deconvoluted using a half-width of 5 cm⁻¹ and an enhancement factor of 2.0. The software used was Win-IR pro 3.0 from Biorad.

2.8 Small-angle x-ray diffraction measurements

Small-angle x-ray diffraction (SAXD) was used to obtain information about the lamellar organization (i.e., the repeat distance of a lamellar phase). The scattering intensity I (in arbitrary units) was measured as function of the scattering vector q (in reciprocal nm). The latter is defined as $q=(4\pi\sin\theta)/\lambda$, in which θ is the scattering angle and λ is the wavelength. From the positions of a series of equidistant peaks (q_n), the periodicity, or d -spacing, of a lamellar phase was calculated using the equation $q_n=2n\pi/d$, with n being the order number of the diffraction peak. One-dimensional intensity profiles were obtained by transformation of the 2D SAXD detector pattern from Cartesian (x,y) to polar (ρ,θ) coordinates and subsequently integrating over θ . All measurements were performed at the European Synchrotron Radiation Facility (ESRF, Grenoble) using station BM26B. The x-ray wavelength and the sample-to-detector distance were 0.113 nm and 0.419 m respectively. Diffraction data were collected on a Frelon 2000 CCD detector with 2048×2048 pixels of 14 μm spatial resolution at 5x magnification. The spatial calibration of this detector was performed using silver behenate ($d=5.838$ nm) and the two strongest reflections of high density polyethylene (HDPE, $d=0.4166$ and 0.378 nm). The SCS was mounted parallel to the primary beam in a temperature controlled sample holder with mica windows. Static diffraction patterns were collected in 1 minute at 25°C.

Is an orthorhombic lateral packing important for the skin barrier function?

2.9 Electron microscopy and ruthenium staining

The SCS was cut into small parts of 1 mm² and fixed for one hour with 2% paraformaldehyde and 2.5% glutaraldehyde in a 0.1 M sodium cacodylate buffer at pH 7.4, at room temperature. After rinsing the samples 3 times with PBS, the samples were post-fixed for one hour with 1% osmium tetroxide in a cacodylate buffer pH 7.4 at 4°C. After rinsing the samples again 3 times with PBS, a second post-fixation followed with 0.5% ruthenium tetroxide in distilled water for 30 min at 4°C. Finally, the samples were rinsed again 3 times with PBS, then dehydrated in a 70% ethanol solution and subsequently processed in a series of 70% ethanol:epoxy resin LX112 at a 2:1 ratio v/v for 30 min, 1:1 for 30 min, 1:2 for 30 min and finally 0:1 for 1 h. Then the samples were polymerized for 2 days at 60°C. Subsequently, ultrathin sections of 100 nm thickness were cut with a Reichert Ultracut E microtome (Depew NY, USA) and after staining with 7% uranyl-acetate and a lead citrate solution according to Reynolds (30), the sections were observed and recorded using a Fei Tecnai 12 Twin spirit electron microscope (Hillsboro OR, USA). Of each filter at least 6 images were recorded in order to make an objective observation of the structure inside the lipid membrane.

3. Results

3.1 Influence of the lateral packing on the permeability of excised human SC and the SCS

In order to determine whether the lateral packing affects the permeability of the SC or the SCS, the BA flux is measured as function of temperature between 28 and 46°C. The temperature is increased in steps of 3°C. In figure 2A the flux of BA through SC and SCS is plotted against the temperature. The studies show that the temperature response of the BA diffusion through SC and SCS is remarkably similar over a wide temperature

range; only at the lowest (28°C) and highest (46°C) temperature a significant difference in BA flux is recorded between SCS and SC.

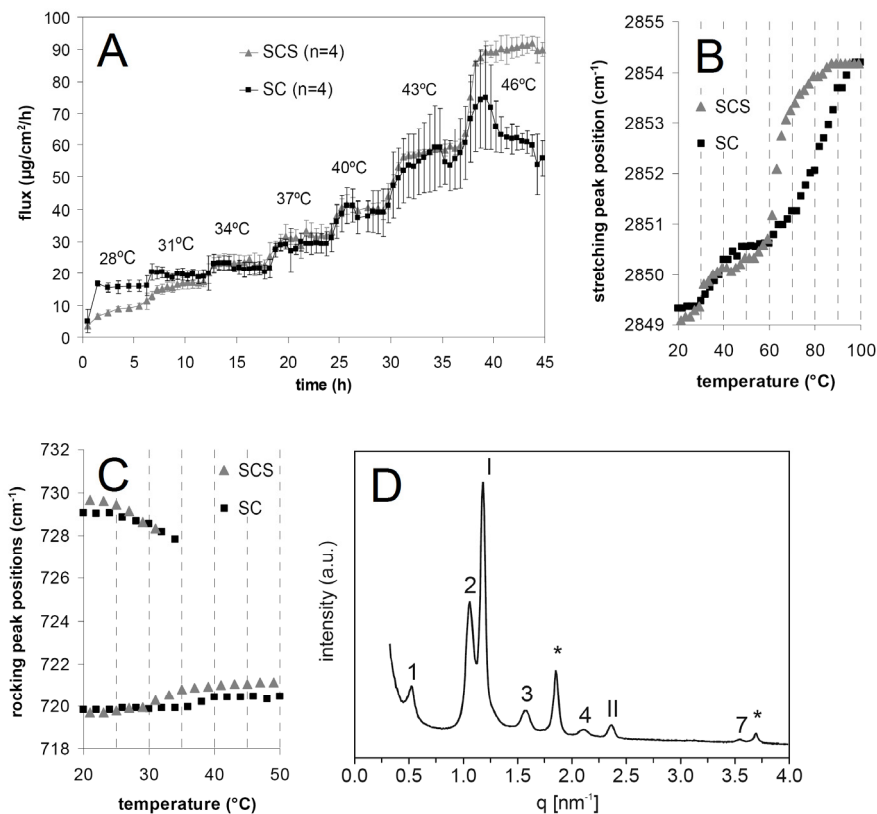


Figure 2: A) The flux of BA through human SC and SCS, at 7 temperature intervals B) FTIR symmetric stretching frequency versus temperature, for SC and SCS C) FTIR rocking frequencies versus temperature, for SC and SCS D) SAXD pattern of SCS. The reflections of the LPP are indicated by Arabic numbers 1-4 and 7, reflections of the SPP are indicated by Roman numbers I and II. Diffraction peaks from crystalline CHOL are indicated by asterisks.

The FTIR CH_2 symmetric stretching frequencies provide information about the conformational ordering of the lipid tails (31, 32). The thermotropic response of the stretching frequencies of SC and SCS is plotted in figure 2B.

Is an orthorhombic lateral packing important for the skin barrier function?

At 20°C, for SC and SCS, the stretching frequencies are 2849.3 and 2849.0 cm^{-1} respectively, which indicates a conformational ordering of the CH_2 chains. Upon increasing the temperature, a gradual shift in the stretching frequencies from 2849.4 to 2850.6 is observed between 28°C and 48°C for SC and from 2849.4 to 2850.1 cm^{-1} between 29 and 39°C for SCS, indicating a transition from orthorhombic to hexagonal lateral packing. A further increase in temperature results in a second much stronger shift in frequency from 2850.6 to 2854.2 cm^{-1} between 60 and 97°C for SC and from 2850.5 to 2854.1 cm^{-1} between 55 and 85°C for SCS. This second shift is indicative for the formation of a liquid phase, with midpoint transition temperatures of 81 and 64°C for SC and SCS respectively.

The FTIR rocking frequencies provide detailed information on the lateral packing. Due to short range coupling, the orthorhombic packing is characterized by a doublet at approximately 720 and 730 cm^{-1} , while the hexagonal packing is characterized by a singlet at a vibration frequency of approximately 720 cm^{-1} (33, 34). In figure 2C the rocking frequencies of the FTIR spectrum of SC and SCS are depicted as function of temperature. At 20°C the rocking frequencies are 719.8 and 729.1 cm^{-1} for SC and 719.7 and 729.7 cm^{-1} for SCS, indicating the presence of an orthorhombic packing. Increasing the temperature results in a gradual shift of the high frequency component to 727.8 cm^{-1} at 34°C for SC and to 728.4 cm^{-1} at 31°C for the SCS. A further increase in temperature turns the high frequency component into a shoulder of the low frequency component. This shoulder disappears at around 39°C for SC and 36°C for SCS. The disappearance of the high frequency component marks the endpoint of the orthorhombic to hexagonal transition. A further increase in temperature does not affect the rocking frequencies of SC or SCS.

The SAXD pattern of SCS is shown in figure 2D. It displays two diffraction peaks that can be attributed to the SPP with a periodicity of 5.3 nm and 5 orders of diffraction attributed to the LPP with a periodicity of 12.0

nm. Also, two reflections indicating the presence of crystalline cholesterol are observed.

3.2 Influence of short chain FFA on the barrier function of SCS

In our studies we also focus on the effect of FFA chain length distribution on the lipid organization. This is of interest as e.g. in SC of human reconstructed skin, the fatty acid chain length is reduced compared to that in SC of normal native skin (27). In addition, the presence of shorter FFA may also play a role in the impaired barrier function in diseased skin (35). The SCS prepared with FFA having a shorter chain length is referred to as short FFA SCS.

In figure 3A the flux of BA through SCS and short FFA SCS is plotted. The studies were performed at 3 temperatures: 15, 25 and 33°C. This figure shows that at all three temperatures a significant difference is observed between the steady state flux across SCS and short FFA SCS.

The thermotropic response of the symmetric CH_2 stretching frequencies of the short FFA SCS is depicted in figure 3B. At 20°C, the stretching frequency is around 2849.4 cm^{-1} , indicating a conformational ordering of the lipid tails. Heating results in a gradual increase of the stretching frequencies to 2850.3 at 49°C. A further increase in temperature results in a shift in frequency from 2850.3 to 2852.2 cm^{-1} between 49 and 67°C, indicative for the transition to a liquid phase. The midpoint temperature of this transition is 58°C. Raising the temperature further results in a gradual increase in CH_2 stretching frequency, up to 2853.6 cm^{-1} at 99°C.

As shown in figure 3C, the rocking vibrations in the FTIR spectrum of short FFA SCS display only a single frequency component at 720.8 cm^{-1} between 20 and 50°C, indicating the absence of an orthorhombic lateral packing.

Is an orthorhombic lateral packing important for the skin barrier function?

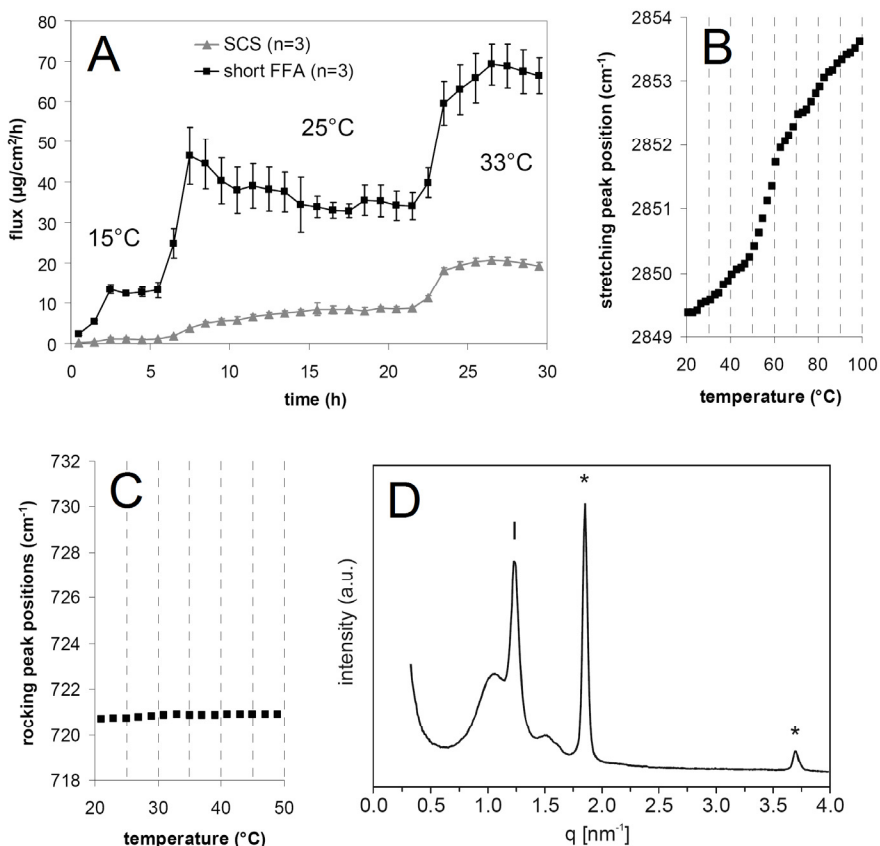


Figure 3: A) The flux of BA through SCS prepared with short chain FFA in comparison with the conventional SCS, at 3 temperature intervals B) FTIR symmetric stretching frequency versus temperature, for the SCS with short chain FFA C) FTIR rocking frequency versus temperature, for the SCS with short chain FFA D) SAXD pattern of the SCS with short chain FFA. One reflection at the position of the first order SPP is indicated by the Roman number I and diffraction peaks from crystalline CHOL are indicated by asterisks.

The SAXD pattern of short FFA SCS displayed in figure 3D shows one sharp diffraction peak at a similar peak position as the 1st order of the

SPP in SCS. Besides this reflection, only very broad peaks are visible around $q = 1.0$ and 1.5 nm^{-1} . This demonstrates that the long range ordering in the short FFA SCS is very different from that in SCS. Also a relatively large amount of phase-separated crystalline CHOL is present in the short FFA SCS, as can be deduced from the high intensity diffraction peaks at $q = 1.85$ and 3.7 nm^{-1} .

3.3 Mixing of short chain FFA with CER and CHOL

When using deuterated FFA (denoted as DFFA), due to a shift in the absorption frequencies, the CD_2 and CH_2 scissoring vibrations of the protonated and deuterated FFA respectively, can be monitored simultaneously in the FTIR spectrum. To determine whether the DFFA and CER participate in one lattice or that phase separation occurs, the CD_2 scissoring mode can be monitored. When FFA and CER participate in an orthorhombic packing, the CH_2 and CD_2 scissoring modes will not interact and therefore the vibrational coupling that results in a doublet in the spectrum will be reduced.

In figure 4A the CD_2 scissoring vibrations of the short chain DFFA mixture are depicted. A doublet with positions at 1086 and 1092 cm^{-1} is observed until a temperature of 62°C is reached. This is indicative for the presence of an orthorhombic lateral packing in this temperature range. However, when the CD_2 scissoring mode in the spectrum of the equimolar mixture of CER, CHOL and short chain DFFA is monitored in figure 4B, only a weak doublet of the CD_2 scissoring mode is observed between 20 and 32°C (see arrows). This demonstrates that only a small portion of all DFFA chains has neighboring DFFA chains and that thus the majority of the short chain DFFA and CER molecules participate in the same orthorhombic lattice.

Is an orthorhombic lateral packing important for the skin barrier function?

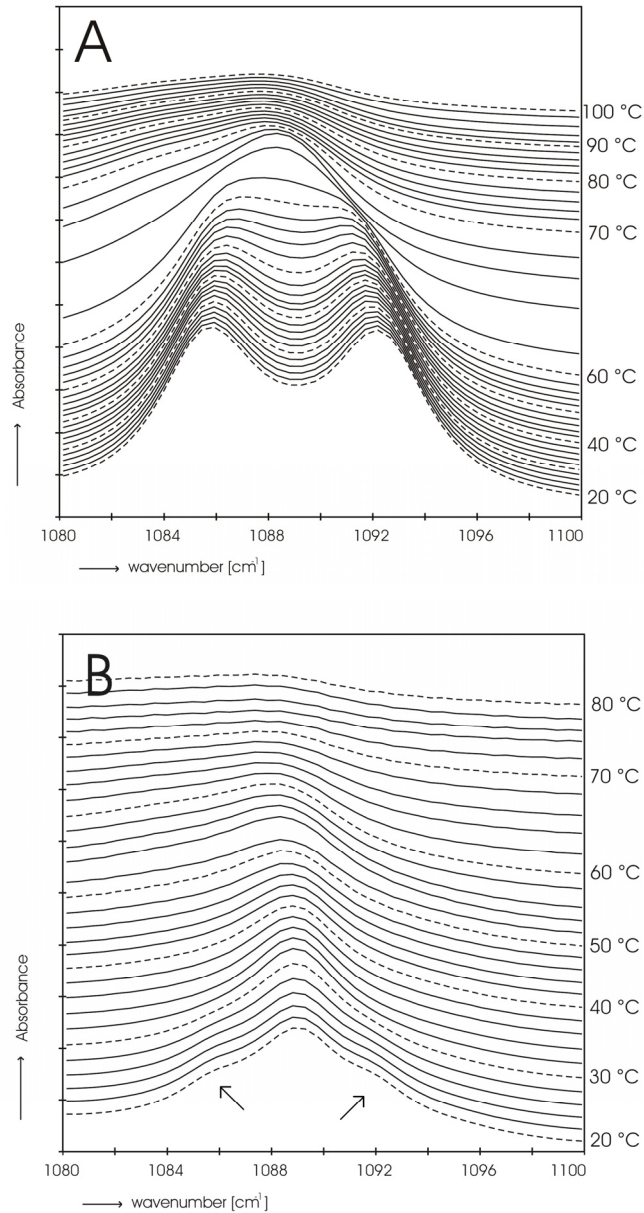


Figure 4: A) Thermotropic CH₂ scissoring spectra of a deuterated short chain FFA mixture depicted from 20 to 100°C. A doublet is observed which disappears at around 62°C. B) Scissoring spectra of DFFA-short in an equimolar mixture with CER and CHOL. Only a weak doublet is observed (indicated by the arrows), which disappears at 32°C.

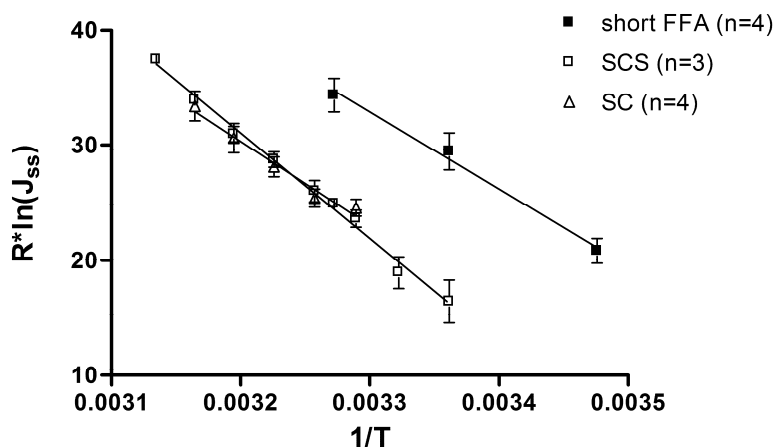


Figure 5: Arrhenius plots for human SC, SCS and short FFA SCS, in which the natural logarithm of the steady state flux (multiplied by the gas constant R), is plotted against the inverse absolute temperature. The linear fit is shown through the flux data of SC and the two models. The error bars in the figure display the standard deviation of the flux data.

3.4 The activation energy for permeation through SC, SCS and the short chain FFA SCS

Figure 5 displays the steady state fluxes obtained at the various temperature intervals for SC, SCS and short FFA SCS, plotted in log scale as function of the reciprocal temperature. Apart from SC at 28 and 46°C and SCS at 15°C (not included because of large flux deviations at these temperatures), for all membranes a linear relationship is observed between the natural logarithm of the steady state flux and the reciprocal temperature. The slope of this linear fit is equal to the activation energy for permeation, see equation 1. Using the same temperature interval for SC and SCS, from 31 to 43°C, the activation energies determined are 73.1 ± 7.1 and 81.9 ± 2.5 kJ/mole for SC and SCS respectively. The appearance of a straight line in figure 5 and thus the existence of only one activation energy in the examined temperature range, indicates that the increase in BA flux as function of

Is an orthorhombic lateral packing important for the skin barrier function?

temperature is not affected by the change in packing from an orthorhombic to a hexagonal phase. The activation energy for permeation of BA through the short FFA model is 66.8 ± 5.9 kJ/mole.

3.5 Lamellar structure of SCS and short chain FFA SCS visualised by electron microscopy

In order to obtain further insight into the lamellar organization of the SCS and short FFA SCS, the SCS are visualized in the electron microscope (EM) after embedding and RuO₄ staining. A typical EM image of the SCS is displayed in figure 6A. In this image it is clear that the SCS contains two distinct phases: domains with the well known broad-narrow-broad pattern (36) and darker domains with a repetitive equidistant spacing. In order to establish whether the broad-narrow-broad structure is correlated to the LPP, membranes were prepared with a twofold higher level of CER EOS (as EOS is responsible for the formation of the LPP (37)) and in the absence of CER EOS. When 30% CER EOS was incorporated, the electron microscopic images display predominantly the broad-narrow-broad sequence and very little regions with an equidistant spacing, see figure 6B. When a membrane was prepared in the absence of CER EOS, no broad-narrow-broad structure is visible in the images, see figure 6C. Instead, domains with short periodicity equidistant lamellae are observed, indicating the formation of the SPP. We measured the spacings of the SPP and LPP from figure 6A-C and found that they are somewhat smaller than determined by SAXD, probably due to the embedding process for EM. The lipid organization of the SCS with short chain FFA is displayed in figure 6D. Although lamellae are visible, this image reveals the absence of a well defined stacking of the lipid lamellae and the absence of a broad-narrow-broad pattern.

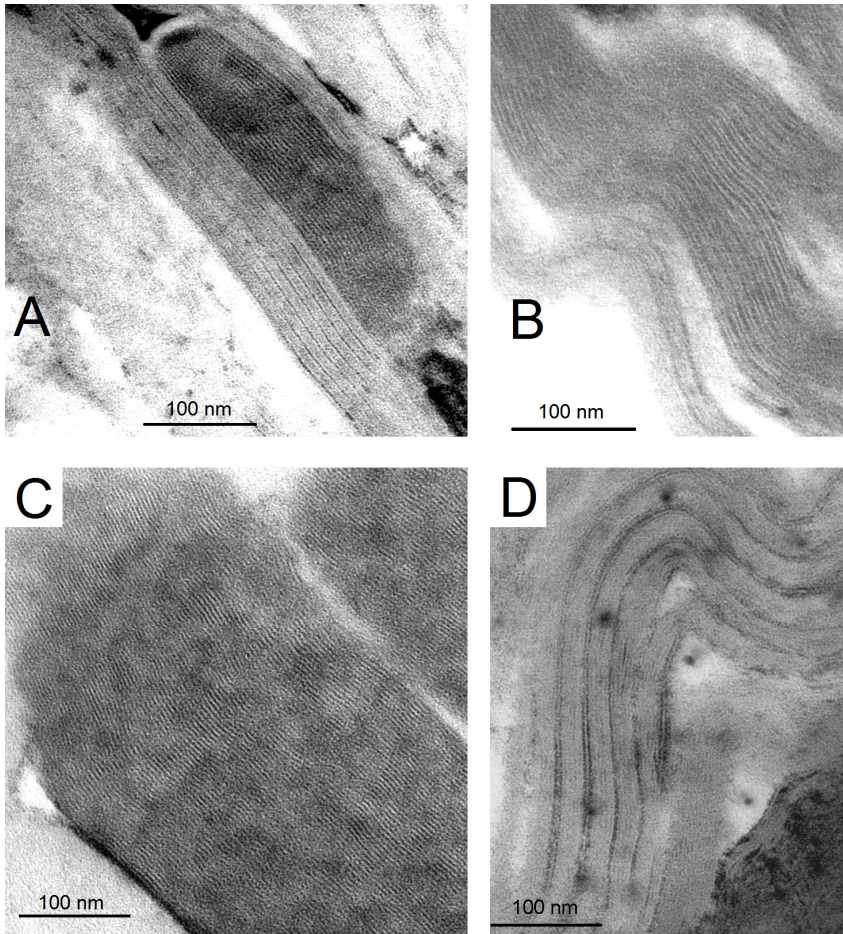


Figure 6: A) Electron microscopy image of the SCS. Two different domains are visible in the micrograph. One domain with the well-known broad-narrow-broad appearance, the other domain with a short repetitive structure. B) EM micrograph of a SCS prepared with a higher level of CER EOS. In this image only lamellae with a broad-narrow-broad pattern are visible. C) Electron microscopy micrograph of a SCS prepared in the absence of CER EOS. In this image only lamellae with a short repetitive pattern are observed. D) EM image of the short FFA SCS. Lamellar structures are visible, but no proper stacking is observed.

Is an orthorhombic lateral packing important for the skin barrier function?

4. Discussion

Although it has been suggested that the presence of the orthorhombic phase is important for the skin barrier function, currently there are almost no data available on the effect of the orthorhombic to hexagonal phase transition and the presence of the LPP on the permeability of compounds. Therefore, in this study we examined the effect of the lateral packing on the permeability of SC and SCS by performing diffusion studies in the temperature interval between 15 and 46°C. In addition, the effect of shorter FFA in the SCS on the lipid organization and permeability was examined.

4.1 The permeability of SCS is very similar to human SC

Around the skin temperature (32°C), the steady state fluxes of BA through SC and SCS did not differ significantly. The steady state flux values are around 20 $\mu\text{g}/\text{cm}^2/\text{h}$ at 32°C, which is very similar to the steady state flux value obtained in a previous study (25). Remarkably, we found that the permeability of SCS to BA closely follows that of human SC at all temperature steps between 31 and 43°C. When comparing SC and SCS in previous studies with PABA, ethyl-PABA and butyl-PABA an excellent correlation between steady state fluxes was also observed (23). Very recently we also noticed that the steady state flux of hydrocortison through SC and SCS is very similar (unpublished results), demonstrating that the SCS mimics the permeation properties of human SC very closely for moderately hydrophilic to moderately lipophilic compounds.

4.2 The activation energy for permeation in SCS and SC is different, but the flux is similar

The E_p values for BA through SC and SCS are consistent with values reported in literature for a range of substances used in skin permeation studies (38). For example, the E_p for acetylsalicylic acid (MW=180, $\log K_{o/w}=1.19$) is 85 kJ/mole (39), for caffeine (MW=194,

$\log K_{o/w}=0.02$) 53 kJ/mole (40), for corticosterone (MW=346, $\log K_{o/w}=1.94$) 97 kJ/mole (41), for ibuprofen (MW=206, $\log K_{o/w}=3.5$) 173 kJ/mole (42) and for water (MW=18, $\log K_{o/w}=1.38$) 57 kJ/mole (2). Mitragotri reports that the E_p for hydrophobic solutes (which also includes BA) is strongly dependent on the molecular size (38). When comparing the E_p calculated for permeation of BA through SC and SCS, the E_p for SC is slightly lower than that for SCS, even though the flux values did not differ significantly between 31 and 43°C. This difference in E_p may be explained by differences in the structure of the SC and SCS: The uniformity in chain length of the synthetic CER in SCS may result in a reduced mismatch between the CER hydrocarbon chains in the lipid lamellae, resulting in a more crystalline structure. Because the environment of the diffusing molecule is affected, this can lead to an increase in E_p (more difficult for the permeant molecule to move through a more crystalline structure).

4.3 Is the orthorhombic lateral packing crucial for a competent SC barrier function?

In previous studies the diffusion of water across pig SC has been measured as function of temperature by Potts and Francoeur (2). From the permeability values an Arrhenius plot can be constructed, which is presented in figure 7. From the linear correlation with the inverse temperature, an E_p of 59.1 ± 2.9 kJ/mole can be calculated. Porcine SC does not exhibit an orthorhombic-hexagonal phase transition (43), demonstrating that in the absence of a phase transition a linear correlation is observed between the log of the steady state flux and the inverse absolute temperature. In human SC and the SCS, the rocking frequencies as function of temperature demonstrated that an orthorhombic to hexagonal phase transition occurs between 30 and 40°C. However, when focusing on the Arrhenius plot of human SC and SCS, a linear relationship is observed similar to that in pig SC. This demonstrates that the orthorhombic-hexagonal phase transition

Is an orthorhombic lateral packing important for the skin barrier function?

does not affect E_p and therefore does not affect the diffusivity of BA across human SC and the SCS (29).

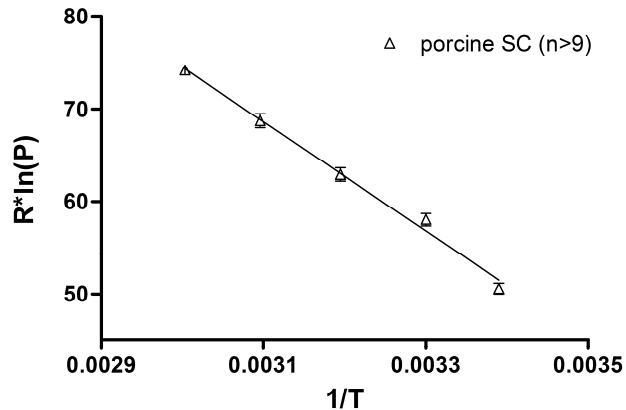


Figure 7: Arrhenius plot for water permeation through porcine SC. The permeation data were presented in an earlier study by Potts and Francoeur (2). Shown in the plot is the linear fit through the flux data. Error bars in the figure represent the standard error of the mean.

Although our studies have only been carried out with BA and the diffusion of other compounds may be more sensitive to the orthorhombic-hexagonal phase transition, our results demonstrate that the presence of the orthorhombic lateral packing seems to be less crucial than suggested in previous studies (21, 26, 44, 45).

In SC of human skin equivalents the lipids form the LPP very similar to that in native SC, but the lateral packing of the lipids is hexagonal (27), very similar to that in porcine SC. Permeation studies have shown that the methyl nicotinate flux across human skin equivalents is 2-fold higher than observed for native human skin (46). However, the results of our present study indicate that the hexagonal lateral packing may not explain this increased permeability.

The results discussed above are in contrast with those of a recent study focusing on the permeation of water through human SC (26). In this study it is reported that the water transport is influenced by the relative population of lipids forming an orthorhombic packing. However, in the latter study the TEWL has been used as a measure for the water transport. Perhaps the difference in physical properties of the solute (water versus BA) or the difference between inside-out permeation (TEWL) and outside-in permeation (BA permeation) can account for the different observations. In a study of Chilcott et al (47), it was shown that TEWL and diffusion of substances, both measured in vitro, do not correlate.

4.4 The formation of ordered lamellar phases is crucial for the SC barrier function

The BA flux through the SCS prepared with short chain FFA is approximately 4-fold higher than that through normal SCS. This was observed at all three temperatures selected in the studies. In addition the E_p is lower than that of normal SCS. When comparing the short FFA SCS with the SCS, differences in lipid organization are noticed. As far as the lateral packing is concerned, at skin temperature a hexagonal lateral packing is observed. However, as discussed above, for BA no obvious difference in diffusivity is expected between a hexagonal and an orthorhombic lateral packing. Therefore, the absence of the orthorhombic packing cannot explain the high permeability observed in the short FFA SCS, provided that the penetration pathlength remains the same in both the hexagonal and orthorhombic lateral packing (see equation 2). As in this model the chain length difference between the short chain FFA and the CER is substantial, phase separation within the crystalline lattice is likely to occur and was therefore examined using SCS prepared with DFFA. These studies, however, demonstrated that the short chain FFA and the CER both participate in the same lattice. Phase separation can therefore not contribute to the increase in BA flux. When focusing on the lamellar organization, the

Is an orthorhombic lateral packing important for the skin barrier function?

lipids in the short chain FFA SCS form different phases than observed in the SCS: in the X-ray diffraction pattern no LPP is noticed and only one reflection can be attributed to the SPP. Instead, broad reflections are observed that are absent in the diffraction pattern of the normal SCS, indicating the absence of a proper stacking of the lipid lamellae. This is confirmed by the electron microscopic studies of the short FFA SCS. In a previous study it was shown that a lack of the LPP results in a 2-fold increased flux of ethyl-para amino benzoic acid (23). Because no LPP is formed and the stacking of the lamellae is less defined, the pathlength through the short FFA membrane may be significantly reduced. The diffusivity of the short FFA membrane (calculated from E_p with equation 1) is only slightly different from the diffusivity of the SCS. Therefore, the absence of the proper lamellar phases may account for the increased flux through the short FFA SCS by reducing the pathlength for permeation (see equation 2).

Interestingly, with EM in the SCS two domains with a different appearance could be distinguished; the broad-narrow-broad pattern and the short repetitive pattern. Although the LPP has been related to the broad-narrow-broad pattern in previous studies (36), until now, this relation was not completely established. For this reason, we prepared a SCS in the absence of the CER EOS and a SCS with 30% CER EOS. X-ray diffraction studies showed that in the absence of CER EOS only the SPP is formed (37), while with 30% CER EOS in our mixture the LPP is predominantly formed (unpublished results). These findings correlate excellently with the presence of mainly broad-narrow-broad pattern in the EM images of the SCS with 30% CER EOS and the presence of only the short repetition pattern in SCS prepared without EOS. Therefore these studies demonstrate that the broad-narrow-broad pattern is indeed directly related to the LPP.

When extrapolating our findings to SC of diseased skin, our present studies suggest that the skin barrier function is more sensitive to a change in the lamellar phases than to a change from an orthorhombic to a hexagonal lateral packing. In lamellar Ichthyosis (48, 49) as well as in psoriasis SC

(unpublished results) the lamellar phases are different from that in SC of healthy human subjects.

In conclusion, we observed that the permeability of BA through human SC and the SCS is not affected by the orthorhombic-hexagonal transition. However, when substituting the long chain FFA for short chain FFA an increased permeability was observed due to a drastic change in the lamellar organization. Our studies indicate that the absence of a proper lamellar organization has a higher impact on the skin barrier function than a change from orthorhombic to hexagonal lateral packing. These findings may provide new insights into the skin barrier function, especially in diseased skin.

Acknowledgments

This work was supported by a grant from the Technology Foundation STW (LGP 7503). We thank the company Cosmoferm B.V. (Evonik) for the provision of the ceramides and the Netherlands Organization for Scientific Research (NWO) for the provision of beam time at the ESRF. Furthermore we thank the personnel at the DUBBLE beam line at the ESRF for their support with the x-ray measurements. Finally, we thank Aat Mulder for the EM studies, Drs Michelle Janssens for additional FTIR measurements and Dr Maria Ponec for valuable discussions about the permeability studies.

Is an orthorhombic lateral packing important for the skin barrier function?

References

1. Motta, S., M. Monti, S. Sesana, R. Caputo, S. Carelli, and R. Ghidoni. 1993. Ceramide composition of the psoriatic scale. *Biochim. Biophys. Acta* 1182:147-151.
2. Potts, R. O., and M. L. Francoeur. 1990. Lipid biophysics of water loss through the skin. *Proc Natl Acad Sci U S A* 87:3871-3873.
3. Simonetti, O., A. J. Hoogstraate, W. Bialik, J. A. Kempenaar, A. H. Schrijvers, H. E. Bodde, and M. Ponec. 1995. Visualization of diffusion pathways across the stratum corneum of native and in-vitro-reconstructed epidermis by confocal laser scanning microscopy. *Arch Dermatol Res* 287:465-473.
4. Wertz, P. W., M. C. Miethke, S. A. Long, J. S. Strauss, and D. T. Downing. 1985. The composition of the ceramides from human stratum corneum and from comedones. *J. Invest. Dermatol.* 84:410-412.
5. Robson, K. J., M. E. Stewart, S. Michelsen, N. D. Lazo, and D. T. Downing. 1994. 6-Hydroxy-4-sphingenine in human epidermal ceramides. *J. Lipid. Res.* 35:2060-2068.
6. Stewart, M. E., and D. T. Downing. 1999. A new 6-hydroxy-4-sphingenine-containing ceramide in human skin. *J. Lipid. Res.* 40:1434-1439.
7. Ponec, M., A. Weerheim, P. Lankhorst, and P. Wertz. 2003. New acylceramide in native and reconstructed epidermis. *J. Invest. Dermatol.* 120:581-588.
8. Masukawa, Y., H. Narita, E. Shimizu, N. Kondo, Y. Sugai, T. Oba, R. Homma, J. Ishikawa, Y. Takagi, T. Kitahara, Y. Takema, and K. Kita. 2008. Characterization of overall ceramide species in human stratum corneum. *J Lipid Res* 49:1466-1476.
9. Bouwstra, J. A., G. S. Gooris, J. A. van der Spek, and W. Bras. 1991. Structural investigations of human stratum corneum by small-angle X-ray scattering. *J. Invest. Dermatol.* 97:1005-1012.
10. Bouwstra, J. A., G. S. Gooris, W. Bras, and D. T. Downing. 1995. Lipid organization in pig stratum corneum. *J. Lipid Res.* 36:685-695.
11. White, S. H., D. Mirejovsky, and G. I. King. 1988. Structure of lamellar lipid domains and corneocyte envelopes of murine stratum corneum. An X-ray diffraction study. *Biochemistry* 27:3725-3732.
12. Bouwstra, J., G. Gooris, and M. Ponec. 2002. The lipid organisation of the skin barrier: liquid and crystalline domains coexist in lamellar phases. *Journal of Biological Physics* 28:211-223.
13. Hatta, I., N. Ohta, K. Inoue, and N. Yagi. 2006. Coexistence of two domains in intercellular lipid matrix of stratum corneum. *Biochim Acta* 1758:1830-1836.

14. Wertz, P. 1991. Epidermal lipids. In *Physiology, Biochemistry and Molecular Biology of the Skin*. L. A. Goldsmith, editor. Oxford University Press, Oxford. 205-235.
15. Swartzendruber, D. C., P. W. Wertz, D. J. Kitko, K. C. Madison, and D. T. Downing. 1989. Molecular models of the intercellular lipid lamellae in mammalian stratum corneum. *J Invest Dermatol* 92:251-257.
16. Bouwstra, J. A., G. S. Gooris, K. Cheng, A. Weerheim, W. Bras, and M. Ponec. 1996. Phase behavior of isolated skin lipids. *J. Lipid Res.* 37:999-1011.
17. Bouwstra, J. A., G. S. Gooris, F. E. Dubbelaar, A. M. Weerheim, and M. Ponec. 1998. pH, cholesterol sulfate, and fatty acids affect the stratum corneum lipid organization. *J Investig Dermatol Symp Proc* 3:69-74.
18. Moore, D. J., and M. E. Rerek. 2000. Insights into the molecular organization of lipids in the skin barrier from infrared spectroscopy studies of stratum corneum lipid models. *Acta Derm Venereol Suppl (Stockh)* 208:16-22.
19. McIntosh, T. J. 2003. Organization of skin stratum corneum extracellular lamellae: diffraction evidence for asymmetric distribution of cholesterol. *Biophys J* 85:1675-1681.
20. Kiselev, M. A., N. Y. Ryabova, A. M. Balagurov, S. Dante, T. Hauss, J. Zbytovska, S. Wartewig, and R. H. Neubert. 2005. New insights into the structure and hydration of a stratum corneum lipid model membrane by neutron diffraction. *Eur Biophys J* 34:1030-1040.
21. Bouwstra, J. A., and M. Ponec. 2006. The skin barrier in healthy and diseased state. *Biochim Biophys Acta* 1758:2080-2095.
22. Kessner, D., A. Ruettinger, M. A. Kiselev, S. Wartewig, and R. H. Neubert. 2008. Properties of ceramides and their impact on the stratum corneum structure. Part 2: stratum corneum lipid model systems. *Skin Pharmacol Physiol* 21:58-74.
23. de Jager, M., W. Groenink, R. Bielsa i Guivernau, E. Andersson, N. Angelova, M. Ponec, and J. Bouwstra. 2006. A novel in vitro percutaneous penetration model: evaluation of barrier properties with p-aminobenzoic acid and two of its derivatives. *Pharm. Res.* 23:951-960.
24. de Jager, M., W. Groenink, J. van der Spek, C. Janmaat, G. Gooris, M. Ponec, and J. Bouwstra. 2006. Preparation and characterization of a stratum corneum substitute for in vitro percutaneous penetration studies. *Biochim. Biophys. Acta* 1758:636-644.
25. Groen, D., G. S. Gooris, M. Ponec, and J. A. Bouwstra. 2008. Two new methods for preparing a unique stratum corneum substitute. *Biochim Biophys Acta* 1778:2421-2429.
26. Damien, F., and M. Boncheva. 2010. The extent of orthorhombic lipid phases in the stratum corneum determines the barrier efficiency of human skin in vivo. *J Invest Dermatol* 130:611-614.

Is an orthorhombic lateral packing important for the skin barrier function?

27. Ponec, M., S. Gibbs, G. Pilgram, E. Boelsma, H. Koerten, J. Bouwstra, and M. Mommaas. 2001. Barrier function in reconstructed epidermis and its resemblance to native human skin. *Skin Pharmacol Appl Skin Physiol* 14 Suppl 1:63-71.
28. Gooris, G. S., and J. A. Bouwstra. 2007. Infrared spectroscopic study of stratum corneum model membranes prepared from human ceramides, cholesterol, and fatty acids. *Biophys J* 92:2785-2795.
29. Barry, B. W. 1983. *Dermatological Formulations: Percutaneous Absorption*. Marcel Dekker, inc, New York.
30. Reynolds, E. S. 1963. The use of lead citrate at high pH as an electron-opaque stain in electron microscopy. *J Cell Biol* 17:208-212.
31. Snyder, R. G., S. L. Hsu, and S. Krimm. 1978. Vibrational-Spectra in C-H Stretching Region and Structure of Polymethylene Chain. *Spectrochimica Acta Part a-Molecular and Biomolecular Spectroscopy* 34:395-406.
32. Wolfangel, P., R. Lehnert, H. H. Meyer, and K. Muller. 1999. FTIR studies of phospholipid membranes containing monoacetylenic acyl chains. *Physical Chemistry Chemical Physics* 1:4833-4841.
33. Snyder, R. G. 1960. Vibrational Spectra of Crystalline N-Paraffins .1. Methylene Rocking and Wagging Modes. *Journal of Molecular Spectroscopy* 4:411-434.
34. Moore, D. J., M. E. Rerek, and R. Mendelsohn. 1997. Lipid domains and orthorhombic phases in model stratum corneum: Evidence from Fourier transform infrared spectroscopy studies. *Biochemical and Biophysical Research Communications* 231:797-801.
35. Ishikawa, J., H. Narita, N. Kondo, M. Hotta, Y. Takagi, Y. Masukawa, T. Kitahara, Y. Takema, S. Koyano, S. Yamazaki, and A. Hatamochi. Changes in the Ceramide Profile of Atopic Dermatitis Patients. *J Invest Dermatol*.
36. Madison, K. C., D. C. Swartzendruber, P. W. Wertz, and D. T. Downing. 1987. Presence of intact intercellular lipid lamellae in the upper layers of the stratum corneum. *J Invest Dermatol* 88:714-718.
37. Bouwstra, J. A., G. S. Gooris, F. E. Dubbelaar, A. M. Weerheim, A. P. Ijzerman, and M. Ponec. 1998. Role of ceramide 1 in the molecular organization of the stratum corneum lipids. *J Lipid Res* 39:186-196.
38. Mitragotri, S. 2007. Temperature dependence of skin permeability to hydrophilic and hydrophobic solutes. *J Pharm Sci* 96:1832-1839.
39. Scheuplein, R. J., and I. H. Blank. 1971. Permeability of the skin. *Physiol Rev* 51:702-747.
40. Akomeah, F., T. Nazir, G. P. Martin, and M. B. Brown. 2004. Effect of heat on the percutaneous absorption and skin retention of three model penetrants. *Eur J Pharm Sci* 21:337-345.

Chapter 3

41. Peck, K. D., A. H. Ghanem, and W. I. Higuchi. 1995. The effect of temperature upon the permeation of polar and ionic solutes through human epidermal membrane. *J Pharm Sci* 84:975-982.
42. Ito, Y., T. Ogiso, and M. Iwaki. 1988. Thermodynamic study on enhancement of percutaneous penetration of drugs by Azone. *J Pharmacobiodyn* 11:749-757.
43. Caussin, J., G. S. Gooris, M. Janssens, and J. A. Bouwstra. 2008. Lipid organization in human and porcine stratum corneum differs widely, while lipid mixtures with porcine ceramides model human stratum corneum lipid organization very closely. *Biochim Biophys Acta* 1778:1472-1482.
44. Bommannan, D., R. O. Potts, and R. H. Guy. 1990. Examination of stratum corneum barrier function in vivo by infrared spectroscopy. *J Invest Dermatol* 95:403-408.
45. Moore, D. J., R. G. Snyder, M. E. Rerek, and R. Mendelsohn. 2006. Kinetics of membrane raft formation: fatty acid domains in stratum corneum lipid models. *J Phys Chem B* 110:2378-2386.
46. Boelsma, E., C. Anderson, A. M. Karlsson, and M. Ponec. 2000. Microdialysis technique as a method to study the percutaneous penetration of methyl nicotinate through excised human skin, reconstructed epidermis, and human skin in vivo. *Pharm Res* 17:141-147.
47. Chilcott, R. P., C. H. Dalton, A. J. Emmanuel, C. E. Allen, and S. T. Bradley. 2002. Transepidermal water loss does not correlate with skin barrier function in vitro. *J Invest Dermatol* 118:871-875.
48. Lavrijsen, A. P., J. A. Bouwstra, G. S. Gooris, A. Weerheim, H. E. Bodde, and M. Ponec. 1995. Reduced skin barrier function parallels abnormal stratum corneum lipid organization in patients with lamellar ichthyosis. *J Invest Dermatol* 105:619-624.
49. Pilgram, G. S., D. C. Vissers, H. van der Meulen, S. Pavel, S. P. Lavrijsen, J. A. Bouwstra, and H. K. Koerten. 2001. Aberrant lipid organization in stratum corneum of patients with atopic dermatitis and lamellar ichthyosis. *J Invest Dermatol* 117:710-717.

Chapter 4

Investigating the barrier function of skin lipid models with varying compositions

Daniël Groen, Dana S. Poole, Gert S. Gooris, Joke A. Bouwstra

Eur J Pharm Biopharm, in press

Abstract

The lipids in the uppermost layer of the skin, the stratum corneum (SC), play an important role in the barrier function. The main lipid classes in stratum corneum are ceramides, cholesterol and free fatty acids. In previous publications a lipid model was presented, referred to as the stratum corneum substitute (SCS), that closely mimics the SC lipid organization and SC barrier function. In the present study, we use the SCS to study the effect of changes in lipid organization on the lipid barrier function using benzoic acid as permeation compound. First, in the SCS we increased the level of one of the three major lipid classes keeping the ratio between the other lipid classes constant. An increased cholesterol level resulted in an increase in phase separated cholesterol and a reduction in the permeability. An increase in ceramide or free fatty acid level resulted in the formation of additional phases, but had no significant influence on the permeability. We also examined models that mimic selected changes in lipid composition reported for dry or diseased skin. The SCS that mimics the composition in recessive X-linked ichthyosis skin displayed a twofold increase in permeability. This increase is possibly related to the formation of an additional, less ordered phase in this model.

1. Introduction

The physical barrier of the human skin is located in the uppermost layer, the stratum corneum (SC). The SC consists of enucleated dead cells (corneocytes) that are surrounded by lipid lamellae. As these lipid lamellae form a continuous pathway in the SC, the lipid domains are considered to play a dominant role in the skin barrier function (4). The main lipid classes in the SC are ceramides (CER), cholesterol (CHOL) and free fatty acids (FFA) (5-9). The lipids are arranged in two crystalline coexisting lamellar phases with repeat distances of 13 and 6 nm, respectively. These lamellar phases are referred to as the long periodicity phase (LPP) and the short periodicity phase (SPP) (10, 11). At the skin temperature of 30-32°C, in human SC the lipids in the lipid lamellae are organized mainly in an orthorhombic lateral packing, although a subpopulation of lipids also forms a hexagonal or even a liquid-like lateral packing (12-14). The lateral and lamellar lipid organization are considered to play an important role in the skin barrier function (14-16). When focusing in more detail on the lipid composition, a wide distribution of FFA chain lengths has been identified. The most abundant chain lengths in the FFA mixture are those of 22 and 24 C atoms (17). As far as the CER are concerned, currently, there are eleven subclasses of CER identified in human SC (5, 6, 9). To understand the change in lipid phase behaviour in diseased and dry skin (18-22), we should unravel the complex phase behaviour in SC. As it is impossible to perform these studies with intact SC, lipid mixtures should be used mimicking the lipid phase behaviour of SC as closely as possible. In previous studies lipid mixtures were prepared using isolated as well as synthetic CER mixtures. These lipid mixtures mimicked the lipid organization of SC very closely and provided useful information on the role the lipid classes play in the lipid phase behaviour (23-25). However, no information was obtained about the relation between lipid organization and the skin barrier function. In order to study this, we developed a skin lipid membrane consisting of a porous substrate covered with a mixture of synthetic CER, CHOL and FFA. This membrane is referred to as the stratum

corneum substitute (SCS). The SCS mimics the lipid organization and lipid orientation in SC very closely. As the lipid composition can easily be modified, the SCS allows us to study the relationship between lipid composition, molecular organization and barrier function in just one model (1, 26, 27). In a previous study it was observed that the LPP plays an important role in the skin barrier function (26). In a recent paper we examined also the effect of the lateral packing on the permeability of the SCS using benzoic acid (BA), a medium lipophilic low molecular weight compound, as model drug (2). This study revealed that an orthorhombic to hexagonal transition does not affect the diffusivity of BA in the SCS.

In the present study, we will first systematically change the CER, CHOL and FFA composition. Subsequently we examine models that mimic some aspects of the changes in lipid composition reported for SC of dry skin (winter xerosis), recessive X-linked ichthyosis and psoriasis skin. The permeability of the in vitro SCS models is assessed by measuring the permeation of BA. To examine the lipid organization in the models, Fourier transform infrared spectrometry (FTIR) and small-angle X-ray diffraction (SAXD) are used.

2. Materials and Methods

2.1 Materials

Synthetic CER(EOS)C30-linoleate, CER(EOS)C30-oleate, CER(NS)C24, CER(NP)C24, CER(NP)C16, CER(AS)C24 and CER(AP)C24 (see figure 1) were generously provided by Cosmoferm B.V. (Delft, The Netherlands). Palmitic acid (C16:0), stearic acid (C18:0), arachidic acid (C20:0), behenic acid (C22:0), tricosanoic acid (C23:0), lignoceric acid (C24:0), cerotic acid (C26:0) and cholesterol were purchased from Sigma-Aldrich Chemie GmbH (Schnelldorf, Germany). Benzoic acid was obtained from Sigma-Aldrich (Zwijndrecht, The Netherlands). Nuclepore polycarbonate filter disks (pore size 50 nm) were purchased from Whatman

(Kent, UK). All organic solvents are of analytical grade and manufactured by Labscan Ltd. (Dublin, Ireland). All other chemicals are of analytical grade and the water is of Millipore quality.

Table 1:

model type	abbreviation	composition and molar ratio	J_{ss} ($\mu\text{g}/\text{cm}^2/\text{h}$)	τ (h)
SC substitute	SCS	CER : CHOL : FFA 1 : 1 : 1	$24 \pm 2^\dagger$	$1.1 \pm 0.5^\dagger$
high CER level		CER : CHOL : FFA 2 : 1 : 1	22.5 ± 1.8	-0.3 ± 0.5
high CHOL level		CER : CHOL : FFA 1 : 2 : 1	9.0 ± 1.5	0.6 ± 0.6
high FFA level		CER : CHOL : FFA 1 : 1 : 2	$25.6 \pm 1.2^\#$	n.a.
psoriasis model	PS SCS	CER : CHOL : FFA 1 : 1.2 : 0.5	14.5 ± 1.1	0.3 ± 0.2
winter xerosis model	WX SCS	CER*: CHOL : FFA 1 : 1 : 1	15.6 ± 2.6	0.9 ± 0.8
recessive X-linked ichthyosis	RXLI SCS	CER : CHOL : FFA : ChSO_4 1 : 1 : 1 : 0.33	46.2 ± 5.5	0.1 ± 0.3

* In the CER composition of the winter xerosis model 50% of the CER(EOS)-linoleate is replaced by CER(EOS)-oleate.

† For the equimolar SCS, J_{ss} and τ were obtained in a previous study (1).

For the SCS with a high FFA level, J_{ss} was determined from the last 4 flux values, therefore τ could not be calculated.

2.2 Preparation of the model lipid mixtures

For the preparation of the SCS models, CHOL, synthetic CER and FFA were used in the appropriate molar ratio according to the different models. In Table 1 the ratios of the main lipid classes are displayed for the models used in this study. The main CER subclasses we have available consist of either a sphingosine (S) or phytosphingosine (P) base, whereas the acyl chain is a nonhydroxy (N), α -hydroxy (A) or ω -hydroxy chain (3). The corresponding nonhydroxy and α -hydroxy CER that are used in this study are denoted as CER NP, CER NS, CER AP and CER AS. The ω -hydroxy CER possesses a longer acyl chain length (C30) and has a linoleic or oleic acid ester-linked to their ω -hydroxy group (indicated with EO). In our study we use two such acylCERs, denoted as CER(EOS)-linoleate and CER(EOS)-oleate. For the ceramides mixture (CER) the following synthCER

composition was selected (see figure 1): CER(EOS)C30-linoleate, CER(NS)C24, CER(NP)C24, CER(AS)C24, CER(NP)C16 and CER(AP)C24 in a 15:51:16:4:9:5 molar ratio, similar as observed in pig SC (25). The acyl chain length of the various CER subclasses is either 30 C atoms (C30), 24 C atoms (C24) or 16 C atoms (C16). For the free fatty acids mixture (FFA), the following composition was selected: C16:0, C18:0, C20:0, C22:0, C23:0, C24:0 and C26:0 at a molar ratio of 1.8:4.0:7.7:42.6:5.2:34.7:4.1 respectively. This chain length distribution is based on the reported FFA composition in SC (17). For each model the appropriate amounts of individual lipids were dissolved in chloroform:methanol (2:1 v/v). After evaporation of the organic solvent under a stream of nitrogen, the lipid mixtures were re-dissolved either in hexane:ethanol 2:1 v/v (for models used in permeability and X-ray studies) or in chloroform:methanol 2:1 v/v (for models used in FTIR studies) at a total lipid concentration of 4.5 mg/ml.

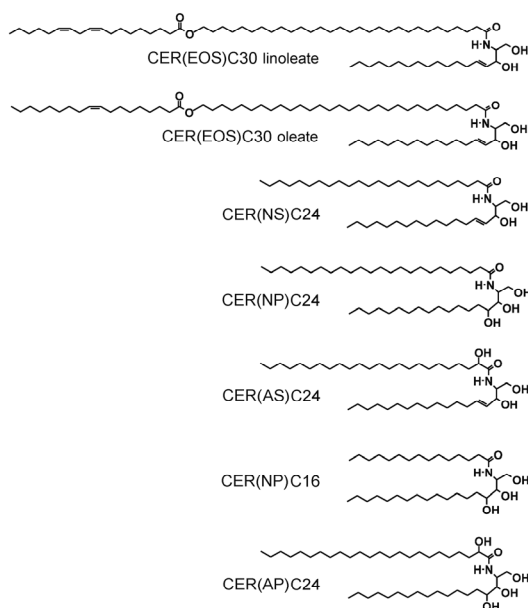


Figure 1: Molecular structure of the synthetic CER selected for the lipid mixtures (see Table 1). The nomenclature is according to Motta et al (3).

2.3 Preparation of SCS models for in vitro permeability studies

A Linomat IV (Camag, Muttenz, Switzerland) extended with a y-axis arm was used to spray lipids in hexane:ethanol solution from a distance of 1 mm onto a porous filter substrate. The spraying flow rate was 5.0 $\mu\text{l}/\text{min}$ at a movement speed of 1.0 cm/s. In an area of $8 \times 8 \text{ mm}^2$ 0.90 mg of lipids was applied per SCS model. After spraying, the SCS was equilibrated at around 80°C. After an equilibration period of at least 10 minutes, the SCS was cooled down to room temperature in approximately 30 minutes.

2.4 Preparation of lipid models for FTIR studies

Sample preparation for FTIR was the same as above, but instead 1.5 mg of lipids in a chloroform:methanol solution was sprayed in an area of $1 \times 1 \text{ cm}^2$ on an AgBr window. The sample was equilibrated for 10 min at around 80°C and slowly cooled down to room temperature in about 30 min. Subsequently, the lipid layer was covered with 25 μl of deuterated acetate buffer pH 5 (50 mM) and stored at 37°C for 24h to fully hydrate the sample. Finally, to homogenize the sample, five freeze-thawing cycles of 3h each were carried out between -20°C and RT (28).

2.5 Permeability studies

In vitro permeation studies were performed using PermeGear inline diffusion cells (Bethlehem PA, USA) with a diffusion area of 0.28 cm^2 . The SCS models were mounted in the diffusion cells and were hydrated for 1 h in phosphate-buffered saline (PBS: NaCl, Na_2HPO_4 , KH_2PO_4 and KCL in MQ water with a concentration of 8.13, 1.14, 0.20 and 0.19 g/l respectively) at pH 7.4 prior to the experiment. The donor compartment was filled with 1.4 ml of BA (MW 122 g/mol) solution in PBS (pH 7.4) at a 2.0 mg/ml concentration. BA has a $\log P_{\text{oct/water}}$ value of about 1.7. The acceptor phase consisted of PBS (pH 7.4), which was perfused at a flow rate of about 2 ml/h. The acceptor phase was stirred with a magnetic stirrer. The volume per collected fraction was determined by weighing. Each experiment was performed under

occlusive conditions, by closing the opening of the donor compartment with adhesive tape. To mimic the in vivo conditions as close as possible the temperature of the SCS was maintained at 32°C during the permeation studies, using a thermo-stated water bath.

Steady state fluxes and lag-times were determined from a plot of the cumulative permeated amount. The steady state flux (J_{SS}) is the slope of the linear part of this graph and the lag-time (τ) is determined by regression of this linear part to the time when the permeated amount is 0.

2.6 FTIR studies

All spectra were acquired on a BIORAD FTS4000 FTIR spectrometer (Cambridge, Massachusetts) equipped with a broad-band mercury cadmium telluride detector, cooled with liquid nitrogen. The sample cell was closed by two AgBr windows. The sample was under continuous dry air purge starting 1 hour before the data acquisition. The spectra were collected in transmission mode, as a co-addition of 256 scans at 1 cm^{-1} resolution during 4 minutes. In order to detect the phase transitions, the sample temperature was increased at a heating rate of 0.25°C/min, resulting in a 1°C temperature rise per recorded spectrum. The spectra were collected between 0°C and 90°C. The software used was Win-IR pro 3.0 from Biorad (Cambridge, Massachusetts). The spectra were deconvoluted using a half-width of 5 cm^{-1} and an enhancement factor of 2.0.

2.7 Determining the midpoint temperature of the melting transition and fitting of the rocking vibrations in FTIR

In FTIR, the frequency of the symmetric stretching maximum as function of temperature depicts the transition of the lipids to a liquid phase (29, 30). The midpoint temperature (T_m) of the melting transition was determined as the temperature at which the frequency increase is halfway between two fitted straight parts of the curve before and after the transition. The straight parts before and after the transition are fitted by linear fits and

the data point closest to the transition that deviates from the linear fit is chosen as the beginning or end point of the melting transition. This method for determining T_m is depicted in figure 2B-ii.

The frequency of the two rocking maxima as function of temperature depict the phase transition from an orthorhombic to a hexagonal lateral packing (31, 32). During this transition, at those temperatures at which no separate peaks could be distinguished but only an asymmetric peak, two components were fitted to the rocking vibrations in order to determine the position of the high-frequency component. The curve-fitting procedure was as follows: First, in the range from 635 to 900 cm^{-1} in the FTIR spectrum a baseline was created with a constant value corresponding to the lowest value in that part of the spectrum. Subsequently the two components present in the spectrum were fitted with two Lorentzian peak shapes using a least squares approximation. The position of the maximum of the high-frequency component was subsequently used in the plot of the rocking frequencies as function of temperature. In this plot, the positions of the high-frequency component are displayed until a temperature is reached at which the high-frequency component could no longer be fitted.

2.8 SAXD studies

X-ray diffraction was used to obtain information about the lamellar organization (i.e., the repeat distance of a lamellar phase) and the orientation of the lamellae. The SCS was mounted parallel to the primary beam in a temperature controlled sample holder with mica windows. Static diffraction patterns were collected for 1 minute at 25°C. The scattering intensity I (in arbitrary units) was measured as a function of the scattering vector q (in reciprocal nm). The latter is defined as $q=(4\pi\sin\theta)/\lambda$, in which θ is the scattering angle and λ is the wavelength. From the positions of a series of equidistant peaks (q_n), the periodicity, or d-spacing, of a lamellar phase was calculated using the equation $q_n=2n\pi/d$, with n being the order number of the diffraction peak. One-dimensional intensity profiles were

obtained by transformation of the two-dimensional SAXD detector pattern from Cartesian (x,y) to polar (ρ,θ) coordinates and subsequently integrating over θ . All measurements were performed at the European Synchrotron Radiation Facility (ESRF, Grenoble) using station BM26B. The X-ray wavelength and the sample-to-detector distance were 0.113 nm and 0.419 m respectively. Diffraction data were collected on a Frelon 2000 CCD detector with 2048×2048 pixels at 14 μm spatial resolution and 5x magnification. The spatial calibration of this detector was performed using silver behenate ($d=5.838$ nm) and the two strongest reflections of high density polyethylene (HDPE, $d=0.4166$ and 0.378 nm).

3. Results

To assess the barrier properties of the various SCS models, the permeation of the model compound BA has been measured at the skin temperature of about 32°C. To correlate permeability with lipid organization, the lipid organization has been examined with FTIR and SAXD. The various model compositions, steady state flux values and lag-times are presented in Table 1.

3.1 Influence of the CER:CHOL:FFA ratio on the barrier function

To determine the role of each of the lipid classes on the lipid composition and permeability, SCS varying systematically in CER:CHOL:FFA composition were examined. The fluxes are provided in Table 1. In this table the flux across SCS with an equimolar CER:CHOL:FFA composition that was reported previously (1), is also provided. In figure 2A-i the BA flux profile across the SCS with a CER:CHOL:FFA molar ratio of 2:1:1 is shown. The steady state flux is 22.5 ± 1.8 $\mu\text{g}/\text{cm}^2/\text{h}$ and the lag-time is -0.3 ± 0.5 h.

Skin lipid models with varying compositions

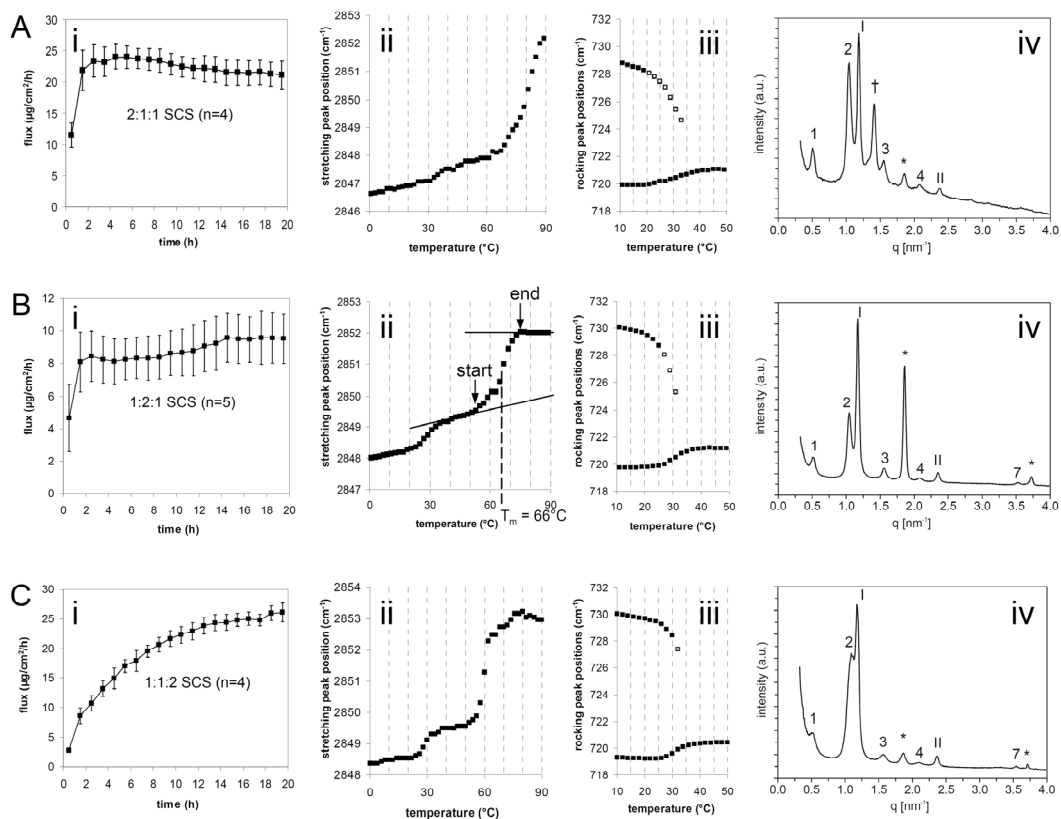


Figure 2: i) Plots of the BA permeation versus time, ii) CH₂ symmetric stretching frequency as function of temperature, iii) thermotropic response of the FTIR CH₂ rocking frequencies and iv) the SAXD pattern of A) SCS in 2:1:1 CER:CHOL:FFA molar ratio, B) SCS in a 1:2:1 CER:CHOL:FFA molar ratio C) SCS in a 1:1:2 CER:CHOL:FFA molar ratio. In the SAXD patterns, the Arabic numbers denote diffraction orders of the LPP, the Roman numbers indicate reflections assigned to the SPP and asterisks mark the reflections of crystalline CHOL. The reflection that was assigned to an additional lamellar phase is indicated by a cross. In the figures depicting the CH₂ rocking vibrations the open squares are calculated with the peak fitting procedure.

The CH₂ symmetric stretching frequencies in the infrared spectrum provide information about the conformational ordering of the lipid tails. The

position of the CH₂ symmetric stretching vibration as function of temperature is plotted in figure 2A-ii. At 20°C this frequency is 2846.9 cm⁻¹, indicating a high conformational ordering. When increasing the temperature, between 30 and 40°C a weak shift is observed in frequency from 2847.1 to 2847.5 cm⁻¹. Although not very pronounced, it indicates an orthorhombic to hexagonal transition. Increasing the temperature leads to another shift in frequency from 2848.1 to 2852.2 cm⁻¹ between 65 and 89°C, revealing the transition to a liquid phase, with a midpoint temperature of T_m = 80°C.

The FTIR rocking frequencies provide detailed information on the lateral packing. Due to short range coupling, the orthorhombic packing is characterized by a doublet at approximately 720 and 730 cm⁻¹, while the hexagonal packing is characterized by a singlet at a vibration frequency of approximately 720 cm⁻¹. The thermotropic response of the rocking frequencies in figure 2A-iii shows a shift of the high frequency component from 728.0 to 724.6 cm⁻¹ between 21 and 33°C, suggesting the transition from an orthorhombic to a hexagonal lateral packing in this temperature region.

The SAXD pattern of the 2:1:1 SCS in figure 2A-iv displays four diffraction peaks that can be ascribed to a LPP with a periodicity of 12.0 nm and two reflections attributed to a SPP with periodicity of 5.3 nm. Furthermore, an additional diffraction peak is observed indicative for an additional phase with a periodicity of 4.4 nm, most likely due to phase separated CER-rich domains. The peak at $q = 1.85 \text{ nm}^{-1}$ indicates the presence of a low level of phase separated crystalline CHOL.

The SCS with elevated CHOL level was also studied. The permeability of the SCS with a CER:CHOL:FFA composition of 1:2:1 is displayed in figure 2B-i. This figure demonstrates that by increasing the CHOL levels the BA flux drastically reduces since the steady state flux is only $9.0 \pm 1.5 \text{ } \mu\text{g}/\text{cm}^2/\text{h}$. The lag-time of this membrane is $0.6 \pm 0.6 \text{ h}$.

The thermotropic response of the CH₂ stretching frequencies is provided in figure 2B-ii. There is a gradual increase in the frequencies from 0

to 20°C. At 20°C, the symmetric stretching frequency is 2848.3 cm⁻¹, denoting the presence of conformational ordered phases. A further increase in temperature from 21 to 37°C results in a shift in frequency from 2848.3 to 2849.1 cm⁻¹, indicative for the orthorhombic-hexagonal phase transition. Upon further heating, between 50 and 79°C a second transition is observed from 2849.4 to 2852.0 cm⁻¹, demonstrating the formation of a liquid phase. The midpoint temperature of this transition is 66°C.

The rocking frequencies are displayed in figure 2B-iii. The orthorhombic to hexagonal transition is shown by a shift of the high frequency component from 729.5 to 725.3 cm⁻¹ between 21 and 31°C.

The SAXD pattern of the 1:2:1 SCS is displayed in figure 2B-iv with diffraction peaks attributed to the LPP and SPP. However, the diffraction peaks attributed to crystalline CHOL have a high intensity, demonstrating a high level of phase separated CHOL.

The level of the third main class of lipids is also increased in the SCS. In figure 2C-i the permeability curve of SCS with a CER:CHOL:FFA molar ratio of 1:1:2 is displayed. From this figure it is clear that a steady state flux is not reached within the 20 h of permeation. The flux value was calculated as a mean of the flux values between 16 and 20 h of permeation and is 25.6 ± 1.2 µg/cm²/h. The lag-time could not be determined due to the absence of a steady state flux.

The thermotropic CH₂ stretching response is provided in figure 2C-ii. At low temperatures the lipid tails are in a conformational ordering as shown by the CH₂ stretching frequency of 2848.6 cm⁻¹ at 20°C. Upon increasing the temperature, a clear shift in frequency from 2848.6 to 2849.5 cm⁻¹ is observed between 22 and 38°C, demonstrating the orthorhombic to hexagonal phase transition. When further increasing the temperature, another shift in wavenumber from 2849.6 to 2852.8 cm⁻¹ is visible between 50 and 72°C denoting the transition to a liquid phase with a midpoint temperature of 60°C.

The orthorhombic to hexagonal phase transition is also monitored by the thermotropic CH_2 rocking response as displayed in figure 2C-iii: A shift of the high frequency component from 729.5 to 727.4 cm^{-1} is observed between 24 and 32°C. When increasing the temperature further a weak orthorhombic component remained in the rocking curve until a temperature of 60°C. This indicates that the majority of the lipids forms a hexagonal lateral packing around 34°C, but a small fraction of phase separated FFA remains in the orthorhombic packing until a temperature of about 60°C is reached (28). At this temperature the crystalline FFA starts to transform into a liquid phase.

The SAXD pattern of the model with high FFA level is displayed in figure 2C-iv. It depicts two diffraction peaks attributed to the SPP with a periodicity of 5.3 nm. Five diffraction peaks could be identified that are attributed to the LPP with a periodicity of 12.0 nm. The two peaks at $q = 1.85$ and 3.7 nm^{-1} indicate the presence of a low level of phase separated crystalline CHOL. The elevated FFA level did not result in an additional phase with a long range ordering.

3.2 The permeability and phase behaviour of SCS with a lipid composition based on that in dry or diseased skin

The lipid organization and barrier properties of models with compositions related to dry skin (winter xerosis), recessive X-linked ichthyosis and psoriasis skin were also examined.

Due to seasonal influences the lipid composition in the SC is reported to undergo changes. Focussing on the CER subclasses, in the winter season the relative level of CER(EOS)-oleate is increased at the expense of CER(EOS)-linoleate (21, 33). To mimic this aspect of the SC composition of dry skin (winter xerosis), 50% of the CER(EOS)-linoleate was replaced by CER(EOS)-oleate in the SCS. The SCS that mimics the composition in SC of dry skin is referred to as WX SCS. The permeation

curve of BA through WX SCS is displayed in figure 3A-i. The steady state flux is $15.6 \pm 2.6 \mu\text{g}/\text{cm}^2/\text{h}$ and the lag-time $0.9 \pm 0.8 \text{ h}$.

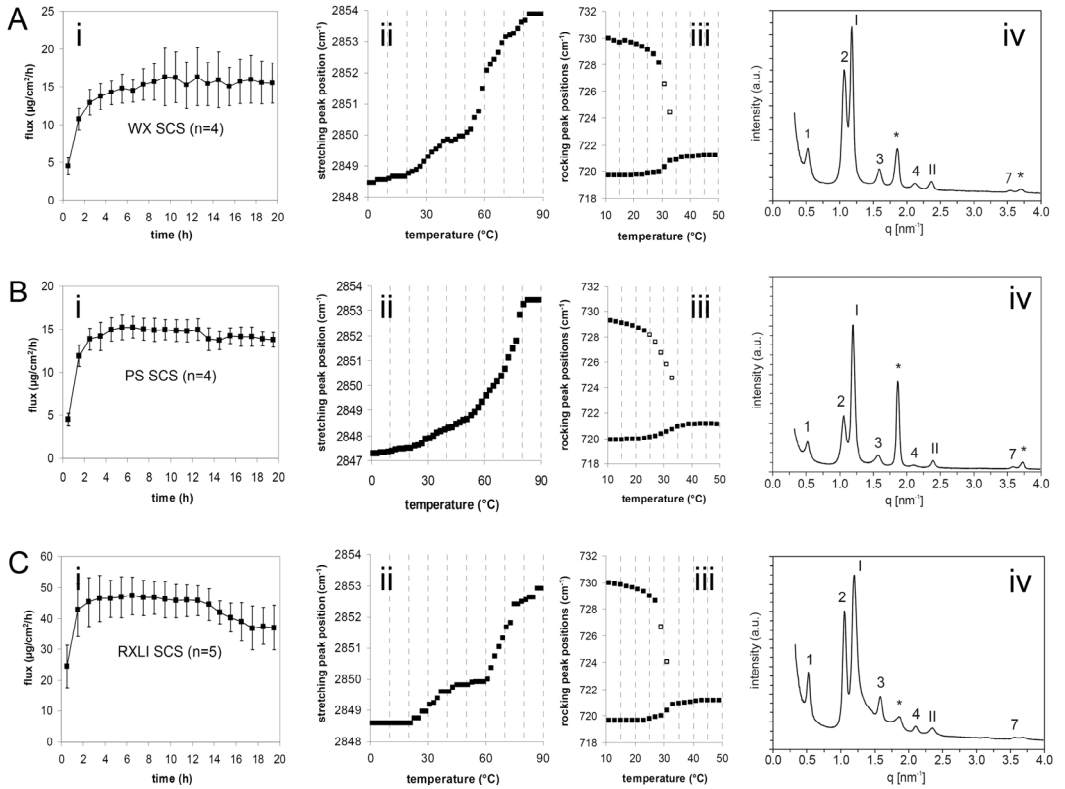


Figure 3: i) Plots of the BA permeation versus time, ii) CH₂ symmetric stretching frequency as function of temperature, iii) thermotropic response of the FTIR CH₂ rocking frequencies and iv) the SAXD pattern of A) WX SCS, B) PS SCS and C) RXLI SCS. In the SAXD patterns, the Arabic numbers denote diffraction orders of the LPP, the Roman numbers indicate reflections assigned to the SPP and asterisks mark the reflections of crystalline CHOL. In the figures depicting the CH₂ rocking vibrations the open squares are calculated with the peak fitting procedure.

The thermotropic response of the CH₂ symmetric stretching peak is plotted in figure 3A-ii. At low temperatures, a gradual increase in frequency is observed up to 2848.7 cm⁻¹ at 20°C. Upon increasing the temperature from 21 to 41°C a shift in wavenumber from 2848.8 to 2849.9 cm⁻¹ is detected, indicating the orthorhombic to hexagonal phase transition. When further increasing the temperature, a liquid phase is formed between 51 and 73°C as denoted by a shift from 2850.1 to 2853.2 cm⁻¹. The midpoint temperature of this transition is 60°C.

The FTIR rocking frequencies displayed in figure 3A-iii show a shift of the high frequency component from 729.1 to 724.4 cm⁻¹ between 25 and 33°C, characteristic for the orthorhombic-hexagonal transition.

The SAXD pattern of WX SCS is shown in figure 3A-iv. It displays two diffraction peaks attributed to a SPP with a periodicity of 5.3 nm and five diffraction peaks assigned to the LPP with a periodicity of 12.0 nm. Crystalline CHOL is also present, as indicated by two diffraction peaks at $q = 1.85$ and 3.7 nm^{-1} .

Besides a change in CER:CHOL:FFA molar ratio, a difference in the CER composition of psoriatic scale, compared to normal human stratum corneum, is reported in literature (3, 20). However, in our present studies we will only focus on the change in CER:CHOL:FFA molar ratio on the permeability, to establish whether this change can account for an increased permeability in psoriasis skin. Based on the results of Motta et al, the CER:CHOL:FFA molar ratio in the SCS model was adapted to 1.0:1.2:0.5 (20). This model is referred to as PS SCS. The flux profile of PS SCS is displayed in figure 3B-i, displaying a steady state flux of $14.5 \pm 1.1 \mu\text{g}/\text{cm}^2/\text{h}$ and a lag-time of $0.3 \pm 0.2 \text{ h}$.

The thermotropic response of the CH₂ stretching vibrations is displayed in figure 3B-ii. The maximum of the symmetric stretching frequencies at 20°C is 2847.5 cm⁻¹. Upon increasing the temperature, a small shift in peak position is visible around 30°C, possibly revealing the orthorhombic to hexagonal transition. Upon further heating, a shift in

wavenumber is visible between 50 and 80°C, indicative for the transition to a liquid phase. This transition has a T_m of 72°C.

The FTIR rocking frequencies in figure 3B-iii show a gradual shift of the high frequency component from 728.2 to 724.8 cm^{-1} between 25 and 33°C, indicating the transition from orthorhombic to hexagonal lateral packing.

The SAXD pattern of PS SCS is depicted in figure 3B-iv. It displays two diffraction orders associated to a SPP, with a periodicity of 5.2 nm. Also, four diffraction peaks assigned to a LPP with a periodicity of 12.0 nm are observed. A high amount of CHOL is phase separated as reflected by the high intensity of the diffraction peaks attributed to crystalline CHOL.

The pathological scaling in recessive X-linked ichthyosis skin is associated with accumulation of abnormally high quantities of ChSO_4 in the SC (18, 19, 22). On this basis, we prepared a model for the lipid composition by addition of ChSO_4 at a molar ratio of 0.33. This model is referred to as RXLI SCS. The permeation curve of BA through RXLI SCS is displayed in figure 3C-i, showing a high steady state flux of $46.2 \pm 5.5 \mu\text{g}/\text{cm}^2/\text{h}$ and a short lag-time of $0.1 \pm 0.3 \text{ h}$.

The FTIR stretching maxima in figure 3C-ii display a constant value of 2848.6 cm^{-1} from 0 to 20°C, indicating conformational ordering of the lipid tails. Upon increasing the temperature, a first shift from 2848.6 to 2849.6 cm^{-1} is observed between 20 and 40°C, representative for an orthorhombic to hexagonal transition. Further increasing the temperature leads to a second shift in wavenumber from 2849.9 to 2852.4 cm^{-1} between 59 and 77°C, representing the transition to a fluid phase with a midpoint temperature of 68°C.

The FTIR rocking frequencies of RXLI SCS in figure 3C-iii reveal a change from orthorhombic to hexagonal transition as shown by a change in high frequency component from 729.0 to 724.0 cm^{-1} between 25 and 31°C.

The SAXD pattern of RXLI SCS is displayed in figure 3C-iv. It displays two diffraction peaks attributed to a SPP with a periodicity of 5.3

nm. The first order reflection of the SPP is broad and contains a shoulder at approximately $q = 1.4 \text{ nm}^{-1}$ which could indicate the formation of an additional phase. Furthermore, five diffraction peaks are observed assigned to the LPP with a periodicity of 12.0 nm. The two diffraction peaks that are associated to crystalline CHOL are low in intensity, indicating a low level of phase separated CHOL.

4. Discussion

In the studies described in this paper we focused on a systematic change in lipid composition to relate lipid composition and organization with permeability. For this purpose we utilized a SC model membrane to unravel the role the various lipid classes play in the skin barrier function. In addition we focused on the lipid permeability in diseased and dry skin. For this purpose we constructed models for the SC lipid composition reported in winter xerosis, psoriasis and recessive X-linked ichthyosis skin. To study the permeability of the various models we used BA as a model drug.

4.1 The order-disorder transition temperature is related to the symmetric CH_2 stretching vibrations of the lipid tails at 20°C

When closely examining the FTIR data of all models it is observed that the models with a high conformational order at room temperature (i.e. low wavenumber of the CH_2 symmetric stretching peak position at 20°C) exhibit a relatively high melting transition midpoint temperature. To gain more insight into this relationship we plotted the CH_2 symmetric stretching vibration at 20°C against the midpoint temperature of the melting transition in each model, see figure 4. Although the midpoint temperature of the melting transition has no physical meaning, as the symmetric stretching peak in FTIR is composed of several vibrational components, it enables us to determine whether this phase transition is related to the conformational order of the lipid chains at 20°C. We also included data of the equimolar SCS and

a model with short chain FFA, examined in a previous study (2). As depicted in figure 4, a linear correlation is observed: the symmetric stretching wavenumber (chain conformation) at 20°C decreases linearly with increasing melting transition T_m .

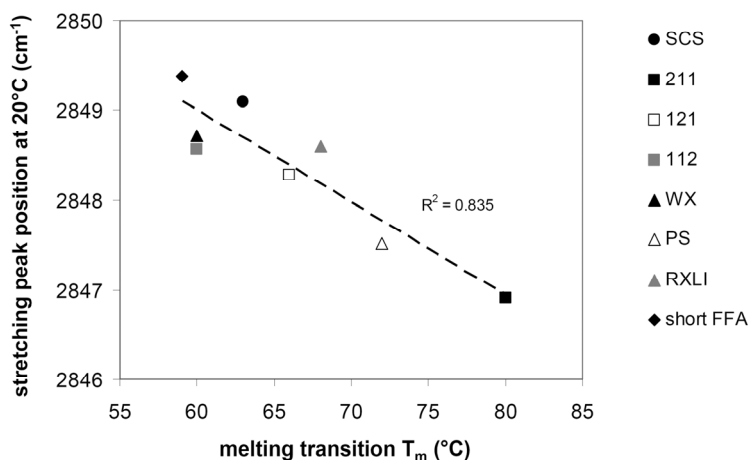


Figure 4: The midpoint temperature of the melting transition as function of the conformational order at 20°C. Depicted are data of all models used in this study plus data of equimolar SCS and of a model with short chain FFA, examined in a previous study (2).

From this graph it is clear that when using the same ceramide composition, an increase in conformational ordering results in an increase in the melting transition T_m . When focusing on those samples in which the FFA content varied, the results are quite remarkable. Although the FFA induces the formation of an orthorhombic lateral packing, it also induces a reduction in the ordering of the chains and a reduction in the T_m . This might be due to the change in headgroup interactions, as it has been suggested (based on pure ceramides but also on mixtures) that an increase in hydrogen bond density in the headgroup region increases the conformational ordering and raises the T_m of the order-disorder transition (34, 35). This suggests that the

addition of FFA increases the packing density but reduces the number of hydrogen bonds.

4.2 Deviation from the equimolar CER:CHOL:FFA ratio observed in human SC does not always result in a decreased barrier function

As it has been suggested that the lipid composition and organization play an important role in the skin barrier, in this study we examined the effect of the lipid composition and organization of the SCS on its permeability. In previous studies we reported the permeability and lipid phase behavior of the equimolar CER:CHOL:FFA SCS, mimicking the lipid composition and skin barrier of healthy subjects (1, 2). The BA steady state flux across this SCS was $24 \pm 2 \mu\text{g}/\text{cm}^2/\text{h}$ and the lag-time was $1.1 \pm 0.5 \text{ h}$ (1). From the FTIR data presented in a recent study (2), the midpoint temperature of the transition from a hexagonal to a liquid phase was 63°C and the orthorhombic-hexagonal transition occurred between 20 and 36°C . In the same study we observed that the flux of BA was more sensitive for a change in the lamellar phases than for a phase change from an orthorhombic to a hexagonal packing. In the present study we varied the lipid composition by increasing the level of either CER, CHOL or FFA. The formation of a hexagonal phase in these studies is not determinative for the changes in flux.

When increasing the level of CER or CHOL by a factor two compared to the equimolar ratio, the X-ray diffraction curves clearly revealed phase separation. In the SCS with 2:1:1 CER:CHOL:FFA an additional 4.4 nm phase was detected, while the CER:CHOL:FFA 1:2:1 SCS resulted in an enhanced level of phase separated crystalline CHOL. The additional 4.4 nm phase did not affect the permeability, while the higher level of phase separated CHOL in the SCS led to a twofold reduction in the permeability. The CHOL domains consist of densely packed three dimensional crystals resulting in many spots and reflections in the WAXD pattern (not shown). If

these three dimensional crystals are not very permeable to BA, it will result in a reduction of the effective diffusion area of the SCS and in an increase in the permeation pathway. This will lead to a reduction in the steady state flux. As far as the 4.4 nm phase is concerned, our results indicate that this phase has a similar layered structure as the SPP as no features in the diffraction pattern are observed indicating the presence of a three dimensional crystalline structure (wide angle X-ray data, unpublished results). This may explain why no change in permeability is observed in the presence of the 4.4 nm phase.

When comparing with the in vivo situation, the 4.4 nm phase was never observed in diffraction patterns of isolated human SC. However, the presence of crystalline CHOL is frequently observed in human SC (11, 36). Therefore, the observation that an increase in phase separated crystalline CHOL results in an increase in the skin barrier function is relevant for the in vivo situation.

In the 1:1:2 CER:CHOL:FFA SCS no phase separation of FFA is observed when focusing on the long range ordering (lamellar phases). However, the presence of a small shoulder was noticed in the high frequency component of the FTIR rocking vibrations. This shoulder was present up to about 60°C and indicates that a low level of FFA forms separate domains within the lipid lamellae. The flux of BA across the 1:1:2 CER:CHOL:FFA SCS displays a very long lag-time. As we used a PBS buffer of pH 7.4 in the donor and acceptor phase and the pK_a of FFA in ceramide containing mixtures is around 6.3 (37), the increase in lag-time may occur by an ionization of the FFA, which may be more pronounced at a high level of FFA, or in phase separated FFA domains within the lipid lamellae.

As far as the diseased skin models are concerned, in these studies we are limited by the information available in literature. Although changes in the composition of the lipid classes have been reported for cosmetically dry skin and for psoriasis, no information is available on the FFA and CER chain

length distribution compared to that in skin of healthy subjects. A reduction in chain length of the CER and FFA may have a profound effect on the lipid organization and permeability. For this reason our studies only provide information on the changes in permeability caused by the reported changes in the composition of the main lipid classes in the various skin diseases.

For both the WX SCS and PS SCS the steady state flux and lag-time is similar to that in the equimolar CER:CHOL:FFA SCS. The lamellar lipid organization of these models is also similar to that in the equimolar SCS and as the lamellar organization is a crucial factor in the skin permeability (2, 14), it is not surprising that the WX SCS and PS SCS have a barrier function that is similar to the equimolar SCS. Although winter xerosis skin is known to be susceptible and displays a faulty desquamation (38, 39) and psoriasis skin is characterized by a deranged keratinization process and an impaired barrier function (40), our results with BA as permeant demonstrate that the reported changes in CER(EOS)-oleate/linoleate ratio in dry skin or in CER:CHOL:FFA ratio in psoriasis skin may not be responsible for the observed impaired barrier function in vivo.

In contrast to the WX and PS models, the permeability of the RXLI model is about twice that of equimolar SCS. Therefore the enhanced permeability indicates that the increased ChSO_4 is expected to be at least partly responsible for the abnormal barrier function observed in RXLI skin (22). The reduced barrier function in our lipid model may partly be explained by the lower level of phase separated crystalline CHOL: The excess ChSO_4 present in this model reduces the amount of crystalline CHOL, similarly as previously observed in a lipid model with isolated CER (41). However, the reduced crystalline CHOL cannot explain the twofold increase in flux as the level of phase separated crystalline CHOL in the 2:1:1 and 1:1:2 CER:CHOL:FFA SCS was also lower, while no increase in permeability was observed. Therefore, other factors should play a role. Previously it was observed that ChSO_4 induces a fluid phase in mixtures with isolated CER, CHOL and FFA (42). Such a fluid phase is expected to increase the

permeability. However, at room temperature (20°C) the frequency of CH₂ symmetric stretching vibrations of the RXLI model was not shifted to a higher wavenumber as compared to equimolar SCS, indicating that the formation of a substantial level of fluid phase in SCS was not induced by the addition of ChSO₄. Perhaps the use of synthetic CER instead of isolated CER precludes the formation of a fluid phase in the RXLI SCS. In order to explain the increased permeability, we investigated the two dimensional SAXD patterns in more detail and examined the equimolar and RXLI SCS also under a polarization microscope. When examining the two dimensional detector image of the RXLI model, we observed that the increased level of ChSO₄ induces a well oriented but broad reflection, close to the position of the first order of the SPP, see figure 5. Also higher order broad reflections of this phase are observed. This indicates that an additional phase is present in the SCS. The less sharp reflections suggest a less ordered phase, which may account for the increased permeability.

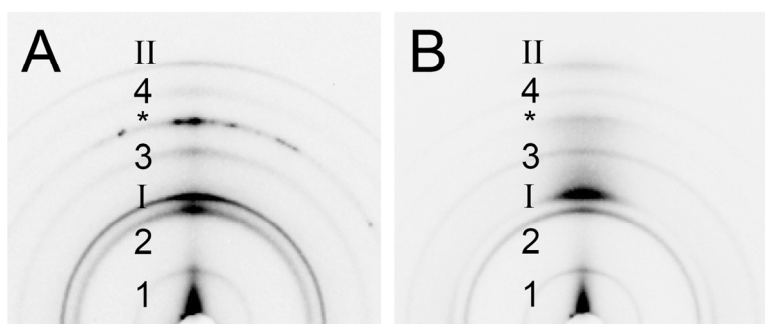


Figure 5: Two dimensional SAXD images. The Arabic numbers 1-4 denote diffraction orders of the LPP, the reflections indicated by Roman numbers I and II are assigned to the SPP and a reflection of crystalline CHOL is indicated with an asterisk. A) Diffraction pattern of the equimolar SCS B) Diffraction pattern of the RXLI model. Broader reflections are located in the centre of the ring at the same position as the 1st and 2nd order of the SPP, indicating an oriented but more disordered additional phase. The intensity of the CHOL reflection is also strongly reduced.

When further examining the RXLI model under a polarization microscope, we observed large patches that are absent in the equimolar SCS, see figure 6, confirming that an additional phase is formed by supplementing ChSO_4 .

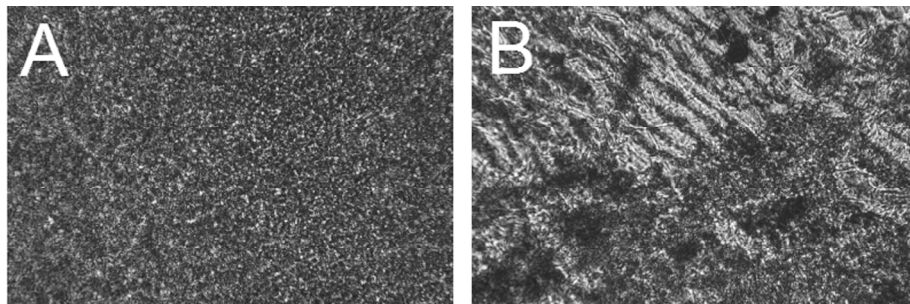


Figure 6: Polarization microscopy images using a 40x magnification. A) Equimolar SCS, displaying a uniform pattern of small domains B) The RXLI SCS, displaying large irregularly shaped domains.

In conclusion, in our studies two SCS models showed a significant change in BA steady state flux; an excess of crystalline CHOL lead to a decreased steady state flux, while an excess of ChSO_4 , as observed in X-linked ichthyosis, led to an increase in the BA steady state flux. While phase separated CHOL is crystalline and therefore possibly difficult to penetrate, there is some evidence that the additional phase induced by ChSO_4 is less ordered in nature accounting for the increased permeability. A change in CER:CHOL:FFA ratio in psoriasis skin and an increase in the CER EOS-oleate/CER EOS-linoleate ratio in dry skin may not be responsible for the impaired skin barrier function in vivo.

Acknowledgments

This work was supported by a grant from the Technology Foundation STW (LGP 7503). We thank the company Cosmoferm B.V. (Evonik) for the provision of the ceramides and the Netherlands Organization for Scientific Research (NWO) for the provision of beam time at the ESRF. Furthermore, we thank the personnel at the DUBBLE beam line at the ESRF for their support with the X-ray measurements. Finally, we thank Dr Maria Ponec for valuable discussions on the permeability studies.

References

1. Groen, D., G. S. Gooris, M. Ponec, and J. A. Bouwstra. 2008. Two new methods for preparing a unique stratum corneum substitute. *Biochim Biophys Acta* 1778:2421-2429.
2. Groen, D., D. S. Poole, G. S. Gooris, and J. A. Bouwstra. 2010. Is an orthorhombic lateral packing and a proper lamellar organization important for the skin barrier function? *Biochim Biophys Acta*.
3. Motta, S., M. Monti, S. Sesana, R. Caputo, S. Carelli, and R. Ghidoni. 1993. Ceramide composition of the psoriatic scale. *Biochim. Biophys. Acta* 1182:147-151.
4. Simonetti, O., A. J. Hoogstraate, W. Bialik, J. A. Kempenaar, A. H. Schrijvers, H. E. Bodde, and M. Ponec. 1995. Visualization of diffusion pathways across the stratum corneum of native and in-vitro-reconstructed epidermis by confocal laser scanning microscopy. *Arch Dermatol Res* 287:465-473.
5. Masukawa, Y., H. Narita, E. Shimizu, N. Kondo, Y. Sugai, T. Oba, R. Homma, J. Ishikawa, Y. Takagi, T. Kitahara, Y. Takema, and K. Kita. 2008. Characterization of overall ceramide species in human stratum corneum. *J Lipid Res* 49:1466-1476.
6. Ponec, M., A. Weerheim, P. Lankhorst, and P. Wertz. 2003. New acylceramide in native and reconstructed epidermis. *J. Invest. Dermatol.* 120:581-588.
7. Robson, K. J., M. E. Stewart, S. Michelsen, N. D. Lazo, and D. T. Downing. 1994. 6-Hydroxy-4-sphingenine in human epidermal ceramides. *J. Lipid. Res.* 35:2060-2068.
8. Stewart, M. E., and D. T. Downing. 1999. A new 6-hydroxy-4-sphingenine-containing ceramide in human skin. *J. Lipid. Res.* 40:1434-1439.
9. Wertz, P. W., M. C. Miethke, S. A. Long, J. S. Strauss, and D. T. Downing. 1985. The composition of the ceramides from human stratum corneum and from comedones. *J. Invest. Dermatol.* 84:410-412.
10. Bouwstra, J. A., G. S. Gooris, W. Bras, and D. T. Downing. 1995. Lipid organization in pig stratum corneum. *J. Lipid Res.* 36:685-695.
11. Bouwstra, J. A., G. S. Gooris, J. A. van der Spek, and W. Bras. 1991. Structural investigations of human stratum corneum by small-angle X-ray scattering. *J. Invest. Dermatol.* 97:1005-1012.
12. Bouwstra, J. A., G. S. Gooris, F. E. Dubbelaar, and M. Ponec. 2001. Phase behavior of lipid mixtures based on human ceramides: coexistence of crystalline and liquid phases. *J Lipid Res* 42:1759-1770.
13. Bouwstra, J. A., G. S. Gooris, F. E. Dubbelaar, and M. Ponec. 2002. Phase behavior of stratum corneum lipid mixtures based on human

- ceramides: the role of natural and synthetic ceramide 1. *J Invest Dermatol* 118:606-617.
14. Bouwstra, J., G. Gooris, and M. Ponc. 2002. The lipid organisation of the skin barrier: liquid and crystalline domains coexist in lamellar phases. *Journal of Biological Physics* 28:211-223.
 15. Hatta, I., N. Ohta, K. Inoue, and N. Yagi. 2006. Coexistence of two domains in intercellular lipid matrix of stratum corneum. *Biochim Biophys Acta* 1758:1830-1836.
 16. White, S. H., D. Mirejovsky, and G. I. King. 1988. Structure of lamellar lipid domains and corneocyte envelopes of murine stratum corneum. An X-ray diffraction study. *Biochemistry* 27:3725-3732.
 17. Wertz, P. 1991. Epidermal lipids. In *Physiology, Biochemistry and Molecular Biology of the Skin*. L. A. Goldsmith, editor. Oxford University Press, Oxford. 205-235.
 18. Williams, M. L., and P. M. Elias. 1981. Stratum corneum lipids in disorders of cornification: increased cholesterol sulfate content of stratum corneum in recessive x-linked ichthyosis. *J Clin Invest* 68:1404-1410.
 19. Elias, P. M., M. L. Williams, M. E. Maloney, J. A. Bonifas, B. E. Brown, S. Grayson, and E. H. Epstein, Jr. 1984. Stratum corneum lipids in disorders of cornification. Steroid sulfatase and cholesterol sulfate in normal desquamation and the pathogenesis of recessive X-linked ichthyosis. *J Clin Invest* 74:1414-1421.
 20. Motta, S., S. Sesana, R. Ghidoni, and M. Monti. 1995. Content of the different lipid classes in psoriatic scale. *Arch Dermatol Res* 287:691-694.
 21. Rogers, J., C. Harding, A. Mayo, J. Banks, and A. Rawlings. 1996. Stratum corneum lipids: the effect of ageing and the seasons. *Arch Dermatol Res* 288:765-770.
 22. Zettersten, E., M. Q. Man, J. Sato, M. Denda, A. Farrell, R. Ghadially, M. L. Williams, K. R. Feingold, and P. M. Elias. 1998. Recessive x-linked ichthyosis: role of cholesterol-sulfate accumulation in the barrier abnormality. *J Invest Dermatol* 111:784-790.
 23. McIntosh, T. J. 2003. Organization of skin stratum corneum extracellular lamellae: diffraction evidence for asymmetric distribution of cholesterol. *Biophys J* 85:1675-1681.
 24. Kuempel, D., D. C. Swartzendruber, C. A. Squier, and P. W. Wertz. 1998. In vitro reconstitution of stratum corneum lipid lamellae. *Biochim. Biophys. Acta* 1372:135-140.
 25. Bouwstra, J. A., G. S. Gooris, K. Cheng, A. Weerheim, W. Bras, and M. Ponc. 1996. Phase behavior of isolated skin lipids. *J. Lipid Res.* 37:999-1011.
 26. de Jager, M., W. Groenink, R. Bielsa i Guivernau, E. Andersson, N. Angelova, M. Ponc, and J. Bouwstra. 2006. A novel in vitro percutaneous penetration model: evaluation of barrier properties

- with p-aminobenzoic acid and two of its derivatives. *Pharm. Res.* 23:951-960.
27. de Jager, M., W. Groenink, J. van der Spek, C. Janmaat, G. Gooris, M. Ponec, and J. Bouwstra. 2006. Preparation and characterization of a stratum corneum substitute for in vitro percutaneous penetration studies. *Biochim. Biophys. Acta* 1758:636-644.
 28. Gooris, G. S., and J. A. Bouwstra. 2007. Infrared spectroscopic study of stratum corneum model membranes prepared from human ceramides, cholesterol, and fatty acids. *Biophys J* 92:2785-2795.
 29. Snyder, R. G., S. L. Hsu, and S. Krimm. 1978. Vibrational-Spectra in C-H Stretching Region and Structure of Polymethylene Chain. *Spectrochimica Acta Part a-Molecular and Biomolecular Spectroscopy* 34:395-406.
 30. Wolfangel, P., R. Lehnert, H. H. Meyer, and K. Muller. 1999. FTIR studies of phospholipid membranes containing monoacetylenic acyl chains. *Physical Chemistry Chemical Physics* 1:4833-4841.
 31. Snyder, R. G. 1960. Vibrational Spectra of Crystalline N-Paraffins .1. Methylene Rocking and Wagging Modes. *Journal of Molecular Spectroscopy* 4:411-434.
 32. Moore, D. J., M. E. Rerek, and R. Mendelsohn. 1997. Lipid domains and orthorhombic phases in model stratum corneum: Evidence from Fourier transform infrared spectroscopy studies. *Biochemical and Biophysical Research Communications* 231:797-801.
 33. Conti, A., J. Rogers, P. Verdejo, C. R. Harding, and A. V. Rawlings. 1996. Seasonal influences on stratum corneum ceramide 1 fatty acids and the influence of topical essential fatty acids. *Int J Cosmet Sci* 18:1-12.
 34. Rerek, M. E., H. Chen, B. Markovic, D. van Wyck, P. Garidel, R. Mendelsohn, and D. J. Moore. 2001. Phytosphyngosine and Sphingosine Ceramide Headgroup Hydrogen Bonding: Structural Insights through Thermotropic Hydrogen/Deuterium Exchange. *J Phys Chem B* 105:9355-9362.
 35. Janssens, M., G. S. Gooris, and J. A. Bouwstra. 2009. Infrared spectroscopy studies of mixtures prepared with synthetic ceramides varying in head group architecture: coexistence of liquid and crystalline phases. *Biochim Biophys Acta* 1788:732-742.
 36. Garson, J. C., J. Doucet, J. L. Leveque, and G. Tsoucaris. 1991. Oriented structure in human stratum corneum revealed by X-ray diffraction. *J Invest Dermatol* 96:43-49.
 37. Gomez-Fernandez, J. C., and J. Villalain. 1998. The use of FT-IR for quantitative studies of the apparent pKa of lipid carboxyl groups and the dehydration degree of the phosphate group of phospholipids. *Chem Phys Lipids* 96:41-52.
 38. Rawlings, A. V., J. Hope, J. Rogers, A. M. Mayo, and I. R. Scott. 1992. Mechanisms of desquamation: new insights into dry flaky skin

- conditions. In Proceedings of the 17th IFSCC International Congress. 865-880.
39. Rawlings, A. V., A. Watkinson, J. Rogers, A. M. Mayo, J. Hope, and I. R. Scott. 1994. Abnormalities in Stratum-Corneum Structure, Lipid-Composition, and Desmosome Degradation in Soap-Induced Winter Xerosis. *Journal of the Society of Cosmetic Chemists* 45:203-220.
 40. Marks, J., S. Rogers, B. Chadkirk, and S. Shuster. 1981. Clearance of Chronic Plaque Psoriasis by Anthralin - Subjective and Objective Assessment and Comparison with Photochemotherapy. *British Journal of Dermatology* 105:96-99.
 41. Bouwstra, J. A., G. S. Gooris, F. E. Dubbelaar, and M. Ponc. 1999. Cholesterol sulfate and calcium affect stratum corneum lipid organization over a wide temperature range. *J Lipid Res* 40:2303-2312.
 42. Bouwstra, J. A., G. S. Gooris, F. E. Dubbelaar, A. M. Weerheim, and M. Ponc. 1998. pH, cholesterol sulfate, and fatty acids affect the stratum corneum lipid organization. *J Investig Dermatol Symp Proc* 3:69-74.

Chapter 5

Model membranes prepared with ceramide EOS, cholesterol and free fatty acids form a very unique lamellar phase

Daniël Groen, Gerrit S. Gooris, Joke A. Bouwstra

Langmuir, vol. 26, no. 6, pp. 4168-75.

Abstract

The lipid matrix present in the human stratum corneum (the thin, uppermost layer of the skin) is considered to play a crucial role in the skin barrier function. The lipid matrix consists of ceramides, cholesterol and free fatty acids. The 13 nm lamellar phase present in the lipid matrix of the stratum corneum is very characteristic and plays an important role in the skin barrier function. One subclass of ceramides with a linoleic acid linked to a very long acyl (referred to as EOS) plays a crucial role in the formation of the 13 nm lamellar phase.

In this paper we focus on the lipid phase behaviour of EOS mixed with cholesterol or with cholesterol and free fatty acids. Our studies reveal that an equimolar ratio of EOS, cholesterol and free fatty acids forms a lamellar phase with a very long repeat distance of approximately 14.7 nm. This phase has an exceptional behaviour as in the thermotropic response the fatty acid chains and the ceramide chains undergo an order-disorder transition at different temperature ranges, while a part of the hydrocarbon chains of ceramides and fatty acids are mixing in the orthorhombic lattice. Based on these observations a molecular model for the 14.7 nm phase has been proposed, in which the lipids are organised in a lamellar phase with three different lipid layers in a symmetric unit cell.

Introduction

The natural function of the skin is to protect the body from unwanted influences of the environment and to prevent the body from desiccation. The main barrier for diffusion of substances across the skin is the outermost layer of the skin, the stratum corneum (2). The stratum corneum is a transparent thin layer of around 15 μm in thickness and consists of hydrophilic corneocytes embedded in lipid regions. The structure of the stratum corneum is often compared to a brick wall, in which the corneocytes form the bricks and the lipids form the mortar. The corneocytes are surrounded by a densely crosslinked protein layer, the cornified envelope. A monolayer of lipids is chemically linked to the cornified envelope and forms the link between the hydrophilic corneocytes and the hydrophobic lipids, which are the major constituents in the intercellular regions (3). As the lipid located in the intercellular regions form the only continuous structure in the stratum corneum, substances always have to cross the intercellular lipid regions before entering the viable epidermis underneath the stratum corneum (4, 5). For this reason the lipid composition and organisation is always considered to play a crucial role in the skin barrier function. The main lipid classes in stratum corneum are ceramides (CERs), cholesterol (CHOL) and free fatty acids (FFAs) in an approximately equal molar ratio (6-8). The lipids form two crystalline lamellar phases with repeat distances of approximately 6 and 13 nm (9-14). The 13 nm lamellar phase is very characteristic for the structure and is considered to be very important for the skin barrier function. When using human stratum corneum, only one group did not report the 13 nm lamellar phase (15). In that publication the set-up of the X-ray beam precluded the detection of reflections corresponding to long spacings and therefore no LPP was reported. The lateral packing of the lipids in the lipid lamellae is mainly orthorhombic, although the hexagonal lateral packing is also formed (10, 16-19). In human stratum corneum at least 11 subclasses of CERs are identified (8). The most important CERs are classified according to their base, which is either a sphingoid base (S), phytosphingoid base (P), or 6 hydroxy sphingoid base (H). Among these

CERs, there are 3 CER subclasses having a very exceptional molecular architecture, referred to as acylCERs (8, 20). The acylCERs have a linoleic acid ester linked to a ω -hydroxy fatty acyl chain with a length of approximately 32 carbon atoms, see Figure 1 (7). Furthermore, the FFAs are mainly saturated having a predominant chain length of 24 to 26 carbon atoms (21). Previous studies using mixtures based on either isolated CERs or synthetic CERs showed that these lipid mixtures resemble very closely the lipid organisation in human stratum corneum (22-24). This simplified synthetic CER mixture consists of one acylceramide (EOS) and 4 other CER subclasses with either a sphingosine or a phytosphingosine base. Using these CER subclasses, mixed with CHOL and FFAs, it was demonstrated that EOS, see Figure 1, is very important for the formation of the 13 nm lamellar phase (24, 25). In additional studies it was observed that the linoleate moiety of the acylCER is in a pseudofluid phase, and that the presence of this pseudofluid phase is also crucial for the formation of the 13 nm lamellar phase (23, 26). When we reduced the number of CERs by selecting only sphingosine-based, phytosphingosine-based or α -hydroxy-based ceramides, it was still possible to form the long periodicity phase (26). However, the composition of the selected CER mixtures affected the lateral packing of the lipids as far as the formation of the orthorhombic phase is concerned.

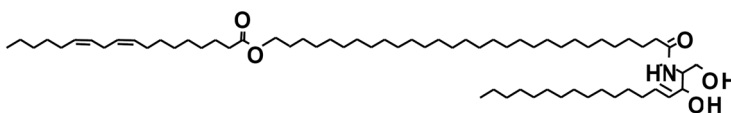


Figure 1: Molecular structure of the most abundant EOS. The nomenclature is according to Motta et al. (1).

In addition several studies were performed on the phase behaviour of single CERs mixed with a single FFA and/or CHOL. Although the lateral packing of these mixtures is often very similar to that observed in stratum corneum, the lamellar phase behaviour and the mixing properties between CERs and FFA are different (27-31).

As EOS plays a crucial role in the formation of the 13 nm lamellar phase, the current study is focussed on the phase behaviour of EOS combined with either only CHOL or with CHOL and FFA. The central questions we wanted to answer in this study are: 1) Is it possible for EOS in a mixture with FFA and CHOL to form the LPP in the absence of the other CER subclasses? and 2) What is the molecular organisation of the phases formed in the equimolar EOS:CHOL:FFA mixture? Our studies reveal that EOS:CHOL:FFA mixtures form a very exceptional lamellar phase that is different from the 13 nm lamellar phase observed in the stratum corneum.

Material and Methods

Materials

Synthetic EOS with an ω -hydroxy chain length of 30 or 27 carbon atoms (deuterated linoleate, referred to as dEOS) was generously provided by Cosmoferm B.V. (Delft, The Netherlands). Palmitic acid (C16:0), stearic acid (C18:0), arachidic acid (C20:0), behenic acid (C22:0), tricosanoic acid (C23:0), lignoceric acid (C24:0), cerotic acid (C26:0), cholesterol and acetate buffer salts were purchased from Sigma-Aldrich Chemie GmbH (Schneidorf, Germany). All organic solvents used are of analytical grade and manufactured by Labscan Ltd. (Dublin, Ireland). The water used is of Millipore quality.

Perdeuterated FFAs (referred to as DFFAs) with a chain length of C16:0 and C22:0 were obtained from Larodan (Malmö, Sweden). The DFFA with chain length of C18:0 and C20:0 were purchased from Cambridge Isotope laboratories (Andover, Massachusetts), while DFFA with a chain length of C24:0 was obtained from ARC laboratories (Apeldoorn, The Netherlands).

Preparation of the lipid mixtures

For the free fatty acids mixture FFA7, the following composition was selected: C16:0, C18:0, C20:0, C22:0, C23:0, C24:0 and C26:0 at molar ratios of 1.8, 4.0, 7.7, 42.6, 5.2, 34.7 and 4.1 respectively. This chain length distribution is based on a FFA composition in SC (32). For FTIR studies, the protonated FFA7 were replaced by protonated FFA5 or deuterated DFFA5 using a slightly different FFA composition, namely C16, C18, C20, C22 and C24 at molar ratios of 1.8, 4.0, 7.6, 47.8 and 38.8 respectively, as not all the FFA were available in the deuterated version. SAXD measurements of mixtures with FFA5 or DFFA5 demonstrated that these mixtures form the same lamellar phases (data not shown).

EOS, dEOS, CHOL, FFA7 or FFA5 or DFFA5 were dissolved in chloroform:methanol (2:1 v/v). The solvents were mixed in appropriate ratios to achieve the required compositions. About 1.5 mg of lipids in solution was sprayed in the centre of a mica strip of 10 x 2 mm (X-ray diffraction studies) or on an AgBr window in 10 x 10 mm area (FTIR studies) using a Camag Linomat IV sample applicator (Muttentz, Switzerland). Spraying was performed at a rate of 5 μ l/min, under a gentle stream of nitrogen gas. Subsequently, each lipid sample was equilibrated at a temperature around the melting point of the lipid mixture, which was either 70 or 80°C dependent on the composition of the mixture. After 10 minutes of equilibration close to the melting temperature range, the sample was cooled down to room temperature.

X-ray diffraction analysis

All samples were measured at the European Synchrotron Radiation Facility (ESRF) in Grenoble (France), at the small-angle X-ray diffraction (SAXD) beam line BM26b. The lipid samples were inserted into a temperature controlled sample holder with two mica windows. Diffraction data were collected on a two-dimensional multi-wire gas-filled area detector with 512×512 pixels of 0.25 mm spatial resolution. The spatial calibration of this detector was performed using silver behenate ($d = 5.838$ nm). Data

acquisition was performed for a period of 10 to 15 min. The scattered intensities were measured as a function of θ , the scattering angle. From the scattering angle the scattering vector (q) was calculated by $q = 4\pi\sin\theta/\lambda$, in which λ is the wavelength at the sample position. One dimensional intensity profiles were obtained by transformation of the two dimensional SAXD pattern from Cartesian (x,y) to polar (ρ,ϕ) coordinates and subsequently, integration over ϕ from 60 to 120 degrees. These diffraction curves were plotted as a function of q (nm^{-1}), the scattering vector in reciprocal space. The positions of the diffraction peaks are identified by their spacing, which is $2\pi/q_n$, in which q_n is the position of the diffraction peak of order n . The repeat distance of a lamellar phase is calculated from the spacings of the various orders of the diffraction peaks attributed to that phase, namely $d=2n\pi/q_n$. When examined as function of temperature, the acquisition time for each sequential measurement was 3 minutes and the heating rate was $1^\circ\text{C}/\text{min}$.

FTIR analysis

All spectra were acquired on a BIORAD FTS4000 FTIR spectrometer (Cambridge, Massachusetts) equipped with a broad-band mercury cadmium telluride detector, cooled with liquid nitrogen. The sample cell was closed by a second AgBr window. The sample was under continuous dry air purge starting 1 hour before the data acquisition. The spectra were collected in transmission mode, as a co-addition of 256 scans at 1 cm^{-1} resolution during 4 minutes. In order to detect the phase transition the sample temperature was increased at a heating rate of $0.25^\circ\text{C}/\text{min}$ resulting in 1°C temperature raise during each measurement. The lipid phase behavior was examined between 20°C and 100°C . The software used was Win-IR pro 3.0 from Biorad (Cambridge, Massachusetts). The spectra were deconvoluted using a half-width of 4 cm^{-1} and an enhancement factor of 1.7.

Results

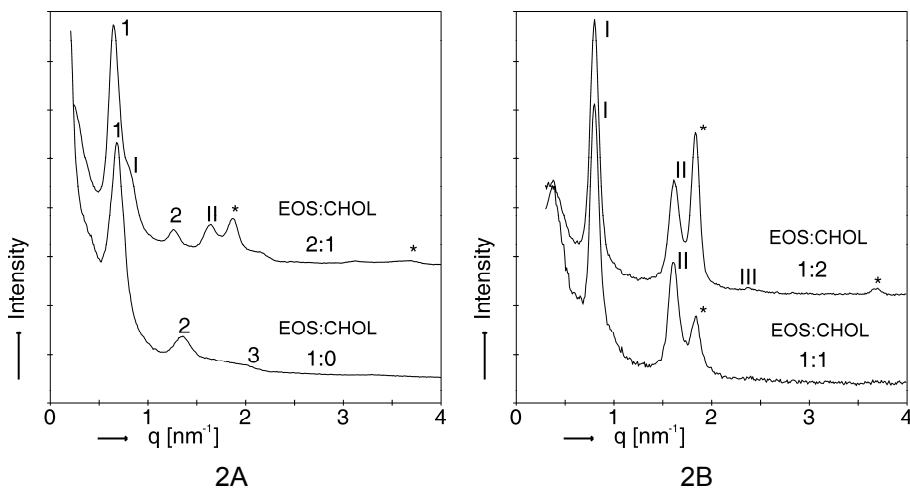


Figure 2: X-ray diffraction patterns of mixtures with EOS:CHOL in different molar ratios. The diffraction peaks indicated by Arabic numbers (1 to 3) are associated to a lamellar phase with a periodicity of approximately 9.8 nm. The peaks indicated by roman numbers (I to III) arise from a shorter lamellar phase with repeat distance of approximately 7.7 nm. The remaining peaks that are present in the diffraction patterns, indicated by asterisks, arise from crystalline cholesterol (repeat distance is 3.4 nm).

Phase behaviour of EOS and EOS:CHOL mixtures

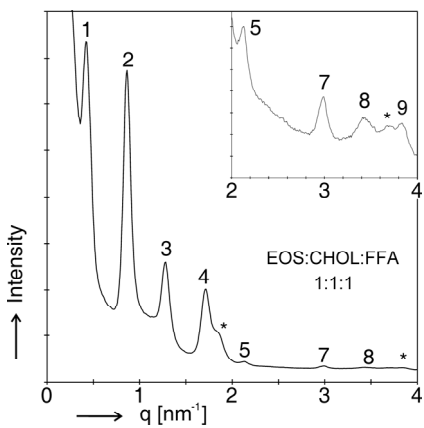
The diffraction profiles of EOS and the EOS:CHOL mixtures are provided in Figure 2A and 2B. The diffraction profile of EOS is characterized by 3 reflections positioned at $q = 0.68, 1.35$ and 2.0 nm^{-1} indicating a lamellar phase with a repeat distance of 9.3 nm. The diffraction pattern of the EOS:CHOL mixture with a molar ratio of 2:1 reveals the presence of at least three reflections ($q = 0.65, 1.26$ and 1.89 nm^{-1}) representing a lamellar phase with a repeat distance of 9.8 nm. The 3rd order peak might also partly be due to phase separated CHOL (33) indicated by reflections located at $q = 1.87$ and 3.74 nm^{-1} . In addition a reflection is observed at a spacing of

3.83 nm ($q = 1.63 \text{ nm}^{-1}$), of which the first order is most probably the shoulder observed at the right-hand side of the peak at $q = 0.64 \text{ nm}^{-1}$ representing a phase with a repeat distance of approximately 7.7 nm. Therefore it seems that in the EOS:CHOL mixture with a 2:1 molar ratio two phases coexist: a lamellar phase with a repeat distance of 9.8 nm and another phase with a repeat distance of approximately 7.7 nm. Increasing the CHOL content to an equimolar EOS:CHOL ratio promotes the presence of the 7.7 nm phase, as is clearly depicted in Figure 2B. The reflections attributed to this phase are located at $q = 0.81$ and 1.62 nm^{-1} . Finally we increased the CHOL content to an EOS:CHOL molar ratio of 1:2. Only the 7.7 nm phase is present ($q = 0.82$ and 1.63 nm^{-1} and a very weak reflection at $q = 2.37 \text{ nm}^{-1}$) together with phase separated CHOL.

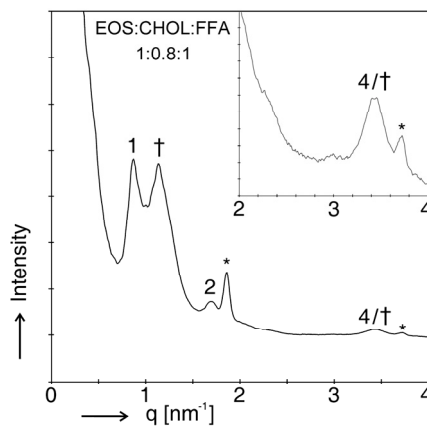
Phase behaviour of EOS:CHOL:FFA7 mixtures

First the phase behaviour of an equimolar EOS:CHOL:FFA7 mixture was studied. As depicted in Figure 3A, a series of peaks is present that can be attributed to only one lamellar phase with a repeat distance of 14.7 nm (reflections at $q = 0.42$ (1st order), 0.86 (2nd), 1.28 (3rd), 1.72 (4th), 2.13 (5th), 2.99 (7th) and 3.41 (8th) nm^{-1}). Choosing this lipid composition a lamellar phase is formed with a longer periodicity than observed in the LPP. In addition two reflections attributed to phase separated crystalline CHOL are present. Reduction in CHOL level to an EOS:CHOL:FFA7 molar ratio of 1:0.8:1 resulted in a diffraction profile with reflections at 0.89 (1st), 1.69 (2nd) and 3.43 (4th) nm^{-1} strongly indicating the presence of a 7.3 nm lamellar phase, see Figure 3B. An additional peak is observed at a spacing of 5.5 nm ($q = 1.13 \text{ nm}^{-1}$), which is attributed to another unknown phase. Reducing the CHOL content further results in the formation of a phase with a repeat distance of around 9.3 nm, very similar to the phase changes of EOS:CHOL mixtures when reducing the CHOL level (not shown). Therefore reducing the CHOL level below an equimolar ratio strongly reduces the formation of the phase with a very long repeat distance of approximately 14.7 nm. From the studies presented in Figure 2 it is clear that in the

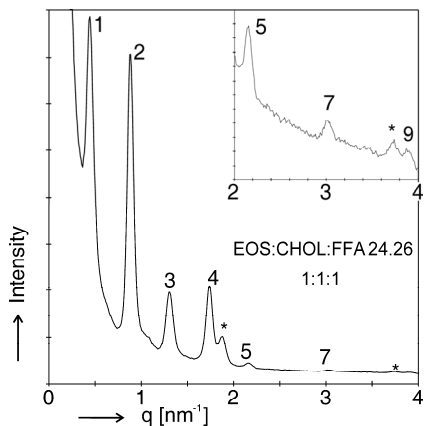
absence of a FFA7 mixture with chain-lengths varying from 16 to 26 carbon atoms, no 14.7 nm lamellar phase is formed, while Figure 3A exhibits reflections all contributing to the 14.7 nm phase.



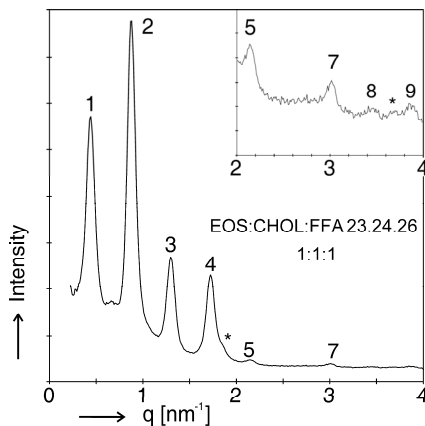
3A



3B



3C



3D

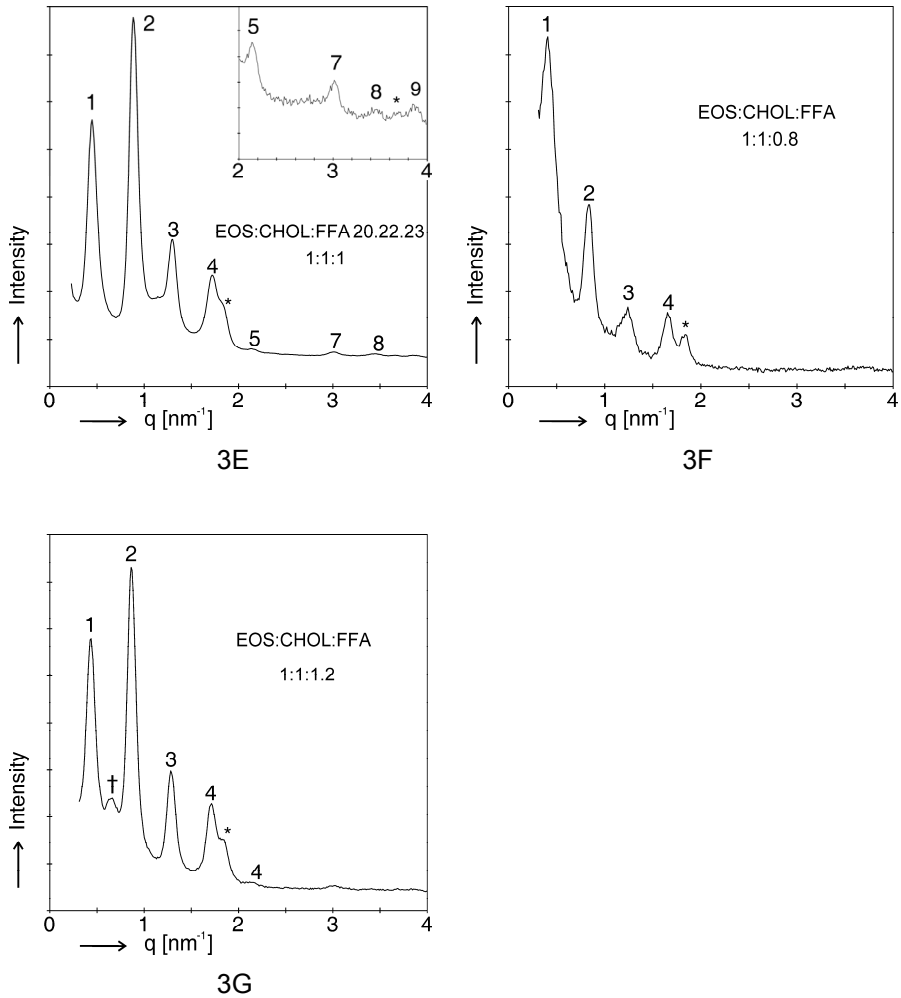


Figure 3: X-ray diffraction patterns of EOS:CHOL:FFA in different molar ratios or with varying FFA composition. In these patterns the Arabic numbers (1 up to 9) denote the diffraction peaks that are associated to the very long periodicity phase (with a repeat distance of around 14.7 nm). If an additional phase is present in a diffraction pattern the peaks associated to this phase are indicated by a dagger (†). Diffraction peaks of crystalline cholesterol are indicated by asterisks.

The next question to be answered is, do we need such a wide variation in chain length distribution in the FFA7 mixture or can we replace this mixture by a less complex one? In order to answer this question we reduced the number of FFA components to only three or two, in which the FFA composition was gradually changed from long chain FFA to shorter chain FFA.

In Figure 3C the diffraction profile of the equimolar EOS:CHOL:FFA24.26 mixture is depicted. (FFA24.26 indicates two fatty acids in equimolar ratio with a chain length of 24 carbon and 26 carbon atoms.) Similarly to the EOS:CHOL:FFA7 mixture 6 reflections are present, which can all be attributed to a lamellar phase with a repeat distance of 14.4 nm (positions of the reflections are at $q = 0.44, 0.87, 1.29, 1.73, 2.16$ and 3.00 nm^{-1}). The presence of crystalline CHOL in separate domains can be deduced from the peaks at 1.87 and 3.74 nm^{-1} . When adding a fatty acid with a chain length of 23 carbon atoms (resulting in an equimolar EOS:CHOL:FFA23.24.26 mixture) a lamellar phase with a repeat distance of 14.5 nm is formed, see Figure 3D. With a further reduction in FFA chain length, using a mixture of equimolar EOS:CHOL:FFA20.22.23, it was still possible to form a 14.4 nm lamellar phase (reflections at $q = 0.44, 0.88, 1.28, 1.71$ and 2.12 and 3.00 nm^{-1}), see Figure 3E. However, the formation of this phase was less reproducible. A further reduction in the FFA chain lengths to FFA16.18.20 did not result in the formation of a lamellar phase with a very long repeat distance (not shown). This indicates that in order to form this phase, fatty acids with a long chain are required.

If we now reduce the number of FFA to only a single FA and study the phase behaviour of EOS:CHOL:FA equimolar ratio by varying the FA chain length between 16 and 24 carbon atoms, the lamellar phase with a repeat distance of around 14.5 nm is not formed in a reproducible manner. Only occasionally this phase is formed when using FA26, FA24 and FA23 (not shown) demonstrating that a limited variation in chain length of the FFA is required to form this lamellar phase with long repeat distance in a reproducible manner.

Finally we investigated whether the level of FFA7 could be reduced or increased while still forming the lamellar phase with the long repeat distance. A reduction of the FFA7 level to an 0.8 molar ratio resulted in the formation of a lamellar phase with a long repeat distance of around 15.1 nm, see Figure 3F. When increasing the FFA7 level to an EOS:CHOL:FFA7 level of 1:1:1.2, the lamellar phase with a long repeat distance (14.4 nm) could still be formed, although a small population of lipids also forms another phase as indicated by the peak position at 0.64 nm^{-1} (dagger in Figure 3G). The EOS:CHOL:FFA7 1:1:1.2 composition was also measured as function of temperature. The data is provided in Figure 4. Increasing the temperature at a heating rate of $1.5^\circ\text{C}/\text{min}$ did not change the lamellar phases until a temperature of around 66°C was reached. At this temperature the reflections attributed to the 14.4 nm lamellar phase reduced in intensity and disappeared at approximately 74°C , while the reflection at 0.64 nm^{-1} disappeared at around 78°C .

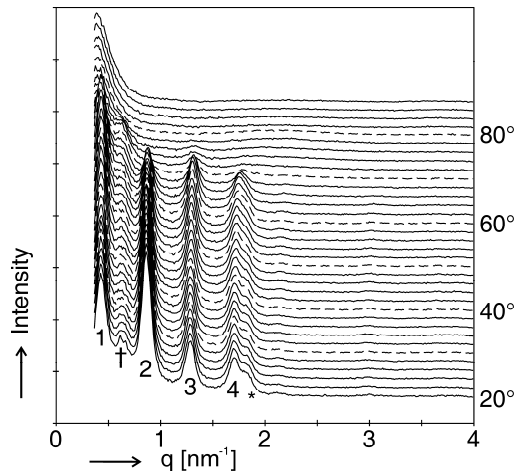
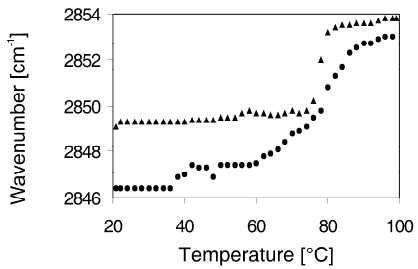
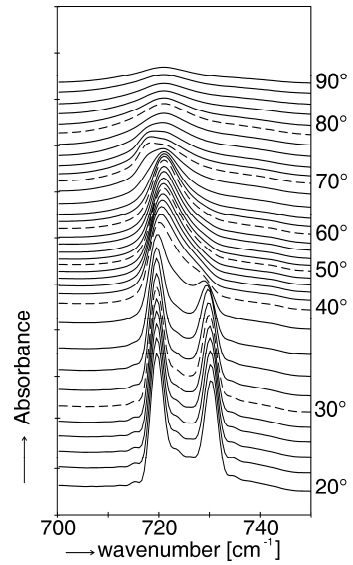


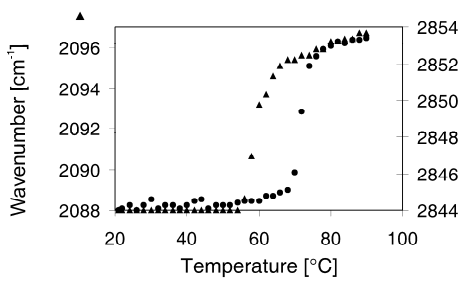
Figure 4: The x-ray diffraction profile of EOS:CHOL:FFA7 1:1:1.2 as a function of temperature. Diffraction peaks associated to the very long lamellar phase (with a periodicity of 14.4 nm) are indicated by Arabic numbers, the additional phase by a dagger (peak position at 0.64 nm^{-1}) and crystalline cholesterol by an asterisk.



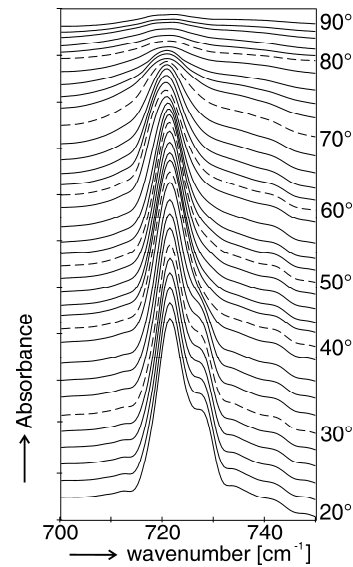
5A



5B



5C



5D

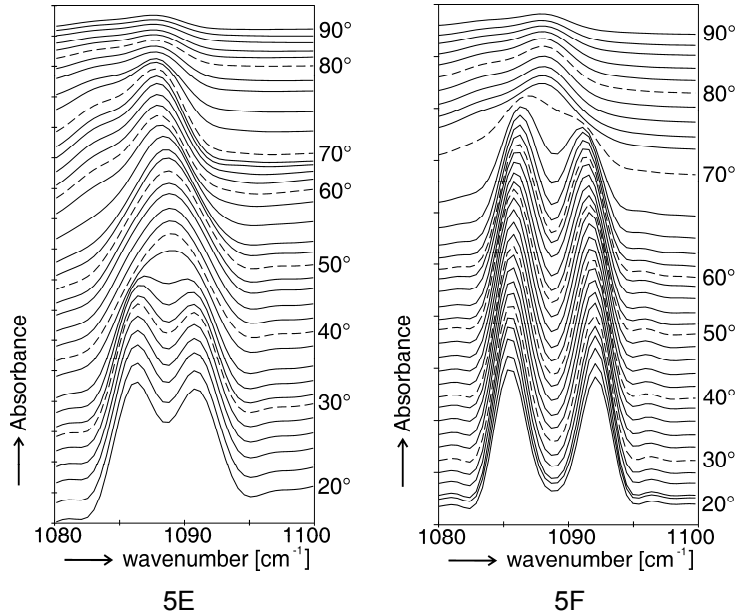


Figure 5: FTIR spectra of EOS:CHOL:FFA5 in different ratios or with DFFA5, as a function of temperature. A) The CH₂ symmetric stretching peak positions of EOS:CHOL 1:1 (triangles) and EOS:CHOL:FFA5 1:1:1 (circles). B) The CH₂ rocking vibrations of EOS:CHOL:FFA5 1:1:1. C) The symmetric stretching peak positions of the CH₂ chains (circles) and CD₂ chains (triangles) in a mixture with EOS:CHOL:DFFA5 1:1:1. D) The CH₂ rocking and E) CD₂ scissoring vibrations of the EOS:CHOL:DFFA5 mixture. F) Scissoring vibrations from a mixture with DFFA5 only.

Conformational ordering and lateral packing of the equimolar EOS:CHOL mixture

The CH₂ symmetric stretching vibrations are a measure for the conformational ordering of the hydrocarbon chains in the mixture. The thermotropic response of the CH₂ symmetric stretching vibration of the equimolar EOS:CHOL mixture is provided in Figure 5A. At 20°C the CH₂ symmetric stretching vibration is located at 2849.2 cm⁻¹. Increasing the temperature to 75°C changes the CH₂ symmetric stretching vibrations only

slightly to 2849.8 cm^{-1} . A further increase in temperature results in large shift to a value of 2853.2 cm^{-1} at 81°C indicating an order-disorder transition in a very narrow temperature region. When focussing on the scissoring vibrations, only one peak is observed at 1467 cm^{-1} , demonstrating that the mixture forms a hexagonal lateral packing (not shown). Possibly a subpopulation of the lipids may also form a liquid phase (see below).

Conformational ordering and lateral packing of the EOS:CHOL:FFA5 and EOS:CHOL:DFFA5 mixtures

To determine the thermotropic conformational ordering of the equimolar EOS:CHOL:FFA5 mixture, the CH_2 symmetric stretching vibrations are measured between 20 and 90°C , see Figure 5A. At 20°C the CH_2 symmetric stretching vibration is located at 2846.4 cm^{-1} . Upon heating no shift in the peak position of the vibration is observed until 38°C , at which a small shift to 2847.4 cm^{-1} is observed. A further increase in temperature to 60°C does not change the CH_2 symmetric stretching vibrations. Above 60°C a gradual shift to higher wave numbers is observed. The midrange temperature of this transition to a disordered phase is at around 78°C . At 90°C the CH_2 symmetric stretching vibrations are at around 2853 cm^{-1} , indicating conformational disordering. The CH_2 rocking and scissoring vibrations of the hydrocarbon chains provide information about the lateral packing of the lipids in the lamellae. The contours of the rocking vibrations in the spectrum reveal a splitting with vibrations at 719.5 cm^{-1} and 730.3 cm^{-1} at 20°C , see Figure 5B. This splitting is caused by a short range coupling between the neighbouring hydrogen atoms of the hydrocarbon chains in the orthorhombic packing. As the magnitude of this splitting approaches 11 cm^{-1} , which is close to its maximum value, it may be concluded that large domains of this orthorhombic packing are formed. However, as the splitting is not complete, a subpopulation of lipids still forms a hexagonal lateral packing. A gradual increase in temperature results in a disappearance of the splitting between 40°C and 42°C . At this temperature only one peak is observed, demonstrating that the lateral packing is mainly hexagonal. These

observations have been confirmed by the scissoring frequencies located in the spectrum at 1463.1 and 1473.3 cm^{-1} (not shown).

When we replace the protonated FFA5 by DFFA5 in the equimolar lipid mixture, information can be obtained on the mixing properties of the FFA and EOS on two levels. Firstly as the vibrations of the deuterated fatty acids and the protonated EOS occur at a different wavenumber, the vibrations can be measured simultaneously. For this reason it is possible to determine whether the transition from an ordered to a disordered phase for the FFA and EOS occurs in the same temperature range. Secondly, as no short range coupling occurs between protonated and deuterated chains in the orthorhombic lattice, it is possible to determine whether the protonated and deuterated lipids participate in the same orthorhombic lattice.

When examining the thermotropic response of CH_2 symmetric stretching vibrations, at 20°C the maximum of the contour is located at 2844.0 cm^{-1} . This peak position does not shift until a temperature of around 50°C, see Figure 5C. At that temperature a gradual increase of the wavenumber of the symmetric stretching vibrations is observed until around 68°C. This suggests an increase in conformational disordering in a subpopulation of protonated chains. A further increase in temperature results in a steep shift in the stretching vibrations to higher wavenumber until 74°C indicating a conformational disordering occurring in a very narrow temperature range. Above 74°C the change in stretching frequency levels off and reaches a value of around 2853.4 cm^{-1} at 90°C. When examining the CD_2 symmetric stretching vibrations of the DFFA5 in the same mixture, the maximum of the CD_2 symmetric stretching contour is at 2088.0 cm^{-1} at 20°C. The peak position does not shift until a temperature of around 54°C. A further increase in temperature results in a steep shift of the maximum peak position to 2095.5 cm^{-1} at 66°C indicating a conformational disordering of the FFA. A further increase in temperature results in a gradual increase in the CD_2 symmetric stretching frequencies to around 2096.7 cm^{-1} at 90°C. The rocking and scissoring CH_2 and CD_2 vibrations provide information on the lateral packing and mixing properties within the orthorhombic phase. These

contours are provided in Figure 5D and 5E, respectively. At 20°C a slight splitting in the CH₂ rocking frequencies is observed with peak positions at 721.4 and 728.0 cm⁻¹. When gradually increasing the temperature, a reduction in the high wavenumber peak intensity starts at 34°C and the splitting disappears at 38°C. The CH₂ scissoring vibrations in the spectrum confirm the disappearance of the CH₂ short range coupling in this temperature region. The CD₂ scissoring contours of the EOS:CHOL:DFFA5 also clearly show a splitting of the peak positions at 20°C. The low frequency and high frequency components are located at 1086.3 and 1090.9 cm⁻¹ respectively. The thermotropic behaviour of the CD₂ scissoring vibrations reveal a disappearance of the splitting between 36 and 40°C. This suggests the disappearance of the orthorhombic packing. For comparison in Figure 5F, the thermotropic behaviour of single DFFA5 contours are provided. These show a splitting at 1085.6 and 1091.2 cm⁻¹. This splitting remains in the temperature range between 20 and 70°C. The slopes forming the dip in between the two scissoring vibrations are much steeper than the slopes forming the dip between the low and high wavenumber of the CD₂ scissoring vibrations in the spectrum of the CER:CHOL:DFFA5 mixture. This shows that at least a subpopulation of DFFA is mixing with the protonated CER, but that a fraction of the DFFA chains are still able to interact and are thus located at neighbouring positions in the orthorhombic lattice.

Conformational ordering of the linoleate moiety in the equimolar mixture of dEOS(C27):CHOL:FFA5

In order to determine whether the linoleate moiety in the equimolar mixture is in a disordered state the CD₂ symmetric stretching vibrations were measured of the equimolar dEOS(C27):CHOL:FFA5 mixture. In this mixture only the linoleate moiety is deuterated, which permits a selective measurement of the deuterated linoleate vibrations. The CD₂ stretching vibrations reveal that already at room temperature the maximum peak is close to 2099.0 cm⁻¹ and almost does not change in peak position until 70°C, then a weak shift occurs to 2101.2 cm⁻¹ which does not change until a

temperature of 90°C is reached (not shown). This obviously shows that the unsaturated linoleate chain is already in conformational disorder at room temperature, but increases slightly in disorder at around 72°C, which is a similar temperature range at which the lamellar phase with the long periodicity disappears.

Discussion

The purpose of the studies described in this paper was to determine whether EOS in the absence of additional CERs is able to form the LPP. For this reason phase behaviour studies were performed with EOS, EOS:CHOL and EOS:CHOL:FFA mixtures. Our studies reveal that only in EOS:CHOL:FFA mixtures a lamellar phase with a very long periodicity of 14.7 nm is formed. However, the periodicity of this lamellar phase is substantially longer than observed for the LPP in stratum corneum and in mixtures prepared from CER:CHOL:FFA (9, 10, 22-24). Particularly, in the case of the synthetic CERs, the CER:CHOL:FFA mixtures mimicking the lipid composition in stratum corneum form a LPP with a repeat distance of approximately 12.2 nm (24). This shows that the lipid arrangement in the 14.7 nm lamellar phase of the EOS:CHOL:FFA mixture is different from that in the LPP of the CER:CHOL:FFA mixtures. From this observation we conclude that EOS requires the presence of other CERs to form the LPP. Examining more closely the molecular organisation of this 14.7 nm lamellar phase might, however, provide useful information on the formation of the LPP, as the presence of EOS and CHOL is crucial for the formation of both lamellar phases.

As also noticed in previous studies (34, 35), the equilibration of the samples is a very important step to obtain lamellar phases with very long repeat distances. For example, in order to obtain the lamellar phase in our equimolar EOS:CHOL:FFA mixture it was required to equilibrate the sample close to the temperature region at which the melting occurs, that is at 80°C. An equilibration temperature of 70°C, which is below the melting

temperature of the sample, does not lead to the formation of the lamellar phase with a very long periodicity (not shown), but results in a diffraction pattern with an undefined lipid phase behaviour indicating an improper mixing of the various compounds. Using a longer equilibration time at elevated temperatures, does not affect the formation of the lamellar phases.

Lipid organisation of the EOS:CHOL:FFA mixtures

Considering the lamellar phase with the long repeat distance varying between 14.4 and 15.1 nm, we noticed exceptional phase behaviour in several aspects. In the discussion below we will refer to this phase as the 14.7 nm lamellar phase, despite the small variations in repeat distance. The combined information obtained with FTIR spectroscopy and X-ray diffraction will be used to provide a molecular arrangement of this lamellar phase. First we will discuss point by point the exceptional phase behaviour of this phase.

a. A slight deviation in CHOL levels from equimolar in the EOS:CHOL:FFA mixture reduces strongly the formation of the 14.7 nm lamellar phase. A deviation in FFA levels proved to be less critical since a small deviation of the FFA molar ratio varying between 1:1:0.8 EOS:CHOL:FFA and 1:1:1.2 EOS:CHOL:FFA still results in the formation of the 14.7 nm lamellar phase.

b. A certain degree of FFA chain length distribution is important for the formation of the 14.7 nm lamellar phase. When reducing the number of FFA components from 7 to 3, it is still possible to form the 14.7 nm lamellar phase, but only when using FFA chain lengths of at least 20 C atoms. This demonstrates that long chain fatty acids are required for the formation of the 14.7 nm lamellar phase.

c. When comparing the thermotropic behaviour in the symmetric stretching absorption of EOS:CHOL and EOS:CHOL:FFA samples, we can conclude that the addition of FFA to the EOS:CHOL mixture results in a higher conformational ordering and a larger temperature range for the melting transition, as the melting starts already at lower temperatures.

d. Substituting FFA by DFFA resulted in several remarkable and apparently contrasting observations. Compared to the DFFA spectrum, the contours of

the CD₂ scissoring frequencies of EOS:CHOL:DFFA are asymmetric and the degree of splitting is clearly reduced, demonstrating that the domain sizes of the deuterated chains in the equimolar EOS:CHOL:DFFA are smaller than the domain sizes in a DFFA mixture only (36). From these observations it is obvious that the short range coupling between DFFA in the EOS:CHOL:DFFA mixture is reduced as compared to a DFFA mixture. Thus, a certain fraction of the hydrocarbon chains of EOS is participating in the same lattice as the DFFA. This is very similar to the observations made in mixtures of CER:CHOL:FFA forming the LPP, reported recently (26, 37).

e. However, the thermotropic response of the conformational disordering shows a very remarkable behaviour: the conformational disordering of the DFFA occurs in a temperature region which is approximately 10°C lower than the temperature region at which the major population of the hydrocarbon chains of EOS transforms from an ordered to a disordered phase. This clearly shows that although a subpopulation of hydrocarbon chains of EOS and DFFA are participating in the same orthorhombic lattice, a large fraction of the EOS and DFFA chains is not located in the same lattice and forms a separate domain.

f. The X-ray diffraction studies revealed that besides the presence of low levels of crystalline CHOL, only a 14.7 nm lamellar phase is formed in the equimolar EOS:CHOL:FFA mixture.

From this and from the observations made above, we can conclude that the 14.7 nm unit cell contains two types of domains: one in which FFA and EOS participate in an orthorhombic lattice and one in which the hydrocarbon chains of EOS and FFA do not mix.

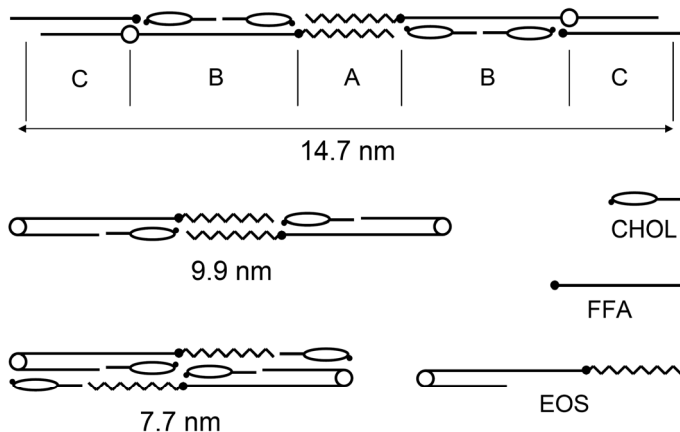


Figure 6: Suggested molecular arrangement for the very long periodicity phase in EOS:CHOL:FFA mixtures and for the two lamellar phases present in EOS:CHOL mixtures.

Proposed molecular arrangement for the 14.7 nm lamellar phase

When combining all observations discussed above, a molecular arrangement for the 14.7 nm lamellar phase can be proposed. Such a molecular arrangement is provided in Figure 6. This arrangement shows three different lipid layers unequal in width. The different layers are referred to as layer A (central part), layer B (layer with ω -hydroxy fatty acid (C30) of EOS) and layer C (FFA containing layer). In the molecular arrangement in Figure 6 the length of the unit cell is determined by the two EOS molecules in linear arrangement, in which the linoleate moieties in the central part of the unit cell are interdigitating. When assuming a 0.127 nm length per C-C bonding, the total length of the unit cell calculated from the molecular structure of the two EOS molecules is 14.7 nm, which is in excellent agreement with the periodicity measured by x-ray diffraction. Furthermore, our measurements also revealed that two different domains are present in the unit cell of the 14.7 nm phase, most probably located in different lipid layers. This conclusion was drawn from the exceptional observation that

protonated and deuterated chains undergo an ordered-disordered transition in clearly different temperature ranges. Therefore, in our proposed arrangement the FFA is located adjacent to the C18 sphingosine chain of EOS in layer C forming the orthorhombic lattice. Furthermore, the FFA and the C18 sphingosine chain are partly interdigitating. The domain in layer B with mainly ω -hydroxy fatty acid (C30) of EOS and CHOL is responsible for the high temperature order-disorder transition of around 75°C. A higher transition temperature is expected as the very long ω -hydroxy fatty acid chain is involved in this transition. Then the question arises, why is the FFA not located adjacent to the EOS C30 chain in layer B? One argument is the large chain length difference between FFA and the C30 chain of approximately 6 to 10 C-atoms. Therefore, these chains do not fit in one lipid layer. In addition, this arrangement cannot explain the difference in temperature range at which the order-disorder transition occurs for the protonated and deuterated chains, as the C18 sphingosine chains are not expected to undergo an ordered-disordered phase transition at a higher temperature than the chains of the FFA. Another possible location for FFA is adjacent to the linoleate moiety of EOS in layer A. However, the linoleate has a high conformational disordering already at 20°C and therefore no short-range coupling between FFA and the linoleate moiety is possible and thus no orthorhombic phase can be formed after addition of the FFA. The final possibility to discuss is an arrangement of the FFA and CHOL in layer C, while the sphingosine chain would be located adjacent to the ω -hydroxy fatty acid chain of EOS. In this case a forked arrangement of the EOS is obtained. However, in this arrangement the reduction in splitting when substituting the FFA by DFFA cannot be explained as the CER and FFA chains are located in different layers.

Then the remaining question is whether the proposed arrangement in Figure 6 fulfils the requirement of an approximately equimolar ratio in the EOS:CHOL:FFA mixture. If indeed EOS is in a linear arrangement, the FFA and EOS might have an interfacial area of approximately 0.20 nm², similarly to that of sphingosine monolayers (38). In contrast, the interfacial area per

CHOL molecule is approximately 0.38-0.40 nm² (39), which is almost twice that of linearly arranged EOS and FFA. Perhaps the orientation of the bulky ring moiety of CHOL is perpendicular to the plane of drawing and a second EOS molecule is located on top of the EOS in the drawing, adjacent to the same CHOL molecule. In this way an equimolar ratio of EOS:CHOL:FFA is indeed achieved.

A suggested molecular arrangement for the lamellar phases in EOS:CHOL mixtures

In the EOS:CHOL mixtures two lamellar phases are observed. At relatively low CHOL levels the repeat distance is approximately 9.8 nm, while at high CHOL levels the 7.7 nm lamellar phase is predominantly present. In the proposed molecular arrangement for the 14.7 nm lamellar phase, the hydroxyl group of the CHOL molecule is located close to the ester bond linking the C30 acyl with the linoleate moiety of EOS. Possibly, a hydrogen bonding between the hydroxyl group of CHOL and the ester group of EOS is stabilizing this arrangement. Furthermore, the linoleate moiety is fully interdigitating. When assuming a 0.127 nm distance per C-C bonding, this arrangement results in a calculated periodicity of 9.9 nm, which is very close to the experimental repeat distance. In this case we cannot distinguish between a forked or a linear arrangement of the EOS, both arrangements are possible. In the figure a forked arrangement is shown. When increasing the CHOL levels in the EOS:CHOL mixture a phase with a shorter repeat distance is found. An arrangement for this shorter repeat period accounting for the higher levels in CHOL content is also proposed in Figure 6. Again, the hydrogen bonding between the hydroxyl group of CHOL and the ester linkage in the EOS molecule might be the important factor that stabilizes the structure. Also, the calculated repeat distance is about 7.7 nm, which again matches with the measured repeat distance for this lamellar phase.

A comparison between the LPP and the 14.7 nm lamellar phase

When we compare the phase behaviour of the LPP with that of the 14.7 nm lamellar phase, some important differences are observed. Most strikingly the 14.7 nm lamellar phase can only be formed when the EOS:CHOL molar ratio in the EOS:CHOL:FFA mixture is close to equimolar, while the LPP can be formed over a wide range of CER:CHOL molar ratios. In case of human CER e.g., the LPP is already formed at a CER:CHOL molar ratio of 1:0.2 in the absence of FFA (40). This means that FFA is not required to form the LPP, while CER and CHOL can replace each other to a certain extent in the LPP. For maintaining the barrier function of the skin, this is a very important observation, as even when dealing with substantial deviations in CER:CHOL molar ratios, the LPP, which is considered to be crucial for the skin barrier function, is still formed in the stratum corneum. In other words, the lipid phase behaviour is not very sensitive to changes in the lipid composition. As far as the role of FFA is concerned, it plays a prominent role in the formation of the orthorhombic lateral packing (41). In contrast to the LPP, in case of the 14.7 nm lamellar phase our results suggest that the three lipid classes including FFA are required to form the 14.7 nm lamellar phase.

Finally, the question rises whether EOS is arranged in the LPP in a linear or in a forked configuration. In the present study we propose a linear arrangement for the EOS in the lamellar phase with a periodicity of around 14.7 nm, as this results in the required mixing of the hydrocarbon chains of FFA and EOS. For other CER mixtures, a linear arrangement is also suggested for AP with a fatty acid chain of 18 carbon atoms (42, 43). However, whether the arrangement of EOS in the LPP is linear or forked remains to be elucidated as very small changes in the environment such as a distribution in chain length of the FFA and CER molecules or a variation in head-group architecture may affect this arrangement. In this paper we reported the phase behaviour of mixtures containing EOS, CHOL and FFA. Our studies showed that the two complimentary methods of X-ray diffraction and FTIR are excellent tools to provide detailed information on the 14.7 nm lamellar phase.

Acknowledgments

We thank the company Cosmoferm B.V. (Evonik) for the provision of the ceramide EOS and the Netherlands Organization for Scientific Research (NWO) for the provision of beam time at the ESRF. Furthermore we thank the personnel at the DUBBLE beam line 26 at the ESRF for their support with the x-ray measurements, as well as the group of crystallography at the University of Amsterdam for additional x-ray measurements.

References

1. Motta, S., M. Monti, S. Sesana, R. Caputo, S. Carelli, and R. Ghidoni. 1993. Ceramide composition of the psoriatic scale. *Biochim Biophys Acta* 1182:147-151.
2. Proksch, E., J. M. Brandner, and J. M. Jensen. 2008. The skin: an indispensable barrier. *Exp Dermatol* 17:1063-1072.
3. Nemes, Z., and P. M. Steinert. 1999. Bricks and mortar of the epidermal barrier. *Exp Mol Med* 31:5-19.
4. Bodde, H. E., M. A. M. Kruithof, J. Brussee, and H. K. Koerten. 1989. Visualisation of normal and enhanced HgCl₂ transport through human skin in vitro. *Int J Pharm* 53:13-24.
5. Talreja, P., N. K. Kleene, W. L. Pickens, T. F. Wang, and G. B. Kasting. 2001. Visualization of the lipid barrier and measurement of lipid pathlength in human stratum corneum. *AAPS PharmSci* 3:E13.
6. Ponc, M., A. Weerheim, J. Kempenaar, A. M. Mommaas, and D. H. Nugteren. 1988. Lipid composition of cultured human keratinocytes in relation to their differentiation. *J Lipid Res* 29:949-961.
7. Wertz, P. W., and D. T. Downing. 1983. Ceramides of pig epidermis: structure determination. *J Lipid Res* 24:759-765.
8. Masukawa, Y., H. Narita, E. Shimizu, N. Kondo, Y. Sugai, T. Oba, R. Homma, J. Ishikawa, Y. Takagi, T. Kitahara, Y. Takema, and K. Kita. 2008. Characterization of overall ceramide species in human stratum corneum. *J Lipid Res* 49:1466-1476.
9. White, S. H., D. Mirejovsky, and G. I. King. 1988. Structure of lamellar lipid domains and corneocyte envelopes of murine stratum corneum. An X-ray diffraction study. *Biochemistry* 27:3725-3732.
10. Bouwstra, J. A., G. S. Gooris, J. A. van der Spek, and W. Bras. 1991. Structural investigations of human stratum corneum by small-angle X-ray scattering. *J Invest Dermatol* 97:1005-1012.
11. Hatta, I., N. Ohta, K. Inoue, and N. Yagi. 2006. Coexistence of two domains in intercellular lipid matrix of stratum corneum. *Biochim Biophys Acta* 1758:1830-1836.
12. Cornwell, P. A., B. W. Barry, C. P. Stoddart, and J. A. Bouwstra. 1994. Wide-angle X-ray diffraction of human stratum corneum: effects of hydration and terpene enhancer treatment. *J Pharm Pharmacol* 46:938-950.
13. Ohta, N., S. Ban, H. Tanaka, S. Nakata, and I. Hatta. 2003. Swelling of intercellular lipid lamellar structure with short repeat distance in hairless mouse stratum corneum as studied by X-ray diffraction. *Chem Phys Lipids* 123:1-8.
14. Fujii, M., Y. Takeda, M. Yoshida, N. Utoguchi, M. Matsumoto, and Y. Watanabe. 2003. Comparison of skin permeation enhancement by 3-l-menthoxypropane-1,2-diol and l-menthol: the permeation of indomethacin and antipyrine through Yucatan micropig skin and

- changes in infrared spectra and X-ray diffraction patterns of stratum corneum. *Int J Pharm* 258:217-223.
15. Garson, J. C., J. Doucet, J. L. Leveque, and G. Tsoucaris. 1991. Oriented structure in human stratum corneum revealed by X-ray diffraction. *J Invest Dermatol* 96:43-49.
 16. Bommannan, D., R. O. Potts, and R. H. Guy. 1990. Examination of stratum corneum barrier function in vivo by infrared spectroscopy. *J Invest Dermatol* 95:403-408.
 17. Bouwstra, J. A., G. S. Gooris, J. A. van der Spek, S. Lavrijsen, and W. Bras. 1994. The lipid and protein structure of mouse stratum corneum: a wide and small angle diffraction study. *Biochim Biophys Acta* 1212:183-192.
 18. Pilgram, G. S., A. M. Engelsma-van Pelt, J. A. Bouwstra, and H. K. Koerten. 1999. Electron diffraction provides new information on human stratum corneum lipid organization studied in relation to depth and temperature. *J Invest Dermatol* 113:403-409.
 19. Boncheva, M., F. Damien, and V. Normand. 2008. Molecular organization of the lipid matrix in intact Stratum corneum using ATR-FTIR spectroscopy. *Biochim Biophys Acta* 1778:1344-1355.
 20. Ponec, M., A. Weerheim, P. Lankhorst, and P. Wertz. 2003. New acylceramide in native and reconstructed epidermis. *J Invest Dermatol* 120:581-588.
 21. Wertz, P. 1991. In *Physiology, Biochemistry and Molecular Biology of the Skin*. L. A. Goldsmith, editor. Oxford University Press, Oxford. 205-235.
 22. Bouwstra, J. A., G. S. Gooris, K. Cheng, A. Weerheim, W. Bras, and M. Ponec. 1996. Phase behavior of isolated skin lipids. *J Lipid Res* 37:999-1011.
 23. Bouwstra, J. A., G. S. Gooris, F. E. Dubbelaar, and M. Ponec. 2002. Phase behavior of stratum corneum lipid mixtures based on human ceramides: the role of natural and synthetic ceramide 1. *J Invest Dermatol* 118:606-617.
 24. de Jager, M. W., G. S. Gooris, M. Ponec, and J. A. Bouwstra. 2005. Lipid mixtures prepared with well-defined synthetic ceramides closely mimic the unique stratum corneum lipid phase behavior. *J Lipid Res* 46:2649-2656.
 25. McIntosh, T. J. 2003. Organization of skin stratum corneum extracellular lamellae: diffraction evidence for asymmetric distribution of cholesterol. *Biophys J* 85:1675-1681.
 26. Janssens, M., G. S. Gooris, and J. A. Bouwstra. 2009. Infrared spectroscopy studies of mixtures prepared with synthetic ceramides varying in head group architecture: coexistence of liquid and crystalline phases. *Biochim Biophys Acta* 1788:732-742.
 27. Brief, E., S. Kwak, J. T. Cheng, N. Kitson, J. Thewalt, and M. Lafleur. 2009. Phase behavior of an equimolar mixture of N-palmitoyl-D-erythro-sphingosine, cholesterol, and palmitic acid, a mixture with optimized hydrophobic matching. *Langmuir* 25:7523-7532.

28. Chen, X., S. Kwak, M. Lafleur, M. Bloom, N. Kitson, and J. Thewalt. 2007. Fatty acids influence "solid" phase formation in models of stratum corneum intercellular membranes. *Langmuir* 23:5548-5556.
29. Moore, D. J., M. E. Rerek, and R. Mendelsohn. 1997. Lipid domains and orthorhombic phases in model stratum corneum: evidence from Fourier transform infrared spectroscopy studies. *Biochem Biophys Res Commun* 231:797-801.
30. Neubert, R., W. Rettig, S. Wartewig, M. Wegener, and A. Wienhold. 1997. Structure of stratum corneum lipids characterized by FT-Raman spectroscopy and DSC. II. Mixtures of ceramides and saturated fatty acids. *Chem Phys Lipids* 89:3-14.
31. Bouwstra, J. A., J. Thewalt, G. S. Gooris, and N. Kitson. 1997. A model membrane approach to the epidermal permeability barrier: an X-ray diffraction study. *Biochemistry* 36:7717-7725.
32. Wertz, P. 1991. Epidermal lipids. In *Physiology, Biochemistry and Molecular Biology of the Skin*. L. A. Goldsmith, editor. Oxford University Press, Oxford. 205-235.
33. Small, D. M. 1986. The Physical Chemistry of Lipids. In *Handbook of Lipid Research*. D. J. Hanahan, editor. Plenum Press, New York.
34. de Jager, M. W., G. S. Gooris, I. P. Dolbnya, W. Bras, M. Ponec, and J. A. Bouwstra. 2004. Novel lipid mixtures based on synthetic ceramides reproduce the unique stratum corneum lipid organization. *J Lipid Res* 45:923-932.
35. Groen, D., G. S. Gooris, M. Ponec, and J. A. Bouwstra. 2008. Two new methods for preparing a unique stratum corneum substitute. *Biochim Biophys Acta* 1778:2421-2429.
36. Snyder, R. G., M. C. Goh, V. J. P. Srivatsavoy, H. L. Strauss, and D. L. Dorset. 1992. Measurement of the growth kinetics of microdomains in binary n-alkane solid solutions by infrared spectroscopy. *J Phys Chem* 96:10008-10019.
37. Gooris, G. S., and J. A. Bouwstra. 2007. Infrared spectroscopic study of stratum corneum model membranes prepared from human ceramides, cholesterol, and fatty acids. *Biophys J* 92:2785-2795.
38. Vaknin, D. 2003. Structure-function relations in self-assembled C18- and C20-sphingosines monolayers at gas/water interfaces. *J Am Chem Soc* 125:1313-1318.
39. Scheffer, L., I. Solomonov, M. J. Weygand, K. Kjaer, L. Leiserowitz, and L. Addadi. 2005. Structure of cholesterol/ceramide monolayer mixtures: implications to the molecular organization of lipid rafts. *Biophys J* 88:3381-3391.
40. Bouwstra, J. A., G. S. Gooris, F. E. Dubbelaar, and M. Ponec. 2001. Phase behavior of lipid mixtures based on human ceramides: coexistence of crystalline and liquid phases. *J Lipid Res* 42:1759-1770.
41. Bouwstra, J. A., G. S. Gooris, F. E. Dubbelaar, A. M. Weerheim, and M. Ponec. 1998. pH, cholesterol sulfate, and fatty acids affect the stratum corneum lipid organization. *J Investig Dermatol Symp Proc* 3:69-74.

Chapter 5

42. Kiselev, M. A., N. Y. Ryabova, A. M. Balagurov, S. Dante, T. Hauss, J. Zbytovska, S. Wartewig, and R. H. Neubert. 2005. New insights into the structure and hydration of a stratum corneum lipid model membrane by neutron diffraction. *Eur Biophys J* 34:1030-1040.
43. Kessner, D., M. A. Kiselev, T. Hauss, S. Dante, S. Wartewig, and R. H. Neubert. 2008. Localisation of partially deuterated cholesterol in quaternary SC lipid model membranes: a neutron diffraction study. *Eur Biophys J* 37:1051-1057.

Chapter 6

New insights into the stratum corneum lipid organization by x-ray diffraction analysis

D. Groen, G. S. Gooris, J. A. Bouwstra

Biophys J, vol. 97, no. 8, pp. 2242-9.

Abstract

The characteristic 13 nm lamellar phase that is formed by lipids in the outermost layer of the skin, the stratum corneum (SC), is very important for the barrier function of the skin. To gain more insight into the molecular organization of this lamellar phase, we performed small-angle x-ray diffraction (SAXD) using various lipid mixtures mimicking the lipid composition in SC. In the SAXD pattern of each mixture at least 7 diffraction orders were observed, attributed to the lamellar phase with a repeat distance ranging from 12.1 to 13.8 nm. Using the sampling method based on the variation in repeat distance, we selected phase angles for the first 6 diffraction orders. Using these phase angles, for the lamellar phase a high resolution electron density distribution could be calculated. Subsequently, from SAXD patterns of isolated SC the electron density distribution of the lamellar phase was also calculated and appeared to be very similar to that in the lipid mixtures. This demonstrates that the lipid mixtures serve as an excellent model for the lipid organization in SC, not only with respect to the repeat distance, but also in terms of the electron density distribution within the unit cell.

Introduction

The skin forms the interface between the human body and the environment. It protects our body against various biological and chemical hazards and from desiccation in a dry environment. The outermost layer of the skin, the stratum corneum (SC), forms the main barrier against diffusion of substances across the skin (3). This layer consists of overlapping flattened dead skin cells. Each cell is surrounded by lipids, which serve as the mortar between the cells. The lipids form multiple sheets of lamellae and are mainly composed of ceramides (CER), cholesterol (CHOL) and free fatty acids (FFA). These lipid classes are present in an approximately equimolar ratio (4). In the SC the lipids form two lamellar phases with repeat distances of approximately 6 and 13 nm, also referred to as the short periodicity phase (SPP) and long periodicity phase (LPP), respectively. Furthermore, the orientation of the lipid lamellae is approximately parallel to the SC surface (5). Within the lipid lamellae the lipids are organized predominantly in a crystalline lateral packing (6, 7). The presence of oriented lipid lamellae as well as the crystalline packing are thought to contribute greatly to the barrier function of the SC.

Previous studies showed that mixtures prepared with either synthetic CER or native CER mixed with CHOL and with FFA mimic the SC lipid organization very closely (8-10). While CER and CHOL play a prominent role in the formation of the two lamellar phases, the addition of FFA is crucial for the formation of the densely packed orthorhombic crystalline structure (8, 11). Furthermore, the presence of CER1, an acyl CER with a linoleic acid linked to a very long ω -hydroxy fatty acid chain (see Fig. 1), is a prerequisite for the formation of the LPP (8, 12, 13).

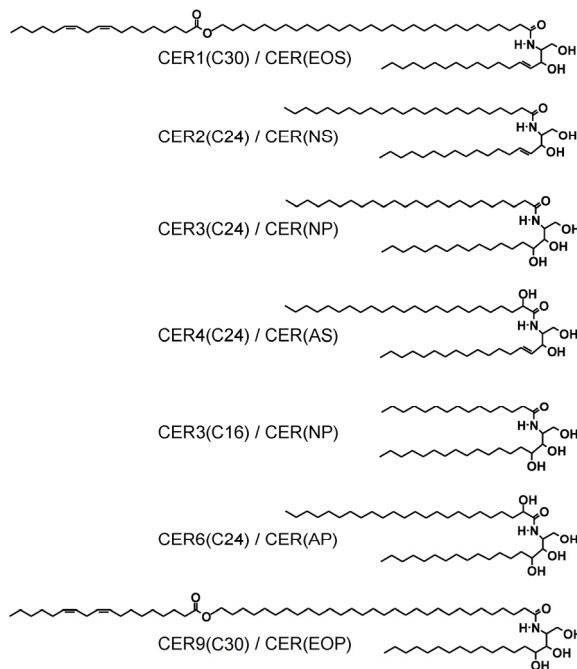


Figure 1: Molecular structure of the synthetic CER used in the lipid mixtures of Table 1. The nomenclature according to Motta et al. (2) is also provided.

Although over the years a lot of information has been gathered on the SC lipid organization and the role the various lipid classes play in this organization (12-15), until now no high-resolution electron density profile of the LPP has been presented. In previous studies, several attempts have been made in order to determine an electron density profile of the LPP. White et al. performed the first calculations using a block-shaped electron density profile (16). Our group performed electron density calculations in which the electron density profiles were simulated by Gauss curves (6, 17). However, both studies suffered from the fact that no swelling of the lamellae was induced and therefore no unique electron density profile could be determined. More recently McIntosh used a mixture of isolated pig CER, CHOL and palmitic acid and performed x-ray diffraction studies (18). Although information was obtained on the distribution of CHOL in the

repeating unit, due to the low resolution of the electron density profile the lipid organization in the repeating unit could not be unravelled. Therefore, the aim of the present study is to obtain more detailed insights into the molecular organization of the LPP by analyzing a large number of x-ray diffraction curves obtained from SC lipid mixtures. In addition, the diffraction curves of SC isolated from pig skin, mouse skin and in vitro cultured skin (that is skin cultured from cells) were also analyzed for comparison. By using 6 reflection orders of the LPP, electron density profiles could be constructed with 1.1 nm resolution. By analyzing these high resolution electron density profiles novel insights on the location of CER1 in the repeating unit could be obtained.

Materials and Methods

Materials

Synthetic CER1(C30) (CER(EOS)), CER2(C24) (CER(NS)), CER3(C24) (CER(NP)), CER4(C24) (CER(AS)), CER3(C16) (CER(NP)), CER6(C24) (CER(AP)) and CER9(C30) (CER(EOP)) were generously provided by Cosmoferm B.V. (Delft, The Netherlands). The moPalmitic acid (C16:0), stearic acid (C18:0), arachidic acid (C20:0), behenic acid (C22:0), tricosanoic acid (C23:0), lignoceric acid (C24:0), cerotic acid (C26:0), cholesterol, cholesterol sulfate and acetate buffer salts were purchased from Sigma-Aldrich Chemie GmbH (Schnelldorf, Germany). All organic solvents used are of analytical grade and manufactured by Labscan Ltd. (Dublin, Ireland). The water used is of Millipore quality.

Isolation of ceramides

Pig or human SC lipids were extracted from isolated SC using the method of Bligh and Dyer (19) and applied on silicagel as published previously (20). The lipid composition of the collected fractions was established by one dimensional high performance thin layer chromatography (21).

Preparation of the lipid mixtures

The isolated or synthetic CER, CHOL and FFA were dissolved in chloroform:methanol (2:1 v/v). The solvents were mixed in appropriate ratios to achieve the required compositions. About 1.5 mg of lipids in solution was sprayed as an unoriented glob of lipids of approximately 1 mm high in the center of a mica strip of 10 x 2 mm using a Camag Linomat IV sample applicator (Muttenez, Switzerland). Only a very small area of approximately 2 mm² is used to ensure a random orientation of the lamellae in the sample. Spraying was performed at a rate of 5 µl/min, under a gentle stream of nitrogen gas. Subsequently, each lipid sample was equilibrated at a temperature around the melting point of the lipid mixture, which was either 60 or 70°C dependent on the composition. When preparing dry lipid mixtures, after 10 minutes of equilibration the sample is cooled down to room temperature. In the case of hydration (11 out of the 12 measured lipid mixtures, see Table 1), after 10 minutes of equilibration at elevated temperatures, acetate buffer (pH 5.0) was added to the sample before cooling down to room temperature and the sample is kept under buffer until measured. To homogenize the hydrated samples, 5 freeze-thawing cycles were carried out between -20°C and room temperature. Composition, equilibration temperature and hydration method of all SC lipid models used for phase calculations are provided in Table 1. The exact composition and preparation method of the mixtures prepared from isolated pig CER were described previously (1). CerA designates a mixture of synthetic ceramides containing CER1, CER2, CER3, CER4, CER3(C16) and CER6 (see also Fig. 1) in a molar ratio of 15:51:16:4:9:5 which closely resembles the CER composition in SC (20). For the free fatty acids mixture (FFA), the following composition was selected: C16:0, C18:0, C20:0, C22:0, C23:0, C24:0 and C26:0 at a molar ratio of 1.8:4.0:7.7:42.6:5.2:34.7:4.1 respectively. This chain length distribution is based on the FFA composition in SC (22).

Table 1: Mixtures used for the determination of phase angles

Lipid mixture composition and molar ratios	symbol in Figs. 3 and 4	hydration	eq. temp. (°C)	repeat distance (nm)
CerA : Chol : FFA 1:1:1	o	pH 5	70	12.3
CerA : Chol : FFA 1:1:1	o	pH 5	70	12.4
CerA : Chol : FFA 1:1:1	o	pH 5	70	12.1
CerA : Chol : FFA : ChSO ₄ 1:1:1:0.1	o	pH 5	70	12.4
PigCER : Chol : FFA 1:1:1	Δ	No	60	12.8
PigCER : Chol : FFA 2:1:1 *	Δ	pH 5	60	13.0
PigCER : Chol : FFA : ISIS 2:1:1:1 *	Δ	pH 5	60	13.0
PigCER : Chol : FFA : IPIS 2:1:1:1 *	Δ	pH 5	60	13.4
PigCER : Chol : FFA : GMIS 2:1:1:1 *	Δ	pH 5	60	13.8
15% synthCER1 + HCER[2..9] : Chol : FFA 1:1:1	◇	pH 5	70	13.5
30% synthCER1 + HCER[2..9] : Chol : FFA 1:1:1	◇	pH 5	70	13.4
CerA : Chol : FFA 1:1:1 †	>	pH 5	70	12.3

Mixtures indicated with (*) are published previously (1). The three moisturizers used in these mixture are isostearyl isostearate (ISIS), isopropyl isostearate (IPIS) and glycerol monoisostearate (GMIS). Cholesterol sulfate is abbreviated to ChSO₄, CER isolated from human SC is abbreviated to HCER and CER isolated from pig SC is abbreviated to PigCER. CerA designates a mixture containing the first 6 synthetic CER presented in Fig. 1. The sample indicated with (†) has an adjusted CerA composition in which a part of the CER1 is replaced by CER9 (8.5% CER1, 6.5% CER9).

X-ray diffraction analysis

All samples were measured at the European Synchrotron Radiation Facility (ESRF) in Grenoble (France), at the small-angle x-ray diffraction (SAXD) beam line BM26b as described previously (10). Data acquisition was performed for a period of 10 to 15 min. From the scattering angle the scattering vector (q) was calculated by $q = 4\pi\sin\theta/\lambda$, in which λ is the wavelength at the sample position and θ the scattering angle. One dimensional intensity profiles were obtained by transformation of the two

dimensional SAXD pattern from Cartesian (x,y) to polar (ρ,φ) coordinates and subsequently, integration over φ from 60 to 120 degrees. Although the integration was performed over a range of φ , the summed intensity over this angle was divided by the number of pixels present in the integration range. This method is similar to a linear scan integration and therefore a correction factor proportional to h is required.

Peak intensities were calculated from the diffraction curve using a mathematical curve fitting procedure. This fitting procedure can be described as follows: First a baseline is created that follows the decaying curve. Secondly, the peaks present in the SAXD pattern are fitted with Gaussian peak shapes by a least squares approximation. When the peak in the SAXD pattern is composed of two overlapping reflections from different phases (for example when a peak exhibits a shoulder), this peak is fitted by two Gaussians. The repeat distance (d) of the LPP and additional phases was determined from the position (q_h) of all non-overlapping reflections attributed to the LPP or additional phase by $d = 2\pi h/q_h$. Vice versa, the position of an overlapping Gaussian was calculated from its lamellar repeat distance by $q_h = 2\pi h/d$ (maximally 3 out of 7 reflections for the LPP were overlapping in a mixture). For clarity, in the figure where a SAXD curve is displayed, the fitted Gaussian peaks are plotted together with the measured diffraction curve.

In order to compare the integrated peak intensities calculated from a SAXD curve originating from different samples (encompassing different signal strengths), a normalization method is required. Our normalization method is adapted from the method presented by Blaurock and Nelander (23). The normalization procedure can be described as follows: In a diffraction pattern, the intensity for each order, $I(h)$, is divided by the total intensity over all orders (the sum of $I(h)$ for $h = 1$ to n) see Eq. 1. In contrast to Blaurock and Nelander, we did not correct for the increase in bilayer repeat distance (D/D_{min}) due to the limited variation in repeat distance observed in the LPP. Subsequently, structure amplitudes were calculated from these normalized

intensities after correction for the Lorentz factor (equal to h) and correction for the linear integration (also by a factor h), see Eq. 1 (24).

$$(1) \quad |F(h)| = \sqrt{I(h)_{norm} \cdot h^2} \quad \text{where} \quad I(h)_{norm} = I(h) / \sum_{h=1}^n I(h)$$

In this equation, $|F(h)|$ is the structure amplitude corresponding to the normalized intensity $I(h)_{norm}$ at diffraction order h and n is the maximum number of orders included in the calculations.

Calculation of an electron density distribution

Sampling of the continuous Fourier transform is performed by plotting the structure amplitudes for all the sets of diffraction data, with each set containing a small variation in repeat distance. Up to 6 orders of diffraction are included in the calculations. In the procedure of selecting the correct phase for each diffraction order, Shannon's sampling theorem (25) is used to construct a continuous curve through one set of diffraction data. Shannon's equation as presented by Franks and Lieb (26) is rewritten as displayed in Eq. 2.

$$(2) \quad F_{cont}(q) = \sum_{h=-n}^n |F(h)| \cdot \varphi(h) \cdot \sin\left(\frac{qd}{2} - \pi h\right) / \left(\frac{qd}{2} - \pi h\right)$$

In this equation $\varphi(h)$ is the phase angle of diffraction order h . The unit cell of the LPP is centrosymmetric as has clearly been shown by the broad-narrow-broad pattern of RuO_4 fixed lipids in SC, visualized in the electron microscope (18, 27). Therefore $\varphi(h)$ is either 0 or 180° and thus the sign of the structure factors is either "+" or "-", respectively. The zero order structure factor $F(0)$ is equal to the positive average electron density of the lamellae and is arbitrarily set to 1 to fit with the data. However, the value of $F(0)$ does not play a role in the calculation of an electron density distribution other than creating an offset value.

With Eq. 2 a continuous function was calculated that fitted with one data set of structure factors calculated from the 6 diffraction peaks of a selected

sample. As for each of the 6 structure factors of this data set a “+” or “-” sign is possible, 64 phase combinations are possible and therefore 64 continuous functions can be calculated. All these continuous functions were calculated and compared with the experimentally determined structure factors of the lipid mixtures presented in Table 1. For each of the 64 curves the fit with experimental data is evaluated by the method of least squares, provided in Eq. 3.

$$(3) \quad R^2 = 1 - \left[\frac{\sum_i (data_i - fit_i)^2}{\sum_i (data_i - \overline{data})^2} \right]$$

In this equation $data_i$ and fit_i represent respectively the i -th experimental value and the i -th fit value and \overline{data} represents the mean of all experimental values. Furthermore, a value of $R^2 = 1$ designates a perfect fit. The phase combination of the curve that most closely fitted with all the experimental data according to the method of least squares was selected as the correct set of phases.

Finally, with the correct phase set, together with a set of structure amplitudes obtained from a selected lipid mixture, an electron density profile $\rho(x)$ for the LPP was calculated using Eq. 4 (28).

$$(4) \quad \rho(x) = F(0) + 2 \sum_{h=1}^n |F(h)| \cdot \varphi(h) \cdot \cos\left(\frac{2\pi hx}{d}\right)$$

In this equation d is the repeat distance of the unit cell and x is the distance from the center of the unit cell.

Results

The small angle x-ray diffraction pattern of a lipid mixture

An x-ray diffraction pattern of a lipid mixture composed of PigCER:CHOL:FFA in a 2:1:1 molar ratio (see Table 1) is provided in Fig. 2A. The rings display a uniform density demonstrating the random orientation of the lipid lamellae. The integrated intensity of these rings over

an angle of 60 degrees is displayed in Fig. 2B. In the diffraction pattern of this mixture, the 7 diffraction orders of the LPP are well separated from the two diffraction peaks assigned to CHOL and to the short periodicity phase. The first 6 diffraction peaks of the LPP from this particular lipid mixture will be used for the calculation of an electron density profile, described below.

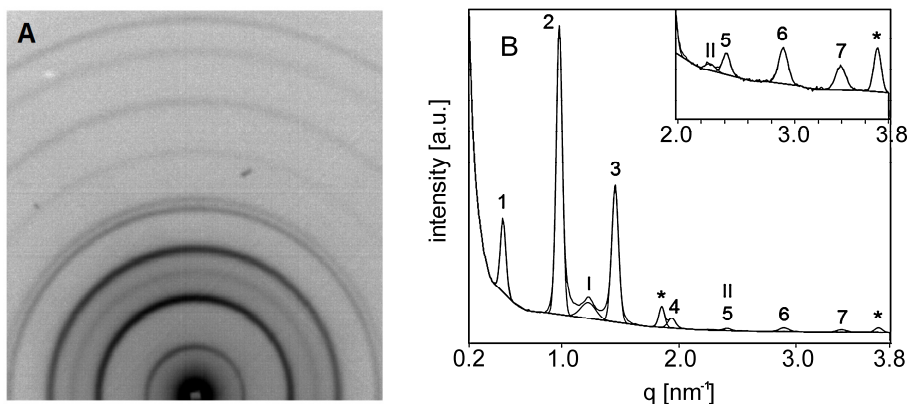


Figure 2: A) The ring-shaped diffraction pattern of a lipid mixture with PigCER:CHOL:FFA in a 2:1:1 molar ratio. B) Result of the integration of (A) over a 60 degree angle. The Gaussian peaks that are fitted to the SAXD pattern are used to determine the peak areas. The diffraction peaks associated to the LPP are indicated by arabic numbers. The other peaks that are present arise from a short lamellar phase (indicated by roman numbers) and crystalline cholesterol (indicated by asterisks).

Determining structure factors and solving the phase problem

For a series of additional lipid mixtures listed in Table 1, small angle x-ray diffraction data are also collected. The data show that all these lipid mixtures form a LPP very similar in length to the LPP observed in SC. However, as shown in Table 1, the lipid mixtures exhibit a small variation in the repeat distance between 12.1 and 13.8 nm.

For each lipid mixture presented in Table 1, a set of structure amplitudes is calculated from the intensities of the various diffraction peaks using Eq. 1. In

Fig. 3 the calculated structure amplitudes are plotted. Each group of structure amplitudes that belong to the same diffraction order (indicated by 1 to 6) is encircled in this figure.

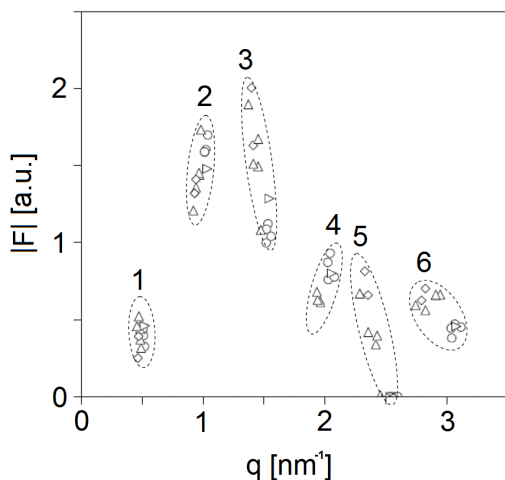


Figure 3: Plot of the structure amplitudes obtained from diffraction patterns of the lipid mixtures presented in Table 1. Encircled are the structure factors that belong to the same order of diffraction, indicated by numbers 1 to 6.

We took 6 orders of diffraction for the calculations as we noticed that by including the 7th order, there was overlap in the position of the structure amplitudes in reciprocal space. Probably this overlap is the result of the different compositions used in our study, because small changes in the unit cell structure are caused only by changes in the higher orders of diffraction. Therefore it is not clear whether there is a phase change between the fourier transform of the 6th and 7th order. From Fig. 3 it is already obvious that the data points sample a continuous function. Each group of structure amplitudes in Fig. 3 (belonging to the same diffraction order) can have either a “+” or a “-” sign as the unit cell of the LPP is considered to be centrosymmetric (27). When including 6 orders of diffraction in the calculations (encircled in Fig. 3), the number of possible phase combinations

is $2^6 = 64$. In order to determine the correct phase combination, first a continuous line is fitted through the set of structure factors of the lipid mixture with PigCER:CHOL:FFA 2:1:1 using Shannon's theorem, see Eq. 2. Subsequently, based on the 6 structure amplitudes of the PigCER:CHOL:FFA 2:1:1 mixture, continuous Fourier functions were calculated for all 64 phase combinations. The correct phase solution is that particular combination of phases for which the continuous Fourier transform fits closely with the structure amplitudes, calculated from the diffraction patterns of the lipid mixtures listed in Table 1. The phase solution that resulted in the best fit of the calculated continuous Fourier transform with the experimental structure amplitudes is plotted in Fig. 4.

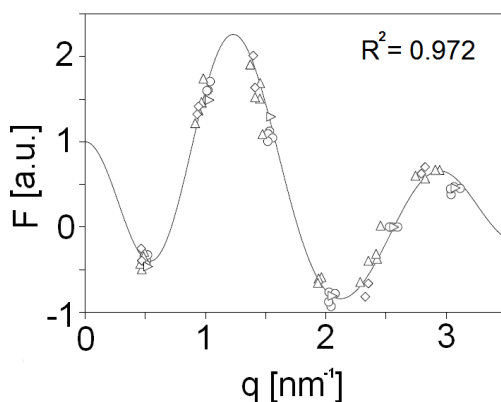


Figure 4: Plot of the continuous Fourier curve, calculated with one set of structure factors from the lipid mixture PigCER:CHOL:FFA in 2:1:1 ratio, is shown fitting through the structure factors of the remaining lipid mixtures in Table 1. The curve and structure factors are calculated using the phase solution with respective phase signs for orders 1 to 6 being - + + - - +.

This phase solution was selected as the best solution according to the method of least squares ($R^2 = 0.972$). For orders 1 to 6, the phase solution resulted in the following combination of signs: - + + - - +. The second best solution with a slightly lower R^2 is the solution with the exact opposite sign

combination of + - - + + -. As the sign combination - + + - - + resulted in the best fit and is in addition in agreement with the sign combination for the first three orders reported by McInStosh using very similar lipid mixtures (16), we considered the - + + - - + sign combination as the correct phase combination. This phase combination will be used to calculate an electron density profile for the LPP.

The electron density profile of the LPP

From the set of structure amplitudes obtained for the selected lipid mixture (PigCER:CHOL:FFA 2:1:1) together with the phase combination - + + - - +, the electron density profile is constructed using Eq. 4. This profile is plotted in Fig. 5, the maximum resolution of details in the profile ($d/2h_{\max}$) is 1.1 nm.

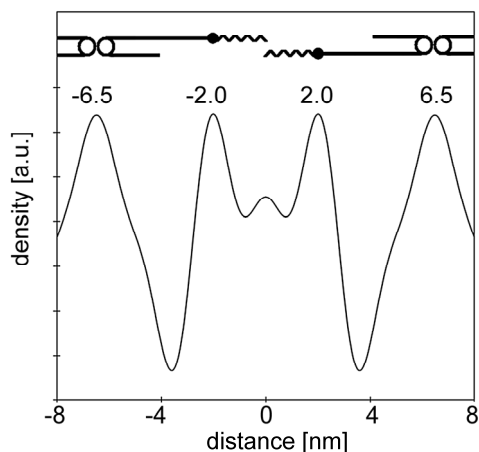


Figure 5: The calculated electron density profile for the LPP in the lipid mixture with PigCER:CHOL:FFA in 2:1:1 molar ratio. Also provided is a model showing the possible location of the CER1 molecule inside the unit cell.

Within the repeating unit of the LPP ($d = 13$ nm), four regions with a high electron density are present. At the boundary of the unit cell two high electron density regions are located around -6.5 and $+6.5$ nm. In addition, closer to the center of the unit cell, two other narrow high electron density

regions are located at -2.0 and +2.0 nm with in between a very small sub-maximum at 0 nm. Model calculations of the electron density of the CER1 and CER2 headgroup relative to the electron density of the CER double alkyl chain (using atomic numbers, following the method of Franks (29)) revealed that the headgroups are about 1.5 times more dense than the alkyl chains (data not shown). Thus, in general the high electron density peaks correspond to the polar headgroups, while the lower electron density regions correspond to the hydrocarbon chains of the lipids. Therefore the electron density profile of Fig. 5 results in a unit cell containing three lipid layers. One lipid layer is located in the center with a width of 4.0 nm and on each side of this central lipid layer two adjacent layers are located, both being 4.5 nm in width.

The smallest detail in the electron density profile in Fig. 5 is located at the center of the unit cell; a small sub-maximum at 0 nm. As 6 orders have been used for the electron density calculation and the sub-maximum is not present in all calculated electron density profiles of the lipid mixtures used, this small sub-maximum is not considered as relevant.

X-ray diffraction profiles of intact SC

In previous studies, the similarity between the repeat distance of the LPP in the lipid model mixtures and in SC has been presented (13, 18, 20, 30). With the new phase information for the structure factors and the related electron density profiles, the next question is whether the electron density profiles of the LPP in the lipid mixtures are also representative for the LPP in SC. This would demonstrate that the lamellar organization in lipid mixtures and in SC is similar, at a high level of detail. In order to determine this, accurate information about the peak intensities of the LPP in SC is required. This information is available for the LPP in mouse SC (17), in SC of cultured skin (i.e. skin generated from isolated skin cells, unpublished results, V.S. Thakoersing, M. Ponec and J.A. Bouwstra) and in pig SC (20). Unfortunately, for SC from human skin the diffraction peaks of the LPP are

not available at a sufficient resolution. For SC isolated from human skin equivalents and from mouse skin, the peak intensities for respectively 6 and 5 diffraction orders of the LPP could be calculated directly from the corresponding diffraction curves using the Gauss fitting procedure. However, in the case of pig SC the diffraction peaks are very broad and overlapping (31). Therefore recrystallisation of the lipids was required, providing much sharper peaks (20). With the peak intensities and the set of phase angles provided above, the structure factors were calculated. The structure factors for the SC are provided in Fig. 6 together with the previously obtained continuous Fourier function of the example lipid mixture PigCER:CHOL:FFA 2:1:1.

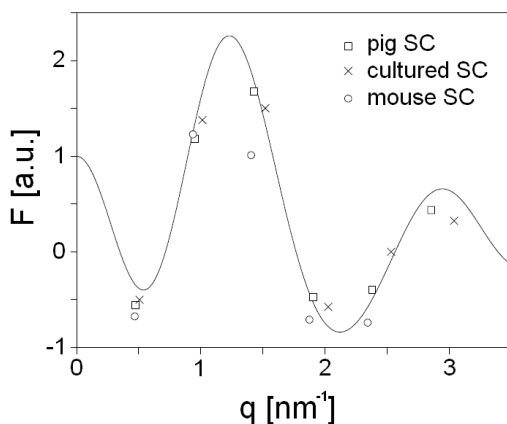


Figure 6: Cultured skin SC, mouse SC and pig SC structure factors, plotted together with the continuous Fourier transform previously displayed in Fig. 4. The structure factors of cultured skin SC and pig SC fit nicely with the continuous Fourier transform, while the structure factors of mouse SC fit to a lesser extent.

It is striking that the 6 structure factors of the LPP detected in SC of cultured skin and the 5 structure factors in pig SC fit well with the continuous Fourier function. However, with respect to the 5 reflections in the diffraction curve of the mouse SC the deviations are larger. The matching of the structure factors of the LPP in pig SC and in SC of cultured skin indicates that the

electron density distribution in the model mixtures is very similar to that in SC. The partial correlating mouse SC structure factors, however, imply that the mouse SC and the model mixtures contain a somewhat different molecular structure for the LPP.

Discussion

The high resolution electron density profile presented in this paper provides a more detailed insight into the molecular organization of the LPP. We combined the x-ray diffraction data of a large number of SC model mixtures in which the lipids form the LPP with a slight variation in repeat distance. With the intensities of 6 reflections we were able to select a set of phase angle combinations, namely - + + - - +. By combining the phase angles with the structure amplitudes of the 6 reflections attributed to the LPP we calculated an electron density profile for the unit cell of the LPP. From the trend that the structure factors of all model mixtures sample the same function (see Fig. 3 and 4), it follows that a very similar electron density profile for the LPP is present in all mixtures, with slight variations due to the variation in the composition of the mixtures. This similarity in electron density profile for the model mixtures prepared with either synthetic CER or isolated CER, demonstrates a very similar molecular organization for the LPP in these mixtures. The similarity at this high level of detail is quite remarkable as the fatty acid chain-length variation and the headgroup variation in the synthetic CER mixture is less abundant than in isolated CER mixtures. In the former only acyl chains with a chain-length of 16, 24 and 30 carbon atoms are present, while in the latter there is a wide variation in acyl chain-length, ranging from approximately 14 to 34 carbon atoms. Furthermore, as we included both dry and hydrated samples, this also suggests that the addition of a buffer at pH 5 does not dramatically change the electron density profile of the unit cell and therefore confirms that almost no swelling of the lamellae is induced, as observed previously (9, 13, 17).

We calculated the structure factors from reflections attributed to the LPP in SC isolated from pig, mouse or cultured skin. The structure factors of the LPP in SC of pig and of cultured skin fitted well with the continuous Fourier transform obtained for the lipid mixtures, demonstrating that the electron density profile in the unit cell of the LPP in the mixtures is very similar to the profile of the LPP in SC of pig and cultured skin. Although the mouse SC exhibits a slightly different organization, the lipid mixtures serve as an excellent model for the lipid organization in SC of pig and cultured skin, not only with respect to the similarity in repeat distance of the LPP (13, 18, 20, 30), but also in mimicking the molecular organization in the unit cell of the LPP. This is a big step forward towards unravelling the molecular organization of the LPP in SC.

Average electron density profiles for the LPP in the mixtures

Our method for determining the phase angles of the structure factors is slightly different from the swelling method that is commonly used. The swelling method is based on increasing a lamellar repeat distance by varying the hydration level of the lipid mixture (29, 32, 33). However, in previous studies it has been observed that at physiological conditions the repeat distance of the LPP in SC or in SC lipid models is almost insensitive to the level of hydration (9, 13, 17). Only when using a high pH value and/or a high cholesterol sulphate content, it is possible to induce swelling in the LPP (18). As we preferred to use lipid mixtures mimicking the physiological conditions as closely as possible, we utilized a variation in repeat distance for the LPP, observed in the SAXD patterns of mixtures with different lipid compositions (see Table 1). The small variation in repeat distance we observed (from 12.1 to 13.8 nm) is probably induced by either a variation in the average lipid chain-length in the different mixtures, or a variation in headgroup architecture. This implies that the structure factors in Fig. 4 sample an average continuous Fourier function, representative for the average electron density in the unit cell of the LPP in the lipid mixtures.

From electron density profile to molecular organization

The electron density profile in Fig. 5 exhibits four high electron density regions inside the unit cell; two electron density peaks are located at the border of the unit cell around -6.5 and +6.5 nm, while two smaller high electron density peaks are located at -2.0 and +2.0 nm from the center of the unit cell. This suggests a unit cell with three lipid bilayers of 4.5, 4.0 and 4.5 nm in width.

The electron density profile in Fig. 5 is supported by several observations: The trilayer arrangement is in agreement with the broad-narrow-broad pattern observed in RuO₄ stained SC as explained by Hill and Wertz (34). Also, in a previous study McIntosh used the swelling method to select a set of phase angles for the first three reflections of a mixture with pigCER:CHOL:palmitic acid 2:1:1 (18). His set of 3 phase angles corresponds to the first 3 we also selected (- + +).

When using the 3 signs and only the first 3 reflections obtained for our mixture, the calculated electron density profile is very similar to the electron density profile obtained by McIntosh. He concluded that only two asymmetric bilayer regions are present in the unit cell of the LPP with a water layer between the outer headgroups in the unit cell. The resolution of the electron density profile was 2 nm, while in our studies the resolution of the electron density profile increased to 1.1 nm. This higher resolution allowed us to determine the electron density peaks at a higher precision. The electron density region between -2.0 and +2.0 nm in our profile corresponds to the water region in the electron density profile of McIntosh. Although this region shows a medium electron density similarly as observed by McIntosh, this medium density level cannot be explained by a water layer for two reasons: 1) This electron density profile is also present in lipid mixtures prepared in the absence of a buffer (see Table 1, the equimolar pigCER:CHOL:FFA mixture). 2) Due to the similarities in the Fourier transform the lipid organization in SC is very similar to that in the lipid mixtures. However, in SC

almost no swelling was observed after hydration at physiological conditions (13, 17).

Constructing a molecular model for the LPP based on the density profile may provide more insight into the molecular organization of the LPP. Because CER1 is crucial for the formation of the LPP and forms the backbone of the molecular structure of the LPP (12, 35), we will only focus on the location of CER1 in the unit cell of the LPP. Furthermore, in previous studies it has been reported that a fluid phase is present in the lipid model mixtures (8, 36) which is correlated to the presence of the CER1 linoleate chain. Therefore, this fluid phase must also be accounted for in the molecular model for the LPP.

Possible location of CER1 in the unit cell

Firstly, due to the large width of the high electron density peaks located at the border of the unit cell, it is likely that two polar headgroups are located in these regions at approximately ± 6 and ± 7 nm. The smaller width of the high electron density peaks around -2.0 and $+2.0$ nm indicates that either a single headgroup or the ω -hydroxy ester bond of CER1 is present in this region. Secondly, the length of the acyl chain of CER1 in mixtures with isolated CER1 can range from 26 to 34 carbon atoms. Assuming a 0.127 nm increase in chain-length per C-C bond (37), the fully extended CER1 acyl chain-length is approximately 3.8 ± 0.5 nm. This length fits into the 4.0 nm distance between the high density peaks at -6 nm and -2.0 nm. As the unit cell is centrosymmetric, two CER1 molecules are present in an opposed configuration in the unit cell. In this configuration, the CER1 headgroup is located at the peak positions of -6 or $+6$ nm and the linoleate tail is located in the central trough of the electron density profile between -2.0 and $+2.0$ nm. In this configuration, the CER1 linoleate tails are almost not interdigitating. In Fig. 5 a schematic representation is provided of the proposed location of CER1 in the unit cell. CER1 plays a prominent role in this molecular arrangement for the LPP as it forms the backbone of the molecular structure

in this unit cell: in the absence of acyl CER the LPP cannot be not formed (6,10,11). Furthermore, in phospholipid bilayer systems, CHOL is known to have an affinity towards saturated hydrocarbon chains as compared to unsaturated chains (38-40). If this can be extrapolated to CER systems, in our model CHOL is expected to be located in the outer lipid layer regions and not in the central trough where the linoleate chains are present. Concerning the location of CER1 and the trilayer electron density profile, this model exhibits important aspects of the sandwich model published previously (35).

Conclusions

In this paper we determined a solution for the electron density distribution of the LPP with high resolution, showing the structure of the LPP in more detail. Furthermore, the electron density distribution in the LPP of the mixtures was found to resemble closely to the density distribution in the LPP of isolated SC samples. This demonstrates that the molecular organization in the mixtures mimics the organization of the LPP in SC. Thus, the lipid mixtures serve as an excellent model for the lipid organization in SC. Finally, additional information must be obtained in order to select the phase angles for higher diffraction orders and to solve the molecular organization of the LPP in more detail. This will be the subject of future studies in our group.

We thank the company Cosmoferm B.V. for the provision of the synthetic ceramides and the Netherlands Organization for Scientific Research (NWO) for the provision of beam time at the ESRF. We thank Dr. Wim Bras and Dr. Kristina Kvashnina from the DUBBLE beam line 26 at the ESRF for their support with the x-ray measurements. Furthermore, we thank Dr. Maja Ponec for critically reading the manuscript and Prof. Yehudi Levine for the in-depth discussions on x-ray diffraction analysis. Finally, we thank M.Sc. Krishna Mohan for the help with calculating the density of a single ceramide molecule.

References

1. Caussin, J., G. S. Gooris, H. W. Groenink, J. W. Wiechers, and J. A. Bouwstra. 2007. Interaction of lipophilic moisturizers on stratum corneum lipid domains in vitro and in vivo. *Skin Pharmacol Physiol* 20:175-186.
2. Motta, S., M. Monti, S. Sesana, R. Caputo, S. Carelli, and R. Ghidoni. 1993. Ceramide composition of the psoriatic scale. *Biochim Biophys Acta* 1182:147-151.
3. Simonetti, O., A. J. Hoogstraate, W. Bialik, J. A. Kempenaar, A. H. Schrijvers, H. E. Bodde, and M. Ponec. 1995. Visualization of diffusion pathways across the stratum corneum of native and in-vitro-reconstructed epidermis by confocal laser scanning microscopy. *Arch Dermatol Res* 287:465-473.
4. Weerheim, A., and M. Ponec. 2001. Determination of stratum corneum lipid profile by tape stripping in combination with high-performance thin-layer chromatography. *Arch Dermatol Res* 293:191-199.
5. Madison, K. C., D. C. Swartzendruber, P. W. Wertz, and D. T. Downing. 1988. The biochemistry and function of stratum corneum. *J Invest Dermatol* 90:110-116.
6. Bouwstra, J. A., G. S. Gooris, J. A. van der Spek, and W. Bras. 1991. Structural investigations of human stratum corneum by small-angle X-ray scattering. *J Invest Dermatol* 97:1005-1012.
7. Gooris, G. S., and J. A. Bouwstra. 2007. Infrared spectroscopic study of stratum corneum model membranes prepared from human ceramides, cholesterol, and fatty acids. *Biophys J* 92:2785-2795.
8. Bouwstra, J. A., G. S. Gooris, F. E. Dubbelaar, and M. Ponec. 2001. Phase behavior of lipid mixtures based on human ceramides: coexistence of crystalline and liquid phases. *J Lipid Res* 42:1759-1770.
9. de Jager, M., W. Groenink, J. van der Spek, C. Janmaat, G. Gooris, M. Ponec, and J. Bouwstra. 2006. Preparation and characterization of a stratum corneum substitute for in vitro percutaneous penetration studies. *Biochim Biophys Acta* 1758:636-644.
10. Groen, D., G. S. Gooris, M. Ponec, and J. A. Bouwstra. 2008. Two new methods for preparing a unique stratum corneum substitute. *Biochim Biophys Acta* 1778:2421-2429.
11. Chen, X., S. Kwak, M. Lafleur, M. Bloom, N. Kitson, and J. Thewalt. 2007. Fatty acids influence "solid" phase formation in models of stratum corneum intercellular membranes. *Langmuir* 23:5548-5556.
12. Bouwstra, J. A., G. S. Gooris, F. E. Dubbelaar, and M. Ponec. 2002. Phase behavior of stratum corneum lipid mixtures based on human ceramides: the role of natural and synthetic ceramide 1. *J Invest Dermatol* 118:606-617.

13. McIntosh, T. J., M. E. Stewart, and D. T. Downing. 1996. X-ray diffraction analysis of isolated skin lipids: reconstitution of intercellular lipid domains. *Biochemistry* 35:3649-3653.
14. Garson, J. C., J. Doucet, J. L. Leveque, and G. Tsoucaris. 1991. Oriented structure in human stratum corneum revealed by X-ray diffraction. *J Invest Dermatol* 96:43-49.
15. Hou, S. Y., A. K. Mitra, S. H. White, G. K. Menon, R. Ghadially, and P. M. Elias. 1991. Membrane structures in normal and essential fatty acid-deficient stratum corneum: characterization by ruthenium tetroxide staining and x-ray diffraction. *J Invest Dermatol* 96:215-223.
16. White, S. H., D. Mirejovsky, and G. I. King. 1988. Structure of lamellar lipid domains and corneocyte envelopes of murine stratum corneum. An X-ray diffraction study. *Biochemistry* 27:3725-3732.
17. Bouwstra, J. A., G. S. Gooris, J. A. van der Spek, S. Lavrijsen, and W. Bras. 1994. The lipid and protein structure of mouse stratum corneum: a wide and small angle diffraction study. *Biochim Biophys Acta* 1212:183-192.
18. McIntosh, T. J. 2003. Organization of skin stratum corneum extracellular lamellae: diffraction evidence for asymmetric distribution of cholesterol. *Biophys J* 85:1675-1681.
19. Bligh, E. G., and W. J. Dyer. 1959. A rapid method of total lipid extraction and purification. *Can J Biochem Physiol* 37:911-917.
20. Bouwstra, J. A., G. S. Gooris, K. Cheng, A. Weerheim, W. Bras, and M. Ponc. 1996. Phase behavior of isolated skin lipids. *J Lipid Res* 37:999-1011.
21. Imokawa, G., A. Abe, K. Jin, Y. Higaki, M. Kawashima, and A. Hidano. 1991. Decreased level of ceramides in stratum corneum of atopic dermatitis: an etiologic factor in atopic dry skin? *J Invest Dermatol* 96:523-526.
22. Wertz, P. 1991. In *Physiology, Biochemistry and Molecular Biology of the Skin*. L. A. Goldsmith, editor. Oxford University Press, Oxford. 205-235.
23. Blaurock, A. E., and J. C. Nelander. 1976. Disorder in nerve myelin: analysis of the diffuse x-ray scattering. *J Mol Biol* 103:421-431.
24. Nagle, J. F., and S. Tristram-Nagle. 2000. Structure of lipid bilayers. *Biochim Biophys Acta* 1469:159-195.
25. Shannon, C. E. 1949. Communication in the presence of noise. *Proc. Inst. Radio Engrs.* 37:10-21.
26. Franks, N. P., and W. R. Lieb. 1979. The structure of lipid bilayers and the effects of general anaesthetics. An x-ray and neutron diffraction study. *J Mol Biol* 133:469-500.
27. Swartzendruber, D. C., P. W. Wertz, D. J. Kitko, K. C. Madison, and D. T. Downing. 1989. Molecular models of the intercellular lipid lamellae in mammalian stratum corneum. *J Invest Dermatol* 92:251-257.

28. Harroun, T. A., J. Katsaras, and S. R. Wassall. 2006. Cholesterol hydroxyl group is found to reside in the center of a polyunsaturated lipid membrane. *Biochemistry* 45:1227-1233.
29. Franks, N. P. 1976. Structural analysis of hydrated egg lecithin and cholesterol bilayers. I. X-ray diffraction. *J Mol Biol* 100:345-358.
30. Kuempel, D., D. C. Swartzendruber, C. A. Squier, and P. W. Wertz. 1998. In vitro reconstitution of stratum corneum lipid lamellae. *Biochim Biophys Acta* 1372:135-140.
31. Bouwstra, J. A., G. S. Gooris, W. Bras, and D. T. Downing. 1995. Lipid organization in pig stratum corneum. *J Lipid Res* 36:685-695.
32. Levine, Y. K., and M. H. Wilkins. 1971. Structure of oriented lipid bilayers. *Nat New Biol* 230:69-72.
33. McIntosh, T. J., and S. A. Simon. 1986. Hydration force and bilayer deformation: a reevaluation. *Biochemistry* 25:4058-4066.
34. Madison, K. C., D. C. Swartzendruber, P. W. Wertz, and D. T. Downing. 1987. Presence of intact intercellular lipid lamellae in the upper layers of the stratum corneum. *J Invest Dermatol* 88:714-718.
35. Bouwstra, J., G. Gooris, and M. Ponc. 2002. The Lipid Organisation of the Skin Barrier: Liquid and Crystalline Domains Coexist in Lamellar Phases. *Journal of Biological Physics* 28:211-223.
36. Gay, C. L., R. H. Guy, G. M. Golden, V. H. Mak, and M. L. Francoeur. 1994. Characterization of low-temperature (i.e., < 65 degrees C) lipid transitions in human stratum corneum. *J Invest Dermatol* 103:233-239.
37. Small, D. M. 1986. The Physical Chemistry of Lipids. In *Handbook of Lipid Research*. D. J. Hanahan, editor. Plenum Press, New York.
38. Smaby, J. M., M. M. Momsen, H. L. Brockman, and R. E. Brown. 1997. Phosphatidylcholine acyl unsaturation modulates the decrease in interfacial elasticity induced by cholesterol. *Biophys J* 73:1492-1505.
39. Needham, D., and R. S. Nunn. 1990. Elastic deformation and failure of lipid bilayer membranes containing cholesterol. *Biophys J* 58:997-1009.
40. Brzustowicz, M. R., V. Cherezov, M. Caffrey, W. Stillwell, and S. R. Wassall. 2002. Molecular organization of cholesterol in polyunsaturated membranes: microdomain formation. *Biophys J* 82:285-298.

Chapter 7

Disposition of ceramide in model lipid membranes determined by neutron diffraction

D. Groen¹, G. S. Gooris¹, D. J. Barlow², M. J. Lawrence², J. B. van Mechelen³, B. Demé⁴, J. A. Bouwstra^{1*}

¹ Leiden/Amsterdam Center for Drug Research, Department of Drug Delivery Technology, Gorlaeus Laboratories, University of Leiden, P.O. Box 9502, 2300 RA Leiden, The Netherlands.

² Pharmaceutical Science Division, King's College London, The Franklin Wilkins Building, 150 Stamford Street, London SE1 9NH, UK.

³ University of Amsterdam, HIMS/FNWI/Kristallografie, Valckenierstraat 65, 1018 XE Amsterdam, The Netherlands

⁴ Institut Laue-Langevin, 6 Rue Jules Horowitz, F38042 Grenoble Cedex 9, France.

Biophys J, vol. 100, no. 6, pp. 1481-9.

Abstract

The lipid matrix present in the uppermost layer of the skin, the stratum corneum, plays a crucial role in the skin barrier function. The lipids are organized into two lamellar phases. To gain more insight into the molecular organization of one of these lamellar phases, we performed neutron diffraction studies. In the diffraction pattern, five diffraction orders were observed attributed to a lamellar phase with a repeat distance of 5.4 nm. Using contrast variation, the scattering length density profile could be calculated showing a typical bilayer arrangement. To obtain information on the arrangement of ceramides in the unit cell a mixture that included a partly deuterated ceramide was also examined. The scattering length density profile of the 5.4 nm phase containing this deuterated ceramide demonstrated a symmetric arrangement of the ceramides with interdigitating acyl chains in the center of the unit cell.

Introduction

The skin forms the interface between the human body and the environment. It protects our body against various biological and chemical hazards and from desiccation in a dry environment. The outermost layer of the skin, the stratum corneum (SC), forms the main barrier against diffusion of substances across the skin (1). This layer consists of overlapping flattened dead skin cells. Each cell is surrounded by lipids, which serve as the mortar between the cells. The lipids form multiple sheets of lamellae and are mainly composed of ceramides (CER), cholesterol (CHOL) and free fatty acids (FFA). These lipid classes are present in an approximately equimolar ratio (2). The lipids are organized in two lamellar phases with repeat distances of approximately 6 and 13 nm, also referred to as the short periodicity phase (SPP) and long periodicity phase (LPP), respectively (3-7). Despite the high level of CHOL, the lipids form predominantly a crystalline lateral packing (4, 8). This is different from phospholipid membranes, in which high levels of CHOL induce the formation of a liquid ordered phase (9-11). In the SC, the CER are a crucial component in the formation of the lamellar phases that constitute the main barrier function. In previous studies we mainly focussed on the formation and molecular organization of the LPP (3, 4, 12-14). In the present study we focus on the molecular organization of the SPP. Not only in SC, but also in membranes of living cells the CER play an important role, especially in the formation of lipid rafts (15, 16).

Previous studies showed that mixtures prepared with either synthetic CER or native CER mixed with CHOL and with FFA mimic the SC lipid organization very closely (17-19). While CER and CHOL play a prominent role in the formation of the two lamellar phases, the addition of FFA is crucial for the formation of the densely packed orthorhombic crystalline structure (17, 20). A more detailed analysis of the lipid composition revealed that the FFA are predominantly saturated and have a wide distribution of chain lengths, in which the chain lengths of 22 and 24 C atoms are most abundantly present (21). In addition, there are eleven subclasses of CER identified in human SC

(22-24). However, in the synthetic CER mixture that we used in our previous studies five subclasses of CER are present mimicking closely the composition of pig SC. These subclasses consist of either a sphingosine (S) or phytosphingosine (P) base, whereas the acyl chain is a nonhydroxy (N), α -hydroxy (A) or ω -hydroxy chain (25). The corresponding nonhydroxy and α -hydroxy CER that are present in this synthetic CER mixture are denoted as CER NP, CER NS, CER AS and CER AP. The molecular structure of these CER is displayed in Fig. 1. In the synthetic CER mixture used in previous studies an ω -hydroxy CER is present (26). This CER possesses a longer acyl chain length (C30) and has a linoleic acid chemically bound to its ω -hydroxy group (indicated with EO). It is denoted as CER EOS. Using these CER subclasses, mixed with CHOL and FFA, it was demonstrated that EOS is very important for the formation of the LPP and that the mixtures closely mimicked the lamellar phase behaviour of mixtures prepared from either isolated human or pig CER (13, 26).

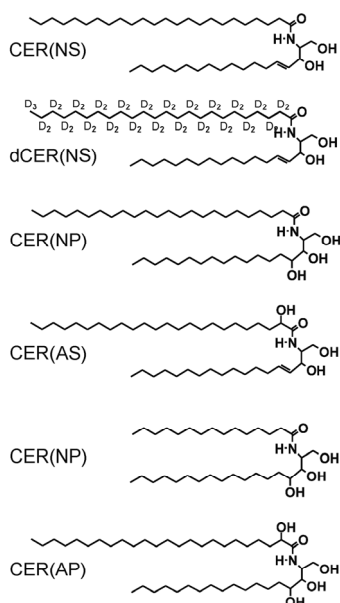


Figure 1: Molecular structure of the synthetic CER used in the mixtures.

Although the above studies were very relevant for providing information on the role the various lipid classes play in the lipid organization, no detailed information was obtained about the localization and molecular arrangement of the molecules within the unit cell. In this respect in several other studies progress has been made using simplified ternary or quaternary lipid mixtures. The mixtures included mainly CER AP with a short acyl chain length of 18 C atoms, CHOL and cholesterol sulfate. In these studies the neutron scattering length density profile was determined of CER rich phases with a short periodicity (27-29). In some studies CER EOS and a single (deuterated) fatty acid were also included, which allowed the localization of the deuterated fatty acid in the unit cell of the phases formed by these simplified mixtures (29).

In the present study we investigate the SPP of SC in more detail, using a complex lipid mixture of synthetic CER, CHOL and FFA that closely mimics the SPP observed in stratum corneum (30). The aim is to obtain information on the localization and conformation of CER NS in the SPP. We chose CER NS, as it is the most abundant CER subclass in the model mixture. As CER EOS is crucial for the formation of the LPP (31), it is excluded from these mixtures. In the studies focussed on the conformation and localization of CER NS in the SPP, part of the CER NS is replaced by CER NS with a perdeuterated acyl chain (dCER NS). First the neutron scattering length density profile of the SPP is determined by using contrast variation. In the second part of our studies information on the arrangement of CER NS in the unit cell of the SPP is obtained by using its partially deuterated counterpart.

Materials and Methods

Materials

Synthetic CER NS (C24), dCER NS (C24), Cer NP (C24), CER AS (C24), CER NP (C16) and CER AP (C24) were generously provided by Cosmoferm B.V. (Delft, The Netherlands). The number given in parentheses denotes the

number of carbon (C) atoms in the acyl chain of the ceramides, all the lipids studied were acyl chain saturated. The palmitic acid (C16:0), stearic acid (C18:0), arachidic acid (C20:0), behenic acid (C22:0), tricosanoic acid (C23:0), lignoceric acid (C24:0), cerotic acid (C26:0), cholesterol and acetate buffer salts were purchased from Sigma-Aldrich Chemie GmbH (Schnelldorf, Germany). The silicon substrates were cut from a wafer (P/Boron (110), thickness $380 \pm 10 \mu\text{m}$) obtained from Okmetic (Vantaa, Finland). All organic solvents used were of analytical grade and manufactured by Labscan Ltd. (Dublin, Ireland). The water used was of Millipore quality.

Preparation of the lipid models

For preparation of the model with protonated lipids, synthetic CER, CHOL and FFA were used. The following synthetic CER composition was selected (see also Fig. 1): CER NS C24, CER NP C24, CER AS C24, CER NP C16 and CER AP C24 in a 60:19:5:11:6 molar ratio which, apart from the absence of CER EOS, closely resembles the CER composition in pig SC (32). For the free fatty acids mixture (FFA), the following composition was selected: C16:0, C18:0, C20:0, C22:0, C23:0, C24:0 and C26:0 at molar ratios of 1.8, 4.0, 7.7, 42.6, 5.2, 34.7 and 4.1 respectively. This chain length distribution is based on the FFA composition in human SC (21). To achieve the desired 1:1:1 ratio of CER:CHOL:FFA, for each model the appropriate amounts of individual lipids were dissolved in chloroform:methanol (2:1) and combined into one solution with a final lipid concentration of approximately 10 mg/ml. This solution was sprayed over an area of $1 \times 3.8 \text{ cm}^2$ on a silicon substrate using a Camag Linomat IV sample applicator (MuttENZ, Switzerland). The spraying rate was $5 \mu\text{L}/\text{min}$ and the solvent was evaporated by a stream of nitrogen gas. The silicon substrate with applied lipid film was then equilibrated twice for 10 minutes at a temperature of approximately 80°C . After each heating step the sample was cooled to RT over approximately 30 min. After equilibration, the lipid layer was immersed in acetate buffer (50 mM, pH 5) and kept at 37°C for 24h to achieve

maximum hydration. After the hydration step the sample was kept at 100% RH until measured in neutron diffraction. This sample preparation leads to oriented multilayers with a low mosaicity, as is demonstrated in Fig. 2.

The same preparation method was used for the model in which 30 mol% of the CER NS was replaced by dCER NS. This “deuterated” sample contains in total 2.5 mol% of deuterated lipids. For the determination of the signs of the structure factors, acetate buffers containing 0, 33, 67 and 100% D₂O were used. When a neutron diffraction measurement of a sample at a selected H₂O:D₂O ratio was completed, the sample was exposed to a buffer with another H₂O:D₂O ratio for a period of 24h at 37°C and subsequently mounted in the chamber for the next neutron diffraction measurement. This procedure was repeated until the sample was measured with all 4 H₂O:D₂O buffer concentrations.

Weighing of the samples to determine the hydration level

To determine the degree of hydration of the mixtures, all samples were weighed in a dry state (24h dehydration over P₂O₅) and fully hydrated state (see procedure above) using a Sartorius SE 2 microbalance (Nieuwegein, The Netherlands). This was performed for both the protonated (in duplicate) and deuterated samples (in triplicate) and the weighing procedure of each sample was repeated 3 times.

X-ray diffraction experiments

Before the neutron diffraction measurements were performed, the equilibration temperature and equilibration period of the lipid mixtures during sample preparation were optimized to form only one lamellar phase with maximum orientation parallel to the silicon support. The samples were measured by X-ray diffraction. An X'pert Pro-alpha diffractometer from PANalytical (Almelo, The Netherlands) was used equipped with a sealed Cu X-ray tube, 0.01 rad primary and secondary Soller slits and an elliptical mirror that produces a convergent beam of Cu K α_1 and K α_2 radiation with

wavelengths of respectively 1.5406 and 1.5444 Å. The analysis of the 1D diffraction patterns was the same as described previously (19).

Neutron diffraction experiments

Experiments were performed on the D16 diffractometer at the Institute Laue-Langevin (ILL, Grenoble, France) operating at $\lambda = 4.75$ Å in the reflection mode. Samples were mounted on a goniometer placed in a sealed temperature-controlled aluminum humidity chamber in the presence of an acetate buffer bath to maintain constant maximum humidity. The temperature in the chamber was kept at 25°C during the measurements. The sample to detector distance was 1.0 m. The intensity of the diffracted beam was recorded by a position sensitive two-dimensional ^3He detector with 128 x 128 channels and 2 mm resolution between channels. The 2D detector readout was integrated in the vertical direction which results in a one-dimensional intensity projection as a function of the detector channel position (2θ). Intensities on the detector surface were corrected by normalization to a water calibration and by subtraction of the empty chamber background. The measurement time per sample varied between 7 and 12 h, depending on the signal to noise ratio during the measurements. A longer measurement time was used for the higher diffraction orders (3 to 5). The lamellar spacing (d) was obtained by fitting the peak positions (in 2θ) of all diffraction orders (h) according to Bragg's law; $2d\sin\theta = h\lambda$. Data analysis was performed using the ILL in-house software LAMP (33). Since it was not possible to integrate over the complete range in omega (due to cut off by the substrate and due to the omega range used in the measurements), we chose to integrate only the peak intensities originating from the lamellae oriented parallel to the silicon support. This was achieved by selecting only the small angle high intensity part of the diffraction peaks at sample rotations of $\Omega = -0.1, 0.0$ and $+0.1$ degrees around the Bragg angle (see also Fig. 2). A summing of these pixel intensities resulted in the total peak intensity value (I_h). Using this integration method we obtain an excellent signal to noise

ratio. Then, the structure factor amplitudes $|F_h|$ were calculated from the total peak intensity (I_h) by:

$$|F_h| = A_h(\theta) \sqrt{h \cdot I_h} \quad (1)$$

Where A_h is the correction factor for sample absorption, which can be calculated via (34):

$$A_h(\theta) = 1 / \sqrt{\frac{\sin \theta}{2\mu L} \left[1 - \exp\left(\frac{-2\mu L}{\sin \theta}\right) \right]} \quad (2)$$

In this equation θ is the Bragg angle, μ the linear attenuation coefficient and L the thickness of the lipid film. With a lipid density of approximately 0.87 g/cm^3 and weight of 10 mg in an area of 3.8 cm^2 , the thickness of the lipid film (L) was calculated to be about $30 \text{ }\mu\text{m}$. The linear attenuation coefficient was calculated from the wavelength used in combination with the density and the chemical composition of the lipid film (35). For the protonated sample μ ranges from 5.48 to 5.09 cm^{-1} for 0% to 100% D_2O respectively and for the deuterated sample $\mu = 5.03$ to 4.65 cm^{-1} . The error in $|F_h|$ was determined from the standard deviation of the summed pixel intensities (σ_I) by:

$$\Delta|F_h| = \frac{A_h \cdot \sigma_{I_h}}{2\sqrt{h \cdot I_h}} \quad (3)$$

If the unit cell of the SPP bilayer is centrosymmetric, the phases of the structure factors are either 0 or π . For this situation, the structure factors display a linear correlation as function of $\text{H}_2\text{O}:\text{D}_2\text{O}$ ratio (34). For a hydrated bilayer we may assume that water is distributed near the hydrophilic headgroups, at the boundaries of the unit cell. Mathematically, a Gaussian water distribution at the boundaries of the unit cell ($\pm d/2$) results in structure factor signs for the water layer being - + - + -. Because the water structure factors are defined as the structure factors at 100% D_2O minus that at 100% H_2O , the signs of the structure factors can be determined from the plot of the $\text{H}_2\text{O}:\text{D}_2\text{O}$ contrast versus the obtained structure factor amplitudes $|F_h|$. The

procedure is as follows: The sign of F_h must be chosen such that F_h at 100% D_2O minus F_h at 0% D_2O results in the correct sign for the h^{th} order of the water layer structure factor.

When the structure factor phase signs are determined, the neutron scattering length density profile for the SPP bilayer, $\rho(x)$, can be calculated via a Fourier transform of the structure factors (36):

$$\rho(x) = \frac{2}{d} \sum_h F_h \cos(2\pi hx / d) \quad (4)$$

Where x is the direction normal to the bilayer surface. The significance of features in the density profile can be visualized by the error in the scattering length density, depicted in the following equation (37):

$$\Delta\rho(x) = \frac{2t}{d} \left[\sum_h (\Delta F_h)^2 \cos^2(2\pi hx / d) \right]^{1/2} \quad (5)$$

Where t is Student's t -statistic. The error in the structure factors (ΔF_h) was determined with Eq. 3. A 99.7% confidence limit for the scattering length density was obtained by using a Student's t -statistic of $t = 2.97$.

Furthermore, after a normalization of the patterns by setting the sum of the structure factor amplitudes (F_1 to F_5) equal for the protonated and deuterated sample, the difference density profile (resulting from the deuterated CER NS tails) can be calculated by subtracting the density of the protonated sample from that of the deuterated sample. To obtain an absolute scaling for the density patterns the total scattering length density (F_0) must be determined and additional information on the features in the difference density pattern is needed. F_0 was calculated using the chemical composition and the mass density of the sample (38, 39).

Results

Optimal sample preparation

Before neutron measurements were performed, the samples were assessed by X-ray diffraction measurements to ensure a proper lamellar organization and orientation. Our original procedure of equilibrating the samples twice for 1 hour at a temperature slightly above the onset of melting, followed by cooling to room temperature, resulted not only in reflections attributed to the SPP, but also in reflections attributed to an additional phase with a repeat distance of 4.4 nm, see Fig. S1A. To examine the formation of this additional phase in more detail, the sample was heated during which diffraction curves were recorded. At 80°C the diffraction peaks attributed to this additional phase disappeared. A subsequent cooling to room temperature resulted in a diffraction pattern with reflections attributed to the SPP with a repeat distance of 5.4 nm and crystalline CHOL only, see Fig. S1B. Based on these results, the lipid mixtures for the neutron diffraction studies were equilibrated for 10 minutes at a temperature of approximately 80°C.

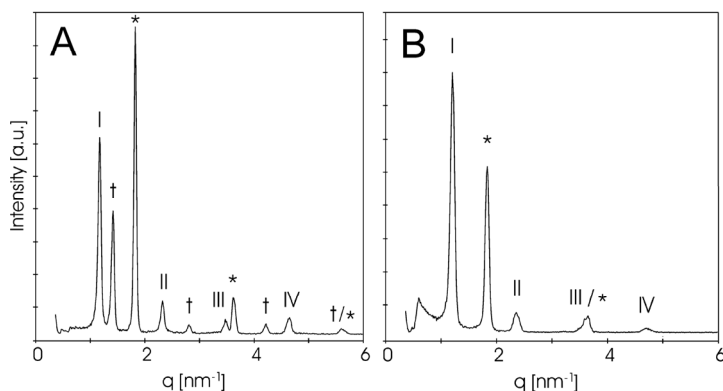


Figure S1: A) X-ray diffraction pattern of the deuterated sample after equilibration at 70°C. B) X-ray diffraction pattern of the deuterated sample after re-equilibration at 90°C. The reflections of the SPP are indicated by Roman numbers I to IV. Reflections of an additional 4.4 nm phase are indicated by a cross and reflections from crystalline CHOL are indicated by asterisks.

Number of water molecules per lipid molecule

Increasing the D₂O concentration in the hydration buffer resulted in a moderate increase in neutron scattering signal, indicating that a relatively low number of water molecules is present in the sample. To determine the amount of water in the samples, the samples are weighed with a microbalance in dry and hydrated state. As expected, between the protonated and deuterated samples no difference in the hydration level was observed. The resulting water:lipid molar ratio determined by weighing is 1.91 ± 0.42 , which indicates that in the lipid mixtures approximately 2 water molecules are present per lipid molecule.

Neutron diffraction pattern

In Fig. 2 a typical example of a diffraction pattern is shown of the mixture containing dCER NS hydrated at 100% D₂O. Three reflections that can be attributed to the SPP are visible at scattering angles of $2\theta = 5.13, 10.16$ and 15.29 degrees, corresponding to a repeat distance of $d = 5.36 \pm 0.04$ nm. In addition, one reflection attributed to crystalline CHOL is visible at $2\theta = 8.0$ degrees. The maximum intensity of the SPP third diffraction order is not visible in Fig. 2, as it is located at the sample rotation of $\Omega = 7.65$ degrees, which is recorded at the second detector position (not shown). The diffraction pattern of the SPP reveals very sharp peaks indicating that a higher number of lipid lamellae is oriented parallel to the substrate surface as compared to other orientations. The mosaicity of the parallelly ordered lamellae was calculated (taking the FWHM of a Gaussian fit to the sharp peak in Ω for orders 1 to 5) to be 0.275 ± 0.014 degrees. A very similar pattern is observed for the protonated sample. The second reflection of CHOL is too low in intensity to be visible in Fig. 2 and its maximum intensity is located at a higher sample rotation of $\Omega = 8.0$ degrees, also recorded at the second detector position. After integration of the peak at this second detector position, the second order of CHOL was determined at $2\theta = 16.0$

Position of ceramide in lipid membrane determined by neutron diffraction

degrees. This reflection did not overlap with the third order reflection of the SPP.

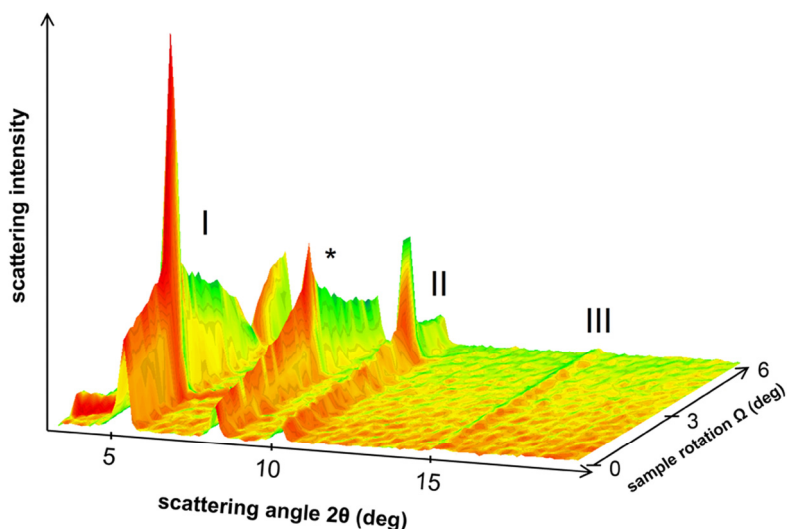


Figure 2: Neutron diffraction profile of the deuterated sample at 100% RH with a buffer of 100% D₂O. The reflections of the SPP are indicated by Roman numbers I to III and a reflection of crystalline CHOL is indicated by an asterisk.

Table 1:

Structure factor amplitudes with errors and absorption correction factors.

[D ₂ O]	F(1)	A ₁	F(2)	A ₂	F(3)	A ₃	F(4)	A ₄	F(5)	A ₅
protonated sample:										
0%	41.23 ± 0.08	1.19	19.67 ± 0.13	1.09	13.99 ± 0.09	1.06	14.17 ± 0.11	1.05	5.19 ± 0.25	1.04
33%	62.83 ± 0.11	1.19	33.72 ± 0.08	1.09	22.65 ± 0.08	1.06	24.52 ± 0.08	1.05	12.65 ± 0.11	1.04
67%	80.82 ± 0.13	1.18	46.56 ± 0.10	1.09	33.91 ± 0.09	1.06	33.27 ± 0.08	1.04	18.37 ± 0.10	1.04
100%	97.22 ± 0.15	1.18	58.39 ± 0.11	1.09	42.64 ± 0.08	1.06	40.96 ± 0.07	1.04	24.93 ± 0.06	1.04
deuterated sample:										
0%	43.68 ± 0.11	1.17	26.04 ± 0.09	1.09	13.99 ± 0.09	1.06	18.03 ± 0.11	1.04	6.10 ± 0.22	1.03
33%	57.52 ± 0.11	1.17	39.33 ± 0.11	1.08	22.45 ± 0.08	1.06	25.52 ± 0.11	1.04	9.80 ± 0.24	1.03
67%	64.57 ± 0.13	1.17	44.72 ± 0.10	1.08	25.97 ± 0.08	1.05	30.60 ± 0.10	1.04	14.21 ± 0.09	1.03
100%	81.48 ± 0.15	1.16	59.71 ± 0.14	1.08	35.96 ± 0.08	1.05	38.48 ± 0.10	1.04	19.56 ± 0.11	1.03

Determination of the phase signs

The absolute structure factor amplitudes with corresponding errors and absorption correction factors are calculated from the diffraction patterns using Eq. 1 to 3. They are provided in Table 1. As shown in the table, the errors in the structure factor amplitudes are small. The linear fits of the structure factor amplitudes with the H₂O:D₂O ratio are displayed in Fig. 3, A and B for the protonated and deuterated sample respectively. From these fits it is clear that the structure factors correlate linearly with the H₂O:D₂O ratio, demonstrating that the lipids in the SPP form a centrosymmetric structure - and this is also true when CER NS is partially substituted by dCER NS. Furthermore, clear differences are observed between the structure factors of the protonated sample and those of the deuterated sample, which indicates a difference between their scattering length density profiles.

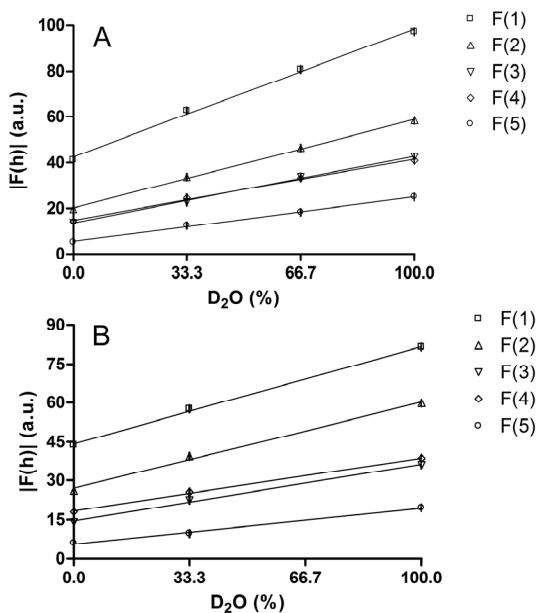


Figure 3: A) Linear fits of the structure factor amplitudes of the protonated sample with the ratio of H₂O:D₂O in the hydration buffer. B) Linear correlation of the structure factor amplitudes of the deuterated sample with the H₂O:D₂O ratio. The error bars represent the standard deviations.

The phase signs are obtained from the H₂O:D₂O plots as follows: A Gaussian water distribution is assumed near the lipid headgroups at the unit cell boundaries ($\pm d/2$). The phase signs for the structure factors of this water layer are, according to its distribution, - + - + -. Subsequently, because the water layer structure factors are defined as the total structure factors at 100% D₂O minus those at 0% D₂O, the structure factor phase signs for the protonated and deuterated sample can be deduced (see Fig. 3, A and B). Since the structure factor amplitudes at 100% D₂O in Fig. 3, A and B are all higher than those at 0% D₂O, the structure factor signs of both the protonated and deuterated sample are also - + - + -, for diffraction orders 1 to 5, respectively.

Scattering length density profiles

The neutron scattering length density profiles of the SPP at 0% D₂O concentration in the protonated and deuterated sample were calculated using Eq. 4. The profiles are displayed in Fig. 4, A and B for the protonated and deuterated sample respectively, with a 99.7% confidence interval calculated with Eq. 5. The profile of the protonated sample displays a high density at the boundaries of the unit cell, a low density in the center and a submaximum at -1.5 and +1.5 nm from the center. Minima in the profile are located at -0.75 and +0.75 nm from the center. The profile of the deuterated sample is very similar to that of the protonated sample, except for an elevated density in the center of the unit cell.

Subsequently, both density patterns are normalized and a difference density pattern is calculated by subtracting the protonated from the deuterated pattern. This difference profile represents the density of the deuterated acyl chains. The resulting difference pattern displays an elevated density in the center of the unit cell. To put the density patterns on an absolute scale as described in the materials and methods, we use information on the molecular structure given by the shape of the difference density pattern as follows: The dCER NS is deuterated along the total length of the acyl chain

(D47). Because the acyl chain is also located in the headgroup region (see Fig. 1) and the intermembrane space is very small (~ 0.1 nm), the neutron scattering length density is expected to increase throughout the entire length of the unit cell.

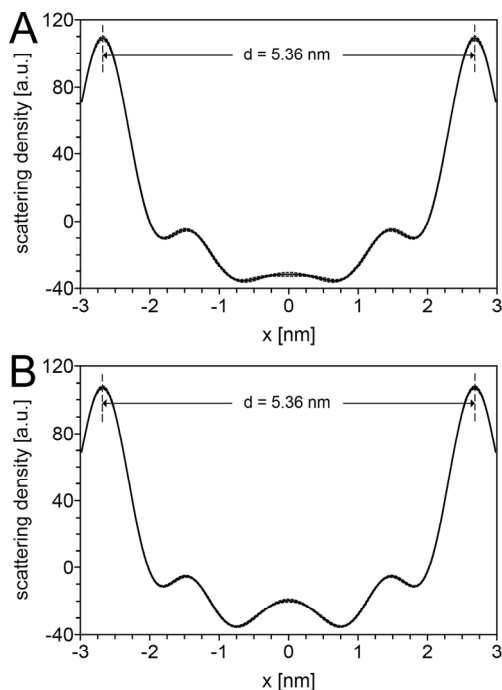


Figure 4: A) Scattering length density profile of the SPP in the protonated sample (solid line). B) Scattering length density profile of the SPP in the deuterated sample (solid line). The dotted lines indicate the 99.7% confidence interval.

Since the shape of the difference density pattern only displays an elevation in the center of the unit cell, this indicates an interdigitation of deuterated acyl chains in the center of the unit cell. We use this information to scale the difference pattern so that the density (D-H) in the center of the unit cell (resulting from 2 overlapping acyl chains) is exactly twice the density in the remaining part of the unit cell (resulting from a single acyl chain). In Fig. 5 the protonated, deuterated and difference density patterns are displayed on

Position of ceramide in lipid membrane determined by neutron diffraction

an absolute density scale. It must be emphasized that the scaling procedure has no influence on the shape of the difference density pattern, only on the range of the scattering length density on the y-axis.

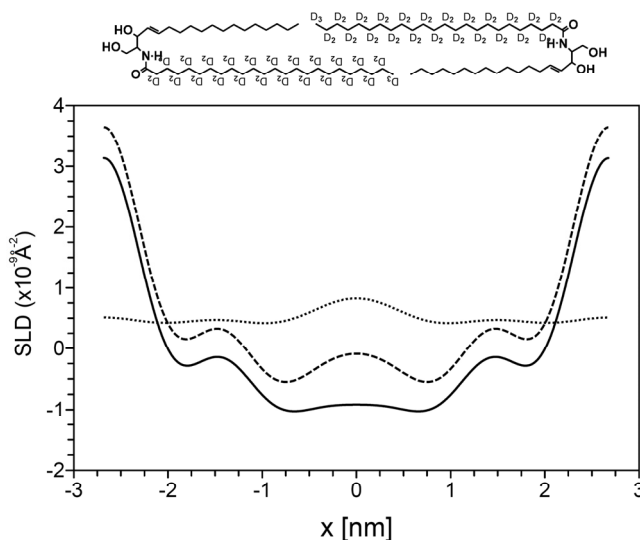


Figure 5: Scattering length density profiles of the SPP in the protonated sample (solid line) and deuterated sample (dashed line) and their difference profile (dotted line) plotted on an absolute density scale. A possible arrangement of the dCER NS molecules in the SPP bilayer is also presented.

Discussion

In human SC the lipids form two lamellar phases referred to as the LPP and SPP (3-7, 40). Very recently, the electron density profile of the unit cell in the LPP was calculated by means of X-ray diffraction studies (14). These studies indicated that in the unit cell of the LPP the lipids are organized in three layers that are almost equally in width. This lipid arrangement, which is very characteristic for the lipid organization in SC, is dictated by the molecular architecture of CER EOS. These studies also demonstrated that the lipid

organization of mixtures prepared from either synthetic CER mixtures or isolated CER mixtures is very similar to that in SC, not only with respect to the repeat distances of the lipid phases, but also with respect to the electron density profile of the unit cell of the LPP. The aim of the present study was to gain more insight into the molecular structure of the SPP. It is well known that the repeat distances of the lamellar phases in mixtures prepared from CER, CHOL and FFA are very insensitive to hydration and that especially for the SPP only a limited number of diffraction orders are obtained with X-ray diffraction. Therefore it is difficult to obtain an electron density profile by X-ray diffraction analysis. In addition, by using a deuterated lipid in neutron experiments information can be obtained about the arrangement of this lipid in the unit cell. For this reason it was decided to perform neutron diffraction studies, as this permits contrast variation by changing the H₂O:D₂O ratio to obtain the phase signs of the structure factors of the various diffraction orders. Using this method we were able to calculate the scattering length density profile of the SPP. However, our final goal is to obtain information on the arrangement of the CER in the unit cell. Therefore we partly replaced the (most abundant) CER NS in the lipid mixture by dCER NS to determine the position of the acyl chain in the unit cell. To the authors' knowledge, these are the first neutron diffraction measurements reported for a lipid mixture that closely mimics the SPP in SC.

In our previous studies, using X-ray diffraction on mixtures with CER, CHOL and FFA prepared in the absence of CER EOS, we were able to form the SPP and partly phase separated crystalline CHOL without the presence of additional phases. However, during the sample preparation for the neutron diffraction experiments, in which we used silicon as the supporting substrate, the equilibration method had to be adjusted to obtain only the SPP and phase separated crystalline CHOL. Our current studies demonstrate that the formation of an additional 4.4 nm phase can be avoided by equilibration of the sample at about 10°C above the melting region of the lipid mixture. The presence of the CHOL is not avoided, as phase separated crystalline CHOL

is also present in SC (3, 4, 41) and the diffraction peaks of CHOL do not interfere with those of the SPP. In previous studies it was shown that at a ratio of CER:CHOL:FFA of 1:0.4:1, CHOL is incorporated in the lamellar phases (unpublished data). From this we may conclude that CHOL is partly dissolved in the lamellar phases. In studies using mixtures with only a few CERs, CHOL and a single fatty acid, phase separation of the fatty acid fraction has been reported (29, 42, 43). However, the mixtures in the latter studies contained a lower number of CER subclasses and only a single fatty acid. Either a mismatch between the CER and fatty acid chain lengths or a different equilibration procedure most probably causes the phase separation in these mixtures. We not only measured the lamellar phases of our mixtures, but we also examined the lateral packing with IR spectroscopy (unpublished results). There was no indication of phase separation between FFA and CER within the lateral packing of the SPP. This suggests that rather homogenous mixtures are formed - not only with respect to the lamellar phase behavior, but also with respect to the lateral packing.

Hydration level of the lipid mixtures

In previous studies on SC or SC lipid models it has been observed that even at 100% humidity the repeat distance of the lipid lamellae is almost insensitive to the level of hydration, suggesting that very little water is present in the headgroup region (12, 30, 44). Our present studies show that on the basis of weight measurements, approximately 2 water molecules are present per lipid molecule. This is a very low hydration level as compared to phospholipid bilayers, that can contain up to 12 (in the gel phase) or even 35 (in the fluid phase) water molecules per lipid molecule (36). In a related study on a SC model mixture with CER EOS, CER AP, CHOL and palmitic acid, the number of water molecules per lipid molecule was estimated to be only 1, based on the available intermembrane space and the molecular volume of H₂O (29). Because of the limited amount of water in the headgroup region, ceramide containing mixtures are less sensitive to the

H₂O:D₂O contrast variation. However, in the present study the change in the structure factor values was significant when increasing the D₂O level from 0 to 100%. This allowed us to determine the phase signs and to calculate a neutron scattering length density profile for the SPP with a high precision. Due to the low water levels in the lipid mixtures, it was decided to hydrate the samples at 100% humidity.

The low hydration level of CER containing mixtures implies that the hydration level of the SC lipid matrix is also very low, as compared to phospholipid layers in a cell membrane. Regarding the barrier function of the lipid matrix in SC, as the amount of water molecules in the headgroup region is very low, the penetration for hydrophilic molecules is expected to be significantly reduced as compared to crystalline phospholipid membranes. Thus, the very low hydration level of the SC lipid matrix may play an important role in the barrier function of the skin.

Bilayer structure of SPP and arrangement of CER NS in unit cell

When considering the scattering length density profiles for the unit cell of the SPP, a high density is located at the boundaries of the unit cell and a low density in the center. This suggests that the headgroups of the lipids are located at the boundaries of the unit cell, while the hydrocarbon chains are located in the center. This is similar to the formation of a typical lipid bilayer driven by hydrophobic-hydrophilic interactions, as often observed for phospholipid membranes (45-47). Furthermore, the experimentally obtained repeat distance of 5.36 nm is in excellent agreement with the bilayer arrangement of two CER molecules: the total length of the extended sphingosine C18 base and C24 acyl chain, when assuming a 0.127 nm length per C-C bond, is 5.33 nm (48). Therefore it is likely that the CER subclasses with an acyl chain length of C24 (90% of the CER) dictates the repeat distance of the SPP unit cell in our systems. This corresponds with our previous findings that the CER dictate the formation of the lamellar phases in SC (14, 31, 49). In a study by McIntosh et al on a mixture with

isolated CER from pig SC, consisting of CER:CHOL:palmitic acid in a 2:1:1 molar ratio, a SPP with a repeat distance of 5.4 nm was also observed (44). In a study by our group using similar mixtures with isolated pig CER, CHOL and FFA a SPP was observed with a repeat distance of 5.2-5.4 nm depending on the CER:CHOL ratio and the presence of FFAs (31). As the mixtures in both studies were prepared in the absence of pig CER EOS, but with the remaining CER isolated from pig SC, the observation of a 5.4 nm repeat distance equals that in our synthetic mixtures suggesting that the SPP in our mixtures is very similar to the SPP present in mixtures prepared with isolated CER.

In a related neutron diffraction study on a mixture with CER AP, CHOL, cholesterol sulphate and palmitic acid, a density profile for a bilayer structure with a smaller periodicity phase of 4.56 nm was presented (27). In that profile the lowest density is located exactly in the center of the unit cell, whereas in our profile the lowest density is located outside the center at a distance of ± 0.75 nm. This difference may be explained by the different CER used: The acyl and sphingosine chains in the CER AP mixture are equal in length (both C18) and thus no interdigitation is expected to occur. Therefore in the CER AP mixture the terminal methyl groups are located in the center of the bilayer, resulting in a low density region at this location. In contrast, in our mixtures the acyl and sphingosine chains are not equal in length, being C24 and C18 respectively. This difference in chain length is likely to result in an interdigitation of the acyl chains which could explain the slightly elevated density observed in the center of the unit cell. This is demonstrated in Fig. 5, in which an arrangement of dCER NS molecules is displayed (discussed into more detail below). The interdigitation is in agreement with the lower density regions on both sides of the elevated density in the center of the unit cell (at ± 0.75 nm), as these minima correlate with the positions of the terminal CH₃ groups of the acyl and sphingosine chains.

The submaxima in the scattering length density profile located at -1.5 and +1.5 nm from the center of the unit cell may be correlated to a

superimposition of CHOL and the methylene chains of CER and FFA. This is similar to the submaxima observed in the profile of the CER AP mixture at ± 1.3 nm from the center of the unit cell, which were also correlated to a superimposition of methylene chains and CHOL (32). Previously, for phosphatidylcholine molecules with unequal chain lengths of C10 and C18, a bilayer arrangement with interdigitating chains was also suggested (45), supporting our present arrangement for the CER.

As far as the arrangement of the CER in the bilayer is concerned, in previous studies an asymmetric fully extended arrangement is suggested for CER NP (50, 51). Whether an asymmetric arrangement also occurs in mixtures prepared with CER, CHOL and FFA can be deduced from our data. First of all, the magnitude of the structure factors correlates linearly with the D_2O concentration, which is only observed in systems with a centrosymmetric unit cell. When dealing with only protonated mixtures this observation does not provide conclusive information, as also in the asymmetric fully extended configuration of the CER a symmetric unit cell is expected. However, when the mixture is prepared with dCER NS, an asymmetric fully extended configuration of the CER will result in an asymmetric density distribution for the deuterated tails, see Fig. 6 A. But since a linear relationship between structure factors and D_2O concentration is observed using this mixture, a symmetric unit cell must be present. Secondly, the elevated density observed in the center of the dCER NS profile can only result from an interdigitation of dCER NS tails in the center of the unit cell, which is only possible when assuming a symmetric arrangement of the CER NS. Therefore, the CER must be arranged symmetrically, either in the hairpin or in the fully extended configuration. These two arrangements are schematically depicted in Fig. 6, B and C. However, with the current data it is not possible to determine whether the CER NS is in the fully extended configuration or in the hairpin configuration, for the following reasons: In the CER containing mixtures, the water level between the headgroups is approximately 2 water molecules per lipid, resulting in a very small

Position of ceramide in lipid membrane determined by neutron diffraction

intermembrane space. In addition, the expected width of a single unfolded headgroup (fully extended conformation) is almost equal to the expected width of two headgroups in the hairpin conformation. Therefore, considering that the maximum resolution in the scattering length density profile is 0.54 nm ($d/2h_{\max}$) and the full width at half maximum of the high density region in the unit cell is 1 nm, it is impossible to distinguish between the two configurations. Thus, the CER molecules in the SPP bilayer structure may be either in the hairpin, or in the fully extended configuration.

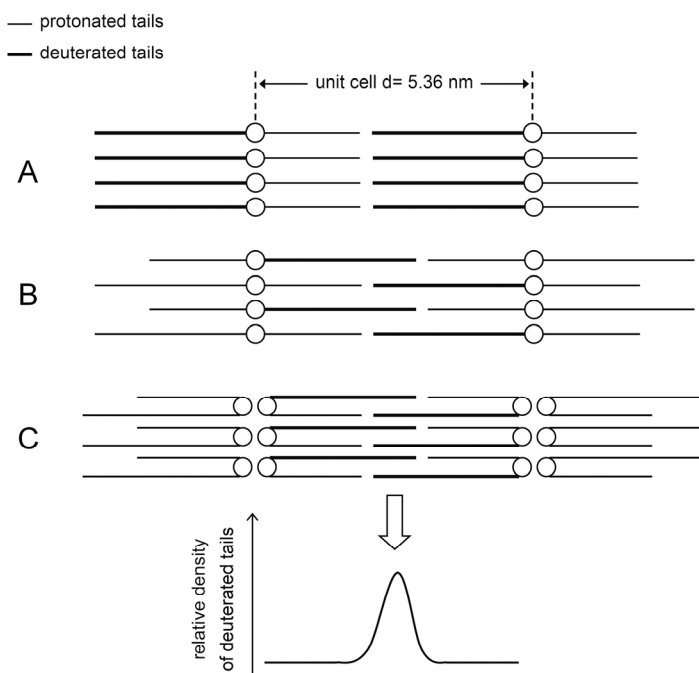


Figure 6: A) Schematic of asymmetrically arranged fully extended dCER NS in the unit cell of the SPP. B) Symmetric arrangement of fully extended dCER NS molecules in the unit cell of the SPP. C) Symmetric arrangement in the unit cell with dCER NS in the hairpin configuration. Only in the arrangements presented in B and C the deuterated acyl chains are interdigitating, resulting in the difference profile that is also displayed in the figure.

Our studies show that a 5.4 nm lamellar phase is formed that consists of homogeneously mixed CER, CHOL and FFA. This is important for the skin barrier function as different lipid domains may lead to an increase in the diffusivity in these lipid membranes. In addition, the low hydration level of the lamellar phase suggests a poor hydrophilic pathway, which minimizes the permeation of hydrophilic compounds across these lamellar phases. Furthermore, the symmetric arrangement observed for the bilayer arrangement of the SPP, excluding the fully extended asymmetric arrangement, may also exist in the LPP as this phase is prepared using the same CER subclasses, with the exception of CER EOS being only present in the LPP.

We may compare our results obtained for the CER in SC lipid models to the role of CER in cell membranes: Previously, monolayers of CER:CHOL in varying ratios were examined to gain insight into the formation of lipid rafts (52). In that study it was concluded that the CER:CHOL mixtures form a crystalline phase with the CER configured in a hairpin structure. This is in agreement with our findings for the CER:CHOL:FFA mixture and it may suggest that a configuration in the hairpin structure is preferred over a fully extended configuration of the CER.

Conclusions

A mixture that, apart from the absence of CER EOS, closely mimics the lipid composition in SC was examined by neutron diffraction. The high resolution density distribution for the 5.36 nm lamellar phase in this mixture demonstrated a bilayer arrangement. The symmetry in the unit cell and the shape of the density profile of deuterated CER NS excluded an asymmetric fully extended arrangement of CER NS in the bilayer. It is for the first time that neutron diffraction studies were performed using deuterated CER providing insights in the arrangement of the SPP.

Position of ceramide in lipid membrane determined by neutron diffraction

This work was supported by a grant from the Technology Foundation STW (LGP7503). We thank the company Cosmoferm B.V. (Evonik) for the provision of the ceramides and we thank the ILL for the allocation of beamtime for neutron diffraction measurements.

References

1. Simonetti, O., A. J. Hoogstraate, W. Bialik, J. A. Kempenaar, A. H. Schrijvers, H. E. Bodde, and M. Ponec. 1995. Visualization of diffusion pathways across the stratum corneum of native and in-vitro-reconstructed epidermis by confocal laser scanning microscopy. *Arch Dermatol Res* 287:465-473.
2. Weerheim, A., and M. Ponec. 2001. Determination of stratum corneum lipid profile by tape stripping in combination with high-performance thin-layer chromatography. *Arch Dermatol Res* 293:191-199.
3. White, S. H., D. Mirejovsky, and G. I. King. 1988. Structure of lamellar lipid domains and corneocyte envelopes of murine stratum corneum. An X-ray diffraction study. *Biochemistry* 27:3725-3732.
4. Bouwstra, J. A., G. S. Gooris, J. A. van der Spek, and W. Bras. 1991. Structural investigations of human stratum corneum by small-angle X-ray scattering. *J. Invest. Dermatol.* 97:1005-1012.
5. Cornwell, P. A., B. W. Barry, C. P. Stoddart, and J. A. Bouwstra. 1994. Wide-angle X-ray diffraction of human stratum corneum: effects of hydration and terpene enhancer treatment. *J Pharm Pharmacol* 46:938-950.
6. Ohta, N., S. Ban, H. Tanaka, S. Nakata, and I. Hatta. 2003. Swelling of intercellular lipid lamellar structure with short repeat distance in hairless mouse stratum corneum as studied by X-ray diffraction. *Chem Phys Lipids* 123:1-8.
7. Hatta, I., N. Ohta, K. Inoue, and N. Yagi. 2006. Coexistence of two domains in intercellular lipid matrix of stratum corneum. *Biochim Biophys Acta* 1758:1830-1836.
8. Gooris, G. S., and J. A. Bouwstra. 2007. Infrared spectroscopic study of stratum corneum model membranes prepared from human ceramides, cholesterol, and fatty acids. *Biophys J* 92:2785-2795.
9. Chachaty, C., D. Rainteau, C. Tessier, P. J. Quinn, and C. Wolf. 2005. Building up of the liquid-ordered phase formed by sphingomyelin and cholesterol. *Biophys J* 88:4032-4044.
10. Clarke, J. A., A. J. Heron, J. M. Seddon, and R. V. Law. 2006. The diversity of the liquid ordered (Lo) phase of phosphatidylcholine/cholesterol membranes: a variable temperature multinuclear solid-state NMR and x-ray diffraction study. *Biophys J* 90:2383-2393.
11. Marsh, D. 2010. Liquid-ordered phases induced by cholesterol: a compendium of binary phase diagrams. *Biochim Biophys Acta* 1798:688-699.
12. Bouwstra, J. A., G. S. Gooris, J. A. van der Spek, S. Lavrijsen, and W. Bras. 1994. The lipid and protein structure of mouse stratum

- corneum: a wide and small angle diffraction study. *Biochim Biophys Acta* 1212:183-192.
13. McIntosh, T. J. 2003. Organization of skin stratum corneum extracellular lamellae: diffraction evidence for asymmetric distribution of cholesterol. *Biophys J* 85:1675-1681.
 14. Groen, D., G. S. Gooris, and J. A. Bouwstra. 2009. New insights into the stratum corneum lipid organization by X-ray diffraction analysis. *Biophys J* 97:2242-2249.
 15. Megha, and E. London. 2004. Ceramide selectively displaces cholesterol from ordered lipid domains (rafts): implications for lipid raft structure and function. *J Biol Chem* 279:9997-10004.
 16. Johnston, I., and L. J. Johnston. 2006. Ceramide promotes restructuring of model raft membranes. *Langmuir* 22:11284-11289.
 17. Bouwstra, J. A., G. S. Gooris, F. E. Dubbelaar, and M. Ponec. 2001. Phase behavior of lipid mixtures based on human ceramides: coexistence of crystalline and liquid phases. *J Lipid Res* 42:1759-1770.
 18. de Jager, M., W. Groenink, J. van der Spek, C. Janmaat, G. Gooris, M. Ponec, and J. Bouwstra. 2006. Preparation and characterization of a stratum corneum substitute for in vitro percutaneous penetration studies. *Biochim Biophys Acta* 1758:636-644.
 19. Groen, D., G. S. Gooris, M. Ponec, and J. A. Bouwstra. 2008. Two new methods for preparing a unique stratum corneum substitute. *Biochim Biophys Acta* 1778:2421-2429.
 20. Chen, X., S. Kwak, M. Lafleur, M. Bloom, N. Kitson, and J. Thewalt. 2007. Fatty acids influence "solid" phase formation in models of stratum corneum intercellular membranes. *Langmuir* 23:5548-5556.
 21. Wertz, P. 1991. Epidermal lipids. In *Physiology, Biochemistry and Molecular Biology of the Skin*. L. A. Goldsmith, editor. Oxford University Press, Oxford. 205-235.
 22. Wertz, P. W., M. C. Miethke, S. A. Long, J. S. Strauss, and D. T. Downing. 1985. The composition of the ceramides from human stratum corneum and from comedones. *J. Invest. Dermatol.* 84:410-412.
 23. Ponec, M., A. Weerheim, P. Lankhorst, and P. Wertz. 2003. New acylceramide in native and reconstructed epidermis. *J. Invest. Dermatol.* 120:581-588.
 24. Masukawa, Y., H. Narita, E. Shimizu, N. Kondo, Y. Sugai, T. Oba, R. Homma, J. Ishikawa, Y. Takagi, T. Kitahara, Y. Takema, and K. Kita. 2008. Characterization of overall ceramide species in human stratum corneum. *J Lipid Res* 49:1466-1476.
 25. Motta, S., M. Monti, S. Sesana, R. Caputo, S. Carelli, and R. Ghidoni. 1993. Ceramide composition of the psoriatic scale. *Biochim. Biophys. Acta* 1182:147-151.
 26. de Jager, M. W., G. S. Gooris, M. Ponec, and J. A. Bouwstra. 2005. Lipid mixtures prepared with well-defined synthetic ceramides

- closely mimic the unique stratum corneum lipid phase behavior. *J Lipid Res* 46:2649-2656.
27. Kiselev, M. A., N. Y. Ryabova, A. M. Balagurov, S. Dante, T. Hauss, J. Zbytovska, S. Wartewig, and R. H. Neubert. 2005. New insights into the structure and hydration of a stratum corneum lipid model membrane by neutron diffraction. *Eur Biophys J* 34:1030-1040.
 28. Ruettinger, A., M. A. Kiselev, T. Hauss, S. Dante, A. M. Balagurov, and R. H. Neubert. 2008. Fatty acid interdigitation in stratum corneum model membranes: a neutron diffraction study. *Eur Biophys J* 37:759-771.
 29. Schroter, A., D. Kessner, M. A. Kiselev, T. Hauss, S. Dante, and R. H. Neubert. 2009. Basic nanostructure of stratum corneum lipid matrices based on ceramides [EOS] and [AP]: a neutron diffraction study. *Biophys J* 97:1104-1114.
 30. de Jager, M., W. Groenink, J. van der Spek, C. Janmaat, G. Gooris, M. Ponec, and J. Bouwstra. 2006. Preparation and characterization of a stratum corneum substitute for in vitro percutaneous penetration studies. *Biochim. Biophys. Acta* 1758:636-644.
 31. Bouwstra, J. A., G. S. Gooris, F. E. Dubbelaar, A. M. Weerheim, A. P. Ijzerman, and M. Ponec. 1998. Role of ceramide 1 in the molecular organization of the stratum corneum lipids. *J Lipid Res* 39:186-196.
 32. Bouwstra, J. A., G. S. Gooris, K. Cheng, A. Weerheim, W. Bras, and M. Ponec. 1996. Phase behavior of isolated skin lipids. *J. Lipid Res.* 37:999-1011.
 33. Richard, D. 2008. <http://www.ill.eu/instruments-support/computing-for-science/data-analysis/>.
 34. Franks, N. P., and W. R. Lieb. 1979. The structure of lipid bilayers and the effects of general anaesthetics. An x-ray and neutron diffraction study. *J Mol Biol* 133:469-500.
 35. NCSR. 2005. www.ncnr.nist.gov/instruments/bt1/neutron.html.
 36. Nagle, J. F., and S. Tristram-Nagle. 2000. Structure of lipid bilayers. *Biochim Biophys Acta* 1469:159-195.
 37. Dante, S., T. Hauss, and N. A. Dencher. 2002. Beta-amyloid 25 to 35 is intercalated in anionic and zwitterionic lipid membranes to different extents. *Biophys J* 83:2610-2616.
 38. Harroun, T. A., J. Katsaras, and S. R. Wassall. 2006. Cholesterol hydroxyl group is found to reside in the center of a polyunsaturated lipid membrane. *Biochemistry* 45:1227-1233.
 39. NCSR. 2010. <http://www.ncnr.nist.gov/resources/sldcalc.html>.
 40. Fujii, M., Y. Takeda, M. Yoshida, N. Utoguchi, M. Matsumoto, and Y. Watanabe. 2003. Comparison of skin permeation enhancement by 3-l-menthoxypropane-1,2-diol and l-menthol: the permeation of indomethacin and antipyrine through Yucatan micropig skin and changes in infrared spectra and X-ray diffraction patterns of stratum corneum. *Int J Pharm* 258:217-223.

41. Bouwstra, J. A., G. S. Gooris, W. Bras, and D. T. Downing. 1995. Lipid organization in pig stratum corneum. *J. Lipid Res.* 36:685-695.
42. Percot, A., and M. Lafleur. 2001. Direct observation of domains in model stratum corneum lipid mixtures by Raman microspectroscopy. *Biophys J* 81:2144-2153.
43. Velkova, V., and M. Lafleur. 2002. Influence of the lipid composition on the organization of skin lipid model mixtures: an infrared spectroscopy investigation. *Chem Phys Lipids* 117:63-74.
44. McIntosh, T. J., M. E. Stewart, and D. T. Downing. 1996. X-ray diffraction analysis of isolated skin lipids: reconstitution of intercellular lipid domains. *Biochemistry* 35:3649-3653.
45. McIntosh, T. J., S. A. Simon, J. C. Ellington, Jr., and N. A. Porter. 1984. New structural model for mixed-chain phosphatidylcholine bilayers. *Biochemistry* 23:4038-4044.
46. Tero, R., H. Watanabe, and T. Urisu. 2006. Supported phospholipid bilayer formation on hydrophilicity-controlled silicon dioxide surfaces. *Phys Chem Chem Phys* 8:3885-3894.
47. Creczynski-Pasa, T. B., M. A. Millone, M. L. Munford, V. R. de Lima, T. O. Vieira, G. A. Benitez, A. A. Pasa, R. C. Salvarezza, and M. E. Vela. 2009. Self-assembled dithiothreitol on Au surfaces for biological applications: phospholipid bilayer formation. *Phys Chem Chem Phys* 11:1077-1084.
48. Small, D. M. 1986. The Physical Chemistry of Lipids. In *Handbook of Lipid Research*. D. J. Hanahan, editor. Plenum Press, New York.
49. de Jager, M. W., G. S. Gooris, I. P. Dolbnya, M. Ponec, and J. A. Bouwstra. 2004. Modelling the stratum corneum lipid organisation with synthetic lipid mixtures: the importance of synthetic ceramide composition. *Biochim Biophys Acta* 1664:132-140.
50. Dahlén, B., and I. Pascher. 1972. Molecular arrangements in sphingolipids. Crystal structure of *N*-tetracosanoylphytosphingosine. *Acta Cryst. B* 28:2396-2404.
51. Rerek, M. E., H. Chen, B. Markovic, D. van Wyck, P. Garidel, R. Mendelsohn, and D. J. Moore. 2001. Phytosphingosine and Sphingosine Ceramide Headgroup Hydrogen Bonding: Structural Insights through Thermotropic Hydrogen/Deuterium Exchange. *J Phys Chem B* 105:9355-9362.
52. Scheffer, L., I. Solomonov, M. J. Weygand, K. Kjaer, L. Leiserowitz, and L. Addadi. 2005. Structure of cholesterol/ceramide monolayer mixtures: implications to the molecular organization of lipid rafts. *Biophys J* 88:3381-3391.

Chapter 8

Summary

The stratum corneum (SC), the thin uppermost layer of the skin, consists of dead flattened skin cells (corneocytes) embedded in a lipid matrix. The lipid matrix is considered to play a crucial role in the skin barrier function. It consists of ceramides (CER), cholesterol (CHOL) and free fatty acids (FFA) forming crystalline lipid lamellae. From studies with native SC and SC lipid models much information has been gained on the phase behavior of the SC lipid matrix. However, little is known about the correlation between SC lipid organization and the permeability of the SC. This is difficult to investigate using native SC, due to its complex structure. Therefore SC lipids were casted on a porous membrane, resulting in a lipid organization and lamellar orientation similar to that in SC. This lipid membrane is referred to as the stratum corneum substitute (SCS) (1, 2). The SCS can be used to perform diffusion studies. Therefore, when modifying the lipid composition and thus the lipid organization in the SCS, it is possible to study the relationship between lipid organization and permeability.

The main objectives of this thesis are 1) to investigate the influence of lipid organization on the barrier function in the SCS and 2) to obtain insights in the molecular organization within the unit cell of the lamellar phases in SC.

Part I: SCS as a tool to study the relation between lipid composition, organization and barrier function in one model

In previous studies the SCS was developed. However, the preparation method of the SCS was suboptimal. For this reason in chapter 2 two new methods were introduced to prepare the SCS, to improve the reproducibility and to increase the efficiency of the preparation method. Subsequently, the properties of the SCS prepared by the three methods, i.e. the manual airbrush method, the rotor airbrush method and the linomat method, were

investigated. The results show that the SCS prepared with the various methods share the properties of a uniform lipid composition and a homogeneous distribution of these lipid components over the substrate. Furthermore, irrespective of the preparation method, the lipids form two crystalline lamellar phases, mimicking the lipid organization and orientation in human SC very closely. In subsequent studies permeation profiles of benzoic acid through SCS were measured. These permeation profiles were very similar to that across human SC. The rotor method increases the efficiency and reproducibility compared to the manual airbrush method, while the linomat method reduces the lipid loss during preparation and results in SCS with a more uniform membrane thickness. Based on these results, the linomat method was selected as the preferred method for preparing the SCS.

After having optimized the quality and the preparation method of the SCS, in subsequent studies the SCS was used to determine the effect of lipid organization on the permeability of the SCS. These studies are described in chapter 3. We examined the effect of the orthorhombic to hexagonal phase transition on the barrier function of SCS and compared that with human SC. This was performed by monitoring the permeability to benzoic acid as function of temperature. Arrhenius plots were constructed. As the slope of the Arrhenius plots below and above the transition temperature was very similar, it was concluded that the orthorhombic to hexagonal phase transition does not affect the diffusivity of benzoic acid across the SCS. The benzoic acid flux as function of temperature across human SC and the SCS was very similar over a temperature region between 31 and 43°C. From the slopes the activation energies were calculated. The activation energy for the diffusivity of benzoic acid appeared to be very similar in SC and SCS. This confirms that the lipids form the main barrier for diffusion in human SC. In subsequent studies the SCS composition was modified by reducing the FFA chain length distribution from around 24 carbon atoms to around 18 carbon atoms in the fatty acid chain. This resulted in a hexagonal packing and a perturbed

lamellar organization. These changes in lipid organization resulted in a significant increased permeability to benzoic acid, which was related mainly to its perturbed lamellar organization. Thus, a proper lamellar organization is more crucial for a competent barrier function than the presence of an orthorhombic lateral packing.

In the studies described in chapter 4 we used the SCS to investigate the effect of changes in lipid organization on the barrier function, again using benzoic acid as model compound. First, in preparing the SCS we increased the level of one of the three major lipid classes (CER, CHOL or FFA) keeping the ratio between the other lipid classes constant. An increased CHOL level induced a higher amount of phase separated CHOL and a reduction in the permeability. An increase in CER or FFA level to twice the original level resulted in the formation of additional phases, but had no significant influence on the permeability. We also examined models that mimic selected changes in lipid compositions reported for dry or diseased skin. In seasonally dry skin (winter xerosis) elevated levels of CER EOS-oleate have been reported. This change in composition was induced in the SCS by replacing 50% of the CER EOS-linoleate by CER EOS-oleate. This change in lipid composition did not induce changes in the lipid organization. Permeation studies revealed a very similar barrier as in the normal SCS. A SCS was also prepared based on an altered CER profile observed in SC of involved psoriasis skin. Its lipid organization and barrier properties were again similar to normal SCS. However, a SCS that mimics an important aspect of the composition in recessive X-linked ichthyosis skin, namely an excess of cholesterol sulfate, displayed a twofold higher permeability as compared to normal SCS. This increase in permeability is possibly related to the formation of an additional, less ordered lipid phase in this model.

It is for the first time that a SC model is used to investigate not only the effect of the lipid composition on the lipid organization, but also to study the relationship between lipid organization and barrier function, which is a very relevant and unique feature of the SCS.

Part II: The molecular organization in the repeating units of the SC lamellar phases

From X-ray diffraction studies using isolated SC it is well known that two lamellar phases are present in the lipid matrix of the SC. One with a unique long periodicity of about 13 nm (the long periodicity phase or LPP) and another with a shorter periodicity of around 6 nm (the short periodicity phase or SPP). However, although a lot of information has been obtained on the lipid phase behaviour of the lipid classes in SC, the molecular arrangement of the CER, CHOL or FFA classes in the unit cell of the lamellar phases is largely unknown. Several studies revealed that CER EOS plays an important role in the formation of the LPP. Therefore, in the studies described in part II of this thesis, we investigated the different lamellar phases in mixtures with CER EOS as the only CER component, in mixtures with all major CER classes present (including CER EOS) and in mixtures with the major CER classes present except for CER EOS.

Firstly, we investigated whether CER EOS in the absence of the other CER subclasses mixed with CHOL and FFA forms similar phases as observed in SC. These studies are described in chapter 5. The phase behaviour was examined using small angle X-ray diffraction (SAXD) and Fourier transformed infrared spectroscopy (FTIR). Our SAXD studies reveal that an equimolar ratio of EOS, CHOL and FFA forms a lamellar phase with an unusual long repeat distance of approximately 14.7 nm, different from that observed in SC. When focusing on the CH₂ stretching frequencies that provide information on the conformational disordering of the lipid chains, an exceptional thermotropic response was measured. The FFA and the CER chains undergo an order-disorder transition in different temperature ranges, indicating that at least a fraction of the FFA and CER do not mix. However, we also noticed by measuring the scissoring vibrations in the FTIR spectrum that a part of the hydrocarbon chains of CER and FFA are mixing in the orthorhombic lattice. Based on these observations, the molecular structure of the CER and the length of the unit cell, a molecular model for the 14.7 nm

lamellar phase has been proposed. This model is composed of three different lipid layers forming a symmetric arrangement in the unit cell. Based on this model and on the periodicity of 14.7 nm of the lamellar phase, it was concluded that the arrangement in the repeating unit is different from that proposed in chapter 6 for the LPP, suggesting that indeed additional CER subclasses are required to form the LPP.

In chapter 6 the molecular structure of the unit cell of the LPP in SC is investigated in detail. This characteristic LPP is suggested to be very important for the barrier function of the skin. To gain more insight into the molecular organization of this unique lamellar phase, we performed SAXD using various lipid mixtures containing all CER subclasses, mimicking the lipid composition in SC. These lipid mixtures formed the LPP with a slight variation in repeat distance. In the SAXD pattern of each mixture at least 6 diffraction orders were observed, attributed to the LPP with a repeat distance ranging from 12.1 to 13.8 nm. Using Shannon's sampling theorem we determined phase angles for the 6 structure factors associated to the first 6 diffraction orders of the LPP. By Fourier synthesis, using the 6 structure factors and phase angles, for the LPP a high resolution electron density distribution could be constructed. The density distribution suggests a unit cell with three lipid bilayers of 4.5, 4.0 and 4.5 nm in width. Subsequently, from SAXD patterns of isolated SC the electron density distribution of the lamellar phase was also constructed and appeared to be very similar to that in the lipid mixtures. This demonstrates that the lipid mixtures serve as an excellent model for the lipid organization in SC, not only with respect to the repeat distance of the LPP, but also in terms of the molecular arrangement within the unit cell.

In chapter 7 the molecular structure of the SPP is investigated into detail. To gain more insight into the molecular organization of the short periodicity lamellar phase we performed neutron diffraction studies on a mixture with all CER subclasses except EOS. In the diffraction pattern, five diffraction orders were observed attributed to the SPP with a repeat distance of 5.4 nm. Using

contrast variation by changing the H₂O/D₂O ratio, the scattering length density profile could be calculated. This density profile suggests a typical bilayer arrangement. To obtain information on the arrangement of the CER in the unit cell, a mixture that included a partly deuterated CER was also examined. The scattering length density profile of the 5.4 nm phase containing this deuterated CER demonstrated a symmetric arrangement of the CER with interdigitating acyl chains in the center of the unit cell.

The lamellar phases play a crucial role in the barrier function of the SC and the studies described above reveal new insights into their molecular structures. It is for the first time that the molecular structure in the lamellar phases is described with this level of detail.

Conclusions

In our first studies, the preparation procedure of the SCS was optimized while a proper lipid organization was maintained. In previous studies it was shown that the SCS closely mimics the human SC concerning lipid organization and barrier function. In the subsequent studies described in this thesis we have shown that the SCS is also a very suitable model for studying the relation between lipid organization and barrier function. Interestingly, based on the results obtained in these studies it appears that the crystalline lateral packing in the SC lipids is of less importance for the barrier function than the presence of the correct lamellar phases. Furthermore, as the formation of the proper lamellar phases is of crucial importance for the skin barrier function, the molecular organization within their repeating units was investigated into more detail. We studied the different lamellar phases present in mixtures with EOS as the only CER, in mixtures with all CER subclasses present and in mixtures with all CER subclasses except EOS. These studies showed a unique very long periodicity phase in the mixture with only CER EOS, of which the molecular arrangement in the unit cell appears to be different from that in the unit cell of the LPP. Studies on mixtures with all CER subclasses revealed the LPP with a trilayer unit cell

and studies on mixtures in absence of EOS demonstrated a SPP with a symmetric ceramide arrangement in the unit cell. Furthermore, based on X-ray studies with native SC, the molecular arrangement in the unit cell of the LPP in the models appears to be very similar to that in native SC. As the LPP is a unique lamellar phase in the SC and is considered to play an important role in the skin barrier function, the latter observation confirms that the mixtures form very relevant models for studying the SC lipid organization.

Perspectives

Although the studies presented in this thesis demonstrate that the SCS is an excellent model for studying the SC lipid organization and barrier function, the permeation studies have been performed with only one model drug (benzoic acid). Benzoic acid was chosen for its medium lipophilicity ($\log P = 1.9$), low molecular weight ($m_w = 122$ Da) and medium water solubility (3.4 g/l), making it a suitable molecule for skin permeation studies. In previous permeability studies similar compounds with a variation in $\log P$ value between 0.6 and 2.6 were also used to compare the flux profile across SCS and human SC, exhibiting an excellent correlation (2). However, very hydrophilic and very lipophilic drugs have not yet been assessed in permeability studies to compare the barrier function of SCS with human SC. This is of interest to perform in future studies. From our studies we may conclude that the SCS is an attractive tool to study the effect of changes in lipid organization on the barrier function. In the studies presented in this thesis models mimicking the composition in SC of winter xerosis, psoriasis and x-linked ichthyosis were evaluated. However, other skin diseases in which the SC lipid composition is affected (and quantified by chromatography methods) can be mimicked as well, by adapting the lipid composition in the SCS. For example, an altered SC lipid composition was also reported for type 2 Gaucher's disease (3-5), lamellar ichthyosis (6) and atopic eczema (7-15). The consequences of such changes in lipid

organization to the contribution of an impaired skin barrier function can in principle be studied using the SCS. Of course one should keep in mind that this is only one aspect of a reduction in skin barrier function. Also changes in the barrier proteins have been reported that affect for example the structure of the cornified envelope or shedding of the corneocytes. These changes are likely to influence the skin barrier function as well. Besides mimicking the composition in diseased skin it is also of interest to use the SCS to investigate the effect of penetration enhancers and moisturizers on the lipid organization and permeability of the SC lipid lamellae.

Concerning the permeation pathway of a permeant molecule through the SC, although the tortuous intercellular pathway has been suggested to be the preferred route for most drug molecules (16), detailed information on the penetration route within a stack of SC lipid lamellae is not available. The permeation through stacks of lamellae within the intercellular spaces in SC itself may also follow a tortuous pathway, effectively lengthening the total permeation pathway through SC or the SCS. By fitting the permeation data of a passive diffusion experiment to the diffusion formula (17), see figure 1A, in theory both the length of the permeation pathway (L) as well as the diffusion constant (D) of the permeant molecule can be calculated. These parameters could lead to new insights on the permeation pathway. However, to successfully determine L and D , it is necessary to accurately determine the partition coefficient (K) by assessing the solubility of the model compound in the donor solution and in the lipids of SC or SCS. Since the SC is a heterogeneous membrane with lipid domains and corneocytes, it is a challenge to obtain a partition coefficient between donor solution and SC lipids. To determine the partition coefficient, the SCS can also replace the SC. For example, with the SCS using benzoic acid as permeant, preliminary measurements revealed a partition coefficient between the SCS lipid film and the donor solution (2 mg/ml benzoic acid in PBS 7.4) of $K = 5.3$ (unpublished data).

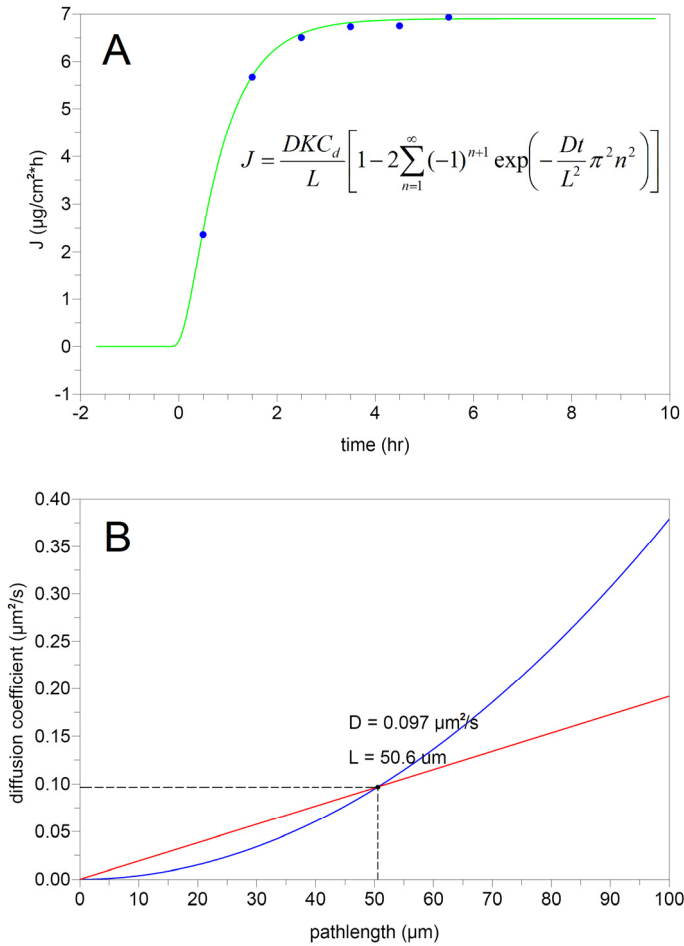


Figure 1: A) Plot of the benzoic acid flux through a SCS model membrane composed of CER, CHOL and FFA in molar ratios of 1:2:1. The dots denote the measured flux values while the solid line denotes the fit of the diffusion formula (also shown in figure A) with the measured flux values. **B)** Solutions for D and L from the fit of the diffusion formula with the flux data in (A). The blue line depicts all possible values for D/L resulting from a fit with the steady state part of the flux data and the red line depicts all values for D/L^2 resulting from a fit with the up-going part of the flux data. A unique solution for both D and L is found when the two lines (denoting both fits) coincide. These values are also depicted in figure B.

Chapter 8

In a first attempt, fitting the diffusion equation to permeation data of benzoic acid through a SCS (with CER:CHOL:FFA composition of 1:2:1) resulted in approximate values for L of 51 μm and D of 0.1 $\mu\text{m}^2/\text{s}$ (see figure 1B, unpublished data). When combining these values with the thickness of the lipid membranes, being around 13 μm , we may conclude that the diffusion occurs partly parallel to the basal plane of the lipid lamellae.

Regarding the molecular structure in the lamellar phases of SC, neutron and x-ray diffraction experiments using SC lipid models can be used for unraveling the lipid arrangement in the LPP and in the SPP. By specifically deuterating one of the major components (CER, CHOL or FFA) more insights can be gained on the location of each of these components, or even on the location of their headgroups or tails in the unit cell. When focusing on the molecular arrangement of the LPP, according to the x-ray results presented in this thesis, the electron density profile of the repeating unit is symmetric and therefore in principle it is possible to perform neutron diffraction studies using $\text{H}_2\text{O}/\text{D}_2\text{O}$ contrast to resolve the density pattern and to locate the position of deuterated (parts of) molecules in the LPP unit cell. However, recent preliminary results suggest that the water in the LPP unit cell is not (or not only) located at the borders of the unit cell (in the headgroup regions, as is normally the case in lipid bilayers), but (also) at specific positions inside the unit cell. Therefore, as the method for resolving the density profile using $\text{H}_2\text{O}/\text{D}_2\text{O}$ contrast is based on the location of the water molecules being only at the borders of the unit cell, it will be a challenge to resolve the molecular structure of the LPP in more detail and to localize several subclasses of ceramides within this repeating unit.

References

1. de Jager, M., W. Groenink, J. van der Spek, C. Janmaat, G. Gooris, M. Ponec, and J. Bouwstra. 2006. Preparation and characterization of a stratum corneum substitute for in vitro percutaneous penetration studies. *Biochim. Biophys. Acta* 1758:636-644.
2. de Jager, M., W. Groenink, R. Bielsa i Guivernau, E. Andersson, N. Angelova, M. Ponec, and J. Bouwstra. 2006. A novel in vitro percutaneous penetration model: evaluation of barrier properties with p-aminobenzoic acid and two of its derivatives. *Pharm. Res.* 23:951-960.
3. Holleran, W. M., E. I. Ginns, G. K. Menon, J. U. Grundmann, M. Fartasch, C. E. McKinney, P. M. Elias, and E. Sidransky. 1994. Consequences of beta-glucocerebrosidase deficiency in epidermis. Ultrastructure and permeability barrier alterations in Gaucher disease. *J Clin Invest* 93:1756-1764.
4. Sidransky, E., M. Fartasch, R. E. Lee, L. A. Metlay, S. Abella, A. Zimran, W. Gao, P. M. Elias, E. I. Ginns, and W. M. Holleran. 1996. Epidermal abnormalities may distinguish type 2 from type 1 and type 3 of Gaucher disease. *Pediatr Res* 39:134-141.
5. Doering, T., R. L. Proia, and K. Sandhoff. 1999. Accumulation of protein-bound epidermal glucosylceramides in beta-glucocerebrosidase deficient type 2 Gaucher mice. *FEBS Lett* 447:167-170.
6. Lavrijsen, A. P., J. A. Bouwstra, G. S. Gooris, A. Weerheim, H. E. Bodde, and M. Ponec. 1995. Reduced skin barrier function parallels abnormal stratum corneum lipid organization in patients with lamellar ichthyosis. *J Invest Dermatol* 105:619-624.
7. Murata, Y., J. Ogata, Y. Higaki, M. Kawashima, Y. Yada, K. Higuchi, T. Tsuchiya, S. Kawainami, and G. Imokawa. 1996. Abnormal expression of sphingomyelin acylase in atopic dermatitis: an etiologic factor for ceramide deficiency? *J Invest Dermatol* 106:1242-1249.
8. Hara, J., K. Higuchi, R. Okamoto, M. Kawashima, and G. Imokawa. 2000. High-expression of sphingomyelin deacylase is an important determinant of ceramide deficiency leading to barrier disruption in atopic dermatitis. *J Invest Dermatol* 115:406-413.
9. Macheleidt, O., H. W. Kaiser, and K. Sandhoff. 2002. Deficiency of epidermal protein-bound omega-hydroxyceramides in atopic dermatitis. *J Invest Dermatol* 119:166-173.
10. Okamoto, R., J. Arikawa, M. Ishibashi, M. Kawashima, Y. Takagi, and G. Imokawa. 2003. Sphingosylphosphorylcholine is upregulated in the stratum corneum of patients with atopic dermatitis. *J Lipid Res* 44:93-102.
11. Ishibashi, M., J. Arikawa, R. Okamoto, M. Kawashima, Y. Takagi, K. Ohguchi, and G. Imokawa. 2003. Abnormal expression of the novel

- epidermal enzyme, glucosylceramide deacylase, and the accumulation of its enzymatic reaction product, glucosylsphingosine, in the skin of patients with atopic dermatitis. *Lab Invest* 83:397-408.
12. Proksch, E., J. M. Jensen, and P. M. Elias. 2003. Skin lipids and epidermal differentiation in atopic dermatitis. *Clin Dermatol* 21:134-144.
 13. Jensen, J. M., R. Folster-Holst, A. Baranowsky, M. Schunck, S. Winoto-Morbach, C. Neumann, S. Schutze, and E. Proksch. 2004. Impaired sphingomyelinase activity and epidermal differentiation in atopic dermatitis. *J Invest Dermatol* 122:1423-1431.
 14. Choi, M. J., and H. I. Maibach. 2005. Role of ceramides in barrier function of healthy and diseased skin. *Am J Clin Dermatol* 6:215-223.
 15. Ishikawa, J., H. Narita, N. Kondo, M. Hotta, Y. Takagi, Y. Masukawa, T. Kitahara, Y. Takema, S. Koyano, S. Yamazaki, and A. Hatamochi. Changes in the ceramide profile of atopic dermatitis patients. *J Invest Dermatol* 130:2511-2514.
 16. Williams, M. L., and P. M. Elias. 1987. The extracellular matrix of stratum corneum: role of lipids in normal and pathological function. *Crit Rev Ther Drug Carrier Syst* 3:95-122.
 17. Barry, B. W. 1983. *Dermatological Formulations: Percutaneous Absorption*. Marcel Dekker, inc, New York.

Samenvatting

Introductie

De hoornlaag, ofwel het stratum corneum (SC), is de dunne bovenste laag van de huid. Het SC bestaat uit platte verhoornde huidcellen (corneocyten) ingebed in een lipidenmatrix. Deze lipiden spelen een zeer belangrijke rol om de doorlaatbaarheid van de huid te minimaliseren en dus ongewenste stoffen buiten het lichaam te houden. Het buiten het lichaam houden van ongewenste stoffen wordt de barrièrefunctie van de huid genoemd. De lipidenmatrix in het SC bestaat voornamelijk uit ceramiden (CER), cholesterol (CHOL) en vrije vetzuren (FFA), die gezamenlijk kristallijne gestapelde lipidenlagen (de zogenaamde lamellen) vormen. Door studies met SC en met lipidenmodellen van SC, is men al veel te weten gekomen over het fasegedrag van de lipiden in het SC. Echter, er is nog weinig bekend over het verband tussen de lipidenorganisatie in het SC en de doorlaatbaarheid van het SC. Door de complexe structuur van het SC bestaande uit eiwitten en lipiden is dit moeilijk te achterhalen. Daarom is er een lipidenmodel ontworpen die de lipidenstructuur in het SC van de huid nabootst. Dit model bestaat uit lipiden aangebracht op een ondersteunend en doorlaatbaar filter. De lipidenorganisatie en de oriëntatie van de lamellen in dit model bootsen die in het SC na. We noemen dit lipidenmodel van het SC het "stratum corneum substituu", ofwel SCS. Het SCS kan gebruikt worden om de permeatie van stoffen te onderzoeken. Door de lipidensamenstelling en daardoor de lipidenorganisatie te veranderen, kunnen we direct een verband leggen tussen de lipidensamenstelling, de lipidenorganisatie en de doorlaatbaarheid van het SCS.

De hoofddoelen van het onderzoek beschreven in dit proefschrift zijn om: 1) de invloed van lipidenorganisatie op de barrièrefunctie van het SCS te onderzoeken en 2) meer inzicht te genereren in de molekuulopbouw van de lamellen in het SC.

Deel I: Het SCS als instrument om de relatie tussen lipiden-samenstelling, organisatie en barrièrefunctie te bestuderen

In eerdere studies is het SCS ontwikkeld, echter, de spraymethode om lipiden op het poreuze membraan aan te brengen was suboptimaal. Daarom worden in het onderzoek beschreven in hoofdstuk 2 twee nieuwe methoden beschreven om het SCS te maken, om zowel de reproduceerbaarheid van het sprayen te verhogen als ook het verlies aan lipiden tijdens het sprayen te beperken. Vervolgens werden de eigenschappen van het SCS onderzocht. De drie methoden om de lipiden te sprayen waren de handmatige airbrushmethode, de rotor-airbrushmethode en de linomatmethode. Uit de resultaten blijkt dat SCS gemaakt met de drie verschillende methoden dezelfde lipiden-samenstelling heeft en dat de lipiden homogeen verdeeld zijn over het substraat. Bovendien vormen de lipiden, ongeacht de gebruikte methode, twee kristallijne lamellaire fasen, waarmee de lipidenorganisatie en oriëntatie in menselijk SC nauwkeurig wordt nagebootst. In de daaropvolgende studies werd de permeatie van benzoëzuur door het SCS gemeten. Hieruit bleek dat de doorlaatbaarheid van het SCS zeer goed overeenkomt met de doorlaatbaarheid van menselijk SC. Wat de drie verschillende methoden betreft: de rotormethode verhoogt de efficiëntie en reproduceerbaarheid in vergelijking met de handmatige airbrushmethode, terwijl de linomatmethode het lipidenverlies tijdens het sprayen sterk vermindert en resulteert in SCS met een meer gelijkmatige dikte van de lipidenfilm over het hele oppervlak. Gebaseerd op deze resultaten werd besloten de linomatmethode in de hieropvolgende studies te gebruiken.

In vervolgstudies werd met behulp van het geoptimaliseerde SCS het effect van de lipidenorganisatie op de doorlaatbaarheid van het SCS bepaald. Deze studies zijn beschreven in hoofdstuk 3. We hebben het effect van de overgang van een zeer dichte orthorombische pakking naar een minder dichte hexagonale lipidenpakking op de barrièrefunctie van het SCS onderzocht en vergeleken met dat in menselijk SC. Dit werd gedaan door de doorlaatbaarheid voor benzoëzuur als functie van de temperatuur in kaart te

brengen. Uit deze metingen werden Arrheniusdiagrammen geconstrueerd. Aangezien de helling van de curves in de Arrheniusdiagrammen boven en onder het overgangstraject nagenoeg hetzelfde is, kunnen we concluderen dat de orthorombisch-hexagonale fase-overgang geen invloed heeft op de diffusie van benzoëzuur door het SCS. Verder was de permeatie van benzoëzuur als functie van temperatuur door het SCS en menselijk SC in het overgangstraject van orthorombisch naar hexagonaal, d.w.z. in het temperatuursgebied tussen de 31 en 43 °C, ook nagenoeg hetzelfde. Van de hellingen in de diagrammen werden activeringsenergieën voor permeatie van benzoëzuur berekend. Het bleek dat de activeringsenergie voor diffusie van benzoëzuur door menselijk SC en SCS erg vergelijkbaar was. Dit bevestigt nogmaals dat de lipiden de voornaamste barrière vormen voor diffusie door het menselijk SC. In de daaropvolgende studies werd de SCS-samenstelling veranderd door de gemiddelde FFA-ketenlengte te verlagen van ongeveer 24 koolstofatomen naar circa 18 koolstofatomen. Dit resulteerde in een hexagonale pakking en een verstoorde lamellaire organisatie. Deze veranderingen in lipidenorganisatie resulteerden in een significant verhoogde doorlaatbaarheid van het SCS voor benzoëzuur. Omdat een orthorombische naar hexagonale overgang nauwelijks invloed heeft op de doorlaatbaarheid, werd de verhoogde doorlaatbaarheid voornamelijk toegeschreven aan de verstoorde lamellaire organisatie. Uit de studies beschreven in hoofdstuk 3 kan geconcludeerd worden dat voor benzoëzuur de juiste lamellaire organisatie in SC belangrijker is voor de barrièrefunctie dan de aanwezigheid van een orthorombische lipidenpakking.

Voor de studies beschreven in hoofdstuk 4 gebruikten we nogmaals het SCS om een systematische verandering in lipidenorganisatie op de lipidenorganisatie en op de barrièrefunctie te onderzoeken, met wederom benzoëzuur als modelstof. In de eerste serie experimenten hebben we de relatieve hoeveelheid van één van de drie hoofdbestanddelen (CER, CHOL en FFA) verhoogd, terwijl de verhouding tussen de andere twee

componenten gelijk bleef. Een dubbele hoeveelheid CHOL resulteerde in een toename van aparte kristallijne gebieden bestaand uit CHOL. Dit leidde tot een verlaging van de doorlaatbaarheid. Een dubbele hoeveelheid CER- of FFA resulteerde in beide gevallen in de vorming van een extra fase, maar dit had geen significante invloed op de doorlaatbaarheid. Daarnaast hebben we ook modellen onderzocht die een verandering in lipidenamenstelling nabootsen die karakteristiek is voor droge of zieke huid. Zo is er in seizoensgebonden droge huid (winter xerosis) een verhoogde hoeveelheid CER EOS-oleaat gemeten ten opzichte van CER EOS-linoleaat. Deze verandering in samenstelling is nagebootst door in het SCS de helft van de CER EOS-linoleaat te vervangen door CER EOS-oleaat. Uit onze röntgenmetingen bleek echter dat dit niet resulteert in een verandering van de lipidenorganisatie. Diffusiestudies met dit aangepaste SCS lieten ook geen verandering in barrièrefunctie zien in vergelijking met onze standaard SCS. Er werd ook een SCS onderzocht waarvan het lipidenprofiel de samenstelling in het SC van psoriasispatiënten benadert. De lipidenorganisatie en barrièrefunctie van dit model waren wederom gelijk aan dat van standaard SCS. Echter, een SCS dat een belangrijk aspect van de specifieke samenstelling in SC van recessief X-linked ichthyosis-patiënten nabootst, namelijk een overmaat aan cholesterolsulfaat, liet een tweemaal hogere doorlaatbaarheid zien ten opzichte van standaard SCS. Deze verhoogde doorlaatbaarheid is mogelijk gerelateerd aan de vorming van een extra, minder goed geordende lamellaire fase in dit model.

Het is voor het eerst dat een lipidenmodel gebruikt is om niet alleen het effect van de lipidenamenstelling op de lipidenorganisatie te onderzoeken, maar ook het effect van de lipidenorganisatie op de barrièrefunctie. Hieruit kunnen zeer relevante conclusies getrokken worden voor met name zieke huid met een afwijkende SC-lipidenamenstelling en barrièrefunctie.

Deel II: De molekuulopbouw van de lamellaire fasen in het SC

Uit röntgendiffractiemetingen met geïsoleerd SC is bekend dat er twee lamellaire fasen aanwezig zijn in de lipidenfractie van het SC. Eén fase met een unieke lange herhalingsafstand van 13 nm (de lange-periodiciteitsfase, ofwel LPP) en één met een kortere herhalingsafstand van ongeveer 6 nm (de korte-periodiciteitsfase, ofwel SPP). Echter, hoewel er al veel bekend is over het fasegedrag van de lipiden in het SC, is de positie van CER-, CHOL- en FFA-molekulen binnen de herhalingsafstand (in de zogenaamde eenheidscel) van de lamellaire fasen grotendeels onbekend. Uit een aantal studies blijkt dat CER EOS, door de bijzondere structuur, een belangrijke rol speelt bij de vorming van de LPP. Vandaar dat we in de studies beschreven in deel II van dit proefschrift de verschillende lamellaire fasen onderzochten in mengsels met CER EOS als enige component, in mengsels met alle CER-klasse(n) (inclusief CER EOS) en in mengsels met alle CER-klasse(n) behalve CER EOS.

Ten eerste onderzochten we of CER EOS in afwezigheid van de andere CER-klasse(n) gemengd met CHOL en FFA dezelfde soort fasen vormt zoals die in SC waargenomen zijn. Deze studies zijn beschreven in hoofdstuk 5. Het fasegedrag werd onderzocht met kleine-hoek röntgendiffractie (SAXD) en Fourier-transformatie-infraroodspectroscopie (FTIR). Uit de SAXD-metingen blijkt dat een equimolair mengsel met CER EOS, CHOL en FFA een lamellaire fase vormt met een bijzonder lange herhalingsafstand van ongeveer 14.7 nm. Deze fase is anders dan de fasen gevormd in menselijk SC. Uit de FTIR metingen bleek dat de FFA- en CER-ketens niet in hetzelfde temperatuurgebied vloeibaar worden. Dit betekent dat tenminste een deel van de FFA- en CER-ketens niet met elkaar mengen. Echter, uit een ander gedeelte van het FTIR spectrum bleek ook dat een deel van de koolstofketens van CER EOS en FFA weldegelijk samen een orthorombische pakking vormen. Gebaseerd op deze waarnemingen, de molekuulstructuur van CER EOS en de lengte van de eenheidscel, is een rangschikking van de FFA-, CER EOS- en CHOL-molekulen in de

eenheidscel van de 14.7 nm lamellaire fase voorgesteld. Dit model bestaat uit drie verschillende lipidenlagen die samen een symmetrische rangschikking binnen de eenheidscel vormen. Gebaseerd op deze rangschikking en op de herhalingsafstand van 14.7 nm werd geconcludeerd dat de molekuulopbouw van deze eenheidscel anders is dan de molekuulopbouw voor de LPP beschreven in hoofdstuk 6. Hieruit blijkt dat er naast CER EOS inderdaad nog meer CER-klassen nodig zijn om de LPP te vormen.

In hoofdstuk 6 wordt de molekuulopbouw binnen de eenheidscel van de LPP in SC in detail onderzocht. Het wordt gesuggereerd dat deze karakteristieke fase erg belangrijk is voor de barrièrefunctie van de huid. Om meer inzicht te krijgen in de moleculaire organisatie van deze unieke fase zijn er SAXD-metingen uitgevoerd met verschillende mengsels die een zodanige samenstelling hadden, dat de lipidenorganisatie in SC werd nagebootst. Echter, deze lipidenmengsels vormden de LPP met kleine verschillen in herhalingsafstand. In het SAXD-patroon van elk van deze mengsels werden tenminste 6 diffractie-orde waargenomen die aan de LPP toegeschreven konden worden, met een herhalingsafstand die varieerde van 12.1 tot 13.8 nm. Met behulp van Shannon's samplingtheorie werden de fasehoeken van de structuurfactoren bepaald die bij de eerste 6 diffractie-orde van de LPP hoorden. Gebruikmakend van de 6 structuurfactoren en fasehoeken werd door middel van Fouriersynthese een hogeresolutie elektronendichtheidsprofiel voor de LPP bepaald. Dit dichtheidsprofiel suggereert een eenheidscel bestaande uit drie opeenvolgende lipidenlagen, met een dikte van 4.5, 4.0 en 4.5 nm. Vervolgens werd met behulp van SAXD-patronen van geïsoleerd SC ook een elektronendichtheidsprofiel van de LPP in SC geconstrueerd. Dit dichtheidsprofiel vertoonde een grote gelijkenis met die van de LPP in de lipidenmengsels. Dit toont aan dat de lipidenmengsels een uitstekend model vormen voor de lipidenorganisatie in SC, niet alleen met betrekking tot de herhalingsafstand van de LPP, maar ook wat betreft de molekuulopbouw in de eenheidscel.

In hoofdstuk 7 wordt de molekuulopbouw van de SPP in detail onderzocht. Om meer inzicht te krijgen in de moleculaire organisatie werden neutronendiffractiestudies uitgevoerd op een mengsel met alle CER-klassen behalve CER EOS. Dit voorkomt de vorming van de LPP. In het diffractiepatroon werden vijf diffractiepieken waargenomen die bij de SPP horen, met een herhalingsafstand van 5.4 nm. Met contrastvariatie (door de verhouding tussen H₂O en D₂O te veranderen) kon het dichtheidsprofiel van de SPP berekend worden. Dit dichtheidsprofiel laat de vorming van een typische bilaag zien. Een mengsel dat een CER bevatte met gedeutereerde vetzuurstaart werd ook onderzocht, om informatie te krijgen over de positie van deze CER-vetzuurstaart in de eenheidscel. Het dichtheidsprofiel van de 5.4 nm fase waarin de CER met gedeutereerde vetzuurstaart aanwezig is correspondeert met 2 ceramiden die tegenover elkaar gesitueerd zijn in de bilaag. De CER hebben een symmetrische verdeling met gedeeltelijk overlappende vetzuurstaarten in het midden van de eenheidscel.

De lamellaire fasen spelen een cruciale rol in de barrièrefunctie van het SC en de studies die hierboven beschreven staan geven nieuw inzicht in de moleculaire rangschikking van lipiden in de lamellen. Het is voor de eerste keer dat de structuur van de lamellaire fasen met zoveel detail beschreven wordt.

Conclusies

In de studies beschreven in het eerste gedeelte van het proefschrift hebben we de spraymethode van het SCS ge-optimaliseerd terwijl de juiste lipidenorganisatie behouden bleef. In eerdere studies was al aangetoond dat het SCS de lipidenorganisatie en barrièrefunctie van menselijk SC nauwkeurig nabootst. Uit de daaropvolgende studies bleek dat het SCS ook een zeer geschikt model is om de relatie tussen lipidenorganisatie en barrièrefunctie te onderzoeken. Interessant genoeg blijkt uit onze resultaten dat het type laterale pakking van de SC-lipiden minder effect heeft op het transport van benzoëzuur dan een verandering van de lamellaire fasen.

Aangezien de vorming van de juiste lipidenfasen cruciaal is voor de barrièrefunctie van de huid, hebben we de moleculaire organisatie in de eenheidscel van deze fasen tot in meer detail bestudeerd. We hebben de verschillende lamellaire fasen bestudeerd in mengsels met alleen CER EOS, in mengsels met 5 CER-klassen aanwezig en in mengsels met dezelfde CER-klassen behalve CER EOS. Uit metingen van het mengsel met CER EOS als enige CER bleek dat in dit mengsel een unieke fase aanwezig is met een zeer lange herhalingsafstand, waarvan de molekuulopbouw in de eenheidscel anders lijkt te zijn dan de molekuulopbouw in de eenheidscel van de LPP. Uit de studies met mengsels waarin alle 5 CER-klassen aanwezig waren bleek dat de eenheidscel van de LPP opgebouwd is uit drie lagen. Studies met mengsels zonder CER EOS lieten een SPP-eenheidscel zien met een symmetrische verdeling van het gedeutereerde CER. Bovendien bleek uit röntgendiffractiestudies met natuurlijk SC dat de molekuulopbouw van de LPP-eenheidscel in onze modellen zeer dicht de de eenheidscel van de LPP in natuurlijk SC benadert. Aangezien de LPP een unieke lamellaire fase is in het SC en geacht wordt een belangrijke rol te spelen in de barrièrefunctie van de huid, bevestigt die laatste observering dat de lipidenmengsels zeer relevante modellen zijn voor onderzoek naar de lamellaire lipidenfasen in het SC.

Curriculum Vitae

Daniël Groen was born on the 3rd of November in 1979 in The Hague. After graduating from the Bonaventura College in Leiden in 1998 he started the study of applied physics at the University of Twente in Enschede. Daniël did his graduation assignment in the group of Biophysical Engineering. In April 2005 he obtained his masters degree in applied physics. In June 2006 he started as a PhD student in the division of Drug Delivery Technology at the Leiden/Amsterdam Center for Drug Research, Leiden University, under the supervision of Prof. Dr. Joke Bouwstra, which resulted in this thesis. From October 2010 till present he is working as a postdoc in the same division, in a research project together with the company Firmenich (Switzerland). In this project he investigates the interaction between perfume raw materials and the stratum corneum lipid organization. From January 2012 he will start in Geneva as a postdoc at Firmenich for one year.

List of publications

2011

Groen, D., Poole, D.S., Gooris, G.S., Bouwstra, J.A. , *Investigating the barrier function of skin lipid models with varying compositions*, *European Journal of Pharmaceutics and Biopharmaceutics*, in press.

Groen, D., Gooris, G.S., Barlow, D.J., Lawrence, M.J., van Mechelen, J.B., Deme, B., Bouwstra, J.A. , *Disposition of ceramide in model lipid membranes determined by neutron diffraction*, *Biophys J*, vol. 100, no. 6, pp. 1481-9.

Groen, D., Poole, D.S., Gooris, G.S., Bouwstra, J.A. , *Is an orthorhombic lateral packing and a proper lamellar organization important for the skin barrier function?*, *Biochim Biophys Acta*, vol. 1808, issue 6, pp. 1529-1537.

2010

Groen, D., Gooris, G.S., Bouwstra, J.A. , *Model membranes prepared with ceramide EOS, cholesterol and free fatty acids form a unique lamellar phase*, *Langmuir*, vol. 26, no. 6, pp. 4168-75.

2009

Groen, D., Gooris, G.S., Bouwstra, J.A. , *New insights into the stratum corneum lipid organization by X-ray diffraction analysis*, *Biophys J*, vol. 97, no. 8, pp. 2242-9.

Bouwstra, J.A., Gooris, G.S., Groen, D., Ponec, M. , *The skin barrier in healthy and diseased state*, *Chemistry and Physics of Lipids*, vol. 160, pp. S16-S16.

2008

Groen, D., Gooris, G.S., Ponec, M., Bouwstra, J.A. , *Two new methods for preparing a unique stratum corneum substitute*, *Biochimica Et Biophysica Acta-Biomembranes*, vol. 1778, no. 10, pp. 2421-2429.